PUBLICACION DE LA REAL SOCIEDAD ESPAÑOLA DE FISICA

ANALES DE FISICA

SERIE B

APLICACIONES, METODOS E INSTRUMENTOS

ISSN 0211-6251

Proceedings of the

Discussion Meeting on

THERMODYNAMICS OF ALLOYS

1990 VOLUMEN 86 Núm. 2 Especial (1-164)

ANALES DE FISICA

Serie A: Fenómenos e Interacciones

Serie B: Aplicaciones, Métodos e Instrumentos

PUBLICACION DE LA REAL SOCIEDAD ESPAÑOLA DE FISICA

Revista Fundada en 1903

DIRECCION PARA ENVIAR LOS MANUSCRITOS

Se recomienda el envío directo a los editores específicos de área. En caso de no corresponder a las áreas anteriores, se enviarán a la Real Sociedad Española de Física. Facultad de Ciencias. Ciudad Universitaria. Madrid – 28040. Teléfono (91) 243 38 79.

Esta publicación ha sido realizada con subvención parcial de la COMISION ASESORA DE INVESTIGACION CIENTIFICA Y TECNICA.

DEPOSITO LEGAL: M. 233 - 1958

Imprime: Gráficas TOMOGRAF, S.A. - Telef. 747 46 07

ANALES DE FISICA Serie B Vol. 86 1990

Proceedings of the

Discussion Meeting on

THERMODYNAMICS OF ALLOYS

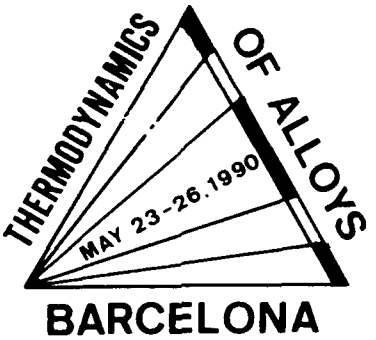

organized by

Grup de Física de Materials Universitat Autònoma de Barcelona
08193-Bellaterra, Spain
in colaboration with
Grupo Especializado de Física del Estado Sólido

Edited by

M.D. Baró
Dept. de Física
Universitat Autònoma de Barcelona
N. Clavaguera
Dept. Estructura i Constituents de la Matèria
Facultat de Física-Universitat de Barcelona
S. Suriñach
Dept. de Física
Universitat Autònoma de Barcelona

ANALES DE FISICA Serie B Vol. 86 1990

LOCAL ORGANIZING COMMITTEE

M.T. Mora (Chairman)
M.D. Baró
S. Bordas
N. Clavaguera
S. Suriñach

SPONSORS

Exmo. Ayuntamiento de Sant Feliu de Guixols
Exma. Diputación Provincial de Gerona
Caixa de Pensions i Estalvis de Barcelona, "La Caixa"
Comisió Interdepartamental de Recerca i Innovació Tecnológica
Direcció General d'Universitats
European Research Office of the U.S. Army
European Research Office of the U.S. Air Force
Comision Interministerial de Ciència i Tecnologia
Vice-Rectorat de Relacions Exteriors i Campus. Universitat Autònoma de Barcelona

FOREWORD

Several attempts have been made in the past by scientists experimentally active in thermodynamics of alloys either to organise discussion meetings or to find a niche at some other conference. All these efforts have not succeeded in establishing a permanent sequence of meetings which would provide a possibility for a recurrent exchange of information and results for the practitioners in this field of science. Two years ago, in April 1988, another discussion meeting was held in Vienna, Austria, with a strong possibility that another attempt would come to naught. By gentle persuasion our Spanish colleagues could be induced to pick up the torch and organise the sequel conference in May 1990 - and with the promise of Prof. Hertz to follow up with a discussion meeting in Nancy, France, in 1992 a series of conferences has been finally established which should provide a sounding board for ideas and results in the field of thermodynamics of alloys.

The present proceedings of the discussion meeting in Sant Feliu de Guixols show the breadth of interests and the international scope. Scientists of nine countries met for four days, presented their results and exchanged experiences. It would be indeed arbitrary to try and select high lights from among the papers presented in these proceedings, and it will be best left to the reader to choose according to his/her interests.

It was very gratifying to note the presence of many younger scientists who by their contributions demonstrated that they are quite ready to continue and promote the field of thermodynamics of alloys. This discussion meeting would not have been possible without the superb organization by Prof. Mora and Prof. Clavaguera, and their coworkers. They not only chose a lovely place on the Costa Brava but also took care to provide a well balanced mix of science and relaxation. The international scientific community owes them a great debt- both for a job extremely well done as far as the conference is concerned and for forging the so far missing link to establish a continuing series of like meetings.

K.L. Komarek
University of Vienna

PREFACE

This especial issue of "Anales de Física" contains the proceedings of the Discussion Meeting on Thermodynamics of Alloys which was held in Sant Feliu de Guixols (Costa Brava, Catalonia) Spain, from 23 to 26 May 1990, organized by the Physics of Materials Group of the Autonomous University of Barcelona

The scientific program covered different aspects of the determination of thermodynamic quantities, possible theoretical modeling and calculations. It consisted of seven plenary lectures of one hour, twenty two oral and ten poster contributions.

The Discussion Meeting was attended by about sixty scientists comming from ten countries, reflecting the interest in the research and development of the thermodynamic problems.

In this proceedings are compiled most of the plenary lectures and the contributed papers presented at the Discussion Meeting. The later were subjected to a fast-refereeing procedure during the Discussion Meeting and revisions have been made if necessary. We express our thanks to all the authors for accepting to keep their papers limited in length and for their cooperation in preparing camera-ready typescripts. Also, thanks are due to the various referees for their critical reading of the papers.

Finally it is our pleasure to announce that the next Discussion Meeting will be held in Nancy, probably in 1992, being chaired by Professor J. Hertz.

Bellaterra/Barcelona, August 1990

M.D. Baró
N. Clavaguera
S. Suriñach
Editors

ANALES DE FISICA Serie B Vol. 86 1990

CONTENTS

ANALES DE FISICA Serie B Vol. 86 1990

DETERMINATION OF THE THERMODYNAMIC PROPERTIES OF FORMATION OF ALLOYS AT HIGH TEMPERATURES

J. HERTZ and J.C. GACHON

Laboratory of Metallurgical Thermodynamics
University of Nancy I - U.R.A CNRS 1108
B. P. 239 - 54506 Vandoeuvre-les-Nancy Cédex (France)

Abstract : The determination of the thermodynamic functions of formation of alloys is examined in the light of the own experience of the authors. At high temperature,where the entropy term becomes important for the stability of each phase it is very important to obtain the two components of the Gibbs function : the enthalpy and the entropy. Experimental measurements of the chemical potential allow, by derivation versus temperature, to deduce the partial enthalpy and the partial entropy. But for an accurate knowledge of the enthalpy, calorimetry is needed. There exist two types of calorimetric method : direct, by reaction between the components of alloys or indirect mixing calorimetry in a solvent. In any case the most efficient way is to "cross" the experimental values obtained for the enthalpies with other results involving the Gibbs function. In this direction the "Calphad" method can be used as a real experimental tool when a good knowledge of the phase diagram is available. It is also possible to "cross" the enthalpies with E.M.F., vapor-pressure, mass-spectrography ... The determination of a complete set of thermodynamic data for each system appears as a real strategic game.

At the beginning of the preparation of this lecture we first thought of speaking only about the experimental ways to measure the thermodynamic properties of formation of alloys. In fact our lab in Nancy is especially an experimental laboratory and, since many years, we have engaged heavy experimental programs in view of determining thermodynamic functions related to the formation of alloys. But considering the strong interaction existing between the real experimental measurements and the estimations of data obtained by optimizations of phase diagrams, we think that it is more equitable to speak about the **"determination"** of thermodynamic properties.

The choice of the method to determine any numerical value in the field of thermodynamics is never predetermined and nobody can pledge his word that any such particular way is the best. In fact any determination of a thermodynamic quantity for any system is based on the analysis of the situation :

1) What has to be done with such a determination?
2) How many time can we spend to obtain it?
3) What is the budget allowed to get it?
4) Does it exist anybody in the world who already got a value of that quantity ? (literature exploration).
5) Is it possible that any technique developped in my surroundings can produce a good direct or indirect information on this numerical value?

If the balance of all these arguments decides your group to undertake the determination of this numerical quantity you are engaged in a **strategic game.**

1 - What kind of thermodynamic properties for alloys?

1 - 1 The Gibbs function

Alloying properties are determined by the Gibbs function **g** and this function can be taken as composed of two parts, the enthalpy and the entropy terms :

$$\mathbf{g = h - T.s} \qquad (1)$$

Any integral quantity, in a multicomponent system, is the sum of its partial quantities:

$$g = \sum_i x_i \mu_i \qquad (2)$$

with $$\mu_i = h_i - T s_i \qquad (3)$$

$$h = \sum_i x_i h_i \qquad (4)$$

$$s = \sum_i x_i s_i \qquad (5)$$

Chemical potentials μ_i, are the partial molar quantities of the Gibbs function. Measurement of any Gibbs function requires the establishment of a reversible equilibrium in a cell and the determination of all the component chemical potentials. The universal method to do that is the mass spectrography in which it is possible to measure independently the chemical potentials of all the species. This is a very heavy and difficult technology which needs very specialised groups. I am not familiar with it and I don't like to speak about it. Recently, Necker has published a very complete review of this question (1). In addition to mass spectrography there exist various other methods to obtain information on the chemical potentials in the system :

- **vapor pressure measurements** and equivalent methods : effusion, isopiestic ....
- **e.m.f measurements.**

Generally speaking, by such methods, we are not able to characterise all the chemical potentials of all the

species. But if we are dealing with binary systems the measurement of one component chemical potential is enough, considering the Gibbs Duhem isobaric - isothermal relation :

$$x_1 \, d\mu_1 + x_2 \, d\mu_2 = 0 \qquad (6)$$

which can be integrated.

1 - 2 The entropies

Generaly speaking entropies are the most difficult quantities to obtain : the unique way to measure directly this kind of function would be the integration of heat capacities, Cp, from 0 to T/K :

$$s = \int_0^T \frac{C_p}{T} dT \quad \text{using the Nernst postulate} \qquad (7)$$

We think that only a few laboratories (or perhaps none) in the world are engaged in such a program of determination of Cp in wide ranges of composition and temperature.

1 - 3 The two derivations of the Gibbs function

In fact, the most information concerning entropies is deduced from Gibbs function measurements. There exist two kinds of derivation of the Gibbs function :

The Gibbs-Helmholz derivation

$$\left(\frac{\partial \quad}{\partial \quad} \right)_{p,x} \qquad (8)$$

The Van t'Hoff derivation

$$h = \left(\frac{\partial g/T}{\partial 1/T} \right)_p \qquad (9)$$

These two formulae express that both enthalpies and entropies can be determined starting only from Gibbs measurements at different temperatures.

1 - 4 The enthalpies

But the best method to measure accurately the enthalpies remains the calorimetry. The heat flow linked to any evolution of a system placed in the cell of a calorimeter, at constant pressure, measures directly the variation ΔH of the system enthalpy.

1 - 5 Crossed strategies

It is often possible to combine the Gibbs integral or partial functions with the enthalpy : if it is possible to measure separately g and h we deduce $s = \frac{h - g}{T}$ without any derivation versus temperature.

1 - 6 General view on the experimental primary informations

Table I summarises the primary methods to obtain experimental function of mixing : it can been seen that, the most often, **integral enthalpies** and **partial Gibbs potentials** are got. Nevertheless for liquid phases the partial enthalpies are also often available.

Table I **Primary experimental information for binaries. Thermodynamic functions of mixing.**

	h_i	h	μ_i	g
Liquid alloys	Direct reaction calorimetry by addition of components	1) Integration of hi 2) Direct reaction calorimetry at various concentrations	Mass spectrography E.M.F vapor pressure effusion /isopiestic	Gibbs-Duhem integration or similar (CALPHAD-modelisation)
Solid solutions		1) Indirect mixing calorimetry in a solvent bath 2) Direct reaction calorimetry starting from components	mass-spectrography E.M.F vapor pressure isopiestic	Gibbs-Duhem integration or similar (CALPHAD-modelisation)
Compounds		1) Indirect mixing calorimetry in a solvent bath 2) Direct reaction calorimetry 3) Precipitation of a compound in a liquid bath 3-1 stoechiometric composition 3-2 Euler equation with partial enthalpies	mass-spectrography E.M.F in a two-phase domain	Gibbs-Duhem integration or similar (CALPHAD- modelisation)

2 - Optimization of phase diagrams (CALPHAD Methods)

There exist also various programs for optimization of phase diagrams. This method can be used either for determining the equilibrium phases in a system under various conditions or also (on the contrary) for estimating the thermodynamic functions of mixing of any phase in the system. The results which are obtained depend slightly on the model used for representation of the Gibbs functions and also on the mathematical method of optimization. Nevertheless there is a universal method to transforme a lot of fragmentary information about thermodynamic properties (for a system) into a **full set of coherent data.** (Table II). We call this method the "CALPHAD method" by reference to the international group devoted to the development of such optimizations. Polynomial developments of the excess Gibbs energy is a rather old idea. Historically, for binaries, the method is related to Margules equation (10), where the excess Gibbs function is expressed by a polynomial development of one mole fraction x

$$g^e = x\,(1-x) \sum_{o}^{n} a_i\, x^i \qquad (10)$$

An improvement was introduced by Redlich and Kister (11) for binaries, using simultaneously the two mole fractions :

$$g^e = x_1\, x_2 \sum_{o}^{n} a_i\, (x_1 - x_2)^i \qquad (11)$$

This kind of development can be easily extended to ternaries and multi-component systems. Hillert (12) has presented a review of these extensions for ternaries. The interest of the first Redlich-Kister asymetric term concerns its identity with the first degree term of orthogonal Legendre polynomials :

$$x_1 - x_2 = 2x - 1 \qquad (12)$$

These orthogonal polynomials have been used by Pelton et al (3) and more recently by our group in Nancy in the program NANCYUN (6)

Table II **Optimization of the phase-diagram**

Ingredient inputs: (fragmentary information)	**modelisation** of the excess Gibbs functions	**output** : full coherent set of data
x (T) line	1) **Polynomial development**	x (T) lines
h_i	"F*A*C*T" Pelton (2)	hi
h	"Lukas" (3)	h
s_i	"Extxd" Oonk and al (4) et (5)	s_i
s	"Nancyun" (6)	s
μ_i	2) **Sublattice model** : Hillert (7)	μi
g	"Thermo-Calc" Sundman and Ågren (8)	g
	3) Hoch and Arpshofen model(9)	
	4) Statistical models	

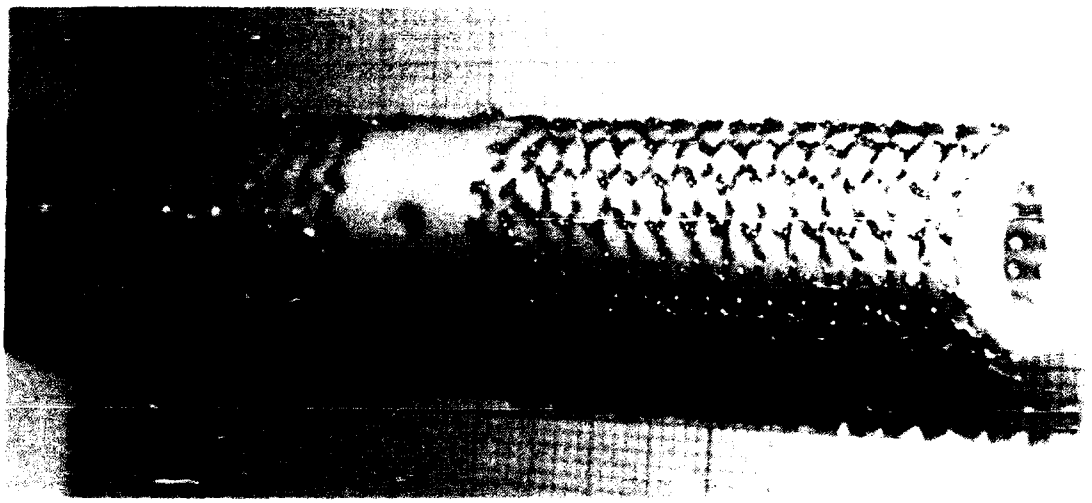

Fig 1-Calvet's type sensor designed by Gachon for service up to 1900K. The thermopile contains about 400 thermocouple-junctions.

3 - High temperature calorimetric data

Now what about the meaning of **high temperature measurements** ? It is possible to define the high temperature domain as the **diffusion** domain, for metallic phases, which is located above about half of the melting temperature of the phase expressed in kelvins. For lead alloys, for instance, high temperature starts at room temperature. But we are sure that the organising committee of this meeting would be somewhat disapointed if we limit this lecture to room temperature experiments. Generaly speaking there exist a lot of new experimental difficulties when working above 1000°C. This is the reason why we have chosen to speak about the determination of **thermodynamic data of mixing above** 1000°C...These new experimental difficulties concern three main points :

I - The choice of the sensor to detect the calorimetric heat effect,

II - The reaction of the metallic substance with the crucible,

III - The high vapor pressure of the alloys which can induce important losses of mater by vaporisation or sublimation, associated with a systematic error for the heat of mixing. To avoid this difficulty, it seems to us, that the best way, when possible, is to obtain a very quick reaction between the condensed phases dropped into the calorimeter, so that the vaporisation process becomes no significant during the reaction measurement. That means that always higher temperatures will be needed.

We would not like to do here a complete review of the calorimetric methods in metallurgy, this has been done very recently by Castanet (14) for the Nato school "Thermochemistry of alloys" and we recommand the lecture of this highly documented review. Previousely, we have also presented a review focusing the application of the calorimetric methods in the field of metallurgy (15). The most important basic principles of calorimetric methods in metallurgy were well described (16) by Predel, Arpshofen and Pool in 1978.

Calorimetric thermopiles for Calvet-type or similar devices are efficient up to 1500°C in special apparatus. But at this high temperature the lifetime of the sensor is often very short and we are considering the sensor as a consumable part of the calorimeter.

Figure 1 shows a new thermopile designed by Gachon. This sensor is made of more than 400 thermocouple junctions made of special platinum alloys. It looks like a real Calvet-type thermopile and it is efficient up to 1600°C in an oxidizing atmosphere and up to 1500°C in a highly reducing one.

Up to 2400°C it is possible to perform semi-quantitative DTA. Commercial cells are built of refractory metals like tungsten and rhenium, and that means that only a reducing atmosphere is allowed (Figure 2).

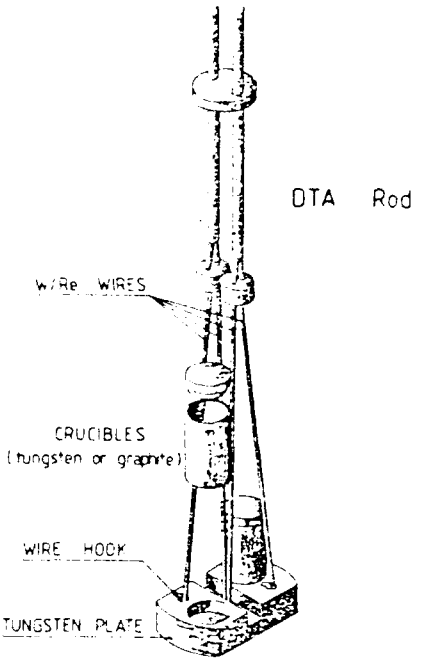

Fig 2-The 2700 K DTA sensor by SETARAM.

3 - 1 Radiation calorimetry

But the real new improvement concerns the use of the radiation signal of the sample, at high temperature, to measure the heat flow. Stefan's law induces that the radiation heat flow becomes predominant at very high temperature. Frohberg (17) has made, with his coworkers, in Berlin, **a levitation calorimeter** based on radiation measurement. The principle of the device is explained on figure 3. Using a twocolor pyrometer it is possible to follow the variation of temperature of the sample during the reaction process and to correct it from the variation of the emissivity coefficient. Frohberg determines the time when the loss of heat, by radiation, is equal to the gain of heat, by electrical induction. At this precise time the extrapoled temperature-versus time curve crosses the correct variation of temperature linked to the reaction (figure 4). The calorimeter is treated as an isoperibolic one. The estimation of the accuracy gives about ± 12 % for an enthalpy of mixing measured at 3000 K. Figure 5 illustrates the results obtained with liquid molybdenum silicon alloys at 3000 K (17). We would like to emphasise that such a procedure avoid any problem of reaction with the crucible (levitation) which induces drastic difficulties in very high temperature calorimeters. Nevertheless the loss of product by vaporization can be a source of difficulties.

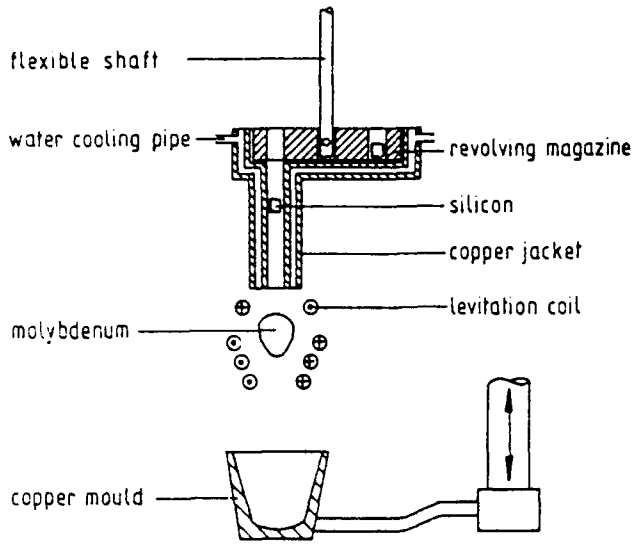

Fig 3-The radiation calorimeter designed by Arpaci and Frohberg (17) with his "levitation crucible".

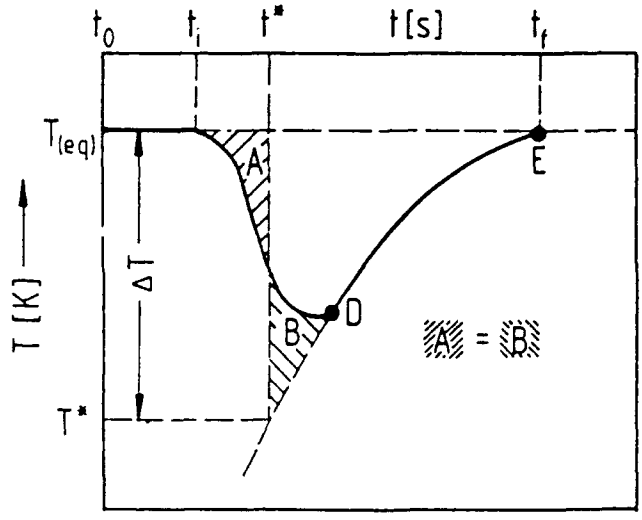

Fig 4-Determination of the time t* where the loss of heath by radiation is compensed by the electrical heating.

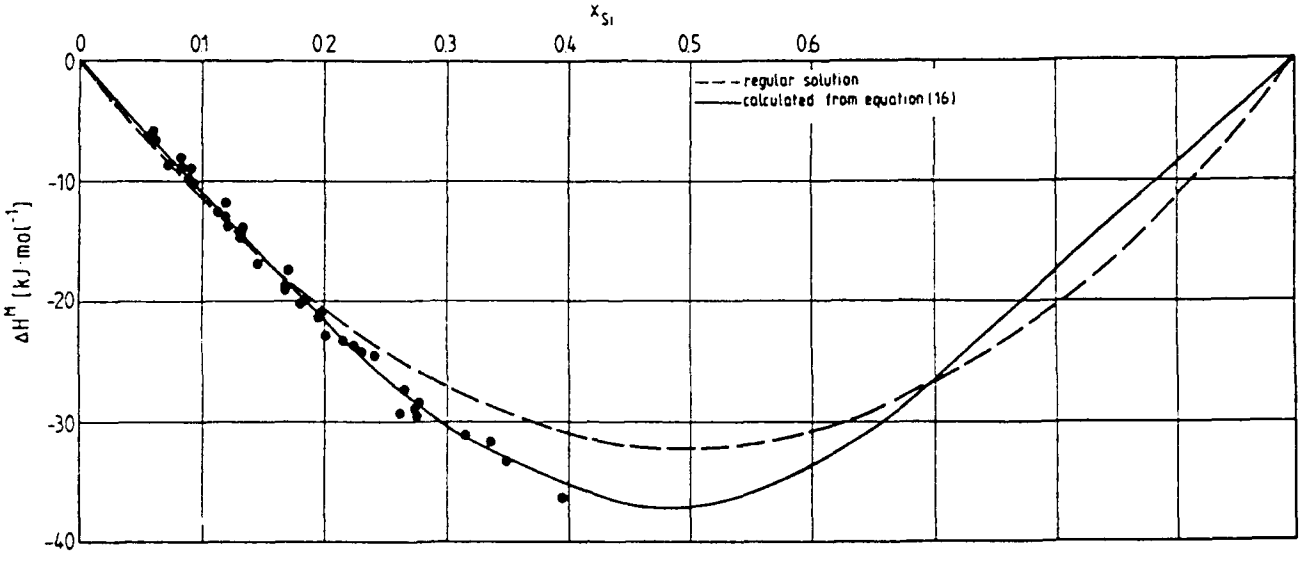

Fig 5- Integral molar heat of mixing of the system molybdenum-silicon measured , near 3000K, by Frohberg and Arpaci (17).

3 - 2 Direct reaction calorimetry for solid and liquid phases

3 - 2 - 1 Liquid Phases

At lower temperatures, liquid alloys can be synthetised directly by dropping small pieces of a pure component in a molten bath, contained in the calorimetric cell, starting either with a pure solvent or with an prealloyed liquid with a well-known composition. We would like to illustrate this technique by an exemple of Franco-Austrian cooperation between the groups of Prof. Bros in Marseille and Prof. Komareck in Vienna. The device is based on a Setaram high-temperature fluxmeter, highly modified (18). Figures 6 and 7 show the partial and integral enthalpies of mixing obtained by Hayer et al (19) for gold-aluminum liquid alloys at various temperatures. We would like to underline the high quality of these measurements.

Predel's group at the MPI of Stuttgart has devoted a lot of studies to the liquid metallic state and built particular calorimeters for the determination of liquid mixing enthalpies. With a well stirred liquid bath it is not necessary to have a full heat-flux recording like in a Calvet type calorimeter.

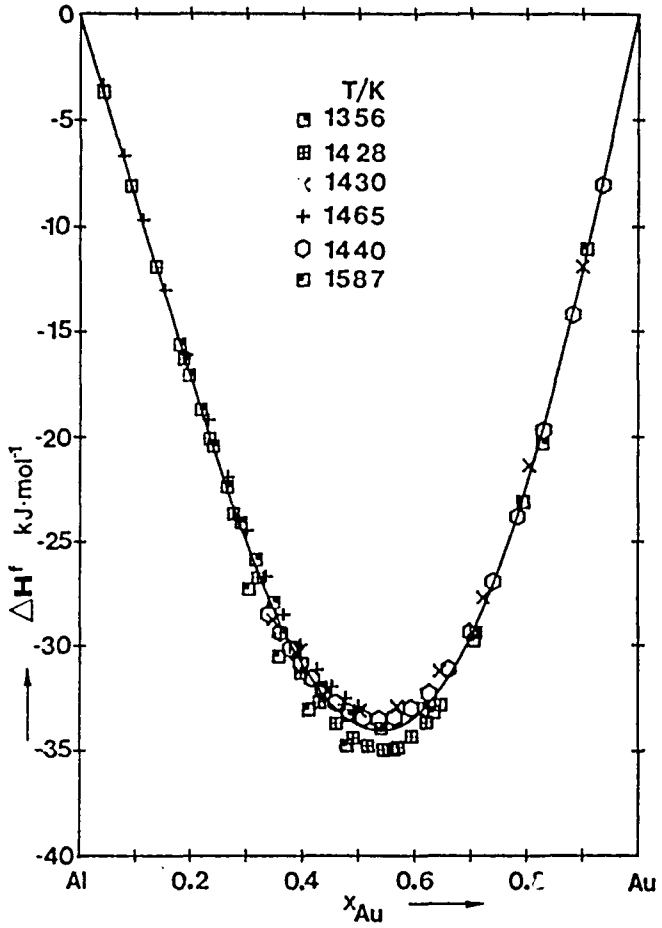

Fig 6- Integral enthapies of liquid (Au, Al) alloys vs composition at different temperatures: after Hayer, Gehringer, Komarek, Gaune-Escard and Bros(19)

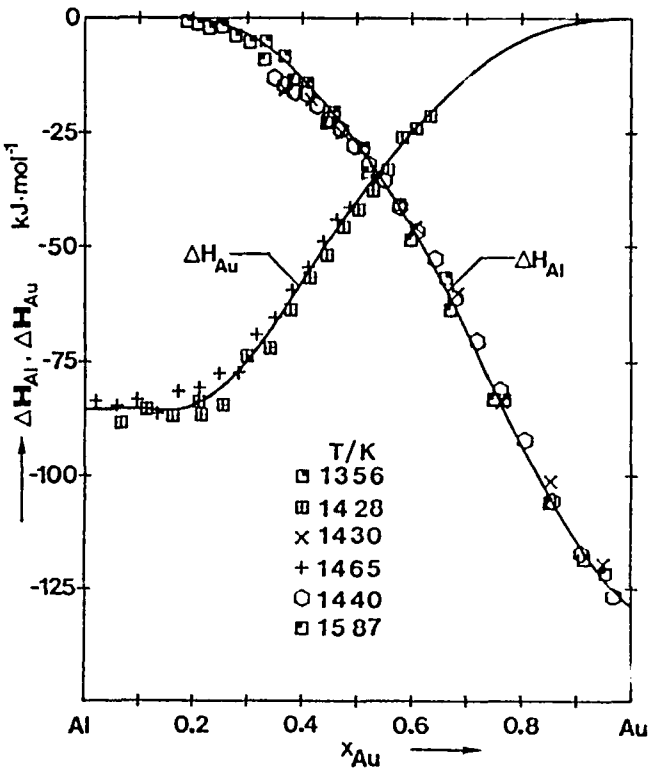

Fig 7- Partial enthalpies of Au and Al , resp, for liquid alloys, after Hayer, Gehringer, Komarek, Gaune-Escard and Bros(19)

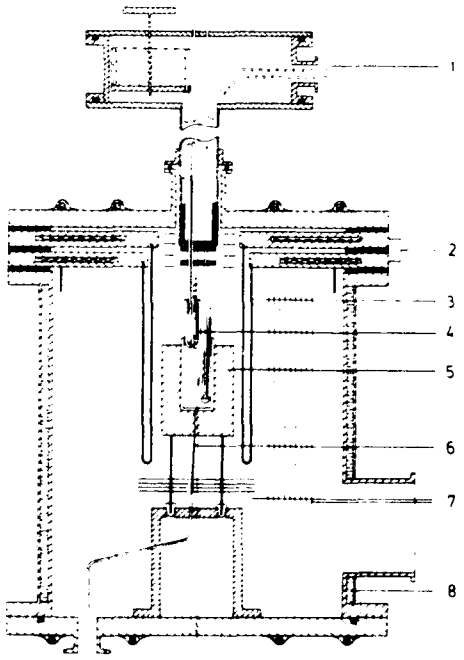

Fig 9- Adaptation of the Predel's initial calorimeter to higher temperature range, (up to 1900K), by Lück and Predel (21).

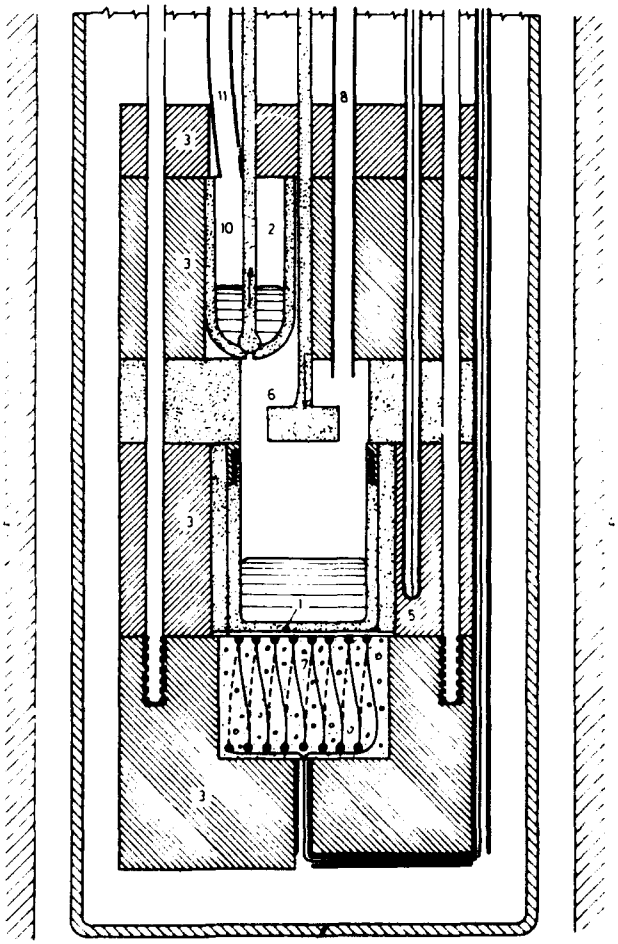

Fig 8- Liquid mixing calorimeter by Predel.

Only a few thermocouples are enough to get a representative knowledge of the heat exchange between the cell and the isothermal block of the calorimeter. Figure 8 shows the principle of the calorimeter as described in a recent review by Sommer (20). The sensor is built in at the bottom of the cell between the crucible and the isothermal block. A stirrer can be pulled to the upper part, when introducing an amount of liquid. The sample is first stored and melted in a particular crucible situated at the top of the cell, maintained at the cell temperature and closed by a stopper. In the initial device the sensor was made from chromel-alumel thermocouples which limited the temperature of use to 1300 K. More recently Lück and Predel (21) built a new version of this calorimeter (figure 9), efficient up to 1900 K. In this new version, only two thermocouples, one placed at the heart of the bath, the second in the block, deliver the thermal signal. Lück, Arpshofen, Predel and Smith (22) have compared the results obtained with this calorimeter or with a SETARAM high temperature fluxmeter in the vicinity of 1800 K. For the liquid (Ni, Ti) alloys they got the same results (figure 10) in the scale of the experimental uncertainty which is of the order of 3 %.

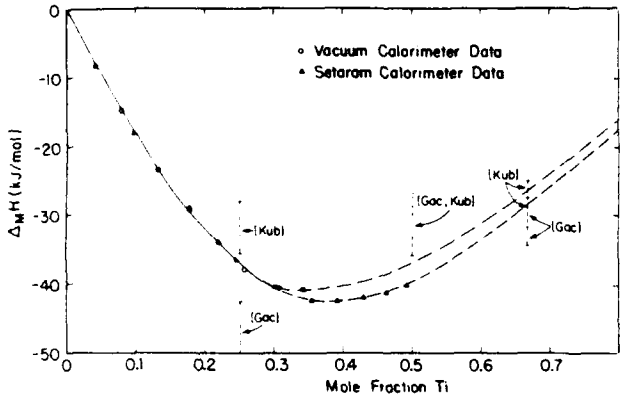

Fig 10- Comparison of the mixing enthalpies of liquid (Ni, Ti) alloys, measured with the vacuum calorimeter or with the SETARAM device, after Lück et al.(22).

A similar technique with a similar device is also used by Dr Castanet in Marseille and also in our own laboratory in Nancy. In Castanet's work we chose, as an exemple, the (In, Te) liquid system, where the variation of the enthalpy of mixing within the temperature range is quite evident (23). Figure 11 illustrates the excess Cp detected in the liquid indium-tellurium alloys between 987 K and 1344 K. This phenomenum is linked to the short-range order which disappears at high temperature. With a similar procedure we have also detected in Nancy an important excess Cp in the nickel-rich part of nickel-hafnium liquid alloys. The discrepancy between the enthalpies of mixing in this system at 1633 and 1743 K, measured by Selhaoui and Gachon (24) is very important (figure 12) and corresponds to an excess mean value of about 80 J/mole K, at $x_{Hf} = 0,15$.

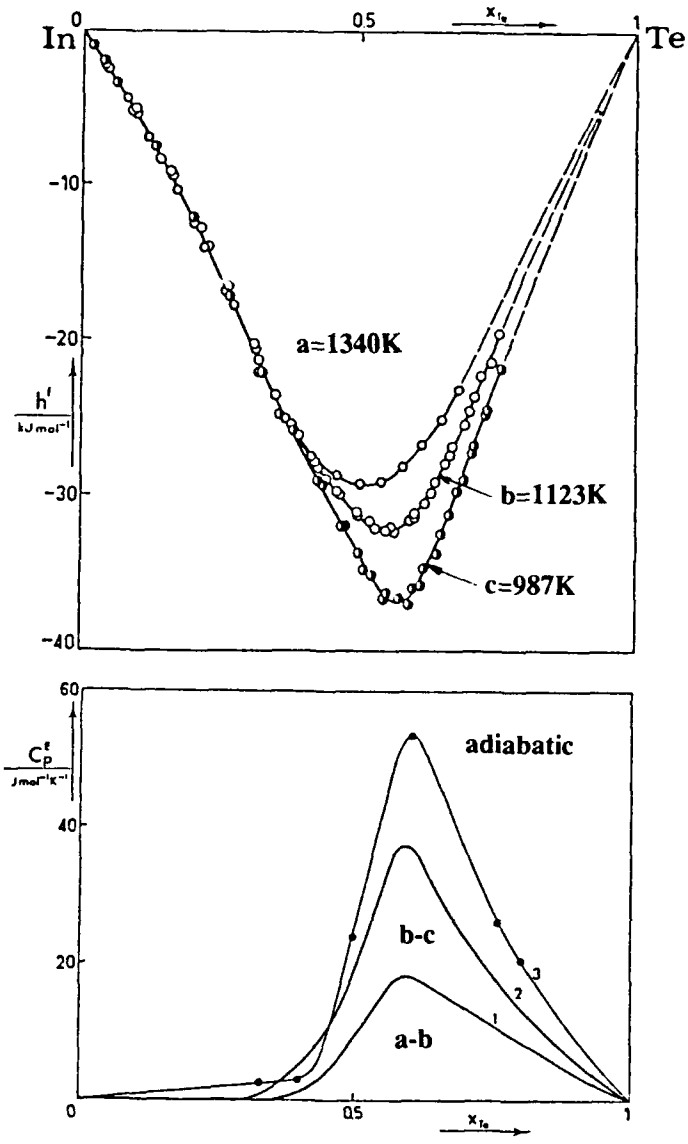

Fig 11- The Indium-Tellurium liquid alloys exhibit very important excess Cp near 1000K. (After Castanet (23))

3 - 2 - 2 Solid phases. This last particular study is also a good introduction to the technique used for measuring the enthalpy of formation of stoichiometric compounds by precipitation in the liquid. The congruent melting point of the Hf_2Ni_7 compound was measured at 1705 K by ATD (24). For this reason the enthalpy curves obtained at 1633 and 1743 K look very different from each other (figure 13). At 1633 K it is clear that the two rectilinear enthalpies of mixing (versus x_{Hf}), obtained on both sides of the compound, cross each other at the x = 0,22 concentration. This can be used to **measure the stoichiometry of the compound.**

We found very impressive the small scattering of the experimental points, at such a high temperature. The mean deviation is only of the order of about ± 200 J/mole.

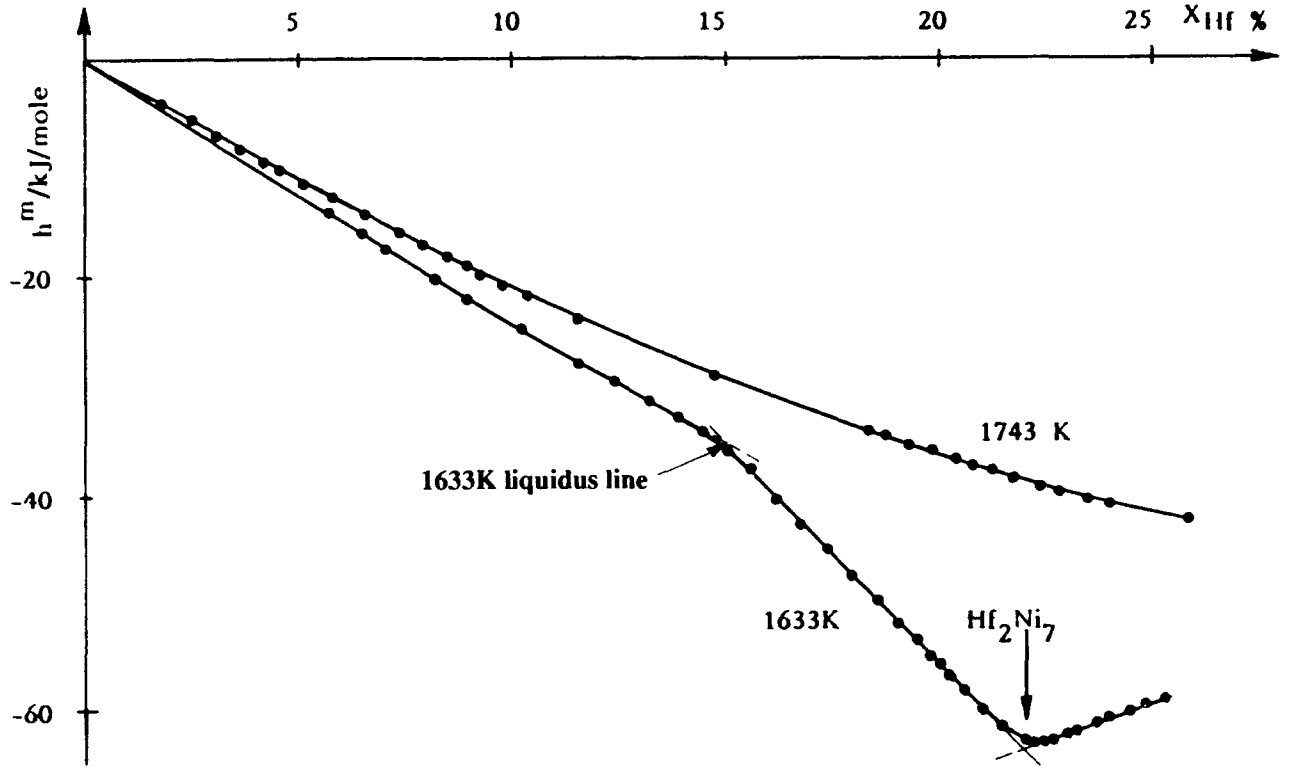

Fig 12- The Hafnium-Nickel liquid alloys exhibit also very high values of excess Cp, near 1700 K. Under the congruent melting point, it is possible to measure directly the stoichiometry and the enthalpy of formation of the $Hf_2 Ni_7$ compound.(After Selhaoui and Gachon (24)).

On the contrary, the accuracy of the calorimeter itself is much lower. Figure 13 exhibits the deviation of the results obtained at 1743 K, when calibrating the calorimeter with pure nickel samples taken at room temperature (24). The standard deviation is about 5 % of the measured value. Nevertheless, in such cases, the results we got for the enthalpy of mixing is highly reproducible. This fact is due to the **"compensation effect"** between the endothermic heat effect of the pure nickel at room temperature when falling into the cell and the exothermic effect of the reaction. As an exemple, at 1633 K, for x_{Hf} = 0,20 we had to measure less than 180 J for a result of 1,3 kJ. This compensation effect is obtained with any highly exothermic reaction. These is one of the most important advantage of the **"direct reaction calorimetry"**.

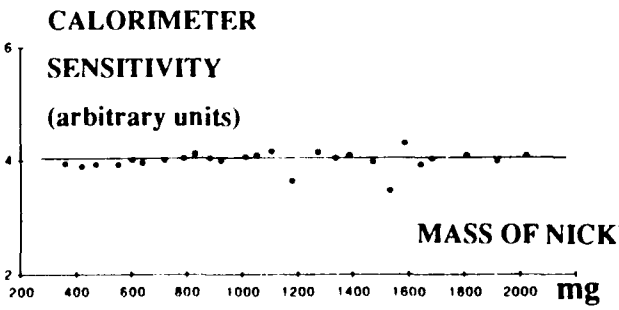

Fig 13- The calibration of the calorimeter : the mean deviation is about 5%.(Selhaoui and Gachon (24)).

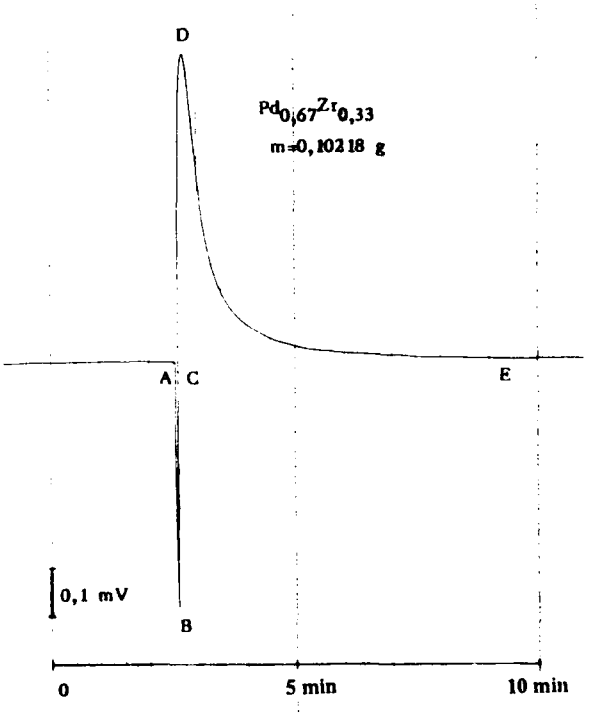

Fig 14- The "compensation effect".

Figure 14 illustrates the compensation effect obtained by synthetising a Pd2Zr compound. In the first step (from A to B) the endothermic cooling of the crucible by the cold sample is apparent. From B to D the exothermic reaction is active, crossing the base line in C. Within a few minutes the total reaction is achieved.

The same technique of precipitation in the liquid was used in our laboratory to measure the enthalpy of formation of the $GaMo_3$ compound. In this particular case, the two "partners" exhibit the most important discrepancy between their melting temperatures : 303 K for Gallium and 2890 K for Molybdenum. High temperature calorimetry near 1500 K allows us to precipitate the compound when dropping small pellets of compressed pure molybdenum pow ' r into the liquid bath. Figure 15 shows the result obtained by Belgacem-Bouzida at 1523 K (25) by this technique. In the two-phase domain, the partial enthalpies of mixing h_{Ga} and h_{Mo} remain constant (fig. 15), and the integral enthalpy of formation of the compound Mo_3Ga is obtained by the Euler equation :

$$h^f (Mo_{0.75}\ Ga_{0.25}) = 0.75\ h_{Mo} + 0.25\ h_{Ga}$$

But it is also quite possible to measure directly the integral enthalpy of the Mo_3 Ga compound by dropping into the cell of the calorimeter a mixture of powders of the two components, weighed and pressed in the right proportions. The results we got (25) by the two techniques are compatible and the precision on the mean value is about 5 % :

Precipitation in the liquid (fig. 15)
h^f ($Ga_{0.25}$ $Mo_{0.75}$, 1573 K) = - 19725 ± 1000 J/mol

Direct integral reaction (2 runs)
h^f ($Ga_{0.25}$ $Mo_{0.75}$, 1423 K) = - 18600 ± 1300 J/mol
Direct integral reaction (3 runs)
h^f($Ga_{0.25}Mo_{0.75}$, 1523 K) = - 17900 ± 1000 J/mol

Reference states for the experiments were solide molybdenum and liquid gallium.

Direct reaction calorimetry is also suitable for various synthesis reactions involving a metal component alloyed with a **non metal**. Berkane and Gachon used this method in our laboratory to measure directly the enthalpies of formation of chromium carbides (26). Table III compares their results with the combustion-calorimetry of carbides, taken in literature (27, 28, 29, 30). It is evident that, (in spite in of the fact that direct reaction calorimetry remains inaccurate), in this case, the precision of this method is five times better than that of the combustion calorimetry.

Another advantage of integral synthesis is to follow the variation of stoichiometry of a carbide. Figure 16, as an example, illustrates the variation of the enthalpy of formation of the Ti_{1-x} C_x phase versus x ($0.32 \leq x < 0.50$), measured by Berkane in our laboratory by direct reaction above 1500°C (31). In these experiments the reaction is not very quick and this is the reason of the relatively important scattering of the results, in particular near the $x < 0.50$ border. It is interesting to observe that the extremum of the enthalpy does probably not correspond to the stoichiometric compound TiC.

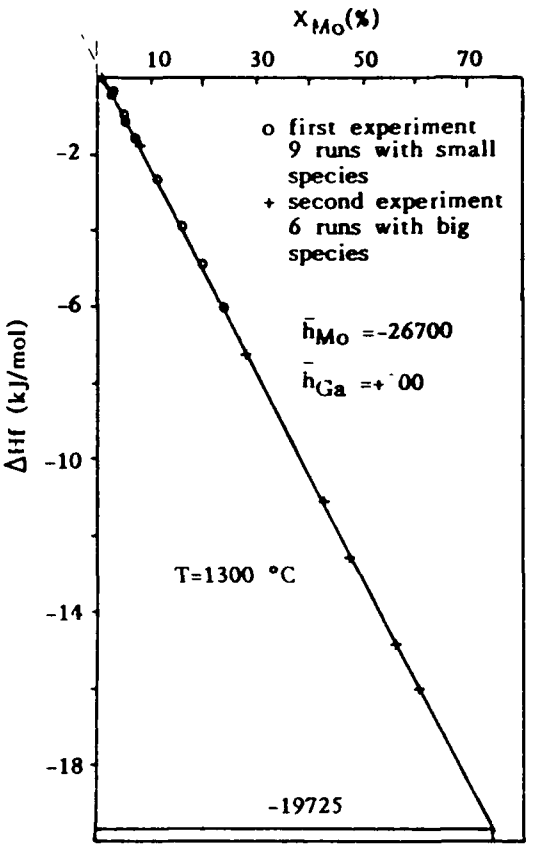

Fig 15- Precipitation of the Mo_3Ga compound in the liquid-solid mixture. By Belgacem-Bouzida, Notin and Hertz (25).

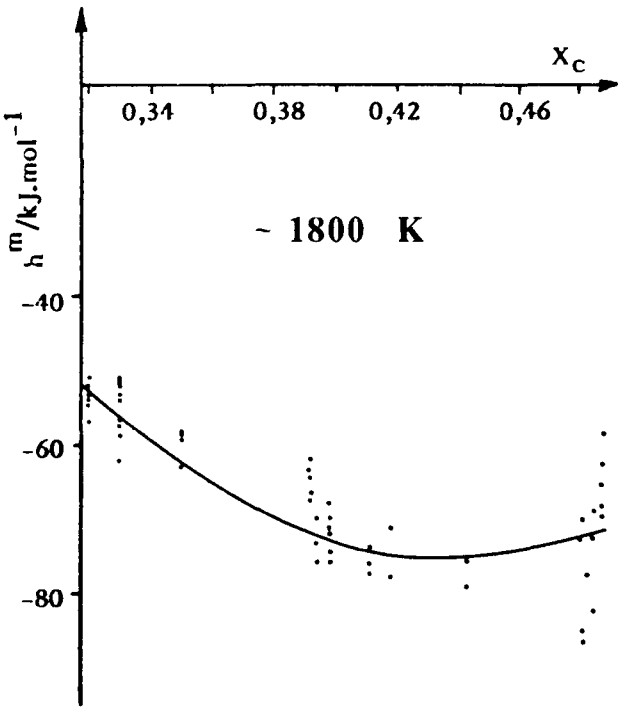

Fig 16- Direct reaction calorimetry between Ti and C, to explore the whole range of non-stoichiometry of the B1 carbide. By Berkane, Gachon and Hertz.(31) The experimental scattering is linked to the long delay needed to obtain the complete reaction.

Table III enthalpies of formation of (Cr, C) compounds

Direct reaction calorimetry at 1723 K and comparison with combustion calorimetry
units : J/mole

	h^f (1723 K) (26)	MAH (27)	MAH revised * by JANAF (28)	MAH revised by KULKARNI and WORREL (29)	DAWSON and SALE (30)
1/29 $Cr_{23}C_6$	- **9400 ± 1000**	- 13700	- 11300	- 9350	- 10200
1/10 Cr7C3	- **10700 ± 1800**	- 18100	- 16100 -	- 14300	- 14900
1/5 Cr_3C_2	- **10000 ± 600**	- 18800	- 17100	- 15600	- 16200

* ***Comments*** *: The results obtained by combustion calorimetry are strongly dependent of the value adopted for the enthalpy of formation of the oxide Cr_2O_3.*

MAH (27) used h^f (Cr_2O_3) = - 276,6 k cal/mole, but this value has been revised by JANAF (28) and by KULKARNI (29).

In any case the uncertainty on this reference enthalpy is about ± 8 kJ for two moles of chromium, inducing in the final result an uncertainty of ± 5500 J for the enthalpy of formation of the carbide

Table IV : Adaptation of the Dench and Kubaschewski procedure

T_2	(Fe) + (Mn)	→	h^m (T_2)	→	(Fe, Mn)	→	0	→	(Fe, Mn)
	h_2 ↑		Kubitz and Hayes		↑ h_1		Dench		↑h_3
T_1	(Fe) + (Mn)	→	0	→	(Fe) + (Mn)	→	h^m (T_1)	→	(Fe, Mn)

Thirty five years before, Kubaschewski and Dench (32,33) proposed another method to obtain the alloying enthalpy of mixing (at room temperature) using an adiabatic device. The operating method consisted to use the calorimeter as a DSC system heating a mixture of the components from room temperature up to high temperature where the reaction took place, the total heat effect being integrated. During a second run, only the heat content of the alloy was characterised. By subtracting the total heat effect of the second run from the first one, they obtained the heat of mixing at room temperature.

The Dench and Kubaschewski calorimetric procedure has been more recently adapted by Kubaschewski and Grundmann (34), and also by Kubitz an Hayes (35) to obtain the enthalpy of mixing at high temperature, instead of room temperature. Table IV give the principle of this modification.

During the second heating, the heat contents of the pure components, taken in the same quantity, is measured without mixing to obtain h^m (T_2) :

$$h^m (T_2) = h_1 - h_2 \qquad (13)$$

While the Dench's initial procedure gave h^m (T_1) :

$$h^m (T_1) = h_1 - h_3 \qquad (14)$$

The results obtained by Kubitz and Hayes (35) for the enthalpies of mixing of the (Fe, Mn) solid f.c.c. solution at 1443 K are presented in figure 17. The enthalpy of formation of the solid phase, in the middle part of the diagram, is about - 3000 J/mole while the magnitude of the heat content between 300 and 1400 K is of order of 25000 J : this is the reason why the results appear relatively scattered. The total measured quantity is about seven times greater than the required mixing enthalpy.

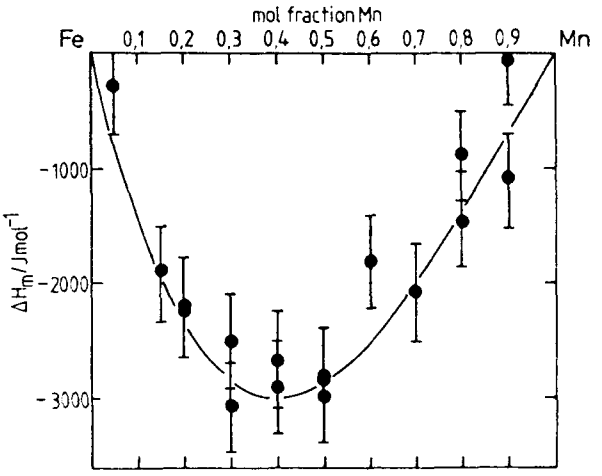

Fig 17- Enthalpies of mixing of the (Fe, Mn) γ alloys at 1443 K
After Kubitz and Hayes (35)

A variant of Kubaschewski's and Dench's method has been developped simultaneously by two groups of the university of Genova respectively led by Professors Iandelli and Ferro. The idea is to use a fluxmetric calorimeter at increasing temperature, to start between the components a reaction which gives a very important heat during the reaction. This exothermal effect is sufficient to achieve the complete reaction, after starting, without any other external heating. Starting temperatures are in the vicinity of 600 K. The first description of such a procedure was given by Palenzona in 1973 (36).

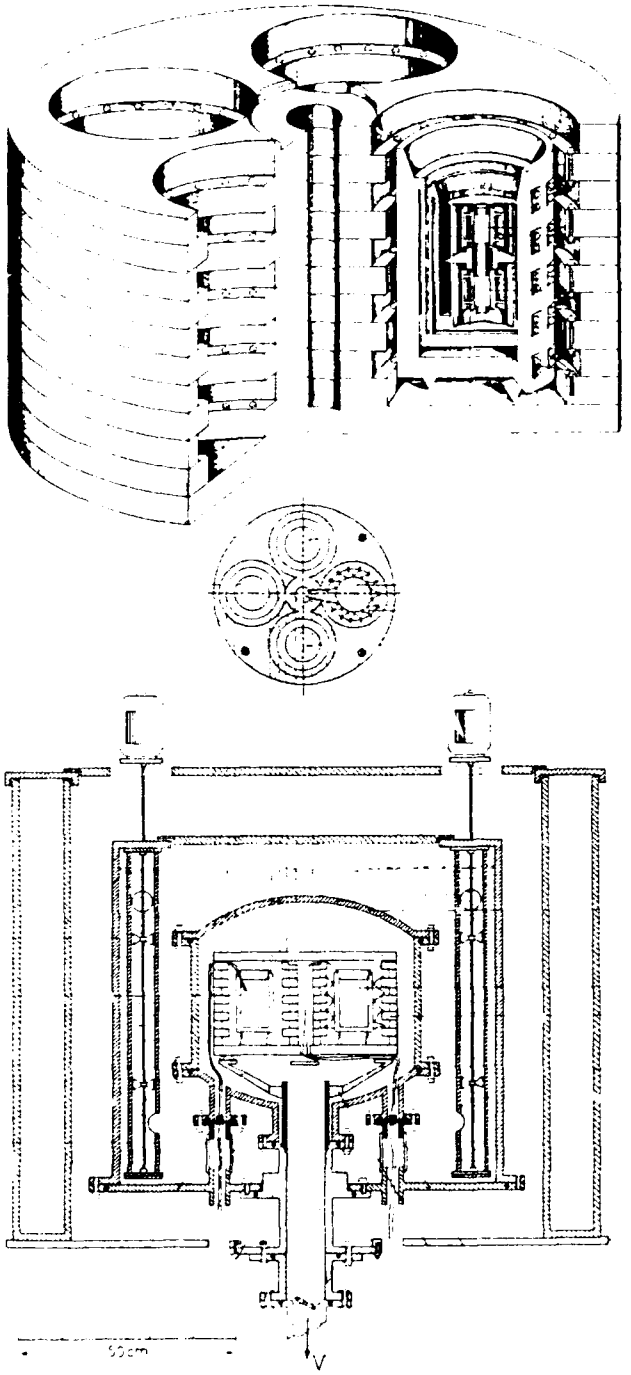

Fig 18- The calorimeter designed by Capelli, Ferro and Borsese for the determination of the enthalpies of formation of solid phases with strong exothermal effect.

Capelli, Ferro and Borsese built, in 1974, a fluxmetric calorimeter containing 4 cells in the same isothermal block (37) (fig. 18). A mixture of the components is heated by an electrical wire up to the start of the alloying reaction. The total heat effect, corresponding to the electrical heating (known energy) and to the chemical reaction, is determined by an isoperibolic procedure. Both methods were widely applied by the two groups for measurements of heats of formation of intermetallic compounds having a high congruent melting temperature and a highly negative enthalpy of formation. In particular, alloys of Ca, Ba, Sr and especially intermetallic compounds with rare-earth components were studied. As an illustration of the results obtained in Genova, we chose to present on figure 19 a comparison between Miedema's model predictions and experimental measurements obtained by Borsese, Borzone and Ferro (38) and by Palenzona and Cirafici (39) for various rare-earth compounds. It is important to underline that the methods used in Genova do not need very high temperature calorimeters.

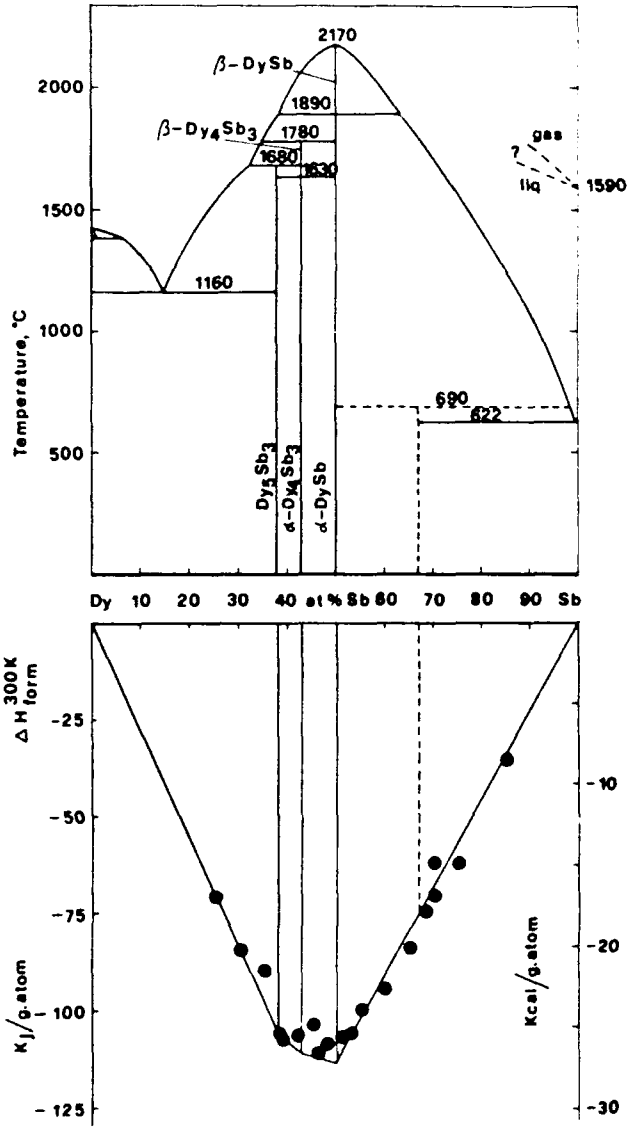

Fig 20- Correspondance between the high melting points of the compounds in the (Dy, Sb) system, (after Mironov et al (40)) and the enthalpies of formation measured by Ferro et al (41).

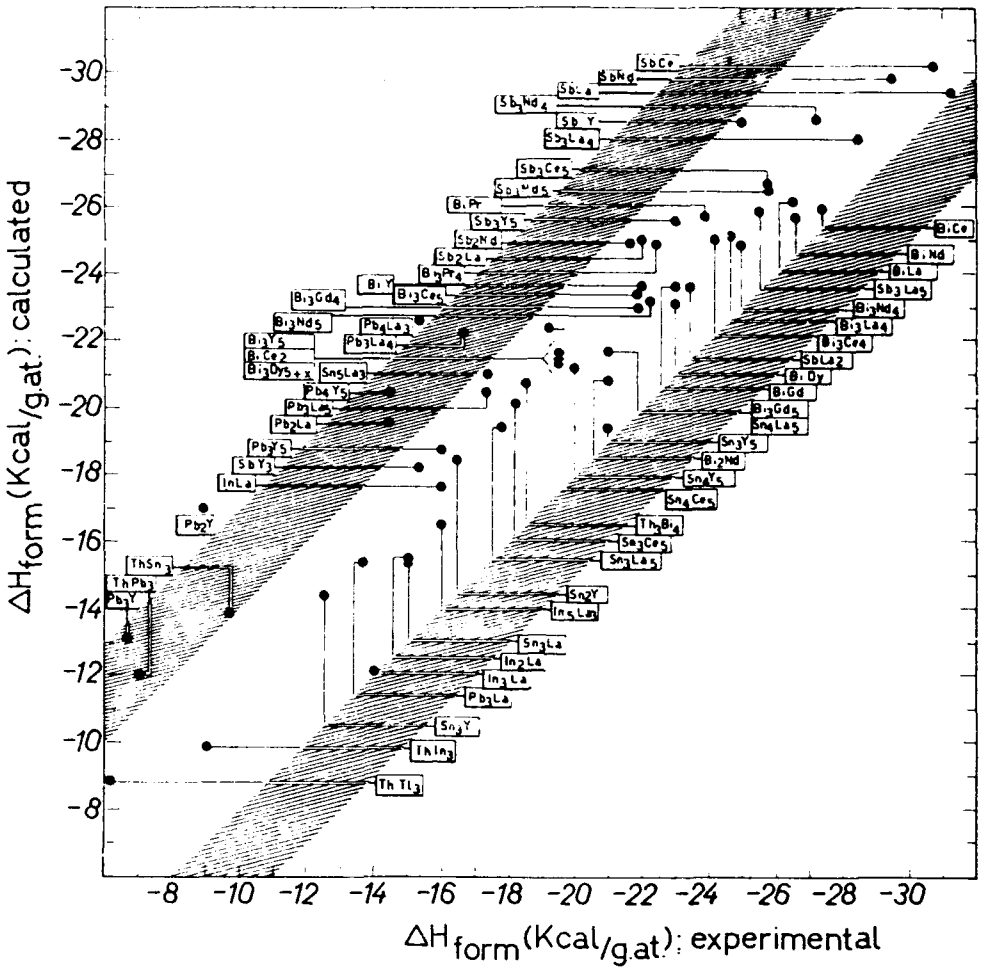

Fig 19- Comparison between Miedema's predictions and experimental enthalpies of formation of rare-earth compounds, measured by Borsese,Borsone and Ferro (38),and by Palenzona and Cirafici (39).

The two groups in Genova are still working on systematic studies of properties of binary and ternary compounds obtained by reaction of a rare earth with low melting temperature components : Bi, In, Sn, Sb, Zn. Due to their highly negative entalpies of formation, these compounds exhibit a series of very high congruent melting temperatures. As a exemple the vapor constrained diagram of Dysprosium antimonides is presented on figure 20, according to the work of Mironov, Abdusalyamova and Burnashev (40). It will be noticed that such diagrams can only be obtained in sealed crucibles, considering the high equilibrium pressure of antimonium. The shape of the liquidus line in the Dysprosium rich part has to be reconsidered for its thermodynamic consistency. Nevertheless the general trend of the diagram is correct and corresponds to the enthalpies of formation measured by Ferro, Borzone and Cacciamani (41) (fig.20). The enthalpies of formation of the rare earth antimonides are summarised on figure 21 after Ferro (42). The enthalpies of formation of the equiatomic compounds of the serie are about -120 kJ/mole of atoms..

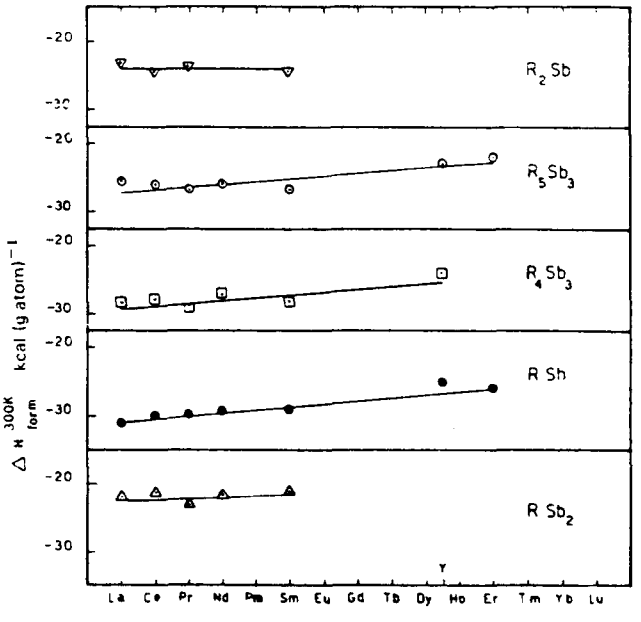

Fig 21- Enthalpies of formation of rare-earth antimonides after Ferro (42).

3 - 3 Indirect mixing calorimetry in a solvent

3 - 3 - 1 Principle of the method

Many laboratories used indirect calorimetry to obtain the mixing enthalpy of solid solutions and compounds. The principle is explained in the following scheme :

T_1	x(A)	+	y (B)	→	Ax By	$h^m(T_1)$
dissolutions:	$h_1\downarrow$		$h_2\downarrow$		$h_3\downarrow$	
T_2	**(final mixed state in a solvent)**					

$$h^m(T_1) = (h_1 + h_2) - h_3 \qquad (15)$$

It consists to obtain the same final mixed state. Starting from the pure components , taken in the right proportions, we get ($h_1 + h_2$) and starting from the presynthetized solid phase we measure (h_3).

3 - 3 - 1- The superiority of this method is evident in the followings cases

a) The compound is unstable at high temperature and disappears by peritectic or peritectoid decomposition,

b) The time needed to achieve the synthesis of the solid phase is too long (for instance, one week, one month ...) and becomes incompatible with direct reaction calorimetry,

c) The quick direct synthesis reaction cannot be achieved in actual calorimetric devices for various reasons : reaction with the crucible, too high temperature needed ...

d) The compound is obtained in particular conditions (like high pressure synthesis) which cannot be realised in calorimetric devices.

3 - 3 - 2 - The choice of the solvent

In the past, many laboratories had chosen an acid aqueous solvent which could be used in room temperature calorimeters. Generaly speaking, in this case, the enthalpies of mixing in the solvent are much too high to allow an accurate measurement. Considering equation (15) the formation enthalpy of the compound is obtained by subtracting two terms one to the other : if the result $h^m(T_1)$ is too small by comparison with the measured mixing enthalpies, the result becomes very inaccurate. It is often the case with acid calorimetry where the mixing enthalpies are ten times higher than the result. Many laboratories use now metallic bathes, but there exist two variants of the method.

a) The liquid metallic bath is used at quasi-infinite dilution : in this particular case, several runs can be realised one after the other with the same bath, depending on the volume of the crucible. This technique is the most-common method and many laboratories are familiar with it.

b) The final mixed state is a concentrated liquid alloy with a **well-know composition**. In this case, any individual run is realised with a mixture of the pure components and the solvent metal, or with a mixture of the compound and the solvent metal, which provides, in the final state, the right composition of the liquid phase. This technique is the original method of Topor and Kleppa, which has been extensively applied to measurements of the enthalpies of formation of refractory borides, silicides and more recently to intermetallic compounds. The solvent metal used is often germanium. Topor and Kleppa have given in a recent synthesis an extensive list of the systems that they have studied by their original technique (43)

As a solvent they use a mixture made of platinum and germanium, or of palladium and germanium, or of copper and germanium, or also of copper and silicium, providing in any case a relatively low melting point for the alloy.

Table V

Comparison between the enthalpies of formation of some equiatomic transition intermetallic compounds measured by mixing calorimetry at 1473 by TOPOR and KLEPPA (43) or measured by direct reaction calorimetry by GACHON (44), by SELHAOUI (24), and by JORDA et al (45).

Compound	enthalpy of formation at room temperature by mixing calorimetry kJ/(mol) (43)	enthalpy of formation near 1500K by direct reaction calorimetry kJ/(mol)
PdTi	- 103,2 ± 12,7	- 106,0 ± 6 (44)
PdZr	- 122,6 ± 7,0	- 124,0 ± 10 (44)
PdHf	- 134,8 ± 7,8	- 131,2 ± 5 (24)
RhZr	- 75,9 ± 3,5	- 75,8 ± 5 (45)
CoHf	- 94,9 ± 6,1	- 102,0 ± 3 (24)
NiHf	- 118,5 ± 4,9	- 95,8 ± 4 (24)
PtTi	- 159,3 ± 12,9	- 154.2 ± 6 (24)
PtZr	- 191,9 ± 12,4	- 180,0 ± 20 (44)
PtHf	- 227,3 ± 13,2	- 226,0 ± 12 (24)

3 - 3 - 4 - Some illustrations of mixing calorimetry

Recently, Topor and Kleppa (43) in Chicago by mixing calorimetry, and Selhaoui (24), Gachon (44) and Jorda et al (45) by direct reaction in Nancy have studied the same systems by the different techniques. The enthalpies of formation of many intermetallic (A, B) transition compounds, with A taken in the (Ti, Zr, Hf) family and B in the triade group, have been established. The published results obtained for the equiatomic phases allow us to make some comparisons : (table V)

i) Generaly speaking the two types of results are compatible

ii) In many cases the estimation of the mean deviation is bigger for the mixing calorimetry : this is quite understandable if we compare the effective published data to the real measured enthalpies, using mixing calorimetry. As an example Topor and Kleppa (46) used the liquid quaternary mixture $Co_{0.05}$ $Hf_{0.05}$ $Pt_{0.2}$ $Ge_{0.7}$ to measure the enthalpy of formation of the CoHf compound. In a series of 2 x 5 runs they got

$$\Delta h^f (CoHf) = (617.2 \pm 2.2) - (716.4 \pm 7.3)$$
$$= 99.2 \pm 7.6 \text{ kJ/mol}$$

iii) Mixing calorimetry gives the enthalpy of formation of the compound at **the room temperature state**, while direct reaction calorimetry at ***high temperature state.***

Nevertheless indirect mixing calorimetry remains the only method when the phase under scrutiny disappears at high temperature. As an example in the molybdenum-gallium system there exist two line-compounds : $GaMo_3$ which decomposes near 2100 K and $GaMo_5$ which decomposes at 1115 K (figure 22). We have seen before that it has been possible (25) to synthetise the $GaMo_3$ compound directly in the cell of the calorimeter and also to obtain the precipitation of this compound in the cell, by adding pure molybdenum to a saturated liquid gallium-molybdenum mixture. On the contrary the determination of the enthalpy of formation of the second compound required indirect mixing calorimetry. Belgacem-Bouzida (25) synthetised the $MoGa_5$ compoud by powder metallurgy at low temperature (680°C, one month annealing). It was possible to dissolve this compound, at 1573 K and infinitite dilution, **in a pure gallium bath** to measure indirectly :

$$\Delta h^f (Mo_{0.26} Ga_{0.84}, 300 \text{ K}) =$$
$$(35645 \pm 2000) - (56170 \pm 2000) =$$
$$- 20525 \pm 3000 \text{J/mol}$$

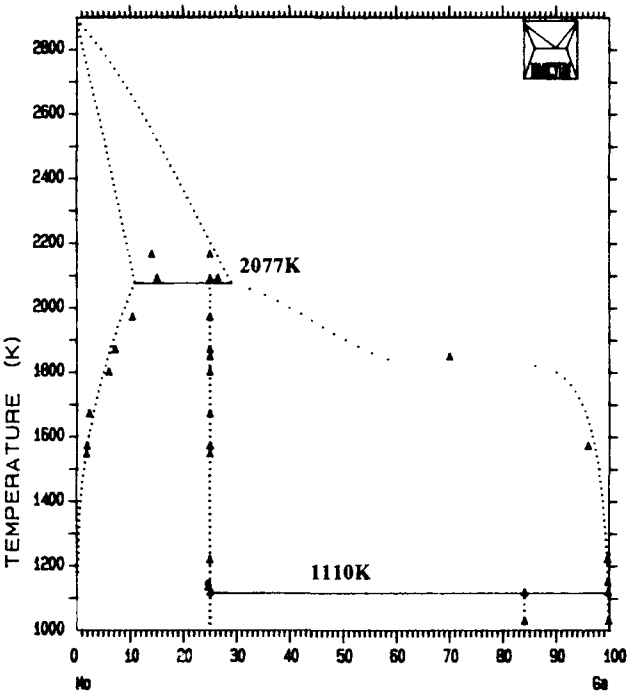

Fig 22- The calculated phase diagram of the (Mo, Ga) system.

An aluminium bath is often chosen to dissolve alloys exhibiting a high oxygen affinity.The dissolution of the first sample is sufficient to avoid any further oxygen trace in the melt. It is a well know fact for the practicians that the first experiment in mixing calorimetry is generally not reliable in contrast of the following runs. Colinet, Pasturel, Percheron-Guégan and Achard (47) have studied the correlation existing between the enthalpies of formation of the $La(Ni_{(1-x)}Co_x)_5$ phase and the affinity ot this phase for hydrogen. A pure molten aluminium bath was used. Figure 23 shows the enthalpies of mixing they got, four time greater than the formation enthalpies of the compounds (same figure). On the other hand they studied the Gibbs enthalpy of hydrogenation-deshydrogenation of the compounds by measuring the pressure equilibrium plateau versus temperature. Figure 24 shows the results obtained. The conclusion was that the more stable the "$LaNi_5$" type compound was, the less stable they found the hydride.

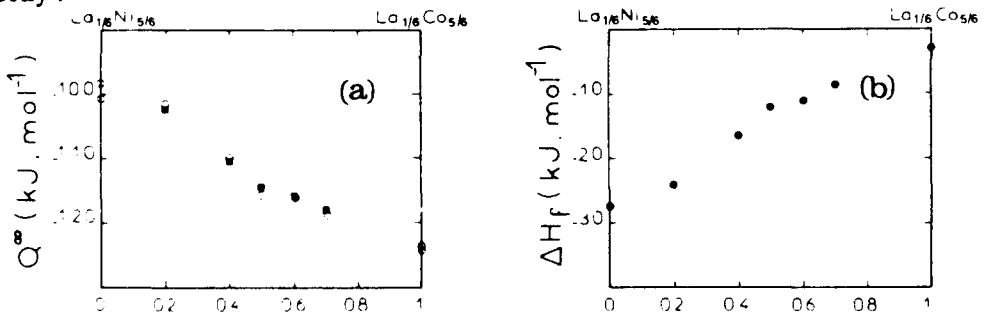

Fig 23- Composition dependence of : (a) the heat of dissolution in Aluminum, at infinite dilution, and (b) the enthalpies of formation of the $La(Ni_{1-x}Co_x)_5$ phase : after Colinet, Pasturel, Percheron-Guégan and Achard (47).

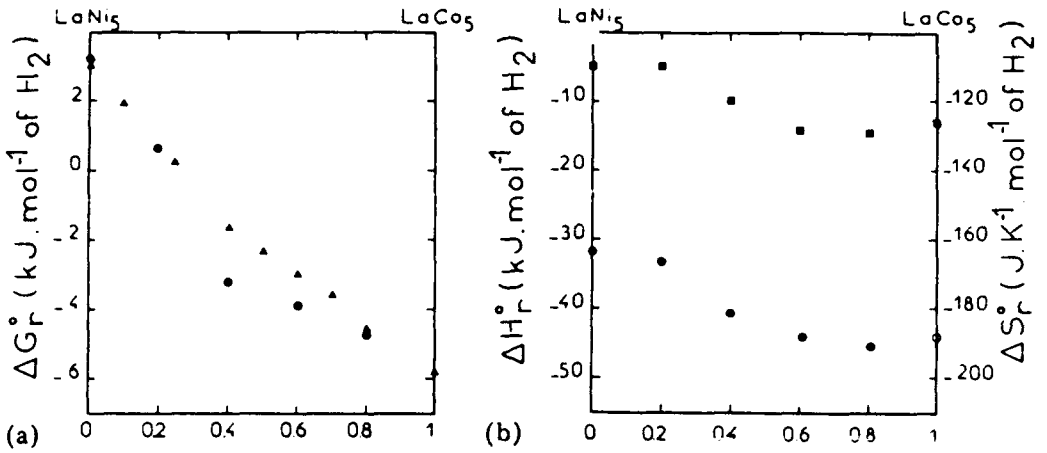

Fig 24- Standard Gibbs energies, enthalpies and entropies of formation of hydrides in the La $(Ni_{1-x}\ Co_x)_5$ solid solution : the more stable the solid solution, (see figure 23), the less stable the hydride. After Colinet, Pasturel, Percheron -Guégan and Achard (47).

4 - Measuring the Gibbs potentials

4 - 1 Vapor pressure measurements

One of the classical technique is the **Knudsen effusion-torsion method** that many laboratories have practised. Fig. 25 represents the apparatus of Hayes and Mc Hugh (48), with which these authors measured the manganese Gibbs potential in various (Fe, Co, Mn) ternary solid alloys. The well known principle is to create a mechanical couple by effusing vapor between two holes bored in the crucible. A thin tungsten torsion wire equilibrates the couple which is measured optically with help of a mirror. In the past time we used the same technique in Nancy. **The most important objection to this method is that the instrument deviation is roughly proportional to the activity** of the volatile component in the crucible whereas **the Gibbs potential is measured in the logarithmic scale of this activity**. As a consequence it is not possible to explore a wide range of chemical potentials by such a technique .

Figure 26 shows the results got by Hayes and Mc Hugh for the binary (Fe, Mn) system at 1350 K. It is clear, on this figure, that the wide domain they explored does not exceed two powers of ten in the manganese activity scale. Activities at 1350 K are represented on the figure 27 by open circles. If we want to obtain the excess entropy of the γ (Fe, Mn) alloys we can observe that 1350 K is very close to the $\beta \rightarrow \gamma$ equilibrium temperature of the pure manganese (1360 K). For this reason the reference state for manganese activities does not vary sensitively when changing β to γ, Mn* reference state. The ideality line is near the diagonal drawn inside the square (fig 27). It appears that the thermodynamic behavior of these alloys seems quasi-ideal at 1350 K. That means :

$$g^e = h^m - Ts^e \approx 0$$

Comparing this result with the enthalpies of mixing measured by Kubitz and Hayes (35) we deduce that the excess entropy of mixing is negative with roughly the same shape as the enthalpy curve (fig 17) in the scale $\left(\frac{1}{1350}\right)$ and a maximum of about (-2,2) J/mol K.

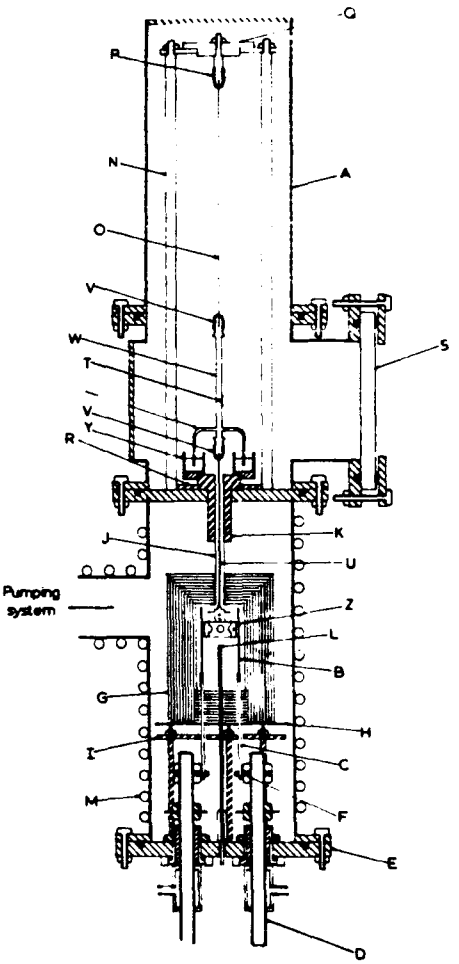

Fig 25- The torsion-effusion apparatus of Hayes and Mc Hugh (48).

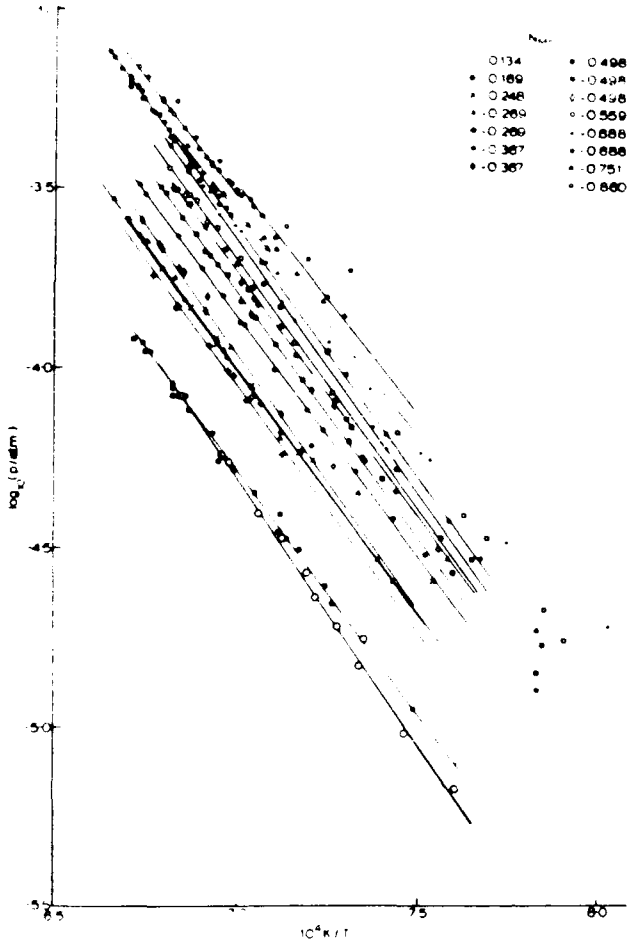

Fig 26- Manganese vapor presure in equilibrium with the (Fe, Mn) solid solutions : after Hayes and Mc Hugh (48).

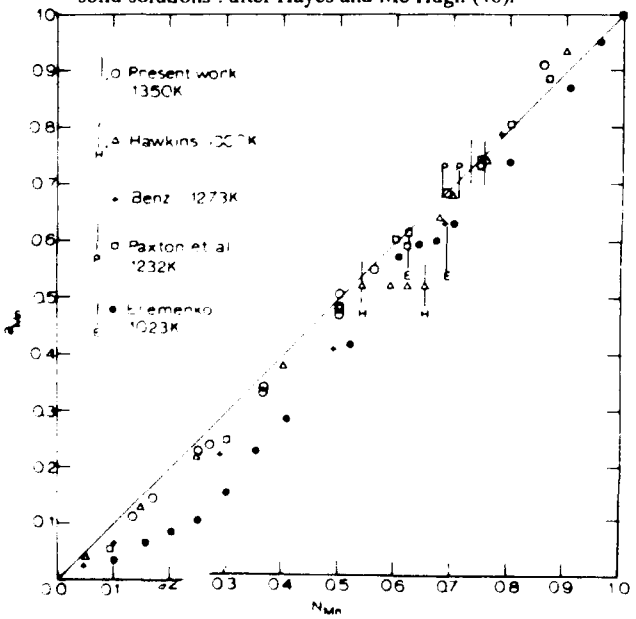

Fig 27- Manganese activity in the solid (Fe, Mn) solid solutions : left side γ phase, right side α phase , | | phase transition. After Hayes and Mc Hugh (48).

The **isopiestic method** developed by Komarek and his group in Vienna (49) seams to me a more efficient way to explore **a wide range of chemical potentials**. It consists to impose the vapor pressure of the most volatile component of the system inside a vessel introduced in a temperature-gradient furnace. The pure volatile component is placed at the lowest temperature while the alloys are slowly elaborated in their equilibrium states, at various temperatures, by gas transfer of the volatile component to the different samples. The time needed to obtain the equilibrium can be very long, up to 3 months. At the end of each experiment, each sample is chemically analysed by measuring its gain of weight. As an example involving also manganese as the volatile component we present on figures 28 and 29 results obtained by Krachler, Ipser and Komareck (50-51) with the non-stoichiometric β Pt Mn and β' Pd Mn B2 ordered phases. It can be observed that the domain which was explored covers a range of about six powers of ten in the manganese activity scale, corresponding to its variations, border to border, in the non-stoichiometric domain of these compounds.

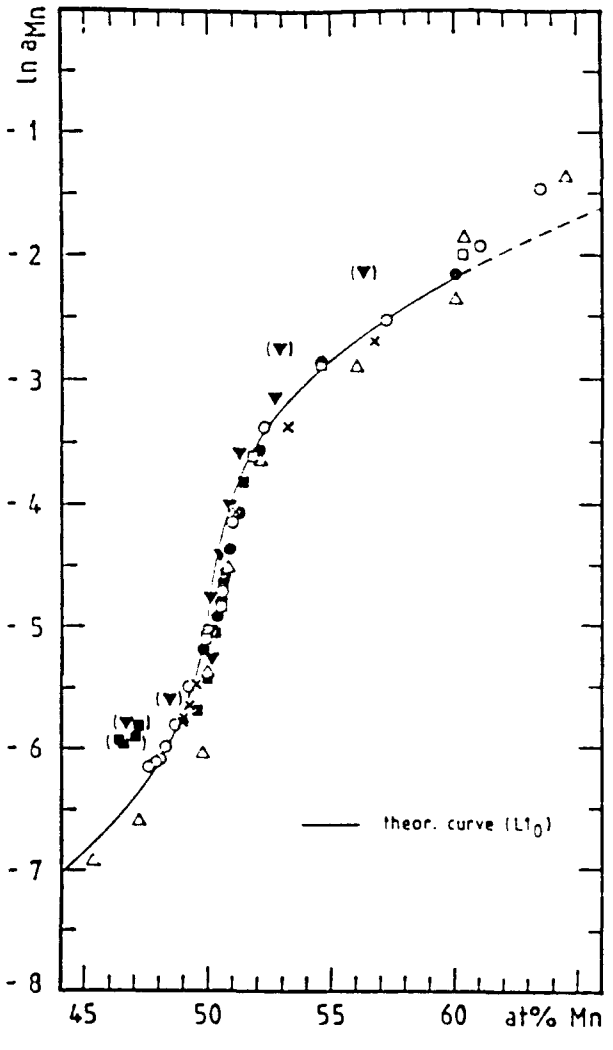

Fig 28- Manganese activity in the β Pt Mn phase at 1273 K. Comparison with a theoretical model, (solid line),by Krachler, Ipser and Komarek (51).

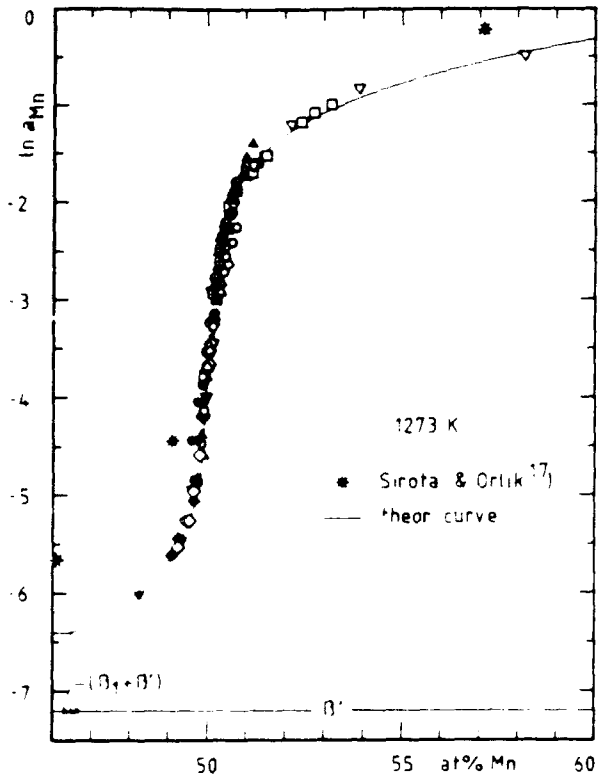

Fig 29- Manganese activity in the β'-PdMn phase at 1273 K. Comparison with a theoretical model, (solid line), by Krachler, Ipser and Komarek (50).

An original Knudsen type method was proposed by Hehenkamp in Göttingen. It consists to trap the effused vapor on frozen targets (water cooled discs) placed in front of the Knudsen-cell orifice and to analyse by electron microprobe the thin films obtained. Fig 30 shows the apparatus (52). The concentration profiles measured on the discs are in very good agreement with the theoretical Clausing's distribution law versus angular deviation in the space, as demonstrated by Hehenkamp and Lüdecke (53). Fig 31 shows an experimental curve which corresponds to the theoretical Clausing's profile.

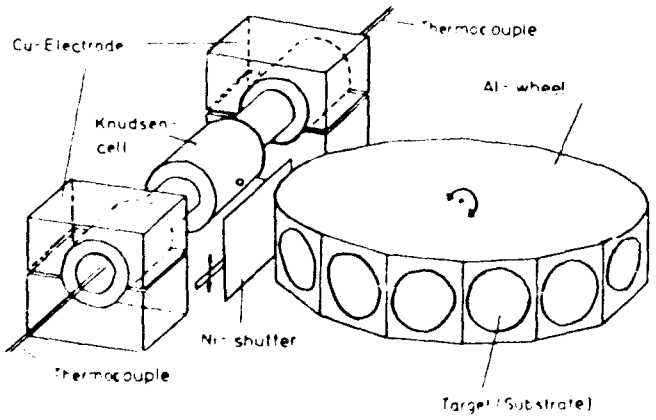

Fig 30- The effusion apparatus for vapor pressure measurements, by Hehenkamp (52).

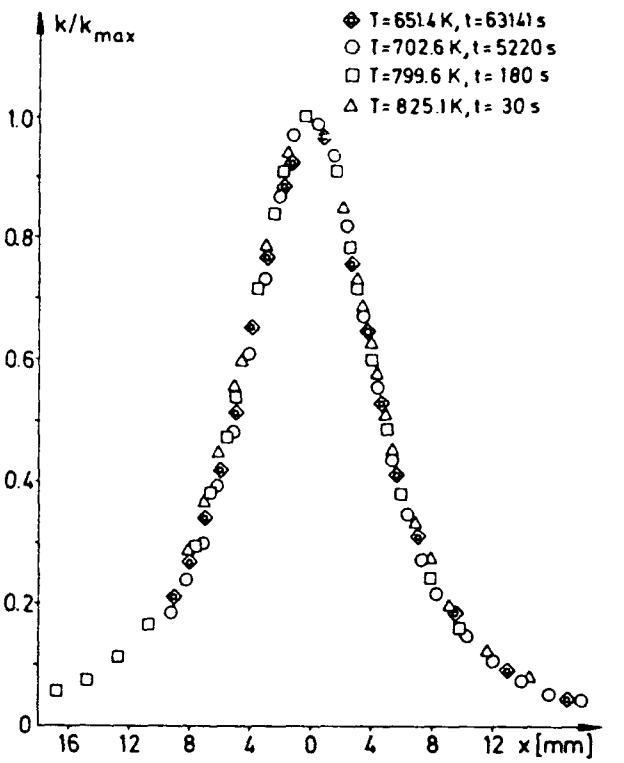

Fig 31- Distribution of Antimony on a Copper substrate for different temperatures and exposure times. The experimental profile corresponds to the theoretical Clausing's spatial distribution law. After Hehenkamp and Lüdecke (53).

By this technique and by diffusion measurements too, the group of Göttingen has studied the thermodynamic behavior of various α c.f.c. dilute solutions. The solvent is either Cu, Ni or Ag and the solute elements are chosen with various valences (Cd or Zn = 2), (In = 3), (Sn = 4), (Sb or As = 5). In any case it appears that the Raoult-Henry law is unsatisfied for very dilute solutions (typically x solute < 5 at %). The Raoult law can be expressed with the Darken function α_1 of the solvent by

$$\mu_1^e = \alpha_1 RT x_2^2 \text{ with } \alpha_1 = \text{constant} \qquad (16)$$

The Lupis stability function φ (54) can be defined in isothermal, isobaric conditions by :

$$\varphi = \frac{d \ln a_1}{d \ln x_1} = \frac{d \ln a_2}{d \ln x_2} = 1 - 2\alpha_1 x_1 x_2 \qquad (17)$$

If Raoult's law is correct, an attractive negative α_1 interaction does correspond to a positive slope associated with a negative curvature for the φ (x_2) curve. On the contrary, Hehenkamp and Lüdecke (53) observe in α silver dilute alloys a positive curvature associated with negative α_1 coefficients. The results obtained with various solutes can be ploted on a single curve when using electronic concentration $\left(\frac{e}{a}\right)$ instead of the mole fraction of the solute (fig 32). The same behaviour appears in the Ni-Sn dilute alloys (fig 33). The Gibbs-Duhem integration of equation (16) gives the excess Gibbs potential of the solute (Henry's law) :

$$\mu_2^e = \alpha_1 RT x_1^2 + \text{constant} \qquad (19)$$

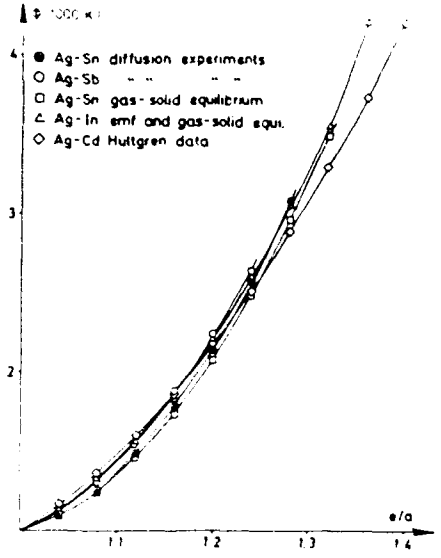

Fig 32- The Lupis stability function for silver alloys, after Hehenkamp (52). The observed curvature does'nt satisfy equation 17 ,with negative α_1.

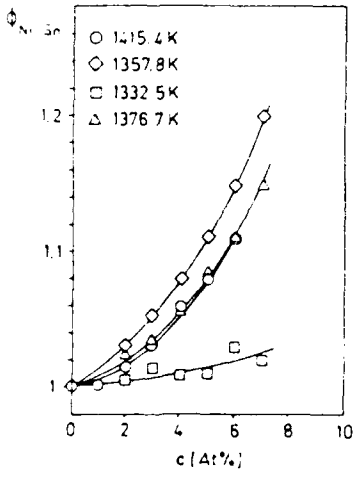

Fig 33- The Lupis stability function in dilute (Ni, Sn) alloys, after Hehenkamp (52).Equation 17 remains unsatisfied for curvature.

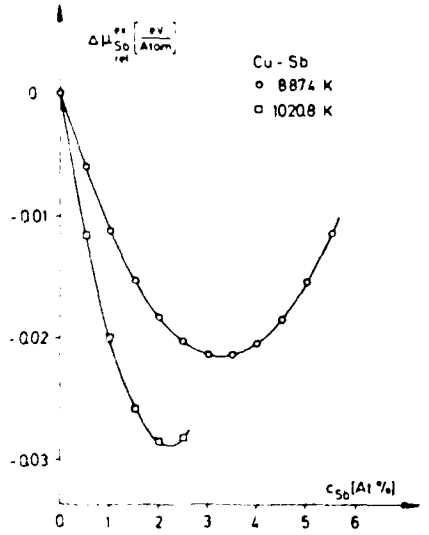

Fig34-Shifted chemical excess potential of Antimony in Copper-base alloys. From equation 19, with α_1 negative, the initial expected slope would be positive.After Hehenkamp (52).

with a negative α_1, a positive slope and a negative curvature are expected, from equation 19, for the $\mu^e{}_2(x_2)$ curve. The contrary is observed in the dilute (**Cu**, Sb) solutions, (fig 34), with a prononced minimum at low concentration, attributed by Hehenkamp (52) to the high difference in metallic radius.

4 - 2 The E.M.F. method and the necessity of the "crossed" strategies.

The most usefull method to determine a Gibbs potential in alloys is the E.M.F technique. The reason why this technique is a so efficient one is linked to the Nernst law :

$$E = \frac{\Delta\mu_i}{n\mathcal{F}} \qquad (20)$$

where $\Delta\mu_i$ is the difference of the Gibbs potential between the two electrodes for the species carrying the charge and nF the transferred charge. The measured quantity is directly proportional to the Gibbs potential and activities are obtained in the logarithmic scale, which offers the possibility of a wide range exploration.

Two types of cells, differing by electrolytes, are generally used for alloys :

- molten salt mixtures,

- solid state electrolytes.

Above 1000°C solid electrolytes are needed. With solid electrolytes the experimental limitations arise from two opposite constraints :

i) at too low temperatures the ionic conductivity is to small to allow any correct measurement (too high impedance of the cell)

ii)- at too high temperatures the electronic conductivity increases, especially when highly reducing equilibria are needed.

It is not the place, here, to develop into details the E.M.F. technique. Several papers have been presented in 1987 at the NATO-ASI "Thermochemistry of Alloys" in Kiel. In particular we recommend Schaller's review (55) devoted to solid-state galvanic cells and the publication of Egan (56) concerning the coulometric titration with a CaF_2 original cell. The most used solid electrolyte is CaF_2 which exhibits an important ionic transference number from very low to very high oxygen activity.

We would like to illustrate on an example the importance of the "crossed strategies" when using Gibbs potential measurements. Recently Du Sichen, Seetharaman an Staffansson (57) measured in Stockholm chromium activities in three mixtures of the (Cr, C) binary system :

a) Cr_3C_2/C b) Cr_7C_3/Cr_3C_2 c) $Cr_{23}C_6/Cr_7C_3$

Three CaF_2 cells were used :

(-)Cr, CrF_2, CaF_2 | CaF_2 | CaF_2, CrF_2, (mixed carbides)(+)

The E.M.F delivered by the cells between 1000 and 1200 K could be fitted by the following three equations :

$$E\ (a)/mV = 72,9 + 0,0589\ T$$

$$E\ (b)/mV = 18,5 + 0,0677\ T$$

$$E\ (c)/mV = 38,3 - 0,01976\ T$$

Figure (35) summarises these equations, for which a rough estimation of the mean deviation is about $\pm$ 3 mV.

The Stockholm group did not use the direct enthalpy measurements we have got (26,31) for his determinations of the h^f and s^f quantities of the carbides. We should like to demonstrate here that the slope derivation method can induce systematic errors that can be avoided by various crossed strategies. The Gibbs function for the three carbides are given in these experiments by

$$g^f\left(\frac{1}{5}Cr_3C_2\right) = \frac{3}{5}2\mathcal{F}E(a)$$

$$g^f\left(\frac{1}{10}Cr_7C_3\right) = g^f\left(\frac{1}{5}Cr_3C_2\right) + \frac{1}{10}\left(2\mathcal{F}E(b) - g^f\left(\frac{1}{5}Cr_3C_2\right)\right)$$

$$g^f\left(\frac{1}{29}Cr_{23}C_6\right) = g^f\left(\frac{1}{10}Cr_7C_3\right) + \left(\frac{23}{29} - \frac{7}{10}\right)\left(2\mathcal{F}E(c) - g^f\left(\frac{1}{10}Cr_7C_3\right)\right)$$

The calorimetric results we got in Nancy (31) have been "crossed" with a CALPHAD optimisation of the phase diagram (26 et 31). It is also possible to "cross" the Gibbs potential measurements with the calorimetric measurements. Table VI shows that the "slope" method can induce heavy systematic errors in the results, which can be avoided by the mixed strategies. On the other hand the two crossed strategies give quite compatible results.

Table VI : Two "crossed" strategies for the determination of the enthalpies and entropies of formation of chromium carbides

1/5 Cr_3 C_2	**E.M.F. after (57)** gf (1100 K) = **- 15945 ± 350**	**h^f (J/mol) (26, 31)** Calorimetry measurements (21) **- 9955 ± 600**	**s^f (J/mol K)** crossing the results **+ 5,44 ± 1**
	Calphad strategy without E.M.F(26)	- 10100	+ 6,43
	Slope method alone by E.M.F (57)	- 8400 ± 450	+ 6,82 ± 0,40
1/10 Cr7 C3	**E.M.F after (57)** g^f (1100 K) = **- 16145 ± 450**	**Calorimetry measurements** (26,31) **- 10700 ± 1800**	**crossing the results + 4,95 ± 2**
	Calphad strategy without E.M.F (26)	- 10791	- 6,48
	Slope method alone by E.M.F (57)	- 7230 ± 430	8,38 ± 0,4
1/29 Cr_{23} C_6	**E.M.F after (57)** gf (1100 k) = **14939 ± 550**	**Calorimetry measurements - 9400 ± 1100**	**crossing the results 5,0 ± 1,5**
	Calphad strategy without EMF (26)	- 9250	3,79
	Slope method alone by E.M.F. (57)	- 7276 ± 340	4,60 ± 0,33

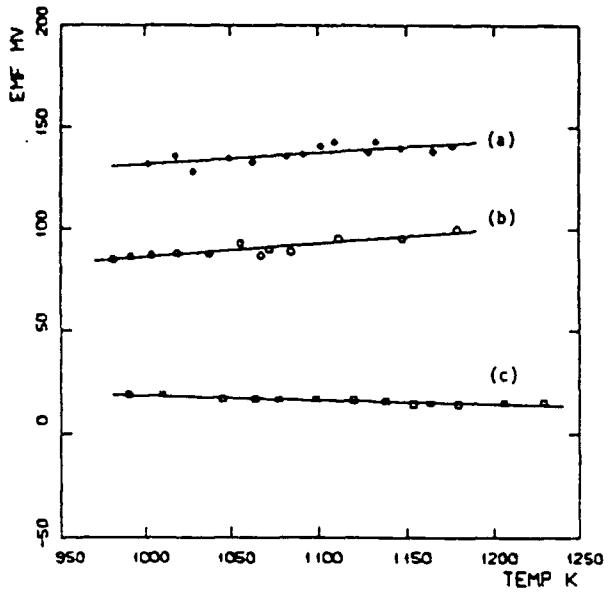

Fig 35- The emf-temperature relationships for cells (a), (b), (c) by Du Sichen, Seetharaman and Staffansson (57).

Conclusion

In this lecture we have tried to explain that the determination of the thermodynamic quantities of mixing is a strategic game. This is true for all systems, organic and inorganic ones. But more attention have to be given to the "crossed" strategies like CALPHAD method or EMF associated with calorimetric measurements, when looking at high temperature domains, (alloys, ceramics). At high temperatures the influence of the entropy of mixing in the Gibbs function becomes very important and for this reason scientists have to be carefull with this quantity often badly known.

Bibliography

(Papers without complete title have not been consulted)

/1/ A. NECKEL
Mass spectrometry determination of thermodynamic mixing effects of alloys
"Thermochemistry of Alloys" KLUWER PUBLISHERS (Eds : H. BRODOWSKY and H.J. SHALLER)
NATO-ASI Series C, Vol 286, (1989), 221-246.

/2/ C.W. BALE, A.D. PELTON and W.T. THOMSON
"F*A*C*T" users guide (1979),Mc Gill University Ecole Polytechnique Montréal.

/3/ H.L. LUKAS, J. WEISS and E. Th. HENIG
Strategies for the calculation of phase diagrams
CALPHAD **6** , (1982), 229-251.

/4/ H. A. J. OONK, P. J. EISINGA and N. BROUWER
CALPHAD **10**, (1986), 1-36

/5/ H. A. J. OONK, J. A. BOUWSTRA and P. J. Van EKEREN
CALPHAD **10**, (1986), 137-161.

/6/ M. RAHMANE
Extension du programme d'optimisation des grandeurs thermodynamiques des systèmes binaires, NANCYUN. Application aux alliages de Calcium (Ca, Al), (Ca, Ni), (Ca, Pb), (Ca, Bi), de Hafnium (Hf, Co), (Hf, Ni) et aux systèmes (Ti, C) et (Mo, Ga).
Thèse de l'Université de Nancy I, 8 juin 1990.

/7/ M. HILLERT and L. I. STAFFANSSON
The regular solution model for stoichiometric phases and ionic melts
Acta Chem. Scand. **24**, (1970), 3618-3626.

/8/ B. SUNDMAN and J. ÅGREN
A regular solution model for phases with several components and sublattices suitable for computer application
J. Phys. Chem. Solids **47**, (1981), 297-301.

/9/ M. HOCH
Application of the Hoch-Arpshofen model to ternary, quaternary and larger systems
CALPHAD **11**, (1987), 219-224.

/10/ M. MARGULES
Sitzungsber. Akad. Wiss. Wien, Mathem. Naturwiss. K 1, 11 a vol **104**, (1895), 1243.

/11/ O. REDLICH and A. T. KISTER
Ind. Engn. Chem. **40**, (1958), 345.

/12/ M. HILLERT
Empirical methods of predicting and representing thermodynamic properties of ternary solid solution phases
CALPHAD **4**, (1980), 1-12.

/13/ C. W. BALE and A. D. PELTON
Mathematical Representation of thermodynamic properties in binary systems and solution of Gibbs-Duhens equation
Met. Trans. **5**, (1974), 2323-2337.

/14/ R. CASTANET
Calorimetric methods in metallurgy
"Thermochemistry of alloys" KLUWER PUBLISHERS (Eds : H. BRODOWSKY and H. J. SCHALLER
NATO-ASIE Series, C. vol 286, (1989), 145-168.

/15/ J. HERTZ
Review of some metallurgical problems suitable to quantitative calorimetric treatement.
J. Thermal. Anal **30**, (1985),1227-1240

/16/ B. PREDEL, I. ARPSHOFEN and M.J. POOL
Calorimetric methods in metallurgy.
Thermochimica Acta **22**, (1978), 211-236

/17/ E. ARPACI and M. G. FROHBERG
Experimental determination of the mixing enthalpies of liquid Molydenum-Silicon alloys
Z. Metallkde. **76**, (1985), 440-444.

/18/ E. HAYER, F. GEHRINGER, K. L. KOMAREK, M. GAUNE-ESCARD and J. P. BROS
AFCAT **18**, (1987), 317-321.

/19/ E. HAYER, F. GEHRINGER, K. L. KOMAREK, M. GAUNE-ESCARD and J. P. BROS
Enthalpy of mixing of liquid (Au + Al) alloys
Z. Metallkde. **80**, (1989), 186-191.

/20/ F. SOMMER
Modern methods in high temperature calorimetry
Journal of Thermal Analysis **33**, (1988), 15-28.

/21/ R. LÜCK and B. PREDEL
The enthalpy of mixing of liquid iron-tin alloys determine by a new high temperature calorimeter
Zeit. Metallkde **76**, (1985), 684-686.

/22/ R. LÜCK, I. ARPSHOFEN, B. PREDEL and J.F. SMITH
Calorimetric determination of the enthalpies of formation of liquid Ni-Ti alloys.
Thermochimica Acta **131** (1988), 171-181.

/23/ R. CASTANET
Structure of liquid metallic alloys from their hermodynamic behaviour
Z. Metallkde **80**, (1989), 737-744.

/24/ N. SELHAOUI
Etude thermodynamique des composés binaires des métaux de transition par calorimétrie à hautes températures. Modélisation numérique de diagrammes de phases. Confrontation expériences-modèles.
Thèse de l'Université de Nancy I, 27 avril 1990.

/25/ BELGACEM-BOUZIDA
Méthodes calorimétriques appliquées aux systèmes métalliques :
1) Thermodynamique du système (Mo, Ga) et première approche du système (Nb, Ga)
2) Mesure automatique des capacités thermiques
Thèse de l'Université de Nancy I, 6 juillet 1989.

/26/ R. BERKANE, J. C. GACHON, J. CHARLES and J. HERTZ
A thermodynamic study of the chromium-carbon system
CALPHAD **11**, (1987), 375-382.

/27/ A. D. MAH
U. S. Bur. Mines, I. R. 7217, (1969).

/28/ M. W. CHASE, J. L. CURNUTT, H. PROPHET, R. A. Mc. DONALD, A. N. SYVERUD
JANAF Thermochemical Tables, Supplement Journal of Phys. and Chem. Reference data 4 n° 1, (1975).

/29/ A. D. KULKARNI and W. L. WORREL
Metall. Trans. **3** (1972), 2363.

/30/ W. M. DAWSON and F.R SALE
Metall. Trans. **8A** , (1977),.15-18.

/31/ R. BERKANE
Etude thermodynamique des carbures de chrome, titane, zirconium et hafnium par calorimétrie à haute température. Modélisation numérique des diagrammes de phases
Thèse de l'université de Nancy I, 10 octobre 1989.

/32/ O. KUBASCHEWSKI and W. A. DENCH
Acta Meta. **3**, (1955), 339.

/33/ W.A. DENCH and O. KUBATSCHEWSKI
J. Iron and Steel Inst. **201**,(1963), 140

/34/ O. KUBASCHEWSKI and J. GRUNDMANN
Application of an adiabatic high temperature calorimeter to the determination of heats of formation in the system Iron-Cobalt- Chromium.
Bericht. Bunsenges. **81**, (1977), 1239-1242.

/35/ R. KUBITZ and F. H. HAYES
Enthalpies of mixing in the Iron-Manganese system by direct reaction calorimetry
Monatsch. Chem. **118**, (1987), 31-41.

/36/ A. PALENZONA
Thermochim. Acta **5**, (1973), 339.

/37/ R. CAPELLI, R. FERRO and A. BORSESE
A direct isoperibol aneroid calorimeter
Thermochimica acta **10**, (1974), 13-23.

/38/ A. BORSESE, G. BORZONE and R. FERRO
Thermochemistry of binary alloys of rare earths : a comparison between experimental and calculated heats of formation
J. of the Less-Com. Met. **70**, (1980), 213-216.

/39/ A. PALENZONA and S. CIRAFICI
Thermochim. Acta **13**, (1975), 357.

/40/ K.E. MIRONOV, M.N. ABDUSALYAMOVA and O.R. BURNASHEV
Izv Akad. Nauk SSSR, Neorg. Mater. **16**, (1980), 1951.

/41/ R. FERRO, G. BORZONE and G. CACCIAMANI
On the thermochemistryof the rare earth antimonides. The Dy-Sb system.
Thermochimica Acta **129**, (1988), 99-113.

/42/ R. FERRO
Contribution to the thermodynamics of rare earth binary alloys.
Journal. of the Less Common Metals **110**, (1985), 53-60.

/43/ L. TOPOR and O.J. KLEPPA
Enthalpies of formation of equiatomic compounds of titanum, zirconium, hafnium with late transition metals : systematic aspects and comparisons with predicted values
J. of the Less-Com. Met. **155**, (1989), 61-73.

/44/ J.C. GACHON
A comparison between computed and measured,enthalpies of formation of binary transition alloys. Accuracy and relativity of model predictions.
J. Phys. Chem. Solids **49**, (1988), 99-113.

/45/ J. L. JORDA, J. C. GACHON, J CHARLES and J. HERTZ
High temperature study of the zirconium- Rhodium System.
J. Thermal Anal **34** (1988), 551-557.

/46/ L. TOPOR and O.J. KLEPPA
Standard enthalpies of formation of CoHf and NiHf
High Temperature Science **25**, (1988), 163.

/47/ C. COLINET, A. PASTUREL, A. PERCHERON-GUEGAN and J.C. ACHARD
Enthalpies of formation and hydrogenation of $La(Ni_{1-x}\ Co_x)_5$ compounds.
J. of the Less-Com. Met. **134**, (1987),109-122.

/48/ F.H. HAYES and G. Mc HUGH
Torsion effusion measurements on Fe-Mn, Co-Mn and Fe-Co-Mn alloys.
"Thermochemistry of alloys" Kluwer Publishers
Eds : H. BRODOWSKY and H.J. SCHALLER
NATO-ASI Series C, vol 286,, (1989), 277-292.

/49/ R. KRACHER, H. IPSER and K.L. KOMAREK
Z. Metallkde **73**, (1982), 731.

/50/ R. KRACHLER, H. IPSER and K.L. KOMAREK
Thermodynamics of the nonstoichiometric phase β'-PdMn
Z. Metallkde **75**, (1984), 724.

/51/ R. KRACHLER, H. IPSER and K.L. KOMAREK
Thermodynamics of the nonstoichiometrie β-PtMn phase
Z. Metallkde **79**, (1988), 96-101

/52/ Th. HEHENKAMP
Thermodynamic behavior of impurity at ans in α range alloys of the noble metals and Nickel
Ber. Bunsenges. Phys. Chem. **87**, (1983), 806-811.

/53/ Th. HEHENKAMP and D. LÜDECKE
Thermodynamic activity of solid α silver antimony alloys
Acta Met. **29**, (1981), 939-950.4

/54/ C.H.P. LUPIS and H. GAYE
Metallurgical Chemistry - Proceeding of the symposium held at Brunel University-N.P.L, (July 1971)
(O. KUBASCHEWSI Editor)
H.M.S.O. (1972), 469-482.

/55/ H.J. SCHALLER
Solid state galvanic cells for thermodynamic investigations.
NATO-ASI Series 286
(H. BRODOWSKY and H.J. SCHALLER Editors).
Kluwer Academic Publishers (1989), 329-358.

/56/ J.J. EGAN
CaF_2 Solid electrolytes used to study thermodynamics of alloys
NATO-ASI Series 286
(H. BRODOWSKY and H.J. SCHALLER Editors).
Kluwer Academic Publishers (1989), 371-398.

/57/ DU SICHEN, S. SEETHARAMAN and L.I. STAFFANSSON
Standard Gibbs Energies of formation of the carbides of chromium by EMF measurements
Metal Trans. **20B**, (1989), 911-917.

APPLICATION OF SOLUTION MODELS TO DIFFUSIVITY STUDIES IN MULTICOMPONENT ALLOYS

J.E. Morral and Yoon-Ho Son

Department of Metallurgy, Institute of Material Science,
University of Connecticut, U-136, Room 111,
97 North Eagleville Road, Storrs, CT 06269-3136, USA

Abstract.-

The "diffusivity" of an n-component alloy is a property matrix, containing $(n-1)^2$ diffusion coefficients, that can be measured by analyzing diffusion couples. The present work is concerned with selecting diffusion couples which will minimize errors that are associated with a variation of the diffusivity with composition. It is proposed that couples be made from alloys with the same determinant of the diffusivity. With this criterion, it is shown that in "ideal solutions" variations in the free energy are not important, while in "regular solutions" the free energy may either increase or decrease the variation depending on the regular solution parameters.

1.- Introduction

Recent developments in diffusion theory and in computer modeling of diffusional reactions have made it possible to make quantitative predictions about complex alloys. These developments have created a need for multicomponent diffusion data.

Although diffusion couples can be used for measuring diffusivities in higher order alloys, the analyses require that the diffusivity be approximately constant in the diffusion zone of the couple. Therefore, both the alloys used in the couple and the change in diffusivity with composition are important.

Each element of the diffusivity matrix is a function of kinetic and thermodynamic properties. These can be approximated with tracer diffusivities and thermodynamic data measured for binary alloys. The present paper is concerned with using this information to design diffusion couples which will give the most accurate diffusivity measurements.

2.- Background

When measuring diffusivities with diffusion couples, the initial concentration differences between alloys in the couple are a primary experimental variable. This variable can be expressed as a "composition vector" (Thompson and Morral, 1986) for an n-component system as:

$$\Delta \mathbf{C}^0 = \left[\Delta C_1^0, \Delta C_2^0, \ldots \Delta C_{n-1}^0\right] \qquad (1)$$

in which the components of the vector are initial concentration differences between the alloys on the left and right side of the couple:

$$\Delta C_i^0 = C_i^R - C_i^L \qquad (2)$$

When using an analysis that assumes "constant diffusivity" both the length and the orientation of the vector must be considered.

It is apparent that the length of the vector must be as small as possible in order to reduce the range of the diffusivity in the diffusion zone. However for ternary and higher order systems the vector orientation will affect the range of the diffusivities as well. In principle there are favorable orientations that minimize errors. The problem is to predict the most favorable orientations.

It is well known (e.g. Kirkaldy and Young, 1987a) that for an n-component system the diffusivity is an (n-1)x(n-1) matrix, [D]. This complicates the problem because each element of the matrix is expected to vary with composition in a different way, as observed for example by Vignes and Sabatier (1969) and by Nesbitt and Heckel (1988). Therefore, it is unlikely that one orientation for the composition vector can eliminate variations in all elements of the diffusivity matrix.

3.- The constant |D| approach

In order to simplify the problem, it will be assumed that maintaining the determinant of [D] constant ($|\mathbf{D}|$ = constant) will limit errors due to variations in [D]. One reason for choosing $|\mathbf{D}|$ over other properties is that it is equal to the product of the eigenvalues of [D]. The eigenvalues are functions of all elements of [D] and are rate constants for the process (Gupta and Cooper, 1971). Another reason for considering $|\mathbf{D}|$ is that it allows kinetic and thermodynamic effects to be considered separately. The basis for the separation is the identity (Kirkaldy, 1958):

$$[\mathbf{D}] = [\mathbf{L}][\mathbf{G}] \qquad (3)$$

in which [L] is a matrix of phenomenological coefficients, associated with a laboratory frame of reference, and [G] is a matrix of second derivatives of the molar free energy with respect to mole fractions:

$$G_{ij} = \left(\frac{\partial^2 G}{\partial N_i N_j} \right)_{N_k \neq N_n} \qquad (4)$$

The determinant of [D] is:

$$| D | = | L | | G | \qquad (5)$$

As will be seen later, the determinants of [L] and [G] are simplified by multiplying and dividing by the determinant of [G] for a system with "ideal" free energy:

$$\left| G^{id} \right| = \frac{(RT)^{n-1}}{\prod_{i=1}^{n} N_i} \qquad (6)$$

The new determinants are $|L'|$ and $|G'|$ as defined by:

$$| L' | = | L | \left| G^{id} \right| \qquad (7)$$

and

$$| G' | = \frac{| G |}{\left| G^{id} \right|} \qquad (8)$$

Equation (8) for $|G'|$ is similar to a function which has been used to test alloy solution stability (Lupis, 1983).

Now the orientation of ΔC° which keeps $|D|$ constant will be calculated. The maximum variation of $|D|$ with composition occurs for the direction given by the gradient of $|D|$:

$$\frac{\nabla | D |}{| D |} = \frac{\nabla | L' |}{| L' |} + \frac{\nabla | G' |}{| G' |} \qquad (9)$$

in which the del operator is defined by:

$$\nabla = \sum_{i=1}^{n-1} \mathbf{i} \left(\frac{\partial}{\partial N_i} \right)_{N_k \neq N_n} \qquad (10)$$

and $\mathbf{i}$ is a unit vector along the i-th concentration axes. It follows that $|D|$ is constant when the "composition vector" is in a direction perpendicular to $|D|$, i.e when:

$$\nabla | D | \cdot \Delta C^0 = 0 \qquad (11)$$

Diffusion couples can be made in directions of constant $|D|$ except in binary systems. For example in a ternary system $|D|$ is constant along a line in the two dimensional composition space. From one diffusion couple prepared along this line, all four D_{ij} constants can be obtained with an analysis (Thompson and Morral, 1986) that combines two different equations for the "square root diffusivity". One equation is a modified form of an equation used in the "Krishstal, Mokrov, Akimov and Zakharov" analysis (1973).

For a quaternary system $|D|$ is constant along a surface in the three dimensional composition space. In this case two diffusion couples must be used, but both composition vectors can be oriented in the surface of constant $|D|$. Regardless of the number of components it is possible to prepare all required diffusion couples with composition vectors that are perpendicular to $|D|$. However, $|D|$ is not known before experiments have been performed, therefore it must be estimated from existing data.

3.1.- A model for $|L'|$

Several assumptions are made in order to estimate $|D|$. First $|L'|$ will be estimated from measured "tracer diffusivities", D_i^*, by assuming that the diagonal "intrinsic" phenomenological coefficients, L_{ii}^I, are given by (Darken, 1947):

$$L_{ii}^I = \frac{D_i^* N_i}{RT} \qquad (12)$$

and the off-diagonal intrinsic coefficients, L_{ij}^I, are zero.

The phenomenological coefficients, L_{ij}, are related to the intrinsic coefficients by (Kirkaldy and Young, 1987b):

$$L_{ij} = \delta_{ij} L_{ij}^I - N_j L_{ii}^I - N_i L_{jj}^I + N_i N_j \sum_{k=1}^{n} L_{kk}^I \qquad (13)$$

in which δ_{ij} is the Kronecker delta. Combining the equations (7), (12) and (13) yields the following expression for $|L'|$:

$$| L' | = \sum_{i=1}^{n} N_i \prod_{j \neq i}^{n} D_j^* \qquad (14)$$

and for the gradient:

$$\frac{\nabla |L|}{\left| L' \right|} = \frac{\sum_{i=1}^{n-1} \mathbf{i} \left(D_i^* - D_j^* \right) \prod_{i \neq j}^{n-1} D_j^*}{\sum_{i=1}^{n} N_i \prod_{i \neq j}^{n} D_j^*} \qquad (15)$$

Equations (14) and (15) model both the atomic mobilities of individual atoms and the composition dependence introduced by the Kirkendall effect.

The free energy matrix [G'] can be calculated when appropriate data is available. Otherwise, it can be modeled. One source of models are phase diagram prediction programs which can be readily modified to give |G'|. When necessary ideal and regular solution models can be employed, as is done in the following.

3.2.- An ideal solution model for |D|

For ideal solutions |G'| is equal to one, as seen from equation (8), therefore:

$$\left| D^{id} \right| = | L' | \qquad (16)$$

Equations (14) and (16) applied to binaries predict that $|D^{id}|$ is the line:

$$\left| D^{id} \right| = N_1 D_2^* + D_1^* N_2 \qquad (17)$$

which is illustrated in Figure 1. Equation (17) predicts a constant value for the variation in |D| with concentration.

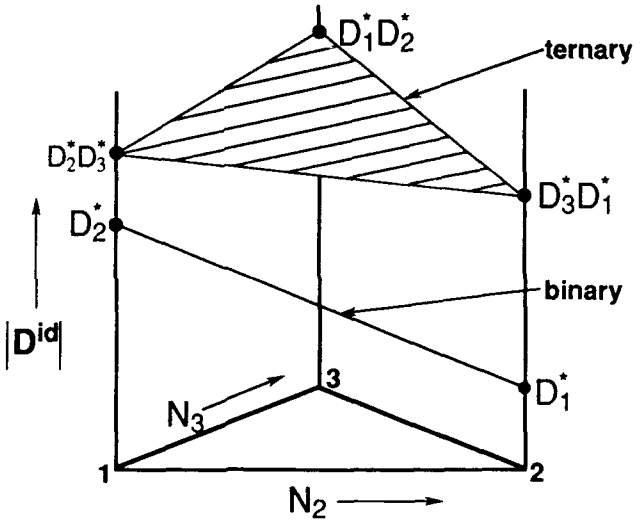

Figure 1: Plots of |D| versus concentration for "ideal" binary and ternary systems. Lines of constant |D| are drawn for the ternary case.

In all relationships given here the tracer diffusivities are assumed constant. It is only because of the Kirkendall effect that there is a concentration dependence of |L'|. If all tracer diffusivities were equal there would be no Kirkendall effect and then |L'| would be a constant equal to:

$$| L' | = \left(D^*\right)^{n-1} \qquad (18)$$

Equation (14) and (16) applied to ternaries predict that |D| is the plane:

$$\left| D^{id} \right| = \left(N_1 D_2^* D_3^* + D_1^* N_2 D_3^* + D_1^* D_2^* N_3\right) \qquad (19)$$

which is illustrated in Figure 1, also. In the ternary case it is possible to prepare diffusion couples along a line of constant |D| by satisfying equation (9), which reduces to the condition:

$$\frac{\Delta C_1^0}{\Delta C_2^0} = - \frac{D_1^* \left(D_3^* - D_2^*\right)}{D_2^* \left(D_3^* - D_1^*\right)} \qquad (20)$$

Equation (20) indicates that when one of the tracer diffusivities is much greater or much less than the others (e.g. by an order of magnitude or more), it is best to make diffusion couples along a line where that component remains constant.

3.3.- Regular Solutions

In the case of regular solutions, |D| is given for binary solutions by the equation:

$$\left| D^{reg} \right| = \left(N_1 D_2^* + D_1^* N_2\right)\left(1 - 2 N_1 N_2 \omega_{12}\right) \qquad (21)$$

The regular solution parameter, ω_{ij}, is defined here by the "regular solution" heat of mixing via the equation:

$$\omega_{ij} = \frac{\Delta H_{mix}^{reg}}{N_i N_j R T} \qquad (22)$$

Equation 21 is the regular solution form of the well known equation (Darken, 1948):

$$D = \left(N_1 D_2^* + D_1^* N_2\right)\left(1 + \frac{\partial \ln \gamma_1}{\partial \ln \gamma_1}\right) \qquad (23)$$

Equation 21 is plotted in Figure 2 for the case of a negative heat of mixing. It can be seen that the effect of a negative heat of mixing adds to that of a slow moving species (the right side of the figure) to cause the greatest variation in |D|, while it subtracts from that of a fast moving species (the left side of the figure). A positive heat of mixing combines in the opposite way.

In ternary regular solutions |D| is a surface, which deviates from a flat plane in a way dictated by the following equations:

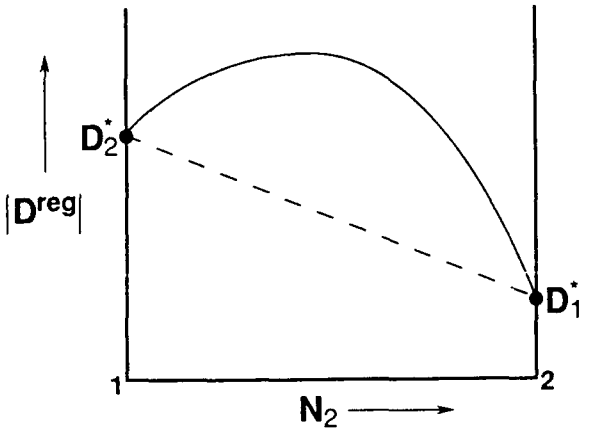

Figure 2: Plot of $|\mathbf{D}|$ for a "regular" binary system that has a negative heat of mixing.

$$|G''| = 1 - 2\,(N_1N_2\omega_{12} + N_2N_3\omega_{23} + N_3N_1\omega_{31}) - N_1N_2N_3\,\Delta\,\omega \qquad (24)$$

in which

$$\Delta\,\omega = \omega_{23}^2 + \omega_{31}^2 + \omega_{12}^2 - 2\,(\omega_{23}\omega_{31} + \omega_{12}\omega_{23} + \omega_{31}\omega_{23}) \qquad (25)$$

A contour map of the $|\mathbf{D}^{reg}|$ surface is given for an example system ($D_1^* = D_2^* = D_3^*$, $\omega_{13} = 0$, $\omega_{12} = -\omega_{23} = 1$) in Figure 3. It can be seen that diffusion couples prepared with composition vectors laying along the contour lines will have different orientations depending on the average composition of the couple.

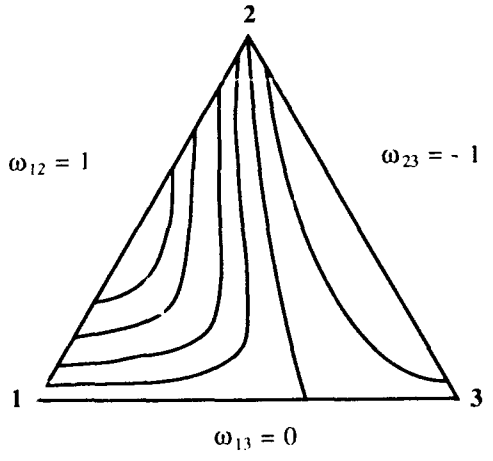

Figure 3: Contour map of $|\mathbf{D}|$ versus composition for a regular ternary system consisting of binaries with positive, negative and zero heats of mixing.

4. Conclusions.-

Diffusion couples for measuring the diffusivities of multicomponent systems with a "constant diffusivity" analysis can be prepared in a systematic way. The procedure is to estimate the determinant of the diffusivity from existing kinetic and thermodynamic data and then to prepare diffusion couples from alloys that have the same value of the determinant. As a general rule this will require having the same concentration, in all alloys, of especially fast or slow moving atoms.

Acknowledgements

The authors are grateful for financial support from the USA National Science Foundation under grant DMR-8711899.

References

Darken, L.S. (1948): Trans. AIME, 174, 184.
Gupta, P.K. and Cooper, A.R. Jr. (1971): Physica, 54, 39.
Krishstal, M.A.; Mokrov, A.P.;Akimov, A.V.; and Zakharov, P.N (1973): Fiz. metal. metalloved. 35, 1234.
Kirkaldy, J.S. (1958): Can. J. Phys. 36, 899.
Kirkaldy, J.S. and Young, D.J. (1987): Diffusion in the Condensed State (London: Institute of Metals) pp. a)154, b)201.
Lupis, C.H.P. (1983) Chemical Thermodynamics of Materials (New York: Elsevier) p. 304.
Nesbitt, J.A. and Heckel, R.W. (1987): Metall. Trans. A 18A, 2075.
Thompson, M.S. and Morral, J.E. (1986): Acta metall. 34, 2201.
Vignes, A. and Sabatier, J.P. (1969): Trans. AIME 245, 1795.

ANALES DE FISICA Serie B Vol. 86 1990

ESTABLISHING PHASE EQUILIBRIA BY MEANS OF THE TEMPERATURE GRADIENT DIFFUSION TECHNIQUE

Walter Lengauer and Peter Ettmayer
Institute for Chemical Technology of Inorganic Materials,
Technical University of Vienna,
Getreidemarkt 9, A-1060 Vienna, Austria

Abstract
The diffusion couple technique for studying phase reactions in order to establish phase diagrams was modified by the introduction of a temperature gradient parallel to the developing diffusion layers. By metallographic preparation and inspection of the diffusion layers phase reactions which occur within relatively small temperature and composition intervals can be observed. Results for the Ti-N system, where this technique was applied, are presented.

1.- Introduction

The interdiffusion of components during heat treatments of binary diffusion couples is known to be well suited for studies concerning phase reactions. It has been proven by several authors (e.g. Heijwegen & Rieck, 1974) that the boundary compositions of the occurring diffusion layers represent equilibrium values. Due to the spatial separation of diffusion layers of phases even when their compositional difference is very small, this technique appears to have considerable potential for establishing phase equilibria even in such binary systems where several compounds occur. This is especially true in view of the development of microanalytical techniques such as EPMA.
The diffusion couple technique has already been described for systems with refractory compounds such as TiN. Results on TiN-Ti interdiffusion have been published by Rennhack et al. (1968), McDonald & Wallwork (1970), Wood & Paasche (1974), Bars et al. (1977), and later by Wolff et al. (1985) and Etchessahar et al. (1987). The results obtained by these authors were quite contradictory, especially with respect to the decomposition temperature of ε-Ti_2N (see Lengauer & Ettmayer 1987). In an attempt to resolve these discrepancies using arc-melting and quenching techniques, two new high-temperature titanium nitride phases were found (Lengauer & Ettmayer 1986a, Lengauer 1986b). These phases are situated adjacent to the ε-phase both with respect to composition and to temperature. Due to the difficulties connected with the restricted homogeneity of arc-melted buttons and metallographic phase identification, a diffusion study was performed. It showed that the high-temperature phases indeed form distinctive diffusion layers characteristic of the phase character of these high-temperature compounds. From a series of diffusion couples annealed at different temperatures three distinct tentative types for a Ti-N phase diagram could be extracted (Lengauer et al. 1989). These are shown in Fig.1. The question concerning the relative composition of ε-Ti_2N and ζ-Ti_4N_{3-x} (Fig.1 type *b* or *c*) as well as whether these two phases overlap with respect to temperature (type *a* on the one hand or type *b* or *c* on the other) had to be left unanswered.
In order to find these answers we modified the isothermal diffusion couple technique by introducting a temperature gradient parallel to the developing layers.
This modification is called the temperature gradient diffusion technique.

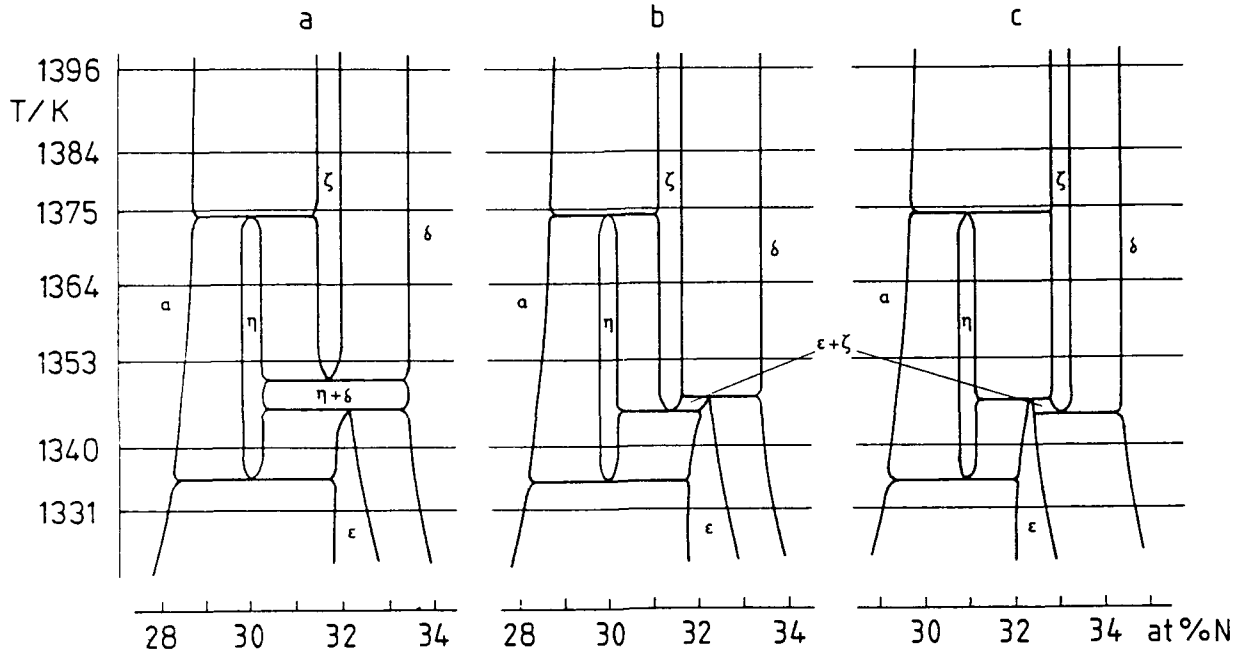

Fig.1
Variants of a portion of the phase diagram of the Ti-N system consistent with results from isothermally annealed diffusion couples.

2.- Experimental

As a first step TiN-Ti diffusion couples were prepared by isothermal reaction of titanium plates with nitrogen in a cold-wall autoclave under strict precautions to avoid oxygen contamination. The temperature was adjusted to a value between the upper and the lower temperature limits of the subsequent tube annealing procedure. After the heating period (the duration of which was dependent on the temperature, e.g. 20 days at 1423 K, (1150°C)) the samples were cooled to room temperature within a few minutes. The resulting samples consisted of a gold colored 30-50μm thick δ-TiN layer surrounding an α-Ti(N) core. At their interface there was a diffusion layer composed of ε-Ti_2N which had formed during the cooling cycle below 1341 K (1068°C).

These samples were aligned and positioned in a Mo-foil holder as illustrated in Fig.2. A temperature profile of the position where they were located is also shown in Fig.2. In order to protect the samples and sample holder from reaction with air, the samples were sealed under Ar in silica tubes. The tubes were placed in turn in a ceramic tube within an electronically temperature controlled SiC-heated furnace (Fig.3). After reaction (typically for 24 h - 5 days) the tubes were quenched in water. While the samples were being pulled out of the furnace the ceramic tube served as a heat buffer.
The temperature profile of the SiC furnace was measured before and after the heat treatments of the samples by introducing a thermocouple in a silica tube and positioning it in exactly the same manner as the samples. Typical deviations in temperature before and after annealing were 1-3 K, depending on the temperature gradient.

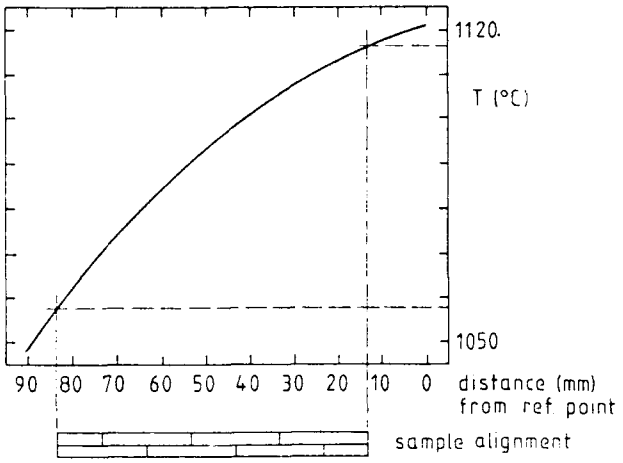

Fig.2
A temperature profile for a gradient diffusion experiment together with a schematic representation of sample alignment.

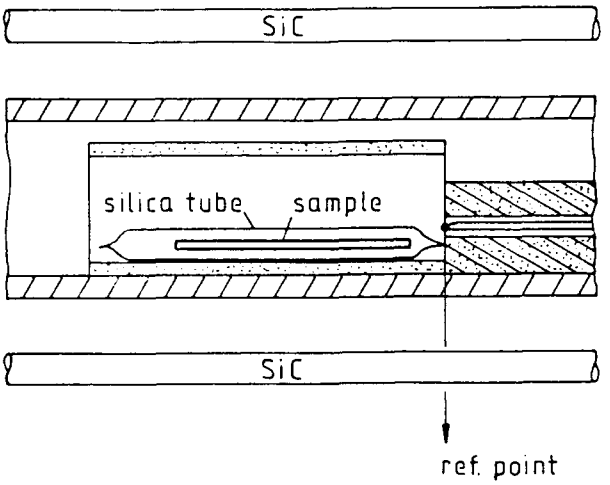

Fig.3
Schematic representation of the internal parts of the SiC furnace for a gradient diffusion experiment.

3.- Results and discussion

The microsections of the samples annealed in the temperature gradient reflect the co-existing phases as a function of temperature and composition. On the axis normal to the diffusion layer the sequence of phases with decreasing nitrogen activity from the surface to the core of the sample can be seen. Paarallel to the temperature axis the change of phase sequence with temperature is reflected. This is the same representation as used for phase diagrams, so that such a sample can be translated directly into a phase diagram.

As shown in Fig.4 the peritectoid decomposition of the ε-Ti_2N phase can be "observed" directly and the decomposition temperature of 1341 K (1068°C) immediately deter-mined, which is in excellent agreement with recent determinations (Etchessahar et al. 1986, Lengauer & Ettmayer 1987).

Similar results could be obtained for all other co-existing phases including the high-temperature phases γ-Ti_3N_{2-x} and ζ-Ti_4N_{3-x}. In the diffusion bands these phases were more difficult to distinguish optically

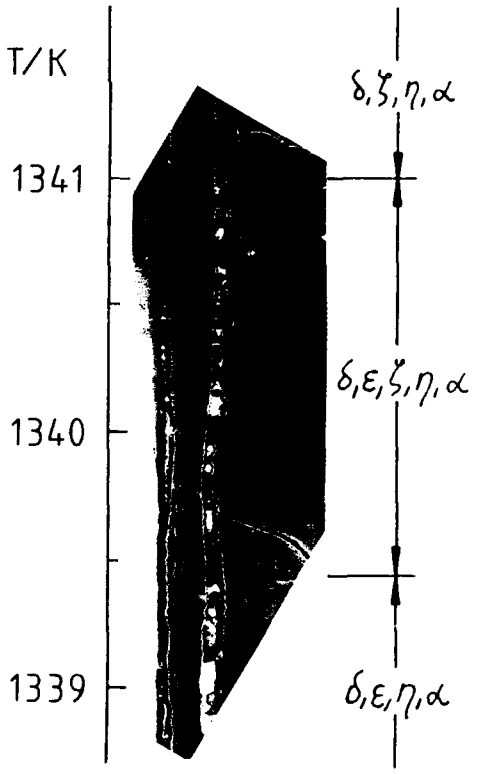

Fig.4
Microsection of a diffusion band reflecting the decomposition of ε-Ti_2N at T = 1341 K (1068°C) as obtained by a gradient diffusion experiment.

since their colors are less intensive in polarized light than those of α-Ti(N) and ε-Ti_2N. However, the microsections of diffusion couples unambiguously reflect the phase sequence in the Ti-N system both as a function of temperature *and* composition. A representation of these phase equilibria is shown in Fig.5. It can be seen that with the temperature gradient technique two three-phase equilibria which occur within a temperature interval of less than 2 K can be observed.

The precision of the technique depends on the temperature gradient and is theoretically much better than 0.1 K. However, if the temperature gradient becomes too small the local thermodynamic equilibrium is strongly influenced by grain size and mechanical stress. It was observed near the thermal stability limit of the ζ-phase that the layer sometimes disappears (and hence the layer sequence changes) when a grain boundary of the adjacent α-phase meets the diffusion band. To avoid this grain size effect the temperature gradient should not be too small. In the present study gradients between 8 K/cm and 50 K/cm were applied with consistent results. The extent of the grain size influence can be observed by comparing opposite surfaces which were located at the same temperature but had a different grain boundary structure. In the most unfavorable cases -- where relatively thin elongated ζ-Ti_4N_{3-x} grains were in contact with the large α-Ti(N) grains near the decomposition temperature of ζ-Ti_4N_{3-x} -- the precision was ± 3 K. In the case of the phase reaction α-Ti(N) + ζ-Ti_4N_{3-x} --> η-Ti_3N_{2-x} the error was about ± 5 K because of difficulties to distinguish the crystallographically closely related compounds η-Ti_3N_{2-x} and ζ-Ti_4N_{3-x}. For the phase equilibria η-Ti_3N_{2-x} --> α-Ti(N) + ε-Ti_2N, ζ-Ti_4N_{3-x} --> η-Ti_3N_{2-x} + ε-Ti_2N and ζ-Ti_4N_{3-x} + δ --> ε-Ti_2N) the diffusion bands did not contain the elongated grain size and the effect was much less pronounced. The precision of the nonvariant three-phase conodes was better than 0.5 K.

The absolute accuracy of the temperature measurement is determined by the accuracy of the Pt/PtRh thermocouples together with the uncertainty of positioning the sample in the furnace (± 1mm) and can be estimated as ±5 K. Further improvement in the positioning of the samples and use of a calibrated thermocouple could increase the accuracy.

It should be noted that there are problems associated with EPMA measurements of titanium nitrides due to the very strong overlap of nitrogen and titanium lines (Bastin et al. 1988). A study is in progress to determine the composition of the layers by means of well characterized Ti-N standards. In the present study the composition was calibrated during probe measurement against ε-Ti_2N assuming that it had a homogeneity range of 32 - 33 at% N. Therefore the compositions of the α-Ti(N) and δ-TiN_{1-x} phases (which both are further away in composition from ε-Ti_2N than the other phases) are too high and too low, respectively. Together with more exact quantitative EPMA measurements, which will be published in the near future, it will be possible to supply better quantitative results with improved precision for the α-Ti(N) and δ-TiN_{1-x} phase boundary.

Acknowledgements

The authors would like to thank the colleagues at the Laboratoire de Metallurgie, INSA, Rennes, France as well as Mr. M. Bohn, IFREMER, Brest, France for their kind help with microprobe measurements. This work was supported by the Austrian Science Foundation FWF under Project No. P 7370.

References

Bars, J.-P.,Etchessahar, E. and Debuigne, J. (1977): J.Less-Common Met. **52**, 51

Bastin, G.F.,Heijligers, H.J.M. and Pinxter, J.F.M. (1988): Microbeam Analysis 290

Etchessahar, E., Bars, J.-P., and Debuigne, J. (1987): J.Less-Common Met. **134**, 123

Heijwegen C.P. and Rieck, G.D. (1974): J. Less-Common Met. **34**, 309

Lengauer, W. and Ettmayer, P. (1986a): J. Less-Common Met. **120**, 153

Lengauer, W. (1988b): J.Less-Common Met. **125**, 127

Lengauer, W., Ettmayer, P., Bars, J. P., Etchessahar,E., Bauer,J. and Debuigne J. (1989): 32nd IUPAC Congress, Stockholm

Lengauer W., and Ettmayer, P. (1987): High Temp.-High Press. **19**, 673

McDonald, N.R. and Wallwork, G.R. (1970): Oxid. Metals. **2**, 263

Pennhack, E.H., Coons, W.C. and Perkins, E.A. (1968): Trans.Met.Soc.AIME **242**, 343

Wolff, L., Bastin, G. and Heijligers, H. (1985): Solid State Ionics **16**, 105

Wood, F.W. and Paasche, O.G. (1974): Microstruct. Sci. **2**, 101

DETERMINATION OF THE ENTHALPY OF FORMATION OF TERNARY Ni_3Al-BASED ALLOYS

Stefan KEK[1], Christoff RZYMAN[2] and Ferdinand SOMMER[1]

[1] Max-Planck-Institut für Metallforschung, Institut für Werkstoffwissenschaft, Seestr. 75, D-7000 Stuttgart 1, F.R.G.

[2] Institute for Metal Research, Polish Academy of Sciences, 30-059 Krakow, Reymonta 25, Poland

Abstract

The enthalpy of formation of ordered ternary alloys with $L1_2$-structure obtained by ternary additions to Ni_3Al was determined by solution calorimetry in liquid aluminium. The concentration dependence of the enthalpy of formation is discussed on the basis of a simple statistical treatment.

1. Introduction

For the development of superalloys and advanced aluminides it is important to know the solid solubility of ternary components in the ordered phase Ni_3Al and their thermodynamic properties. In this work results of solution calorimetry are presented to determine the enthalpy of formation as a function of ternary additions to Ni_3Al. The results are discussed in a simple Bragg-Williams model taking into account the site preference of the ternary additions.

2. Experimental

A previously described calorimeter (Sommer et al. 1980, Oehme et al. 1978) was used to determine the heats of formation by solution calorimetry. The alumina reaction crucible contains an aluminium bath (about 1.3 mol aluminium with a purity of 99.9%). Calibration was carried out by adding at least seven aluminium samples of mass about 0.2 g which have a known enthalpy content from room temperature (Hultgren et al. 1973a). The individual additions of the alloys and their components had masses of about 0.3 g. The temperature change occuring during the dissolution process is determined by a Ni-NiCr thermopile situated directly below the reaction crucible. The resulting heat effects are recorded and the area under the ΔT vs. time curve corresponds to the enthalpy of dissolution ΔH^I. In all experiments the calorimeter was evacuated and flushed with high purity argon (purity 99.999%) five times at different temperatures during heating and then measurements were done at a constant temperature in steady argon atmosphere with continuous stirring through out the experiments. The Al_2O_3 stirrer has an effective blade area of 3 cm^2.

The alloys were made from metals with a purity of 99.98% or higher. Melting was carried out in an induction furnace under argon atmosphere to produce chillcast cylinders of diameter 7mm. After individual heat treatment and rapidly cooling to room temperature the homogeneity of the alloys were confirmed by X-ray analysis using the Guinier technique and metallographic examination.

3. Experimental results

The experimental results for the thermal effects of dissolution ΔH^I of nickel, cobalt, iron, manganese, chromium, copper, gallium, silicon and of the binary and ternary alloys in liquid aluminium are given in Tables 1-9 as a function of the concentration of all additional elements. ΔH^I includes the change in heat content of the samples from room temperature to the temperature of measurement. The thermal effects at infinite dilution $\Delta H^{I,0}$ were obtained by extrapolation to $x_{Al} = 1$. $\Delta H^{I,0}$ is obtained as mean value or by using a linear concentration dependence. The uncertainity is given by the addition of the standard error of calibration and dissolution of the metals and alloys. The partial enthalpies of mixing at infinite dilution $\Delta \overline{H}_i^0$ of liquid components in liquid aluminium (see Table 11) have been obtained by subtracting the heat content from room temperature to 1123 K and the enthalpy of melting of the elements from $\Delta H_i^{I,0}$ (Hultgren et al. 1973a). The enthalpy of melting was extrapolated to 1123 K. The temperature dependence of the $\Delta \overline{H}^0$-values of iron and nickel in liquid aluminium indicates the existence of chemical short range order, which is described in thermodynamic models as the formation of associates with a definite stoichiometry (Sommer et al. 1988). The heat of formation ΔH^f of the intermetallic phases at room temperature are calculated directly from the measured $\Delta H^{I,0}$-values:

$$\Delta H^f_{A_{x_A}B_{x_B}C_{x_C}} = x_A \Delta H^{I,0}_A + x_B \Delta H^{I,0}_B + x_C \Delta H^{I,0}_C - \Delta H^{I,0}_{A_{x_A}B_{x_B}C_{x_C}} \quad (1)$$

The values obtained are given in Table 10 and some of the concentration dependences are presented in Fig. 1-5. The reference state of the ΔH^f-values given in Table 10 and of the extrapolated values calculated with eqn. (2) and (3) is the me-

chanical mixture of the pure components in their stable crystal structure at room temperature.

The enthalpy of formation of a ternary alloy is calculated from their separately measured $\Delta H^{E,0}$-values and literature value for the heat content of aluminium (Hultgren et al. 1973a) (see eqn. (1)). The high accuracy of the enthalpy of formation values given in Table 10 could only be achieved because the individual $\Delta H^{E,0}$-values have been obtained in most cases with a standard error below 1%. The standard error of the compounds given in Table 10 has been calculated by taking square root of the added squares of the four standard errors of the $\Delta H^{E,0}$-values of the compound and the components. The squared errors of the $\Delta H^{E,0}$-values of the components have been added according to their mole fractions.

4. Discussion

Between Ni_3Al and Ni_3Si, Ni_3Al and Ni_3Ga exist a continous homogeneity of $L1_2$-phase at 1273 K (Ochiai et al. 1984). Ni_3Al and Ni_3Mn also show continous solubility below 700 K (Wachtel et al. 1988). The results of X-ray analysis of our heat treated samples also show these continous solid solubilities and only Ni_3Mn samples contain, even after 56 d heat treatment, a small volume part of disordered fcc solid solution. The solubility limit is 25 at.% for copper at 1173 K and 30 at.% for cobalt at 1073 K (Ochiai et al. 1984). The investigated alloys with chromium and iron also show $L1_2$-structure.

The site preference for ternary components in the unit cell of Ni_3Al with $L1_2$ can be estimated from the direction of the solubility lobe in a ternary region (Ochiai et al. 1984). A ternary addition X which occupies mostly cube corner sites has a lobe in the direction Ni_3Al-Ni_3X, an addition which occupies mostly face centered sites has a lobe in the direction Ni_3Al-X_3Al and an addition which substitutes both sites has maximum solubility extension in a direction in between. A simple explanation of this behaviour can be obtained from the atomic radii of Ni (1.25 Å) and Al (1.43 Å) in relation to the atomic radius radius of the ternary addition, because an ordered structure can be easily destabilized by an unfitting atomic radius. Values of atomic radius used for the elements (Pearson 1970) are obtained considering a coordination number of 12. If the atomic radius of the ternary component is approximately equal to that of nickel or aluminium then it can easily substitute one of these elements. Therefore copper (1.28 Å) and cobalt (1.25 Å) substitute nickel. From experimentally determined atomic volume of Al in Ni solid solution, as a function of concentration and atomic volume of Ni_3Al, one obtains a partial atomic volume of Al in Ni_3Al. The effective radius for coordination number 12, determined by this partial volume, amounts to 1.31 Å. The effective atomic radius of Al in Ni_3Al is therefore 1.31 Å (Kolatschek 1988) and not 1.43 Å as for the pure element. The charge transfer and the covalent bond between the atoms in Ni_3Al, as shown by recent electron theory calculations (Morinaga et al. 1984), cause the change of atomic radius in this compound. From similar investigations the effective radius of gallium in Ni_3Ga results is 1.33 Å (Kolatschek 1990) and that of Mn in Ni_3Mn is 1.34 Å (Pearson 1958). Gallium and manganese can therefore substitute aluminium easily. Considering the effective radius of Si, 1.22 Å (Ellner 1981), silicon should substitute nickel, but silicon substitutes aluminium (see Fig. 3) because the electronic configuration of silicon is much more similar to aluminium compared to nickel. The effective radii of iron (1.29 Å) (Pearson 1958) and chromium (1.29 Å) (Taylor and Floyd 1952) allow in accordance with the experimental results a substitution of all sites in Ni_3Al. Enomoto et al. 1989 and Wu et al. 1989 have obtained with the cluster variation method more detailed informations about the site preference of ternary addition in an A_3B compound with the $L1_2$ structure depending on the relative magnitude of the pair interactions. The concentration dependence of the heat of formation along the quasibinary cut Ni_3Al-Ni_3X should be determined mainly by the ΔH^f-values of Ni_3Al and Ni_3X. The results for X = Ga, Mn and Si support this (see Fig. 1-3). A simple statistical treatment which describes the concentration dependence of ΔH^f and accounts for the site preference of X in an ordered $L1_2$ alloy can be obtained from the Bragg-Williams model. Taking only nearest neighbour and concentration independent interactions into account for the special case where the ternary additions occupy only cube corner sites the following equation results (Ochiai et al. 1984).

$$\Delta H^f_{(x)} = 12\left[\left(\frac{1}{4} - X_X\right) V_{Ni\,Al} + X_X V_{Ni\,X}\right] \qquad (2)$$

$$\text{with} \quad V_{Ni\,Al} = \frac{\Delta H^f_{Ni_3Al}}{3}$$

$$V_{Ni\,X} = \frac{\Delta H^f_{Ni_3X}}{3}$$

According to eqn. (2) ΔH^f exhibits a linear concentration dependence. The experimentally obtained results for Ni_3Al-Ni_3Mn also show a linear concentration dependence with the exception of Ni_3Mn because it was only partially ordered. The extrapolated value for a completely ordered Ni_3Mn amounts to -12 ± 1.5 kJ mol^{-1} (see Fig. 2). The ΔH^f-values for Ni_3Al-Ni_3Si follow linear concentration dependence only with a big scatter which results in a value -49 ± 2 kJ mol^{-1} for Ni_3Si with $L1_2$-structure (see Fig. 3). This value is in agreement with results obtained from phase diagram calculations (Nash 1987) and is in disagreement with the value of -36 kJ mol^{-1} obtained by reaction calorimetry (Oelsen et al. 1936). These experimental results show that $\Delta H^f_{(x)}$ along Ni_3Al-Ni_3X can be

described with eqn. (2) if the ΔH^f of binary bordering phases are known.

If the ternary additions occupy only face centered sites then considering only nearest neighbour and concentration independent interactions the following relation is obtained (Ochiai et al. 1984).

$$\Delta H^f_{(x)} = 12\left[\left(\frac{1}{4}-\frac{X_X}{3}\right)V_{NiAl}+\frac{X_X}{3}V_{XAl} + \frac{2}{3}X_X\left(1-\frac{4}{3}X_X\right)V_{NiX}\right] \quad (3)$$

$$\text{with} \quad V_{XAl} = \frac{\Delta H^f_{X_3Al}}{3}$$

The experimental results for Ni_3Al-X_3Al can be described quantitatively with eqn. (3) using experimental data of the base binary systems (see Fig. 4). The interaction parameter ($V_{NiAl} = -13.5$, $V_{AlCo} = -9.50$, $V_{NiCo} = 0.1$ kJ mol^{-1}) are obtained from $\Delta H^f_{Ni_3Al}$, " $\Delta H^f_{Co_3Al}$ " (Henig et al. 1980) and " $\Delta H^f_{Ni_3Co}$ " (Hultgren et al 1973b). The heat of formations obtained for Ni-Al-Cu alloys can be used to calculate with eqn. (3) the enthalpy of formation of a hypothetical Cu_3Al compound with $L1_2$ structure. The ΔH^f-value obtained with $V_{NiCu} = -0.6$ kJ mol^{-1} (Hultgren et al. 1973b) amounts to -37 kJ mol^{-1}. The Ni-Al-Cr alloys investigated have concentrations near the quasibinary cut Ni_3Al-Cr_3Al. The experimental $\Delta H^f_{(x)}$-values correspond well to the values obtained from eqn. (3) using $V_{AlCr} = -3$, $V_{NiCr} = 0.3$ kJ mol^{-1} (Hultgren et al. 1973b).

The $\Delta H^f_{(x)}$-values within a ternary phase with $L1_2$ structure can therefore be calculated with a simple Bragg-Williams model taking into account only nearest neighbour interactions using interaction parameters which are fixed from ΔH^f-values of the binary base systems. The experimental $\Delta H^f_{(x)}$-values can also be used to determine the parameters of the pair interactions within the cluster variation method and to calculate the site preference of ternary additions.

Acknowledgement. The financial support of this work by the Deutsche Forschungsgemeinschaft is gratefuly acknowledged.

References

Batalin, G. I., Beloborodova, E. A., Shalpak, A. N., Nikolaenko, J. V. and Kurach, V. P. (1981): Russ. J. Phys. Chem. **55**, 888.

Dannöhl, H. D. (1971): PhD Thesis, University of Stuttgart.

Ellner, M. (1981): J. Less Common Metals **78**, P21.

Enomoto, M. and Harada, H. (1989): Metall. Trans. **20A**, 649.

Esin, Yu. O., Bobrov, N. T., Petrushevskiy, M. S. and Gel'd, P. V. (1973): Russ. J. Phys. Chem. **47**, 1103.

Henig, E. T., Lukas, H. L. und Petzow, G. (1980): Z. Metallkde. **71**, 398.

Hultgren, R., Desai, P. D., Hawkins, D. T., Gleiser, M., Kelly, K. K. and Wagman, D. D. (1973): Selected Values of the Thermodynamic Properties of the Elements (Ohio, ASM Metals Park).

Hultgren, R., Desai, P. D., Hawkins, D. T., Gleiser, M. and Kelly, K. K. (1973): Selected Values of Thermodynamic Properties of Binary Alloys (Ohio, ASM Metals Park).

Kolatschek, K. (1988): Diploma Work, University of Stuttgart.

Kolatschek, K. (1990): PhD Thesis, University of Stuttgart.

Kubaschewski, O. (1958): Trans. Farad. Soc. **54**, 814.

Lee, J. J. and Sommer, F. (1980): Z. Metallkde. **76**, 750.

Martosudirjo, S. and Pratt J. N. (1976): Thermochimica Acta **17**, 183.

Mathieu, J. C., Jounel, B., Desré, P. and Bonnier E. (1967): Proc. Conf. Thermodynamics of Nuclear Materials, Vienna. 767.

Morinaga, M., Yukawa, N., and Adachi, H. (1984): J. Phys. Soc. Japan **53**, 653.

Nash, P. and Nash, A. (1987): Bull. Phase Diagr. **8**, 6.

Ochiai, S., Yoshihiro, O. and Suzuki, T. (1984): Acta Metall. **32**, 289.

Oehme, G. and Predel B. (1976): Thermochimica Acta **22**, 267.

Oelsen W. and Middel, W. (1936): Mitt. Kaiser Wilhelm Inst. Eisenforsch. **18**, 132.

Oelsen W. and Middel, W. (1937): Mitt. Kaiser Wilhelm Inst. Eisenforsch. **19**, 1.

Pearson, W. B. (1958): A Handbook of Lattice Spacings and Structure of Metals and Aloys (Oxford: Pergamon).

Pearson, W. B. (1972): The Crystal Chemistry and Physics of Metals and Alloys (New York: Wiley).

Petrushevskiy, M. S., Esin, Yu. O., Gel'd, P. V., and Sandakov, V. M. (1972): Russ. Metall. **No. 6** , 149.

Predel B., Vogelbein W., and Schallner, U. (1975): Thermochimica Acta **12**, 367.

Sandakov, V. M., Esin, Yu. O. and Gel'd, P. V. (1971): Russ. J. Phys. Chem. **45**, 1020.

Sandakov, V. M., Esin, Yu. O., Gel'd, P. V. and Shantarin, V. D. (1971): Russ. J. Phys. Chem. **45**, 1150.

Sommer, F., Lee, J. J. and Predel, B. (1980): Z. Metallkde. **71**, 818.

Sommer, F., Schott, J. and Krull H.-G. (1988): J. Less Common Metals **144**, 53.

Taylor, A. and Floyd, R. W. (1952): J. Inst. Metals **80**, 577.

Wachtel, E., Vincent, M. and Predel, B. (1988): Z. Metallkde. **79**, 252 and 330.

Wu, Y. P., Tso, N. C., Sanchez, J. M. and Tien, J. K. (1989): Acta Metall. **37**, 2835.

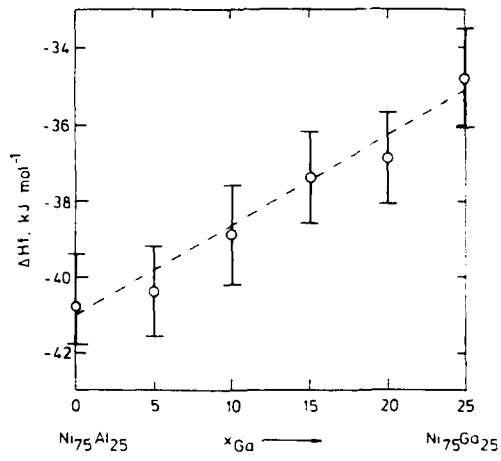

Fig. 1. Enthalpy of formation of Ni-Al-Ga alloys at room temperature (- - - calculated from eqn. (2)).

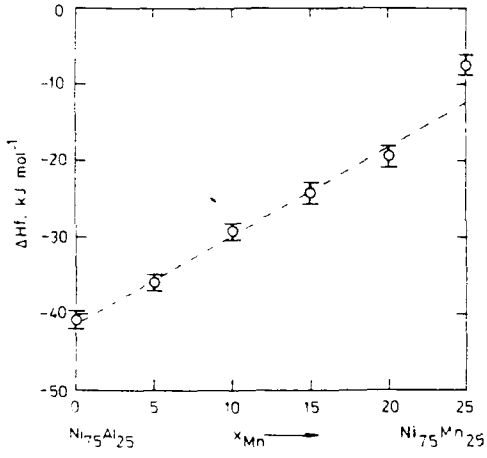

Fig. 2. Enthalpy of formation of Ni-Al-Mn alloys at room temperature (- - - calculated from eqn. (2)).

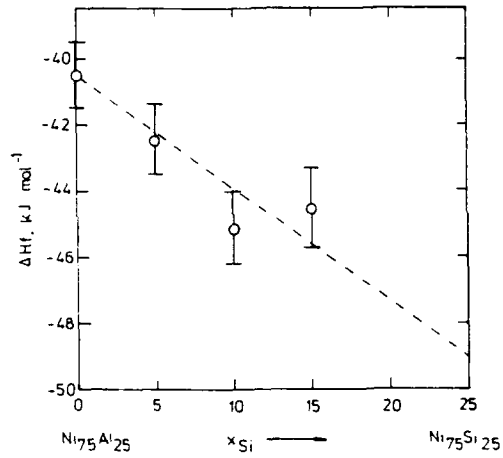

Fig. 3. Enthalpy of formation of Ni-Al-Si alloys at room temperature (- - - calculated from eqn. (2)).

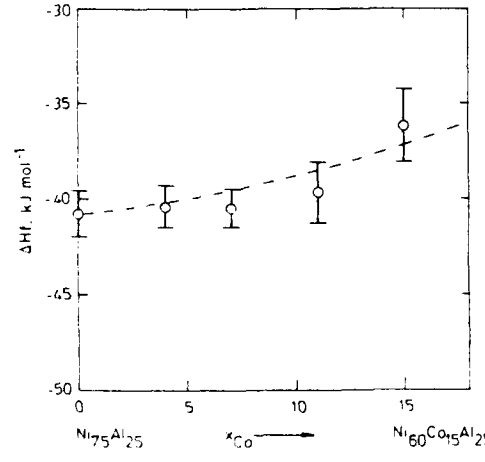

Fig. 4. Enthalpy of formation of Ni-Al-Co alloys at room temperature (- - - calculated from eqn. (3)).

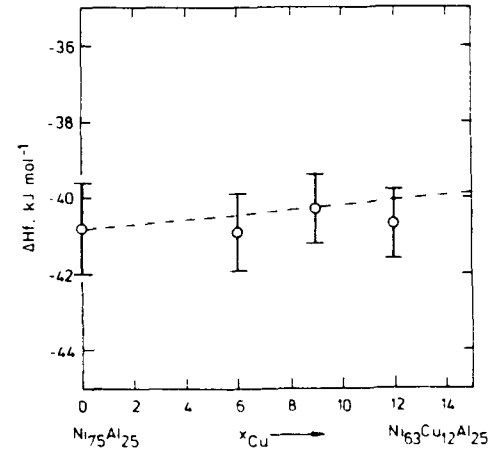

Fig. 5. Enthalpy of formation of Ni-Al-Cu alloys at room temperature (- - - calculated from eqn. (3)).

Table 1. Experimental values of the enthalpy of dissolution of cobalt, copper, gallium, nickel, manganese, silicon, iron and chromium from room temperature in liquid aluminium at 1123 K (x, $at.\%$, ΔH $kJmol^{-1}$).

x_{Co}	ΔH^E_{Co}	x_{Cu}	ΔH^E_{Cu}	x_{Ga}	ΔH^E_{Ga}	x_{Ni}	ΔH^E_{Ni}	x_{Mn}	ΔH^E_{Mn}	x_{Si}	ΔH^E_{Si}	x_{Fe}	ΔH^E_{Fe}	x_{Cr}	ΔH^E_{Cr}
0.16	−109.6	1.17	0.91	0.17	33.9	0.35	−107.2	0.24	−40.9	0.22	53.3	0.45	−76.9	0.19	−29.2
0.26	−109.9	2.32	0.71	0.45	31.1	0.71	−108.9	0.47	−41.1	0.42	53.4	0.75	−79.5	0.46	−25.0
0.29	−111.4	3.48	0.65	0.80	31.4	1.10	−111.0	0.69	−37.8	0.63	56.1	1.04	−83.0	1.00	−27.7
0.46	−109.7	4.62	0.53	1.05	31.2	1.54	−111.4	0.90	−39.1	0.86	55.9	1.31	−78.7	1.64	−28.1
0.51	−110.4	5.72	0.22	1.43	31.7	1.97	−110.6	1.13	−40.8	1.05	56.5	1.62	−79.0		
0.52	−110.4	6.80	0.09	1.82	33.0	2.39	−110.9	1.32	−39.7	1.20	57.3	1.92	−84.0		
0.69	−110.9	7.89	0.08	2.19	31.6	2.80	−112.0	1.60	−39.6	1.36	56.5				
0.79	−111.4	9.01	−0.04	2.44	31.5	3.15	−112.6	1.90	−41.1						
0.80	−104.2	10.1	−0.20	2.58	33.3										
0.96	−108.6	11.0	−0.10	2.87	30.3										
1.02	−106.6	12.0	−0.22	3.16	31.5										
1.08	−103.6	13.0	−0.31	3.50	30.9										
1.27	−103.2	13.8	−0.45	3.81	30.3										
1.29	−103.9	14.8	−0.57	4.07	31.8										
1.46	−107.0	15.0	−0.51												
1.50	−103.5														
$\Delta H^{E,0}_{Co}$ =		$\Delta H^{E,0}_{Cu}$ =		$\Delta H^{E,0}_{Ga}$ =		$\Delta H^{E,0}_{Ni}$ =		$\Delta H^{E,0}_{Mn}$ =		$\Delta H^{E,0}_{Si}$ =		$\Delta H^{E,0}_{Fe}$ =		$\Delta H^{E,0}_{Cr}$ =	
−108.0 ±1.8		0.86 ±0.13		31.7 ±0.6		−110.4 ±1.3		−40.0 ±0.6		55.6 ±1.2		−79.4 ±1.6		−27.5 ±1.3	

Table 2. Experimental values of the enthalpy of dissolution of $Ni_{75}Al_{25}$, $Mn_{25}Ni_{75}$ and $Ni_{75}Ga_{25}$ from room temperature in liquid aluminium at 1123 K (x, $at.\%$, ΔH $kJmol^{-1}$).

x_{Ni}	$\Delta H^E_{Ni_{75}Al_{25}}$	$x_{Mn,Ni}$	$\Delta H^E_{Mn_{25}Ni_{75}}$	$x_{Ni,Ga}$	$\Delta H^E_{Ni_{75}Ga_{25}}$
0.11	−33.5	0.38	−83.5	0.29	−39.6
0.24	−33.5	0.75	−84.5	0.61	−39.9
0.40	−34.6	1.08	−84.3	0.93	−40.7
0.48	−30.9	1.42	−86.0	1.26	−40.2
0.60	−34.6	1.76	−85.0	1.60	−40.4
0.74	−30.7	2.03	−84.7	1.94	−41.6
0.84	−34.2	2.41	−86.3	2.28	−38.9
1.02	−30.8	2.82	−84.2	2.63	−38.8
1.12	−34.2			2.98	−40.8
1.29	−31.4			3.36	−39.9
1.57	−31.4				
1.88	−34.0				
2.19	−32.5				
2.52	−32.4				
2.88	−32.8				
$\Delta H^{E,0}_{Ni_{75}Al_{25}}$ =		$\Delta H^{E,0}_{Mn_{25}Ni_{75}}$ =		$\Delta H^{E,0}_{Ni_{75}Ga_{25}}$ =	
−33.4 ±0.4		−84.8 ±0.8		−40.1 ±0.5	

Table 3. Experimental values of the enthalpy of dissolution of $Co_4Ni_{71}Al_{25}$, $Co_7Ni_{68}Al_{25}$, $Co_{11}Ni_{64}Al_{25}$ and $Co_{15}Ni_{60}Al_{25}$ from room temperature in liquid aluminium at 1123 K (x, $at.\%$, $\Delta H\ kJmol^{-1}$).

$x_{Co,Ni}$	$\Delta H^E_{Co_4Ni_{71}Al_{25}}$	$x_{Co,Ni}$	$\Delta H^E_{Co_7Ni_{68}Al_{25}}$	$x_{Co,Ni}$	$\Delta H^E_{Co_{11}Ni_{64}Al_{25}}$	$x_{Co,Ni}$	$\Delta H^E_{Co_{15}Ni_{60}Al_{25}}$
0.23	−32.1	0.26	−31.9	0.17	−33.0	0.32	−32.4
0.40	−34.6	0.69	−33.4	0.39	−33.7	0.65	−39.3
0.60	−32.2	1.20	−32.4	0.57	−35.3	1.01	−38.4
0.85	−33.6	1.36	−33.5	0.77	−37.8	1.36	−37.8
1.09	−34.3	1.71	−33.4	0.96	−32.4	1.72	−37.3
1.27	−34.1	2.05	−34.1	1.14	−31.8	2.08	−41.4
1.55	−33.4	2.41	−35.2	1.31	−33.6	2.43	−38.2
1.77	−35.0	2.78	−34.0	1.66	−39.3	2.88	−37.4
		3.16	−34.0	1.79	−32.0		
$\Delta H^{E,0}_{Co_4Ni_{71}Al_{25}}$ = −33.7 ±0.7		$\Delta H^{E,0}_{Co_7Ni_{68}Al_{25}}$ = −33.5 ±0.5		$\Delta H^{E,0}_{Co_{11}Ni_{64}Al_{25}}$ = −34.3 ±1.3		$\Delta H^{E,0}_{Co_{15}Ni_{60}Al_{25}}$ = −37.8 ±1.7	

Table 4. Experimental values of the enthalpy of dissolution of $Ni_{75}Al_{20}Si_5$, $Ni_{75}Al_{15}Si_{10}$ and $Ni_{75}Al_{10}Si_{15}$ from room temperature in liquid aluminium at 1123 K (x_i $at.\%$, $\Delta H\ kJmol^{-1}$).

$x_{Ni,Si}$	$\Delta H^E_{Ni_{75}Al_{20}Si_5}$	$x_{Ni,Si}$	$\Delta H^E_{Ni_{75}Al_{15}Si_{10}}$	$x_{Ni,Si}$	$\Delta H^E_{Ni_{75}Al_{10}Si_{15}}$
0.24	−29.4	0.37	−26.0	0.28	−25.7
0.47	−27.6	0.74	−24.7	0.63	−26.0
0.75	−30.4	1.05	−26.1	0.98	−27.0
1.04	−29.9	1.39	−25.8	1.34	−26.9
1.32	−28.2	1.79	−27.6	1.71	−26.3
1.58	−30.1	2.16	−26.1	2.11	−26.3
1.88	−32.0	2.50	−26.9	2.52	−26.3
2.18	−31.9	2.82	−26.1	2.88	−25.6
2.47	−31.3				
2.65	−29.4				
2.97	−29.6				
$\Delta H^{E,0}_{Ni_{75}Al_{20}Si_5}$ = −30.0 ±0.6		$\Delta H^{E,0}_{Ni_{75}Al_{15}Si_{10}}$ = −26.2 ±0.4		$\Delta H^{E,0}_{Ni_{75}Al_{10}Si_{15}}$ = −26.3 ±0.4	

Table 5. Experimental values of the enthalpy of dissolution of $Ni_{69}Cu_6Al_{25}$, $Ni_{66}Cu_9Al_{25}$ and $Ni_{63}Cu_{12}Al_{25}$ from room temperature in liquid aluminium at 1123 K (x_i $at.\%$, $\Delta H\ kJmol^{-1}$).

$x_{Ni,Cu}$	$\Delta H^E_{Ni_{69}Cu_6Al_{25}}$	$x_{Ni,Cu}$	$\Delta H^E_{Ni_{66}Cu_9Al_{25}}$	$x_{Ni,Cu}$	$\Delta H^E_{Ni_{63}Cu_{12}Al_{25}}$
0.24	−28.1	0.30	−23.7	0.29	−17.6
0.50	−27.1	0.62	−23.5	0.59	−20.8
0.77	−26.0	0.98	−22.4	0.89	−19.3
1.03	−25.4	1.36	−22.8	1.24	−20.5
1.35	−25.2	1.73	−23.4	1.39	−20.5
1.68	−27.0	2.11	−23.8	1.96	−19.8
2.03	−26.2	2.49	−24.9	2.33	−19.8
2.66	−26.6	2.88	−24.6	2.70	−19.7
3.02	−27.0	3.27	−25.0	3.08	−20.7
				3.47	−22.2
$\Delta H^{E,0}_{Ni_{69}Cu_6Al_{25}}$ = −26.5 ±0.4		$\Delta H^{E,0}_{Ni_{66}Cu_9Al_{25}}$ = −23.8 ±0.4		$\Delta H^{E,0}_{Ni_{63}Cu_{12}Al_{25}}$ = −20.1 ±0.5	

Table 6. Experimental values of the enthalpy of dissolution of $Mn_5Ni_{75}Al_{20}$, $Mn_{10}Ni_{75}Al_{15}$, $Mn_{15}Ni_{75}Al_{10}$ and $Mn_{20}Ni_{75}Al_5$ from room temperature in liquid aluminium at 1123 K (x_i *at.*%, ΔH *kJmol*$^{-1}$).

$x_{Mn,Ni}$	$\Delta H^E_{Mn_5Ni_{75}Al_{20}}$	$x_{Mn,Ni}$	$\Delta H^E_{Mn_{10}Ni_{75}Al_{15}}$	$x_{Mn,Ni}$	$\Delta H^E_{Mn_{15}Ni_{75}Al_{10}}$	$x_{Mn,Ni}$	$\Delta H^E_{Mn_{20}Ni_{75}Al_5}$
0.32	−41.2	0.38	−50.8	0.33	−57.8	0.34	−66.1
0.65	−41.0	0.75	−50.8	0.70	−60.4	0.70	−68.1
0.98	−41.7	1.14	−51.3	1.09	−61.7	1.06	−68.7
1.48	−41.5	1.53	−50.1	1.49	−62.4	1.46	−70.0
1.81	−41.0	1.94	−52.0	1.88	−60.2	1.85	−70.0
2.14	−40.7	2.35	−51.5	2.27	−58.9	2.28	−72.2
2.52	−42.0	2.76	−51.8	2.67	−62.4	2.78	−67.8
2.91	−42.3	3.17	−53.0	3.07	−61.7		
		3.59	−53.5	3.50	−61.0		
		4.02	−53.1	4.00	−58.9		
$\Delta H^{E,0}_{Mn_5Ni_{75}Al_{20}}$ = −41.4 ±0.5		$\Delta H^{E,0}_{Mn_{10}Ni_{75}Al_{15}}$ = −51.8 ±0.6		$\Delta H^{E,0}_{Mn_{15}Ni_{75}Al_{10}}$ = −60.5 ±1.0		$\Delta H^{E,0}_{Mn_{20}Ni_{75}Al_5}$ = −69.0 ±1.0	

Table 7. Experimental values of the enthalpy of dissolution of $Ni_{75}Al_{20}Ga_5$, $Ni_{75}Al_{15}Ga_{10}$, $Ni_{75}Al_{10}Ga_{15}$ and $Ni_{75}Al_5Ga_{20}$ from room temperature in liquid aluminium at 1123 K (x_i *at.*%, ΔH *kJmol*$^{-1}$).

$x_{Ni,Ga}$	$\Delta H^E_{Ni_{75}Al_{20}Ga_5}$	$x_{Ni,Ga}$	$\Delta H^E_{Ni_{75}Al_{15}Ga_{10}}$	$x_{Ni,Ga}$	$\Delta H^E_{Ni_{75}Al_{10}Ga_{15}}$	$x_{Ni,Ga}$	$\Delta H^E_{Ni_{75}Al_5Ga_{20}}$
0.26	−34.8	0.23	−37.2	0.24	−38.8	0.31	−39.2
0.49	−33.4	0.46	−35.0	0.51	−36.0	0.63	−37.8
0.70	−34.1	0.76	−37.7	0.78	−35.4	0.96	−38.0
0.91	−33.9	1.06	−34.8	1.06	−36.8	1.38	−36.4
1.21	−33.3	1.36	−34.9	1.38	−37.4	1.67	−38.0
1.51	−35.3	1.69	−33.5	1.72	−36.8	2.03	−37.1
1.82	−33.6			2.03	−37.8	2.39	−38.1
2.12	−32.8			2.38	−37.0	2.76	−38.1
2.44	−34.8			2.72	−37.3	3.15	−37.5
2.83	−33.3			3.13	−38.3	3.41	−38.0
$\Delta H^{E,0}_{Ni_{75}Al_{20}Ga_5}$ = −33.9 ±0.4		$\Delta H^{E,0}_{Ni_{75}Al_{15}Ga_{10}}$ = −35.5 ±0.8		$\Delta H^{E,0}_{Ni_{75}Al_{10}Ga_{15}}$ = −37.2 ±0.5		$\Delta H^{E,0}_{Ni_{75}Al_5Ga_{20}}$ = −37.8 ±0.4	

Table 8. Experimental values of the enthalpy of dissolution of $Ni_{74}Al_{23}Fe_3$, $Ni_{73}Al_{22}Fe_5$, $Ni_{71}Al_{22}Fe_7$ and $Ni_{72}Al_{18}Fe_{10}$ from room temperature in liquid aluminium at 1123 K (x_i *at.*%, ΔH *kJmol*$^{-1}$).

$x_{Ni,Fe}$	$\Delta H^E_{Ni_{74}Al_{23}Fe_3}$	$x_{Ni,Fe}$	$\Delta H^E_{Ni_{73}Al_{22}Fe_5}$	$x_{Ni,Fe}$	$\Delta H^E_{Ni_{71}Al_{22}Fe_7}$	$x_{Ni,Fe}$	$\Delta H^E_{Ni_{72}Al_{18}Fe_{10}}$
0.31	−35.3	0.35	−38.1	0.2	−36.9	0.9	−42.9
0.65	−37.1	0.68	−39.2	0.41	−37.2	1.2	−43.7
1.1	−37.5	1.0	−38.3	0.82	−35.4	1.6	−44.6
1.9	−37.3	1.6	−38.6	1.61	−37.5	1.7	−42.2
2.2	−37.3	1.95	−40.2	1.82	−37.9		
				2.1	−38.0		
$\Delta H^{E,0}_{Ni_{74}Al_{23}Fe_3}$ = −37.0 ±2.3		$\Delta H^{E,0}_{Ni_{73}Al_{22}Fe_5}$ = −38.9 ±1.5		$\Delta H^{E,0}_{Ni_{71}Al_{22}Fe_7}$ = −37.4 ±0.6		$\Delta H^{E,0}_{Ni_{72}Al_{18}Fe_{10}}$ = −43.3 ±0.6	

Table 9. Experimental values of the enthalpy of dissolution of $Ni_{72}Al_{23}Cr_5$, $Ni_{70}Al_{22}Cr_8$ and $Ni_{67}Al_{21}Cr_{12}$ from room temperature in liquid aluminium at 1123 K (x, $at.\%$, ΔH $kJmol^{-1}$).

$x_{Ni,Cr}$	$\Delta H^E_{Ni_{72}Al_{23}Cr_5}$	$x_{Ni,Cr}$	$\Delta H^E_{Ni_{70}Al_{22}Cr_8}$	$x_{Ni,Cr}$	$\Delta H^E_{Ni_{67}Al_{21}Cr_{12}}$
0.3	−36.8	0.29	−35.1	0.27	−34.1
0.7	−34.8	0.96	−36.7	0.51	−34.8
0.98	−37.3	1.24	−36.9	0.85	−34.9
1.28	−36.3	1.58	−37.7	1.09	−33.6
1.66	−35.2			1.36	−36.7
1.96	−36.9			1.67	−35.7
$\Delta H^{E,0}_{Ni_{72}Al_{23}Cr_5}$ = −36.1 ±0.9		$\Delta H^{E,0}_{Ni_{70}Al_{22}Cr_8}$ = −36.6 ±0.7		$\Delta H^{E,0}_{Ni_{67}Al_{21}Cr_{12}}$ = −35.0 ±0.4	

Table 10. The enthalpy of formation of intermetallic phases at room temperature (ΔH^f, $kJmol^{-1}$).

$Ni_{75}Al_{25}$	−40.6±1.0		$Ni_{75}Al_{20}Si_5$	−42.5±1.1		$Mn_5Ni_{75}Al_{20}$	−35.9±1.1		$Ni_{74}Al_{23}Fe_3$	−39.1±1.9	
$Ni_{75}Al_{25}$	−37.6	[1]	$Ni_{75}Al_{15}Si_{10}$	−45.3±1.0		$Mn_{10}Ni_{75}Al_{15}$	−29.3±1.1		$Ni_{73}Al_{22}Fe_5$	−38.0±1.7	
$Ni_{75}Al_{25}$	−40.2	[2]	$Ni_{75}Al_{10}Si_{15}$	−44.2±1.1		$Mn_{15}Ni_{75}Al_{10}$	−24.3±1.4		$Ni_{71}Al_{22}Fe_7$	−38.8±1.4	
$Ni_{75}Al_{25}$	−37.6±5	[3]				$Mn_{20}Ni_{75}Al_5$	−19.5±1.4		$Ni_{72}Al_{18}Fe_{10}$	−37.8±1.4	
			$Ni_{69}Cu_6Al_{25}$	−40.9±1.0							
$Mn_{75}Ni_{25}$	−7.5±1.3		$Ni_{66}Cu_9Al_{25}$	−40.3±0.9		$Ni_{75}Al_{20}Ga_5$	−40.4±1.2		$Co_4Ni_{71}Al_{25}$	−40.4±1.1	
			$Ni_{63}Cu_{12}Al_{25}$	−40.7±0.9		$Ni_{75}Al_{15}Ga_{10}$	−38.9±1.3		$Co_7Ni_{68}Al_{25}$	−40.4±1.0	
$Ni_{75}Ga_{25}$	−34.8±1.0					$Ni_{75}Al_{10}Ga_{15}$	−37.4±1.2		$Co_{11}Ni_{64}Al_{25}$	−39.5±1.6	
$Ni_{75}Ga_{25}$	−26.6±0.7	[4]	$Ni_{72}Al_{23}Cr_5$	−36.7±1.4		$Ni_{75}Al_5Ga_{20}$	−36.9±1.2		$Co_{15}Ni_{60}Al_{25}$	−36.0±1.9	
$Ni_{75}Ga_{25}$	−27.4	[5]	$Ni_{70}Al_{22}Cr_8$	−35.2±1.4							
			$Ni_{67}Al_{21}Cr_{12}$	−34.9±1.3							

1. (Kubaschewski 1958), 2. (Oelsen 1937), 3. (Hultgren et al. 1973b), 4. (Martosudirjo et al. 1976), 5. (Predel et al. 1975).

Table 11. The partial enthalpies of mixing at infinite dilution of cobalt, manganese, gallium, chromium, iron, nickel, copper and silicon in liquid aluminium at different temperatures ($\Delta\overline{H}^0$ $kJmol^{-1}$).

$\Delta\overline{H}^0_{Co}$			$\Delta\overline{H}^0_{Mn}$			$\Delta\overline{H}^0_{Ga}$			$\Delta\overline{H}^0_{Cr}$		
−140.6 ±1.5	(1100 K)	[1]	−83.8 ±0.6	(1123 K)	[2]	−3.5	(1023 K)	[4]	−71.8 ±1.3	(1123 K)	[2]
−150.8 ±1.8	(1123 K)	[2]	−64.6	(1626 K)	[3]	−4.0 ±0.6	(1123 K)	[2]			
$\Delta\overline{H}^0_{Fe}$			$\Delta\overline{H}^0_{Ni}$			$\Delta\overline{H}^0_{Cu}$			$\Delta\overline{H}^0_{Si}$		
−128.5	(971 K)	[5]	−151.1	(1023 K)	[6]	−34.2	(1023 K)	[6]	−11.5	(962 K)	[5]
−119	(1023 K)	[6]	−149.4 ±1.3	(1123 K)	[2]	−34.2 ±0.1	(1123 K)	[2]	−16.6 ±1.2	(1123 K)	[2]
−120.3 ±1.6	(1123 K)	[2]	−149.1 ±1.9	(1158 K)	[7]	−33.9 ±0.3	(1191 K)	[7]	−8.7	(1760 K)	[11]
−110.8 ±3.0	(1212 K)	[7]	−136.4	(1923 K)	[9]	−38 ±3	(1473 K)	[10]			
−95.2	(1873 K)	[8]									

1. (Henig et al. 1980), 2. (this work), 3. (Esin et al. 1973), 4. (Hultgren et al. 1973b), 5. (Mathieu et al. 1967), 6. (Dannöhl 1971), 7. (Lee et al. 1985), 8. (Petrushevskiy et al. 1972), 9. (Sandakov et al. 1971a), 10. (Sandakov et al. 1971b), 11. (Batalin et al. 1981).

SOLID-STATE THERMODYNAMICS: KNUDSEN CELL MASS SPECTROMETRY AND HIGH-TEMPERATURE X-RAY DIFFRACTION

Hugo F. FRANZEN

Department of Chemistry, Iowa State University and
Ames Laboratory-DOE, Ames, Iowa 50011 USA

Abstract. -
Application of the Knudsen effusion technique to the determination of vaporization thermodynamics using simultaneous mass-loss and mass spectrometric methods of vapor pressure determination is described. The results obtained for the aluminides of the early transition metals (Zr, Nb, Mo and Ta) are reviewed.

1. - Knudsen effusion

The Knudsen effusion method is used to determine partial vapor pressures by the measurement of rates at which vapor species pass through an orifice in an isothermal enclosure containing a vaporizing condensed sample. A number of conditions must be met if such measurements are to accurately yield partial pressures, the most important of which are: 1) the sample and container must not interact significantly with the environment or with each other, 2) the transport rate must be accurately known as a function of pressure, temperature and molecular mass (here, as is generally true for Knudsen effusion, this means pressures sufficiently low that the equations of kinetic theory are valid), 3) the rate of vapor flow through the orifice must be sufficiently low relative to the rate of collision of vapor with the condensed phase that the solid and its surface are essentially equilibrated with the vapor, 4) the quantity of material that creeps or diffuses through the orifice must be negligible and 5) the crucible interior must have an essentially uniform temperature. When these conditions are met, and when the orifice channel results in negligible back reflection of the vapor (when the Clausing factor is unity), the number of molecules of the i'th species leaving the crucible in unit time is

$$R_i = \frac{dn_i}{dt} = \frac{P_i a}{\sqrt{2\pi m_i kT}}$$

where P_i is the equilibrium partial pressure of the i'th species, a is the orifice area, M_i is the molecular mass, k is Boltzmann's constant, and T is the temperature of the crucible interior.

2. - Mass spectrometry

Our experimental technique is to use a mass spectrometer to examine the vapor arising from a Knudsen crucible that is suspended from one arm of a microbalance (Fig. 1). Since we use a computer to assist in the collection of data we call the technique the Computer Assisted Simultaneous Mass-Loss and Mass-Spectrometric technique, or CASMLMS for short. This technique has strengths and weaknesses that will be discussed below with respect to conditions 1-5.

The mass spectrometer provides for the identification of the vapor species by ionization by electron impact followed by mass analysis by quadrapole mass spectrometry and detection of the ion current, I_i^+, using a multiplier. The effusing molecules pass through the ionizing region of the mass spectrometer at an average speed, S_i, determined by the crucible temperature, T

$$S_i = \frac{\sqrt{3kT}}{m_i}$$

and the number passing through the region per unit time is proportional to the effusion rate, R_i (is equal to R_i times a geometric factor equal to the fraction of all effusing molecules that arrive in the ionizing region). Thus, since the ion current is proportional to R_i and inversely proportional to S_i, the ion current is given by

$$I_i^+ = \alpha_i P_i / T$$

where α_i depends upon species dependent quantities such as the ionization cross section, the mass analyzer transmission, the multiplier efficiency and the isotopic abundances, as well as the electron beam current and the geometric factors mentioned above.

The CASMLMS technique thus provides the capability of two simultaneous measurements related to the partial pressures and, when there is a single vapor species, as in the studies discussed here, to the total pressure. The mass-loss

measurement allows a calculation of the total pressure in the case of a single species, but requires measurement times between tens and hundreds of minutes. The mass-spectrometric measurement provides a quantity (I^+T) proportional to pressure but with a measurement time on the order of seconds, or less. Thus, one advantage of the CASMLMS technique is that simultaneous measurement of mass loss and ion current over 1/2 to 10 hr intervals provides calibration of the mass spectrometer which can in turn be used to make many pressure determinations over much shorter time periods through the measurement of I^+T alone. The sensitivity of the mass spectrometer also permits the determination of the variation of ion current over relatively short time intervals, an important capability for considering condition 3, as will be discussed below.

Another benefit of simultaneous measurement is that the proportionality between I^+T and $T^{\frac{1}{2}}\Delta m/\Delta t$ can be checked at various times during data collection, and changes in instrument sensitivity or in vaporization processes that might otherwise go undetected can be noted and the resulting errors can be avoided.

3. - Experimental methods

3.1 - Sample-container interactions

Sample-container interactions may result in the chemical alteration of the condensed sample and of the vapor. An example of an interaction of the first kind is solid-solution formation. For example, a transition-metal aluminide, TAl_x, in a crucible could interact to yield transition-metal in solid solution in the crucible material. In such a case the stoichiometry, and therefore the thermodynamics, of the vaporization process would be uncertain. Since high-temperature data concerning solid-solution formation from aluminides are generally not available prior to a vaporization study, an important initial step in such a study is the investigation of such processes and the selection of an appropriate crucible material. In the work discussed here it was determined by the fact of no observable mass gain of the crucible that there is no detectable solid solution formed when the aluminides of Zr,Nb,Mo and Ta vaporize from a tungsten Knudsen crucible.

3.2. - Sample-vapor interactions

Interaction with the gas phase, given the highly reactive nature of the early transition metals towards oxygen, requires the careful consideration of the oxygen partial pressure in the interior of the crucible. The rates at which vapor species enter and leave the Knudsen crucible are given by the Knudsen equation (given above). The rate at which oxygen enters the crucible is the rate at which $H_2O(g)$ enters the cell (the residual gas at 10^{-7} torr, our working vacuum, is principally $H_2O(g)$). The rate at which oxygen leaves the cell is at least equal to the rate at which $Al_2O(g)$ leaves the crucible. The total oxygen within the cell will thus be less than the amount given by

$$R_{H_2O}^{enter} = R_{Al_2O}^{depart}$$

or

$$\frac{R_{H_2O}^{res}}{\sqrt{18T^{res}}} = \frac{P_{Al_2O}}{\sqrt{70\ T}}.$$

Assuming chemical equilibrium within the crucible,

$$K(T) = \frac{P_{Al_2O}}{P_{O_2}^{1/2}\ P_{Al}^2},$$

where K(T) can be found, for example, in the JANAF tables (Chase, et al. 1985). Combining

$$P_{O_2}^{1/2} = \frac{1}{P_{Al}^2\ K(T)}\ \frac{\sqrt{70T}}{\sqrt{18T^{res}}}\ P_{H_2O}.$$

For a typical set of conditions, T = 1700 K, T^{res} = 1700 K (because of radiation shields), K(T) = 2×10^{15}; $P_{Al} = 10^{-7}$ atm and $P_{H_2O}^{res} = 10^{10}$ atm, the steady-state value of P_{O_2} is calculated to be less than about 10^{-22} atm.

Thus, the stability of $Al_2O(g)$ under the conditions of a typical aluminide vaporization assures a condition within the cell that is far more reducing than the residual atmosphere that can be achieved by pumping, and is therefore sufficiently reducing to make oxidation of the condensed sample a negligible effect. The $Al_2O(g)$ pressure calculated for the conditions given above is 2×10^{-10} atm, a value which is several orders of magnitude below P_{Al} and thus does not interfere with measurement of P_{Al} by mass-loss.

3.3. - Rate considerations

The condition for molecular flow is readily considered. As a simple rule, the boundary for the onset of the molecular flow regime is taken to be given by a mean-free path that is substantially larger (say 10x) than the orifice diameter and data collection is restricted to this regime. The third condition, i.e., the establishment of solid-vapor equilibrium, is frequently tested by examining the

effect of orifice area upon vaporization rate. If the ratio of vaporization rate to orifice area is independent of orifice area it can be assumed with confidence that the sampled vapor is essentially at equilibrium with the condensed phase. However, if the vaporization reaction is incongruent, and therefore involves changing chemical composition of condensed material, then R/a generally does depend significantly upon a. In this case, if the deviation from equilibrium is not too large, then R/a can be plotted vs. a and extrapolated to a = 0. However, in practice such measurements are time consuming and the availability of orifice areas is limited, and therefore some uncertainty is attached to thermodynamic data obtained in this way.

On the other hand, the data obtained from such studies, and information about the chemical behavior of systems at temperature, are frequently of sufficient value that the studies are carried out in spite of this limitation. The investigations of transition-metal aluminides (T = Zr, Nb, Mo, Ta) to be discussed below fall into this category. In these studies the following technique was devised to check for a significant kinetic barrier. After a measurement of pressure at a given temperature the sample temperature was dropped to a temperature below which measurable vaporization occurred ($P_{calc} < 10^{-10}$ atm) but above which solid-state diffusion is believed to be fairly rapid ($T > 0.5\ T_{melt}$), and the sample was annealed for ten hours or more. The sample was then rapidly (< 1 minute) heated back to the original temperature and the ion current was rapidly measured. If the ion-current returned to within ±10% of the previously measured value the measurement was accepted. If the ion-current returned to a higher value and then decayed with time at constant temperature it was inferred that diffusion limited vaporization was occurring and the measurement was rejected. Since the enthalpy of vaporization is greater (roughly about two times) than the energy of activation for diffusion, it is expected that the rate of vaporization will increase with temperature more rapidly than the rate of diffusion. Thus, in the work summarized here, it was anticipated, and indeed observed, that there would be, for a given system and a given orifice, a temperature above which measurements of thermodynamic partial pressures were not possible by virtue of diffusion limited rates, and only data collected at temperatures below the diffusion limited cut-off were accepted.

3.4. - Surface diffusion and creep

The mass-spectrometer, because of the existence of a movable shutter, is capable of providing a crude measurement of the effective orifice area. Thus, as the vapor species is shut-off from the ionizing region there results an s-type curve (Fig. 2) of I^+ vs shutter position, and the width of "half maximum" of the s-curve is a measure of the orifice projected along the lines of flight of the molecules. The occurrence of creep or diffusion along the surface of the orifice channel and out onto the crucible surface results in a diffuse enlargement of the effective orifice area and can be detected by determination of a shutter profile.

3.5. - Temperature measurement and uniformity

The fifth condition, of isothermal conditions within the crucible is extremely critical. A necessary but insufficient condition for an isothermal crucible is that vaporizing sample not be transported to regions of the crucible other than the region of the source sample. One of the experimental factors of importance in vaporization studies is that they are typically at high temperatures (>1500°K) and at these temperatures radiative heat transfer is important (radiative heat transfer increases as the fourth power of T). Thus, our experimental design includes radiation shields that are designed to produce, in so far as is possible, an isothermal enclosure in which the crucible is suspended. The temperature is measured using a W–Re alloy thermocouple inside a Ta shield with BeO insulators, and the tip of this thermocouple is located within ca. 1 mm of the Knudsen crucible. Prior to a vaporization study the thermocouple is calibrated by intercomparison with a Pt–Rh alloy thermocouple that is placed inside the crucible.

The effectiveness of this calibration, and of the radiation shielding is difficult to estimate. The criterion used in this work to determine whether there are or are not serious temperature measurement errors is a standard in high-temperature vaporization studies, namely the comparison of enthalpy changes determined by second- and third-law calculation.

4. - Data reduction

Using the free energy function $(G^\circ_T - H^\circ_{298})/T = fef$ and considering a reaction such as

$$TAl_x(s) = TAl_y(s) + (y-x)Al(g)$$

for which $\Delta G^\circ_T = RT \ln P_{Al}$, it follows that

$$\Delta fef = -R \ln P_{Al}^{y-x} - \Delta H^\circ_{298}/T,$$

or

$$\Delta fef + R \ln P_{Al}^{y-x} = -\Delta H^\circ_{298}/T.$$

This equation can be used in two independent ways. The first is to plot the left-hand side vs T^{-1} and determine the slope. One ΔH°_{298} value results from a least slope determination for a given data set. This slope is a best-fit measure of ΔH°_{298} if the differences between the fef values:

$$\text{fef} = \frac{H^\circ_T - H^\circ_{298}}{T} - S^\circ_T,$$

$$= \frac{1}{T}\int_{298}^{T} Cp^\circ\, dT - \int_{0}^{T} Cp^\circ/T\, dT - S^\circ_0$$

are known with sufficient accuracy over the temperature interval of the measurements. This result depends only on the 0th, 1st and 2nd laws of thermodynamics, i.e., only entropy differences, and not absolute entropies enter into the calculation. The second way to obtain ΔH°_{298} values from the equation under discussion is to use values for Δfef, which typically depend upon the validity of the third law ($\lim_{T\to 0} \Delta S^\circ = 0$), P_{Al} and T and calculate a different ΔH°_{298} value for each measured T, P_{Al} pair.

It should be remarked that Cp data for all reactants and products between 0 K and T > 1500°K are seldom available and therefore estimations are usually required in order to do the calculations. However, heat capacity data are frequently well known for vapor species from spectroscopic measurements, and the estimation of heat capacities of solids is a thoroughly considered problem and fairly good estimates of the uncertainties involved are available.

The two methods of data reduction, called the second-law and third-law methods, provide two methods for checking for significant temperature measurement errors. First, the ΔH°_{298} values obtained by the third-law method are checked for systematic variation over the temperature ranges. The ΔH°_{298} values should all be the same within acceptable uncertainty, and variation outside of magnitudes that could result from inaccurate estimates in fef's is indicative of temperature measurement or gradient error. The second check is accomplished by comparing the average third-law value with the single second-law value for ΔH°_{298}. A significant disparity between these values is indicative of temperature measurement errors.

5. - Results for Mo-Al

One of our early studies was of the Mo-Al system (Shilo and Franzen 1982) and the quality of the results is typical of our studies by CASMLMS. Fig. 3 shows aluminum pressure isotherms, Fig. 4 shows a second-law plot of ln P_{Al} vs T^{-1} for the Mo_3Al_8–Mo_3Al vaporization and Fig. 5 shows a plot indicating the proportionality between the pressures derived from mass-loss and mass-spectrometrically obtained data. Table 1 lists the enthalpies of formation of the Mo-rich intermetallics as determined in this work. Fig. 6 shows the phase diagram reported for the Mo-Al system together with some points determined from the breaks in our isotherms. Note that our phase boundaries were determined at temperature, and that MoAl, for which data were obtained, is unstable with respect to disproportionation below 1740°K. These results illustrate the power of the effusion method to determine chemical information at temperature and in a highly reducing environment.

6. - Summary of enthalpies of vaporization for transition-metal aluminides

The second column of Table 2 lists the enthalpies of atomization per gram atom, i.e., ΔH°_{298} for the reaction

$$\frac{1}{1+x}\,TAl_x(s) = \frac{1}{1+x}\,T(g) + \frac{x}{1+x}\,Al(g)$$

where T is Zr (Kematick and Franzen 1984), Nb (Shilo et al. 1982), Mo (Shilo and Franzen 1982) or Ta (Schmidt and Franzen 1986) and the x values are those for which we were able to make an enthalpy determination. The $\Delta H^\circ_{vap,298}$ values for the transition metals were obtained from the Atomic Energy Review (for Zr, No. 6 (Alcock, et al. 1976), for Nb, No. 2 (Lavrentev and Gerassimov 1968), for Mo, No. 7 (Brewer and Lamoreaux 1980)) and for Ta the JANAF tables (Chase 1985), and that for Al was taken from (Hultgren, et al. 1973). It is found that in each system these cohesive or bond energies can be fit to a two parameter equation

$$\frac{\Delta H^\circ_{vap}\,(T_mAl_n)}{(m+n)} = \left(\frac{m}{m+n}\right) A + \left(\frac{n}{m+n}\right) B,$$

where the A and B values determined by least squares are given in Table 3. The values given in column 3 of Table 2 are those calculated using the values of Table 3. Column 4 of Table 2 lists the difference between the calculated and observed quantities.

The fit between calculated and observed values of enthalpies of vaporization or cohesive energies shown by the data of Table 2 suggests the following interpretation: When an intermetallic compound forms it does so in such a way as to realize a maximum bond energy. For example, in the case of the aluminides of zirconium (Kematick and Franzen 1984), Zr brings to the intermetallic

compounds the capacity to form bonds yielding 154.3 kcal per g atom and Al brings the capacity to yield 88.5 kcal. The observed stoichiometries and structures are those that provide the framework within which the elements can realize this bonding potential to within about ±1 kcal per g atom. If this potential is not realized in a hypothetical compound, then that compound will be unstable with respect to disproportionation, and will not be observed. This interpretation is supported not only by the data of Table 2 and similar data for other systems (Schmidt 1986), but also by the well known fact that enthalpy changes accompanying solid-state phase transitions are very much smaller than the vaporization enthalpies of the compounds, i.e., changes in structure occur between phases for which bond energies are very nearly the same.

7. - High-temperature X-ray diffraction (HTXRD)

In the last several years we have been using a high-temperature X-ray diffractometer capable of providing X-ray diffraction patterns for samples at temperatures up to 2000°C to examine heterogeneous behavior in far greater detail than has been possible using the Knudsen technique alone. For example, Fig. 7 shows the diffractometer patterns for Ta–Ru samples at room temperature, 1000 K, 1173 K and 1433 K showing the consecutive cubic —> tetragonal and tetragonal --> orthorhombic transitions. Fig. 8 shows the phase diagram inferred from the diffraction study.

8. - The Lu-S system

An interesting example of the complementary uses of Knudsen effusion and HTXRD was provided by an investigation of the Lu–S system. Some years ago (Franzen and Hariharan 1979) we found that $Lu_{0.75}S$ vaporizes congruently and reported (Hariharan et al. 1981) an unusual partially ordered superstructure of NaCl-type for Lu_3S_4. Now, by virtue of HTXRD studies, we have a somewhat different view of the system. The key experiment was the formation of a sample by the decomposition of Lu_2S_3 with the α-Al_2O_3-type structure by vaporization from a W Knudsen cell, and further examination of this sample by HTXRD. We found: 1. that the sample obtained by decomposition of Lu_2S_3, which we call $Lu_{2+x}S_3$, no longer has the α-Al_2O_3 structure, but has a powder pattern identical to that of the $Lu_{0.75}S$ sample obtained in prior studies, 2. that this $Lu_{2+x}S_3$ transforms to NaCl-type at high temperatures (above about 1200°C), and 3. the intensities of the $Lu_{2+x}S_3$ powder pattern are not fit well by a calculation based upon the Lu_3S_4 structure, we reported previously. A Rietveld full-profile refinement of the powder diffraction data for room-temperature $Lu_{2+x}S_3$ showed that it has the Sc_2S_3-type structure (Dismukes 1964) a vacancy ordered superstructure of NaCl-type.

A phase diagram that summarizes these findings is shown in Fig. 9. The congruently vaporizing phase is $Lu_{0.75}S$ with the defect NaCl-type (random vacancies) structure. When cooled to a sufficiently low temperature the Sc_2S_3-type phase precipitates out of the random solid solution (this is a first-order, order-disorder process). This behavior was difficult to discern in part because the strong reflections from both the NaCl-type and the Sc_2S_3-type phases overlap and are separated only by maximum resolution (Guinier) and then only for some S/Lu ratios. The HTXRD experiment showed that $Lu_{2+x}S_3$ with the Sc_2S_3-type structure transforms to NaCl-type at high-temperature, and thus that a supposed congruently vaporizing Lu_3S_4 does not intervene between the NaCl-type and the Sc_2S_3-type phase. The phase to which the Lu_3S_4 structure corresponds remains to be explained. It seems likely, perhaps even necessary, that this structure does not correspond to an equilibrium phase. There were many twinned crystals found in the search for a single crystal of Lu_3S_4, and the final structure (Hariharan et al. 1981) obtained for Lu_3S_4 is a highly unusual partially ordered structure. It is therefore, probable that the structure was determined from a crystal, perhaps one of many different such crystals, within which the ordering from NaCl-type to Sc_2S_3-type was incomplete when the sample was quenched to room temperature.

9. - Conclusions

The CASMLMS technique for the study of high-temperature chemical behavior and the determination of enthalpy changes for reactions at high temperatures was described. The conditions that must be met in order that a Knudsen effusion study can produce meaningful thermodynamic results, and the methodology for considering these conditions in the case of the CASMLMS technique were reviewed. It was shown that the transition-metal aluminides provide nearly ideal examples for study by this technique. The results of four such studies were used to demonstrate a "chemical-bonding" interpretation for the formation of intermetallic compounds. The HTXRD technique, especially in combination with Knudsen effusion, was shown to provide a uniquely powerful method for analyzing heterogeneous behavior at high-temperature.

Acknowledgement

The Ames Laboratory-DOE is operated for the U. S. Department of Energy by Iowa State University under Contract No. W-7405-Eng-82. This research was supported by the Office of Basic Energy Sciences, Materials Sciences Division.

References

Alcock, C. B., Jacob, K. T., and Zador, S. (1976): Atomic Energy Review, No. 6, ed., O. Kubaschewski (International Atomic Energy Agency, Vienna), p. 7.

Brewer, L. and Lamoreau, R. H. (1980): Atomic Energy Review, No. 7, ed., Brewer, L. (International Atomic Energy Agency, Vienna), p. 11.

Chase, M. W., Jr., Davies, C. A., Downey, J. R., Jr., Frurip, D. J., MacDonald, R. A., and Syverud, A. N. (1985): JANAF Thermochemical Tables, 3rd ed., (American Chemical Society and the American Institute of Physics for the National Bureau of Standards).

Dismukes, J. P. and White, J. G. (1964): *Inorg. Chem.* 3, 1220.

Franzen, Hugo F. and Hariharan, Alleppey V. (1979): *J. Chem. Phys.* 70, 4907.

Hariharan, A. V., et al. (1981): D. R. Powell, R. A. Jacobson and H. F. Franzen, *J. Solid State Chem.* 36, 148.

Hultgren, R., Desai, P. D., Hawkins, D. T., Gleiser, M., Kelley, K. K., and Wagman, D. D. (1973): Selected Values of the Thermodynamic Properties of the Elements, American Society for Metals, Metals Park, OH.

Kematick, R. J. and Franzen, H. F. (1984): *J. Solid State Chem.* 54, 226.

Lavrentev, V. I. and Gerassimov, Ya. I. (1968): Atomic Energy Review, No. 2, ed., Kubaschewski, O. (International Atomic Energy Agency, Vienna), p. 7.

Schmidt, Stephen R. and Franzen, Hugo F. (1986): *J. Less-Common Met.* 116, 73.

Shilo, I., Franzen, H. F. and Schiffman, R. A. (1982): *J. Electrochem. Soc.* 129, 1608.

Shilo, I. and Franzen, H. F. (1982): *J. Electrochem. Soc.* 129, 2613.

Table 1

Compound	ΔH_f° (kcal/mol) per gram atom 2nd Law	3rd Law
Mo_3Al_8	−11.2 (3)	−9.4 (1)
MoAl	−6.6 (4)	−7.5 (2)
Mo_3Al	−6.6 (5)	−5.1 (1)

Table 2

	ΔH°_{vap} (kJ/g atm) Obs	Calc	Δ
$ZrAl_3$	104.7	105.2	+0.5
$ZrAl_2$	111.3	110.7	−0.4
Zr_2Al_3	115.8	115.0	−0.8
ZrAl	121.9	121.6	−0.3
Zr_5Al_4	125.2	125.2	—
Zr_3Al_2	127.4	128.1	+0.7
Zr_5Al_3	128.6	129.8	+1.2
$NbAl_3$	134.8	134.9	+0.1
Nb_2Al	166.2	164.3	−1.9
Nb_3Al	168.2	170.2	+2.0
Mo_3Al_8	111.3	111.1	−0.2
MoAl	124.6	128.6	+1.0
Mo_3Al	144.3	142.6	−1.7
$TaAl_3$	111.5	111.2	−0.3
Ta_2Al_3	126.4	126.3	−0.1
Ta_2Al	153.4	153.3	−0.1
Ta_3Al	162.0	161.7	−0.3
Ta_4Al	167.3	166.8	−0.5

Enthalpies of vaporization (atomization) as determined by CASMLMS

Table 3

	A(kcal)	B(kcal)
Zr–Al	154.3	88.5
Nb–Al	187.7	117.2
Mo–Al	159.1	93.0
Ta–Al	187.0	85.9

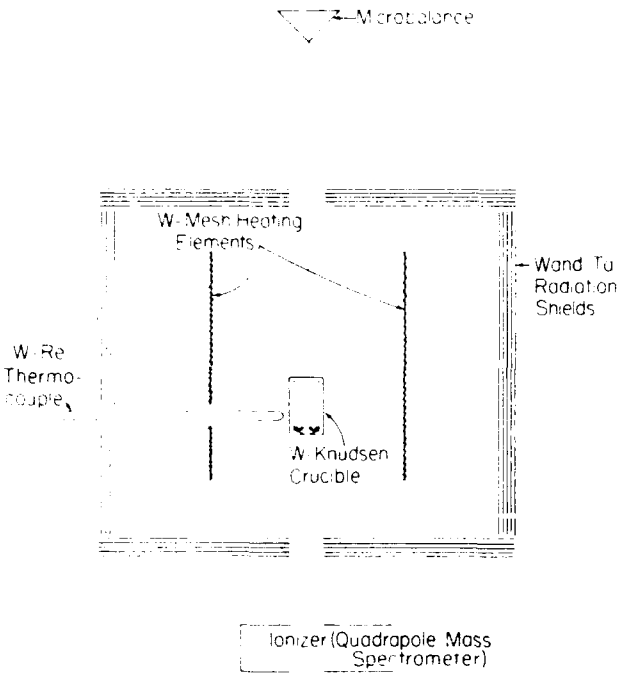

1. Mass-Loss, Mass-Spectrometer Apparatus for Knudsen Effusion Studies

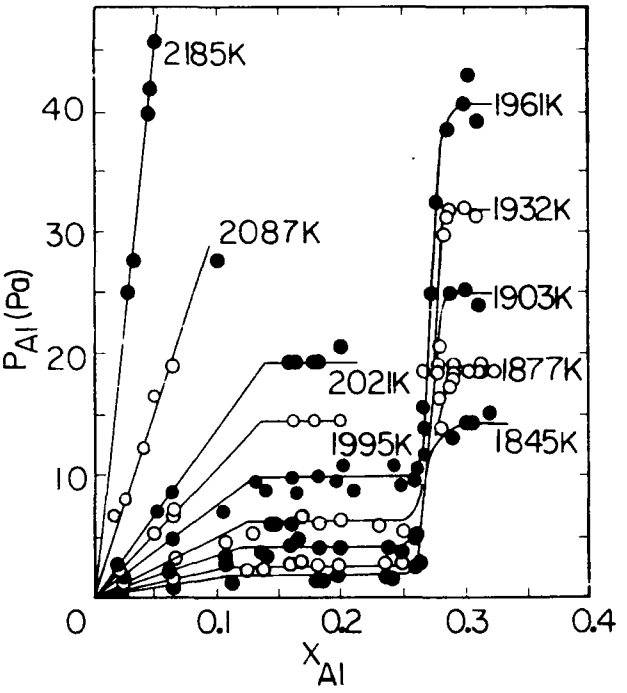

3. Vapor Pressure Isotherms for the Mo_3Al_8-Mo_3Al Reaction

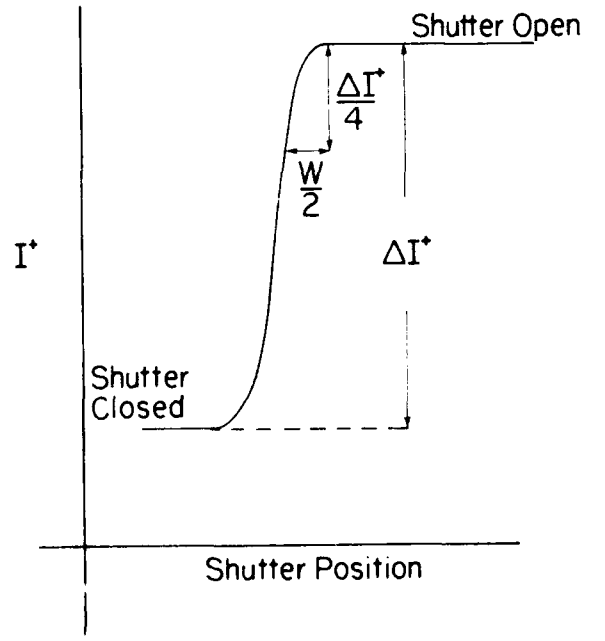

2. Schematic Shutter Profile

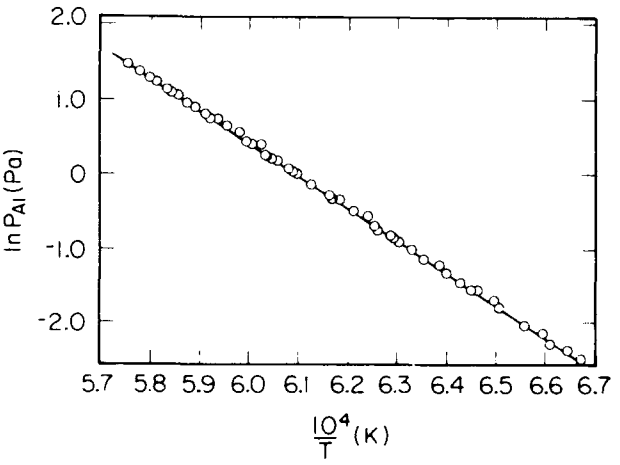

4. lnP vs. T^{-1} for the Mo_3Al_8-Mo_3Al Reaction

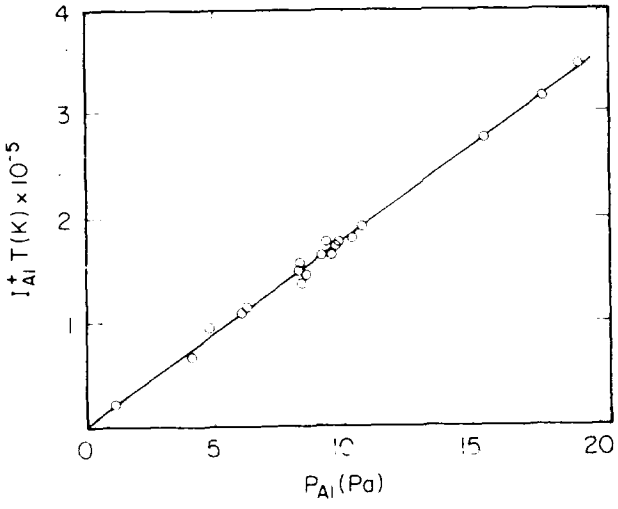

[illegible] Current vs. Aluminum Pressure as Determined by Mass Ross (Mo-Al System)

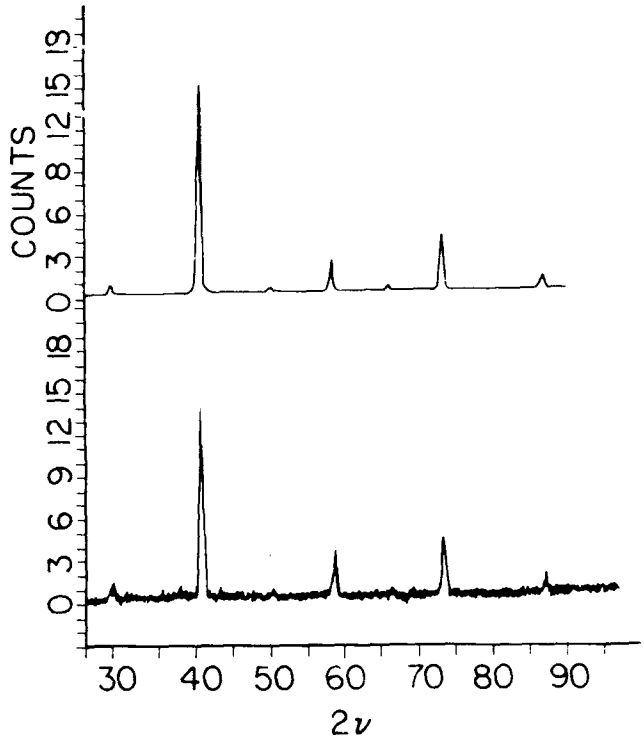

7a. Calculated and observed X-Ray Diffraction Pattern for Cubic Ruta

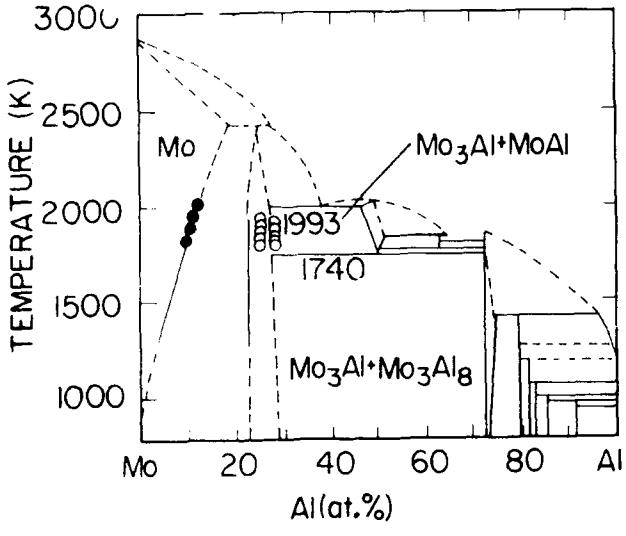

[illegible] Mo-Al Phase Diagram

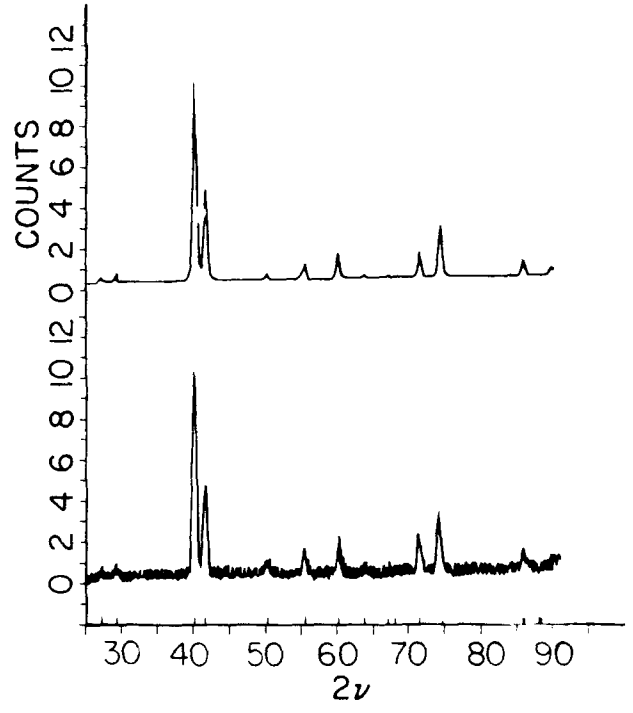

7b Calculated and observed X Ray Diffraction Pattern for Tetragonal Ruta

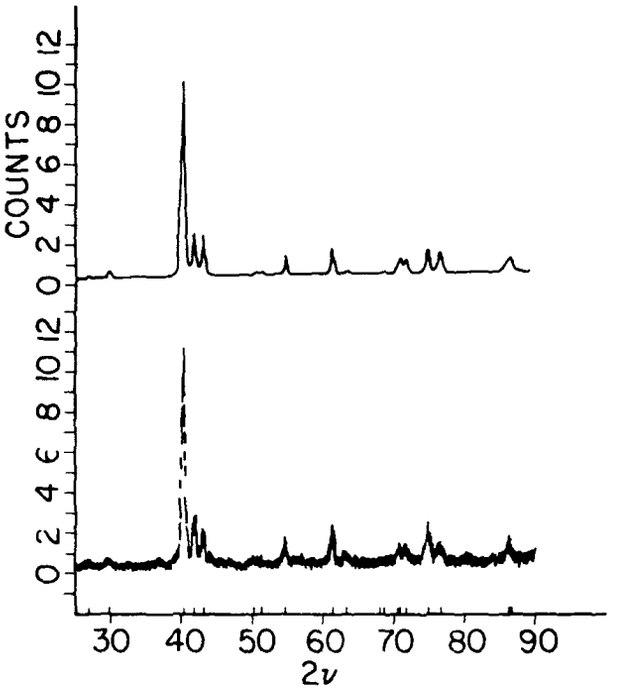

7c. Calculated and observed X-Ray Diffraction Pattern for Orthor ombir ruta.

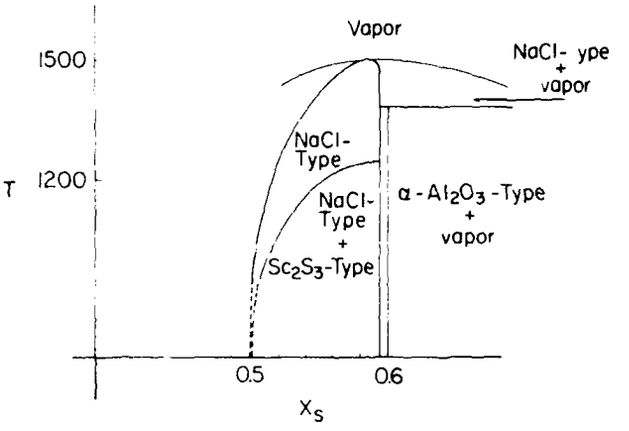

9. Schematic Lu-S Phase Dragram in the $LuS-Lu_2S_3$ Region at Elevated Temperatures

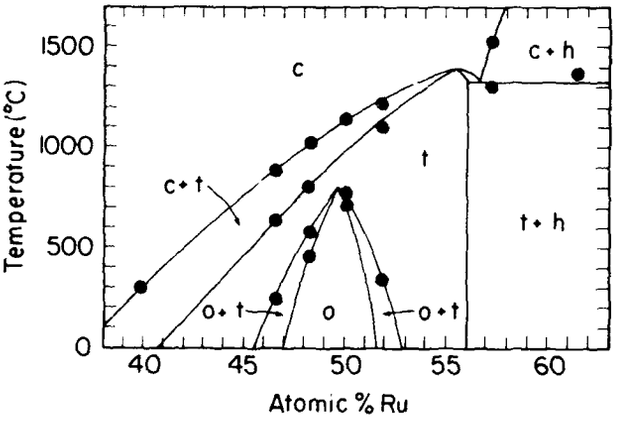

8. Ru-Ta Temperature-Compositon Phase Dragram.

SIMPLE FORMS OF THE GIBBS-DUHEM INTEGRATION FOR k–GASEOUS MULTICOMPONENT SYSTEMS

Zhi-Chang WANG, Reinhard LÜCK and Bruno PREDEL

Max-Planck-Institut für Metallforschung
Institut für Werkstoffwissenschaft
Seestrasse 75, D-7000 Stuttgart 1
F. R. Germany

Abstract. -

Three alternative simple procedures for the Gibbs–Duhem integration have been presented for di-gaseous quaternary systems in order to calculate unknown activities of two components from known activities of the other two components. Extension to k–gaseous $(k+2)$–component systems has also been given, here k is any positive integer. Each one only requires one set of integration and one set of differentiation for a homogeneous phase. The differentiation can be omitted when one of them is applied to a multiphase and its boundary. The results have been extended to k–gaseous c–component systems with $c \geq k+2$.

1. – Introduction

As is well known, if the activity of one component has experimentally been known in a ternary or multicomponent system, activities of all other components in the system could be calculated by using one of the procedures of the Gibbs-Duhem integration proposed by Darken (1950), Wagner (1952), Schuhmann (1955), Gokcen (1960), Arita and St. Pierre (1977), Chou (1978), Korpachev et al. (1979), Wang (1981) as well as Wang and Chou (1984), respectively.

If there exist two or more volatile components in the systems, however, activities of all these volatile components could be measured simultaneously, for example, by using isopiestic method, Knudsen effusion method or chemical equilibrium method. It is therefore required to present new forms of the Gibbs-Duhem integration to calculate the unknown activities of the involatile components in the systems from the known activities of the two or more components.

Nagamori and Yazawa (1988) first presented such an procedure of the Gibbs–Duhem integration for quaternary systems involving two volatile components and two involatile components. As pointed out by them, however, their equations are very complex. The unknown activity of the third component in a quaternary system $1-2-3-4$, for example, should be calculated by the following equation:

$$\begin{aligned} ln a_3 &= (ln a_3)_{x_2=0} \\ &+ \int_0^{x_2} \frac{y x_2}{(1-x_1-x_2)^2} \left(\frac{\partial x_1}{\partial y}\right)_{p_2,p_1} \left(\frac{\partial ln p_2}{\partial x_2}\right)_{y,p_1} dx_2 \\ &+ \int_0^{x_2} \frac{-y(1-x_1)}{(1-x_1-x_2)^2} \left(\frac{\partial ln p_2}{\partial y}\right)_{x_2,p_1} dx_2 \\ &+ \int_0^{x_2} \frac{-x_2}{1-x_1-x_2} \left(\frac{\partial ln p_2}{x_2}\right)_{y,p_1} dx_2 \\ &(y = const. \quad \text{and} \quad p_1 = const.) \end{aligned} \tag{1}$$

from known activities of the first and second components and from the known initial condition of the 1-3-4 ternary subsystem, using three sets of differentiation and three sets of integration, according to eqns. (33)-(37) in the reference; where x_1, x_2, x_3, x_4 and a_1, a_2, a_3, a_4 are atomic (or mole) fractions and activities of components 1, 2, 3 and 4 in the quaternary system, respectively; p_1 and p_2 are partial pressures of the components 1 and 2, respectively; and y is a composition ratio defined by

$$y = \frac{x_4}{x_3 + x_4}. \tag{2}$$

Notice that the symbols x and y here have different meaning from those defined by Nagamori and Yazawa (1988). The purpose of this paper is to simplify the procedure mentioned above and to extend the results to k-gaseous $(k+2)$-component systems and k-gaseous c-component systems, here $c \geq k+2$ and k refers to any positive integer.

2. – Three alternative simple procedures for quaternary systems

Let μ_1, μ_2, μ_3 and μ_4 be the chemical potentials of the components 1, 2, 3 and 4, respectively, in the $1-2-3-4$ quaternary system, let G be the molar Gibbs free energy of the system and let the superscript E refer to excess functions. Basic thermodynamic equations for the quaternary system may be

$$G^E = x_1\mu_1^E + x_2\mu_2^E + x_3\mu_3^E + x_4\mu_4^E, \tag{3}$$

$$dG^E = \mu_1^E dx_1 + \mu_2^E dx_2 + \mu_3^E dx_3 + \mu_4^E dx_4 \tag{4}$$

and

$$x_1 d\mu_1^E + x_2 d\mu_2^E + x_3 d\mu_3^E + x_4 d\mu_4^E = 0. \tag{5}$$

2.1. – Procedure A.

From eqn. (3)

$$\langle A_{\{q\}}\rangle \equiv \frac{G^E}{x_3+x_4} = \frac{x_1\mu_1^E + x_2\mu_2^E}{x_3+x_4} + (1-y)\mu_3^E + y\mu_4^E. \quad (6)$$

Differentiating eqn. (6) and comparing the results with eqn. (5), we have

$$d\langle A_{\{q\}}\rangle = \mu_1^E d\frac{x_1}{x_3+x_4} + \mu_2^E d\frac{x_2}{x_3+x_4} + (\mu_4^E - \mu_3^E)dy, \quad (7)$$

which yields

$$\langle A_{\{q\}}\rangle = (\langle A_{\{q\}}\rangle)_{x_1=0} + \int_0^{\frac{x_1}{x_3+x_4}} \mu_1^E d\frac{x_1}{x_3+x_4} \quad (y = const. \text{ and } \frac{x_2}{x_3+x_4} = const.), \quad (8)$$

$$\langle A_{\{q\}}\rangle = (\langle A_{\{q\}}\rangle)_{x_2=0} + \int_0^{\frac{x_2}{x_3+x_4}} \mu_2^E d\frac{x_2}{x_3+x_4} \quad (y = const. \text{ and } \frac{x_1}{x_3+x_4} = const.) \quad (9)$$

and

$$\mu_4^E - \mu_3^E = (\frac{\partial\langle A_{\{q\}}\rangle}{\partial y})_{\frac{x_1}{x_3+x_4},\frac{x_2}{x_3+x_4}}. \quad (10)$$

Since

$$d\frac{x_1}{x_3+x_4} = \frac{1}{(1-x_1)^2}(1+\frac{x_2}{x_3+x_4})dx_1$$

at the condition of y=const. and $x_2/(x_3+x_4)$=const. as well as

$$d\frac{x_2}{x_3+x_4} = \frac{1}{(1-x_2)^2}(1+\frac{x_1}{x_3+x_4})dx_2$$

at the condition of y=const. and $x_1/(x_3+x_4)$=const., eqns. (8) and (9) can, respectively, be rewritten as

$$\frac{\langle A_{\{q\}}\rangle}{1+x_2/(x_3+x_4)} = \frac{G^E}{1-x_1} = (G^E)_{x_1=0} + \int_0^{x_1}\alpha_1 dx_1 \quad (y = const. \text{ and } \frac{x_2}{x_3+x_4} = const.) \quad (11)$$

and

$$\frac{\langle A_{\{q\}}\rangle}{1+x_1/(x_3+x_4)} = \frac{G^E}{1-x_2} = (G^E)_{x_2=0} + \int_0^{x_2}\alpha_2 dx_2 \quad (y = const. \text{ and } \frac{x_1}{x_3+x_4} = const.), \quad (12)$$

where α is a known function defined by

$$\alpha_1 = \frac{\mu_1^E}{(1-x_1)^2} \quad \text{and} \quad \alpha_2 = \frac{\mu_2^E}{(1-x_2)^2}. \quad (13)$$

Multiplying eqn. (10) by y and combining the results with eqn. (6), we have

$$\mu_3^E = \{\frac{\partial[\langle A_{\{q\}}\rangle/y)}{\partial(1/y)}\}_{\frac{x_1}{x_3+x_4},\frac{x_2}{x_3+x_4}} - \frac{x_1\mu_1^E + x_2\mu_2^E}{x_3+x_4}. \quad (14)$$

From eqns. (10) and (14)

$$\mu_4^E = \{\frac{\partial[\langle A_{\{q\}}\rangle/(1-y)]}{\partial[1/(1-y)]}\}_{\frac{x_1}{x_3+x_4},\frac{x_2}{x_3+x_4}} - \frac{x_1\mu_1^E + x_2\mu_2^E}{x_3+x_4}. \quad (15)$$

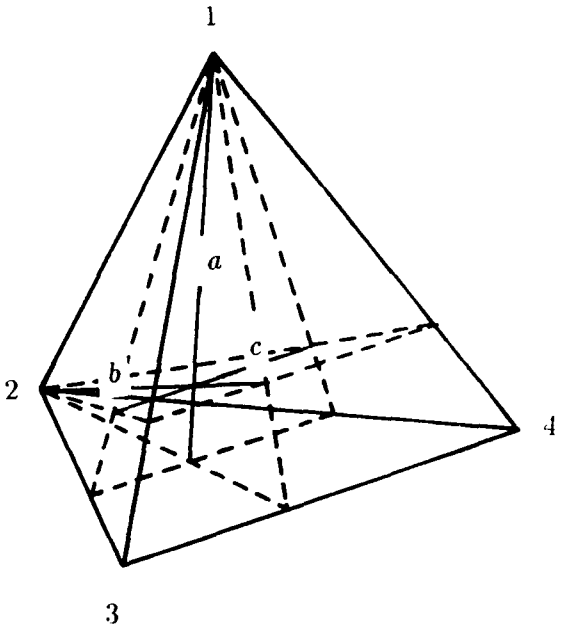

Figure 1. Integration and differentiation paths for the procedure A in a quaternary system 1-2-3-4. *a*, integration path for eqn. (11), *b*, integration path for eqn. (12) and *c*, differentiation path for eqns. (14) and (15).

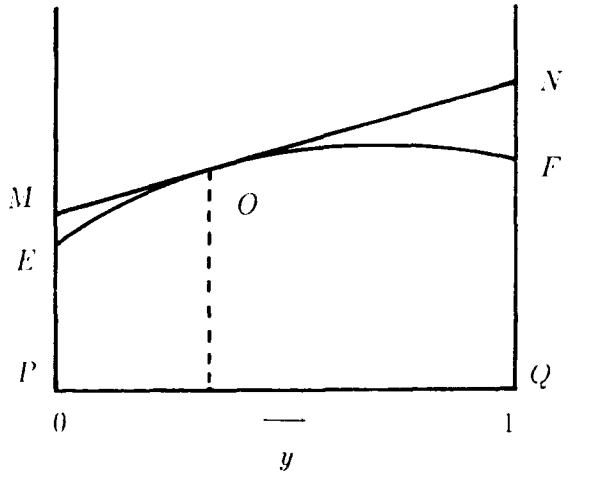

Figure 2. Relation between partial molar quantities and $\langle A_{\{q\}}\rangle$, $\langle B_{\{q\}}\rangle$ or $\langle C_{\{q\}}\rangle$. $MP = \mu_3^E + \frac{x_1\mu_1^E + x_2\mu_2^E}{x_3+x_4}$ and $NQ = \mu_4^E + \frac{x_1\mu_1^E + x_2\mu_2^E}{x_3+x_4}$ when EOF denotes $\langle A_{\{q\}}\rangle$ against y at constant $x_1/(x_3+x_4)$ and $x_2/(x_3+x_4)$; $MP = \mu_3^E + RTln(x_3+x_4)$ and $NQ = \mu_4^E + RTln(x_3+x_4)$ when EOF denotes $\langle B_{\{q\}}\rangle$ against y at constant a_1 and a_2; as well as $MP = \mu_3^E + \frac{x_2\mu_2^E + RTx_2[1+ln(x_3+x_4)]}{x_3+x_4} + RTln(x_3+x_4)$ and $NQ = \mu_4^E + \frac{x_2\mu_2^E + RTx_2[1+in(x_3+x_4)]}{x_3+x_4} + RTln(x_3+x_4)$ when EOF denotes $\langle C_{\{q\}}\rangle$ against y at constant a_1 and $x_2/(x_3+x_4)$.

Curves a and b in Fig. 1 illustrate the alternative integration paths expressed, respectively, in eqns. (11) and (12), while the curve c, the differentiation path expressed in both eqns. (14) and (15). After $\langle A_{\{q\}}\rangle$ has been calculated in terms of either eqn. (11) or (12), both μ_3^E and μ_4^E may be calculated at the same time in terms of eqns. (14) and (15) along the curves of $x_1/(x_3+x_4)$=const. and $x_2/(x_3+x_4)$=const. as illustrated in Fig. 2. Only one set of integration and one set of differentiation is required.

From eqn. (10)

$$\int_0^1 (\mu_4^E - \mu_3^E)dy = (\langle A_{\{q\}}\rangle)_{1-2-4\ ternary} - (\langle A_{\{q\}}\rangle)_{1-2-3\ ternary} \quad (\frac{x_1}{x_3+x_4} = const. \text{ and } \frac{x_2}{x_3+x_4} = const.). \tag{16}$$

Similarly,

$$\int_0^1 (\mu_2^E - \mu_1^E)d\frac{x_2}{x_1+x_2} = (\langle A_{\{q\}}\rangle)_{1-3-4\ ternary} - (\langle A_{\{q\}}\rangle)_{2-3-4\ ternary} \quad (\frac{x_3}{x_1+x_2} = const. \text{ and } \frac{x_4}{x_1+x_2} = const.). \tag{17}$$

Equations (16) and (17) can, respectively, be used for checking the thermodynamic consistency between the data of the quaternary system and its binary and ternary subsystems.

2.2. – Procedure B.

Equation (6) can be rewritten as

$$\langle B_{\{q\}}\rangle \equiv \frac{G^E - x_1\mu_1^E - x_2\mu_2^E}{x_3+x_4} + RTln(x_3+x_4) = (1-y)\mu_3^E + y\mu_4^E + RTln(x_3+x_4). \tag{18}$$

Differentiating eqn. (18) and comparing the results with eqn. (5), we have

$$d\langle B_{\{q\}}\rangle = -RT\frac{x_1}{x_3+x_4}dlna_1 - RT\frac{x_2}{x_3+x_4}dlna_2 + (\mu_4^E - \mu_3^E)dy \tag{19}$$

since

$$dln(x_3+x_4) = -\frac{x_1}{x_3+x_4}dlnx_1 - \frac{x_2}{x_3+x_4}dlnx_2.$$

Equation (19) yields

$$\langle B_{\{q\}}\rangle = (\langle B_{\{q\}}\rangle)_{a_1=0} - RT\int_0^{a_1}\frac{x_1/a_1}{x_3+x_4}da_1 \quad (y = const. \text{ and } a_2 = const.), \tag{20}$$

$$\langle B_{\{q\}}\rangle = (\langle B_{\{q\}}\rangle)_{a_2=0} - RT\int_0^{a_2}\frac{x_2/a_2}{x_3+x_4}da_2 \quad (y = const. \text{ and } a_1 = const.) \tag{21}$$

and

$$\mu_4^E - \mu_3^E = \{\frac{\partial\langle B_{\{q\}}\rangle}{\partial y}\}_{a_1,a_2}. \tag{22}$$

Multiplying eqn. (22) by y and combining the results with eqn. (18), we have

$$\mu_3^E = \{\frac{\partial\langle B_{\{q\}}\rangle/y)}{\partial(1/y)}\}_{a_1,a_2} - RTln(x_3+x_4). \tag{23}$$

From eqns. (22) and (23)

$$\mu_4^E = \{\frac{\partial[\langle B_{\{q\}}\rangle/(1-y)]}{\partial[1/(1-y)]}\}_{a_1,a_2} - RTln(x_3+x_4). \tag{24}$$

Curves a and b in Fig. 3 illustrate the alternative integration paths expressed respectively in eqns. (20) and (21) and the curve c, the differentiation path for both eqns. (23) and (24). Therefore, after $\langle B_{\{q\}}\rangle$ has been calculated in terms of either eqn. (20) or (21), both μ_3^E and μ_4^E may be calculated at the same time in terms of eqns. (23) and (24) along the curves of a_1=const. and a_2=const. as illustrated in Fig. 2. The procedure also involves one set of integration and one set of differentiation.

2.3. – Procedure C.

Equation (6) can also be rewritten as

$$\langle C_{\{q\}}\rangle \equiv \frac{G^E - x_1\mu_1^E + RTx_2[1+ln(x_3+x_4)]}{x_3+x_4} + RTln(x_3+x_4) = \frac{x_2\mu_2^E}{x_3+x_4} + (1-y)\mu_3^E + y\mu_4^E + \frac{RTx_2[1+ln(x_3+x_4)]}{x_3+x_4} + RTln(x_3+x_4). \tag{25}$$

Differentiating eqn. (25) and comparing the results with eqn. (5), we have

$$d\langle C_{\{q\}}\rangle = -RT\frac{x_1}{x_3+x_4}dlna_1 + \{\mu_2^E + RTln(x_3+x_4)\}d\frac{x_2}{x_3+x_4} + (\mu_4^E - \mu_3^E)dy \tag{26}$$

since

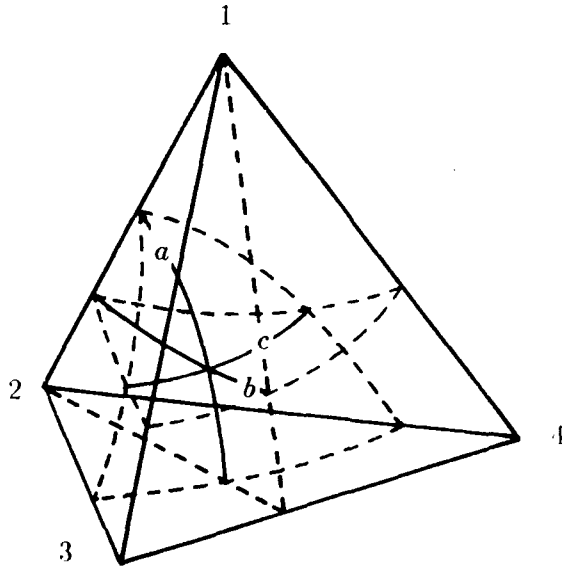

Figure 3. Integration and differentiation paths for the procedure B in a quaternary system 1-2-3-4: a, integration path for eqn. (20), b, integration path for eqn. (21) and c, differentiation path for eqns. (23) and (24).

$$d\frac{(1-x_1)ln(x_3+x_4)}{x_3+x_4} = \frac{1-x_1}{x_3+x_4}dln(x_3+x_4) + ln(x_3+x_4)d\frac{x_2}{x_3+x_4}$$

and

$$\frac{1-x_1}{x_3+x_4}dln(x_3+x_4) = -\frac{x_1}{x_3+x_4}dlnx_1 - d\frac{x_2}{x_3+x_4}.$$

Equation (26) yields

$$\langle C_{\{q\}}\rangle = (\langle C_{\{q\}}\rangle)_{a_1=0} - RT\int_0^{a_1}\frac{x_1/a_1}{x_3+x_4}da_1 \quad (y = const. \text{ and } \frac{x_2}{x_3+x_4} = const.), \tag{27}$$

$$\langle C_{\{q\}}\rangle = (\langle C_{\{q\}}\rangle)_{x_2=0} + \int_0^{\frac{x_2}{x_3+x_4}}\{\mu_2^E + RTln(x_3+x_4)\}d\frac{x_2}{x_3+x_4} \quad (y = const. \text{ and } a_1 = const.) \tag{28}$$

and

$$\mu_4^E - \mu_3^E = (\frac{\partial\langle C_{\{q\}}\rangle}{\partial y})_{a_1,\frac{x_2}{x_3+x_4}}. \tag{29}$$

Multiplying eqn. (29) by y and combining the results with eqn. (25), we have

$$\mu_3^E = (\frac{\partial\{\langle C_{\{q\}}\rangle/y\}}{\partial\{1/y\}})_{a_1,\frac{x_2}{x_3+x_4}} - \frac{x_2\mu_2^E}{x_3+x_4} - RTln(x_3+x_4) - \frac{RTx_2[1+ln(x_3+x_4)]}{x_3+x_4}. \tag{30}$$

From eqns. (29) and (30)

$$\mu_4^E = (\frac{\partial\{\langle C_{\{q\}}\rangle/(1-y)\}}{\partial\{1/(1-y)\}})_{a_1,\frac{x_2}{x_3+x_4}} - \frac{x_2\mu_2^E}{x_3+x_4} - RTln(x_3+x_4) - \frac{RTx_2[1+ln(x_3+x_4)]}{x_3+x_4}. \tag{31}$$

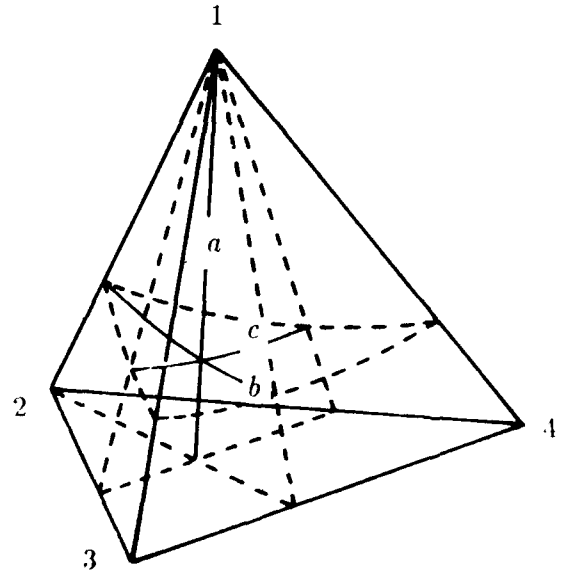

Figure 4. Integration and differentiation paths for the procedure C in a quaternary system 1-2-3-4: a, integration path for eqn. (27), b, integration path for eqn. (28) and c, differentiation path for eqns. (30) and (31).

Curves a and b in Fig. 4 illustrate the alternative integration paths expressed, respectively, in eqns. (27) and (28) and the curve c, the differentiation path for both eqns. (30) and (31). Therefore, after $\langle C_{\{q\}}\rangle$ has been calculated in terms of either eqn. (27) or (28), both μ_3^E and μ_4^E may also be calculated at the same time in terms of eqns. (30) and (31) along the curves of a_1=const. and $x_2/(x_3+x_4)$=const. as illustrated in Fig. 2. The procedure also only involves one set of integration and one set of differentiation.

3. – Activities in multiphase regions–

The three procedures mentioned above can be applied to both homogeneous phases and multiphases. When applied to multiphase regions, the procedure B may further be simplified. In such a case, eqns. (23) and (24) can, respectively, be rewritten as

$$RTlna_3 = (\frac{\partial\{(\langle B_{\{q\}}\rangle + RT[(1-y)lnx_3 + ylnx_4 - ln(x_3+x_4)])/y\}}{\partial\{1/y\}})_{a_1,a_2}, \tag{32}$$

$$RTlna_4 = (\frac{\partial\{(\langle B_{\{q\}}\rangle + RT[(1-y)lnx_3 + ylnx_4 - ln(x_3+x_4)])/(1-y)\}}{\partial\{1/(1-y)\}})_{a_1,a_2}. \tag{33}$$

Since every tie–line in any multiphase region and at its boundary is a common isoactivity line for all the four components, $\{\langle B_{\{q\}}\rangle + RT[(1-y)lnx_3 + ylnx_4 - ln(x_3+x_4)]\}$ against y corresponding to every tie–line should be a straight line. The intercepts of its extension should be equal to $RTlna_3$ at the axis of $y = 0$ and $RTlna_4$ at the axis of $y = 1$. The differentiation calculation can therefore be omitted and only one set of integration is required.

4. – Extension to k – gaseous (k + 2) – component systems–

In this section we discuss how to calculate unknown activities of both $(k+1)$–th and $(k+2)$–th components from known activities of other k components in $(k+2)$–component systems.

Let t be a composition ratio defined by:

$$t = \frac{x_{k+2}}{x_{k+1}+x_{k+2}}. \tag{34}$$

Extending eqns. (6) and (7) to k–gaseous $(k+2)$–component systems, we have

$$\langle A_{\{k+2\}}\rangle \equiv \frac{G^E}{x_{k+1}+x_{k+2}} = \frac{\sum_i x_i\mu_i^E}{x_{k+1}+x_{k+2}} + (1-t)\mu_{k+1}^E + t\mu_{k+2}^E, \tag{35}$$

$$d\langle A_{\{k+2\}}\rangle = \sum_i \mu_i^E d\frac{x_i}{x_{k+1}+x_{k+2}} + (\mu_{k+2}^E - \mu_{k+1}^E)dt; \tag{36}$$

where $i \in \{1,2,\cdots,k\}$. Equation (36) yields

$$\frac{\langle A_{\{k+2\}}\rangle}{1+\sum_{i^*} x_{i^*}/(x_{k+1}+x_{k+2})} = \frac{G^E}{1-x_i} = (G^E)_{x_i=0} + \int_0^{x_i}\alpha_i dx_i \quad (t = const. \text{ and } all\ \frac{x_{i^*}}{x_{k+1}+x_{k+2}} = const.) \tag{37}$$

and

$$\mu_{k+2}^E - \mu_{k+1}^E = (\frac{\partial\langle A_{\{k+2\}}\rangle}{\partial t})_{all\ \frac{x_i}{x_{k+1}+x_{k+2}}}; \tag{38}$$

where $i^* \in \{1,2,\cdots,k\}$ but $i^* \neq i$. From eqns. (35) and (38)

$$\mu^E_{k+1} = \{\frac{\partial(\langle A_{\{k+2\}}\rangle/t)}{\partial(1/t)}\}_{all\ \frac{x_i}{x_{k+1}+x_{k+2}}} - \frac{\sum_i x_i\mu^E_i}{x_{k+1}+x_{k+2}}, \quad (39)$$

$$\mu^E_{k+2} = \{\frac{\partial[\langle A_{\{k+2\}}\rangle/(1-t)]}{\partial[1/(1-t)]}\}_{all\ \frac{x_i}{x_{k+1}+x_{k+2}}} - \frac{\sum_i x_i\mu^E_i}{x_{k+1}+x_{k+2}}. \quad (40)$$

Therefore, the whole calculation only involves one set of integration along the curves of t=const. and all $x_{i^*}/(x_{k+1}+x_{k+2})$=const. and one set of differentiation along the curves of all $x_i/(x_{k+1}+x_{k+2})$=const.

Extending eqns. (18) and (19) to $k-$gaseous $(k+2)-$component systems, we have

$$\begin{aligned}\langle B_{\{k+2\}}\rangle &\equiv \frac{G^E - \sum_i x_i\mu^E_i}{x_{k+1}+x_{k+2}} + RTln(x_{k+1}+x_{k+2}) \\ &= (1-t)\mu^E_{k+1} + t\mu^E_{k+2} + RTln(x_{k+1}+x_{k+2}), \quad (41)\end{aligned}$$

$$d\langle B_{\{k+2\}}\rangle = -RT\sum_i \frac{x_i}{x_{k+1}+x_{k+2}} dlna_i + (\mu^E_{k+2} - \mu^E_{k+1})dt. \quad (42)$$

Equation (42) yields

$$\begin{aligned}\langle B_{\{k+2\}}\rangle &= \{\langle B_{\{k+2\}}\rangle\}_{a_i=0} - RT\int_0^{a_i} \frac{x_i/a_i}{x_{k+1}+x_{k+2}} da_i \\ &\quad (t = const. \quad \text{and} \quad all\ a_{i^*} = const.), \quad (43)\end{aligned}$$

$$\mu^E_{k+2} - \mu^E_{k+1} = (\frac{\partial\langle B_{\{k+2\}}\rangle}{\partial t})_{all\ a_i}. \quad (44)$$

From eqns. (41) and (44)

$$\mu^E_{k+1} = (\frac{\partial\{\langle B_{\{k+2\}}\rangle/t\}}{\partial\{1/t\}})_{all\ a_i} - RTln(x_{k+1}+x_{k+2}), \quad (45)$$

$$\mu^E_{k+2} = (\frac{\partial\{\langle B_{\{k+2\}}\rangle/(1-t)\}}{\partial\{1/(1-t)\}})_{all\ a_i} - RTln(x_{k+1}+x_{k+2}). \quad (46)$$

Therefore, the whole calculation only involves one set of integration along the curves of t=const. and all a_{i^*}=const. and one set of differentiation along the curves of all a_i=const.

Extending eqns. (25) and (26) to $k-$gaseous $(k+2)-$component systems, we have

$$\begin{aligned}\langle C_{\{k+2\}}\rangle &\equiv \frac{G^E - \sum_j x_j\mu^E_j + RT[1+ln(x_{k+1}+x_{k+2})]\sum_l x_l}{x_{k+1}+x_{k+2}} \\ &+ RTln(x_{k+1}+x_{k+2}) \\ &= (1-t)\mu^E_{k+1} + t\mu^E_{k+2} + RTln(x_{k+1}+x_{k+2}) \\ &+ \frac{\sum_l x_l\mu^E_l}{x_{k+1}+x_{k+2}} + \frac{RT[1+ln(x_{k+1}+x_{k+2})]\sum_l x_l}{x_{k+1}+x_{k+2}}, \quad (47)\end{aligned}$$

$$\begin{aligned}d\langle C_{\{k+2\}}\rangle &= -RT\sum_j \frac{x_j}{x_{k+1}+x_{k+2}} dlna_j \\ &+ \sum_l \{\mu^E_l + RTln(x_{k+1}+x_{k+2})\} d\frac{x_l}{x_{k+1}+x_{k+2}} \\ &+ (\mu^E_{k+2} - \mu^E_{k+1})dt \quad (48)\end{aligned}$$

where $j \in \{1,2,\cdots,h<k\}$ and $l \in \{h+1, h+2,\cdots,k\}$. Equation (48) yields

$$\begin{aligned}\langle C_{\{k+2\}}\rangle &= (\langle C_{\{k+2\}}\rangle)_{a_j=0} - \int_0^{a_j} \frac{x_j/a_j}{x_{k+1}+x_{k+2}} da_j \quad (t = const. \\ &\quad all\ a_{j^*} = const. \quad \text{and} \quad all\ \frac{x_l}{x_{k+1}+x_{k+2}} = const.), \quad (49)\end{aligned}$$

$$\begin{aligned}\langle C_{\{k+2\}}\rangle &= (\langle C_{\{k+2\}}\rangle)_{x_l=0} \\ &- \int_0^{x_l} \{\mu^E_l + RTln(x_{k+1}+x_{k+2})\} dln\frac{x_l}{x_{k+1}+x_{k+2}} \\ &\quad (t = const. \quad all\ a_j = const. \quad \text{and} \\ &\quad all\ \frac{x_{l^*}}{x_{k+1}+x_{k+2}} = const.) \quad (50)\end{aligned}$$

and

$$\mu^E_{k+2} - \mu^E_{k+1} = (\frac{\partial\langle C_{\{k+2\}}\rangle}{\partial t})_{all\ a_j,\ all\ \frac{x_l}{x_{k+1}+x_{k+2}}}; \quad (51)$$

where $j^* \in \{1,2,\cdots,h<k\}$ but $j^* \neq j$ and $l^* \in \{h+1, h+2,\cdots,k\}$ but $l^* \neq l$. From eqns. (47) and (51)

$$\begin{aligned}\mu^E_{k+1} &= (\frac{\partial\{\langle C_{\{k+2\}}\rangle/t\}}{\partial\{1/t\}})_{all\ a_j,\ all\ \frac{x_l}{x_{k+1}+x_{k+2}}} \\ &- RTln(x_{k+1}+x_{k+2}) - \frac{\sum_l x_l\mu^E_l}{x_{k+1}+x_{k+2}} \\ &- \frac{RT[1+ln(x_{k+1}+x_{k+2})]\sum_l x_l}{x_{k+1}+x_{k+2}}, \quad (52)\end{aligned}$$

$$\begin{aligned}\mu^E_{k+2} &= (\frac{\partial\{\langle C_{\{k+2\}}\rangle/(1-t)\}}{\partial\{1/(1-t)\}})_{all\ a_j,\ all\ \frac{x_l}{x_{k+1}+x_{k+2}}} \\ &- RTln(x_{k+1}+x_{k+2}) - \frac{\sum_l x_l\mu^E_l}{x_{k+1}+x_{k+2}} \\ &- \frac{RT[1+ln(x_{k+1}+x_{k+2})]\sum_l x_l}{x_{k+1}+x_{k+2}}. \quad (53)\end{aligned}$$

Therefore, the whole calculation only involves one set of integration along either the curves of t=const., all a_{j^*}=const., and all $x_l/(x_{k+1}+x_{k+2})$=const. or the curves of t=const., all a_j=const., and all $x_{l^*}/(x_{k+1}+x_{k+2})$=const.; and one set of differentiation along the curves of all a_j=const. and all $x_l/(x_{k+1}+x_{k+2})$=const.

5. – Discussion–

For $k-$gaseous $c-$ component systems where activities of the k components have been known, the procedure A yields

$$\langle A_{\{c\}}\rangle \equiv \frac{G^E}{x_{k+1}+x_{k+2}} = \frac{\sum_i x_i\mu^E_i + \sum_m x_m\mu^E_m}{x_{k+1}+x_{k+2}} + (1-t)\mu^E_{k+1} + t\mu^E_{k+2} \quad (54)$$

$$\begin{aligned}\frac{\langle A_{\{c\}}\rangle}{1+\sum_{i^*} x_{i^*}/(x_{k+1}+x_{k+2}) + \sum_m x_m/(x_{k+1}+x_{k+2})} &= \frac{G^E}{1-x_i} \\ = (G^E)_{x_i=0} + \int_0^{x_i} \alpha_i dx_i \\ (t = const., \quad all\ \frac{x_{i^*}}{x_{k+1}+x_{k+2}} = const. \quad \text{and} \\ all\ \frac{x_m}{x_{k+1}+x_{k+2}} = const.), \quad (55)\end{aligned}$$

$$\mu^E_m = (\frac{\partial\langle A_{\{c\}}\rangle}{\partial\frac{x_m}{x_{k+1}+x_{k+2}}})_{t,\ all\ \frac{x_i}{x_{k+1}+x_{k+2}},\ all\ \frac{x_{m^*}}{x_{k+1}+x_{k+2}}}, \quad (56)$$

$$\mu^E_{k+1} = \{\frac{\partial(\langle A_{\{c\}}\rangle/t)}{\partial(1/t)}\}_{all\ \frac{x_i}{x_{k+1}+x_{k+2}}, all\ \frac{x_m}{x_{k+1}+x_{k+2}}} - \frac{\sum_i x_i\mu^E_i + \sum_m x_m\mu^E_m}{x_{k+1}+x_{k+2}} \quad (57)$$

and

$$\mu^E_{k+2} = \{\frac{\partial[\langle A_{\{c\}}\rangle/(1-t)]}{\partial[1/(1-t)]}\}_{all\ \frac{x_i}{x_{k+1}+x_{k+2}}, all\ \frac{x_m}{x_{k+1}+x_{k+2}}} - \frac{\sum_i x_i\mu^E_i + \sum_m x_m\mu^E_m}{x_{k+1}+x_{k+2}}; \quad (58)$$

where $i, i^* \in \{1, 2, \cdots, k\}$ but $i^* \neq i$ and $m, m^* \in \{k+3, k+4, \cdots, c\}$ but $m^* \neq m$; the procedure B yields

$$\begin{aligned}\langle B_{\{c\}}\rangle &\equiv \frac{G^E - \sum_i x_i\mu^E_i}{x_{k+1}+x_{k+2}} + RTln(x_{k+1}+x_{k+2}) \\ &+ RT[1+ln(x_{k+1}+x_{k+2})]\frac{\sum_m x_m}{x_{k+1}+x_{k+2}} \\ &= (1-t)\mu^E_{k+1} + t\mu^E_{k+2} + RTln(x_{k+1}+x_{k+2}) \\ &+ RT[1+ln(x_{k+1}+x_{k+2})]\frac{\sum_m x_m}{x_{k+1}+x_{k+2}} \\ &+ \sum_m \frac{x_m\mu^E_m}{x_{k+1}+x_{k+2}}, \end{aligned} \quad (59)$$

$$\begin{aligned}\langle B_{\{c\}}\rangle &= (\langle B_{\{c\}}\rangle)_{a_i=0} - \int_0^{a_i} \frac{x_i/a_i}{x_{k+1}+x_{k+2}} da_i \\ &\quad (t = const., \quad all\ a_{i^*} = const. \quad and \\ &\quad all\ \frac{x_m}{x_{k+1}+x_{k+2}} = const.), \end{aligned} \quad (60)$$

$$\mu^E_m + RTln(x_{k+1}+x_{k+2}) = (\frac{\partial\langle B_{\{c\}}\rangle}{\partial\frac{x_m}{x_{k+1}+x_{k+2}}})_{t,\ all\ a_i,\ all\ \frac{x^*_m}{x_{k+1}+x_{k+2}}}, \quad (61)$$

$$\begin{aligned}\mu^E_{k+1} &= (\frac{\partial\{\langle B_{\{c\}}\rangle/t\}}{\partial\{1/t\}})_{all\ a_i,\ all\ \frac{x_m}{x_{k+1}+x_{k+2}}} - RTln(x_{k+1}+x_{k+2}) \\ &- RT[1+ln(x_{k+1}+x_{k+2})]\frac{\sum_m x_m}{x_{k+1}+x_{k+2}} - \frac{\sum_m x_m\mu^E_m}{x_{k+1}+x_{k+2}} \end{aligned} \quad (62)$$

and

$$\begin{aligned}\mu^E_{k+2} &= (\frac{\partial\{\langle B_{\{c\}}\rangle/(1-t)\}}{\partial\{1/(1-t)\}})_{all\ a_i,\ all\ \frac{x_m}{x_{k+1}+x_{k+2}}} \\ &- RTln(x_{k+1}+x_{k+2}) \\ &- RT[1+ln(x_{k+1}+x_{k+2})]\frac{\sum_m x_m}{x_{k+1}+x_{k+2}} \\ &- \frac{\sum_m x_m\mu^E_m}{x_{k+1}+x_{k+2}} \end{aligned} \quad (63)$$

and the procedure C yields

$$\begin{aligned}\langle C_{\{c\}}\rangle &\equiv \frac{G^E - \sum_j x_j\mu^E_j}{x_{k+1}+x_{k+2}} + RTln(x_{k+1}+x_{k+2}) \\ &+ RT[1+ln(x_{k+1}+x_{k+2})]\frac{\sum_l x_l + \sum_m x_m}{x_{k+1}+x_{k+2}} \\ &= (1-y)\mu^E_{k+1} + y\mu^E_{k+2} + \frac{\sum_l x_l\mu^E_l + \sum_m x_m\mu^E_m}{x_{k+1}+x_{k+2}} \\ &+ RTln(x_{k+1}+x_{k+2}) \\ &- RT[1+ln(x_{k+1}+x_{k+2})]\frac{\sum_l x_l + \sum_m x_m}{x_{k+1}+x_{k+2}}, \end{aligned} \quad (64)$$

$$\begin{aligned}\langle C_{\{c\}}\rangle &= (\langle C_{\{c\}}\rangle)_{a_j=0} - \int_0^{a_j} \frac{x_j/a_j}{x_{k+1}+x_{k+2}} da_j \quad (t = const. \\ &\quad all\ a_{j^*} = const. \quad all\ \frac{x_l}{x_{k+1}+x_{k+2}} = const. \\ &\quad and \quad all\ \frac{x_m}{x_{k+1}+x_{k+2}} = const.), \end{aligned} \quad (65)$$

$$\begin{aligned}\langle C_{\{c\}}\rangle &= (\langle C_{\{c\}}\rangle)_{x_l=0} - \int_0^{\frac{x_l}{x_{k+1}+x_{k+2}}} \{\mu^E_l + RTln(x_{k+1}+x_{k+2})\} \\ &\quad \cdot dln\frac{x_l}{x_{k+1}+x_{k+2}} \quad (t = const. \quad all\ a_j = const. \\ &\quad all\ \frac{x_{l^*}}{x_{k+1}+x_{k+2}} = const. \\ &\quad and \quad all\ \frac{x_m}{x_{k+1}+x_{k+2}} = const.), \end{aligned} \quad (66)$$

$$\mu^E_m + RTln(x_{k+1}+x_{k+2}) = (\frac{\partial\langle C_{\{c\}}\rangle}{\partial\frac{x_m}{x_{k+1}+x_{k+2}}})_{t,\ all\ a_j,\ all\ \frac{x_l}{x_{k+1}+x_{k+2}}, all\ \frac{x_{m^*}}{x_{k+1}+x_{k+2}}} \quad (67)$$

$$\begin{aligned}\mu^E_{k+1} &= (\frac{\partial\{\langle C_{\{c\}}\rangle/t\}}{\partial\{1/t\}})_{all\ a_j,\ all\ \frac{x_l}{x_{k+1}+x_{k+2}},\ all\ \frac{x_m}{x_{k+1}+x_{k+2}}} \\ &- \frac{\sum_l x_l\mu^E_l + \sum_m x_m\mu_m}{x_{k+1}+x_{k+2}} - RTln(x_{k+1}+x_{k+2}) \\ &- RT[1+ln(x_{k+1}+x_{k+2})]\frac{\sum_l x_l + \sum_m x_m}{x_{k+1}+x_{k+2}}, \end{aligned} \quad (68)$$

and

$$\begin{aligned}\mu^E_{k+2} &= (\frac{\partial\{\langle C_{\{c\}}\rangle/(1-t)\}}{\partial\{1/(1-t)\}})_{all\ a_j,\ all\ \frac{x_l}{x_{k+1}+x_{k+2}},\ all\ \frac{x_m}{x_{k+1}+x_{k+2}}} \\ &- \frac{\sum_l x_l\mu^E_l + \sum_m x_m\mu_m}{x_{k+1}+x_{k+2}} - RTln(x_{k+1}+x_{k+2}) \\ &- RT[1+ln(x_{k+1}+x_{k+2})]\frac{\sum_l x_l + \sum_m x_m}{x_{k+1}+x_{k+2}}; \end{aligned} \quad (69)$$

where $j, j^* \in \{1, 2, \cdots, h < k\}$ but $j^* \neq j$; $l, l^* \in \{h+1, h+2, \cdots, k\}$ but $l^* \neq l$; and $m, m^* \in \{k+3, k+4, \cdots, c\}$ but $m^* \neq m$. After $\langle A_{\{c\}}\rangle$, $\langle B_{\{c\}}\rangle$ or $\langle C_{\{c\}}\rangle$ has been calculated by one set of integration and all μ^E_m have been calculated by $(c-k-2)$ sets of differentiation, both μ^E_{k+1} and μ^E_{k+2} can be calculated by one set of differentiation. Only one set of integration and $(c-k-1)$ sets of differentiation are required for the whole calculation.

Acknowledgment

One of the authors (Wang) is greatly indebted to the Max-Planck Society for financial support and to the Shanghai Institute of Nuclear Research, Academia Sinica for a leave during the period.

Reference

Arita, M. and St. Pierre, G. R. (1977): Trans. Japan Inst. Met., 18, 552.
Chou, K.-C. (1978): Sci. Sinica, 21, 73.
Darken, L. S. (1950): J. Amer. Chem. Soc., 72, 2909.
Gokcen, N. A. (1960): J. Phys. Chem., 64, 401.
Korpachev, V. G., Vatolin, N. A. and Sryvalin, I. T. (1979): Dokl. Akad. Nauk SSSR, 245, 392.
Nagamori, M. and Yazawa, A. (1988): Trans. JIM, 29, 798.
Schuhmann, Jr. R. (1955): Acta Metall., 3, 219.
Wagner, C. (1952): Thermodynamics of Alloys (Addision-Wesley) p 19.
Wang, Z.-C. (1981): Acta Metall. Sinica, 17, 168.
Wang, Z.-C. and Chou, K.-C. (1984): Sci. Sinica Ser. A, 27, 1093.

OXYGEN PARTIAL PRESSURE OF Y-Ba-Cu-O FROM DIRECT MEASUREMENTS

F. Faupel and Th. Hehenkamp
Institut für Metallphysik, Universität Göttingen, 3400 Göttingen, FRG

Abstract

The oxygen partial pressure of $YBa_2Cu_3O_{6+x}$ was measured directly as function of temperature and composition under isochoric conditions with minimized free volume. Since this technique does not require major diffusion of oxygen for equilibration it is applicable down to T < 200 °C. Different from isobaric measurements the composition range near x = 1 is accessible. The partial enthalpy of oxygen $\Delta\bar{H}(x)$ was derived from the data. A strong decrease of $\Delta\bar{H}(x)$ was found for x > 0.9. Based on pressure-composition isothermes the thermodynamic factor was calculated. The latter drastically increases as x approaches 1. The present investigation indicates that the stability of oxygen saturated $YBa_2Cu_3O_{6+x}$ towards oxygen desorption has largely been overestimated, particularly at low temperatures.

1. - Introduction

The oxygen content of $YBa_2Cu_3O_{6+x}$ can be reversibly changed in the range $0 < x < 1$ (Hazen et al. 1987). The superconducting properties of the material strongly depend on the composition. Highest T_c values are obtained near x = 1 (Engler et al. 1987). Therefore knowledge of the O_2 partial pressure as function of temperature and composition is indispensable.

Usually measurements are carried out at constant oxygen pressure, and the composition is recorded as function of temperature, e.g. by means of thermogravimetry (Gallagher 1987, Musbah and Chang 1989). These measurements require long range diffusion of oxygen for equilibration and are, therefore, restricted to relatively high temperatures. In addition, the most interesting concentration range near x = 1 is not accessible.

In the present paper we report $p_{O_2}(x, T)$ values, which have been obtained from direct measurements under isochoric conditions with minimized free volume. This technique (Faupel et al. 1989) avoids the aforementioned drawbacks of the isobaric measurements. The partial enthalpy of oxygen as well as the thermodynamic factor, which affects chemical diffusion of oxygen, are determined from the data.

2. - Experimental Procedure

Y-Ba-Cu-O powder of 99 % purity and T_c = 92 K was kindly provided by Hoechst company. In addition, 1-2-3 material was prepared by solid state reaction from $BaCuO_2$ and $Y_2Cu_2O_5$ as described by Chunlin et al. (1988). Oxygen saturation was obtained by an annealing program in flowing O_2, which involves a final ramp between 400 and 300 °C for 50 h. The samples exhibited a T_c of 92 K (midpoint) with a sharp transition range in resistivity of $\simeq$ 3 K and excellent susceptibility values. X-ray measurements showed the Y-Ba-Cu-O to be orthorhombic and single phase. DTA measurements revealed the presence of about 1 % of impurity phases (Faupel et al. 1990). No significant differences in the oxygen partial pressures were observed between this powder and the Hoechst material.

For the pressure measurements an Al_2O_3 crucible with Y-Ba-Cu-O powder was placed within a furnace in a vacuum pumped quartz tube with minimized free volume. Pressure was monitored outside the furnace by a piezoresistive gauge. The inner dimensions of the quartz tubing were large enough to achieve a constant pressure in the whole volume in the pressure range investigated. The quartz tube could optionally be connected by a throttle to a quadrupole mass spectrometer chamber in order to analyze the gas phase (Faupel et al. 1989). Substantial amounts of water were detected in most samples. They were stored in dry atmosphere, though. Therefore, the water was removed by evacuation, and the final oxygen loading was carried out directly in the set-up for pressure measurements. Additionally, remaining traces of H_2O were trapped by a Peltier cooling unit. A computer was used for data acquisition and for increasing the temperature by steps of typically 35 °C. The pressure was allowed to equilibrate after each step. No major diffusion of oxygen was required for equilibration because of the extremely small free volume. Typical changes in composition caused by oxygen evolution were of the order of $\Delta x = 0.01$ at 1 bar O_2. Δx was calculated by means of the ideal gas law from the amount of powder (7 g), the pressure, and the free volume. The latter was essentially given by a dead volume of about 1 ml within the furnace around the Al_2O_3 crucible and a dead volume of $\simeq$ 1.5 ml at room temperature. The equilibrium pressure of the samples was generally reached in less than 30 min, while much longer periods are needed even at high temperatures for any technique involving major changes in composition (Faupel et al 1989).

The oxygen concentration of the samples was determined by taking oxygen saturated $YBa_2Cu_3O_{6+x}$ as reference with x = 1. The oxygen content was reduced in a

well defined way by evolving a certain amount of O_2 into a large calibrated volume (66.6 ml). The ideal gas law was employed to calculate the change in composition.

3. - Results and Discussion

An Arrhenius plot of log (p_{O_2}) vs. 1/T is shown in Fig. 1 for various values of x. Here x refers to the original oxygen concentration. x slightly decreases with increasing pressure due to the effect of the finite free volume alluded to above. This leads to a small curvature

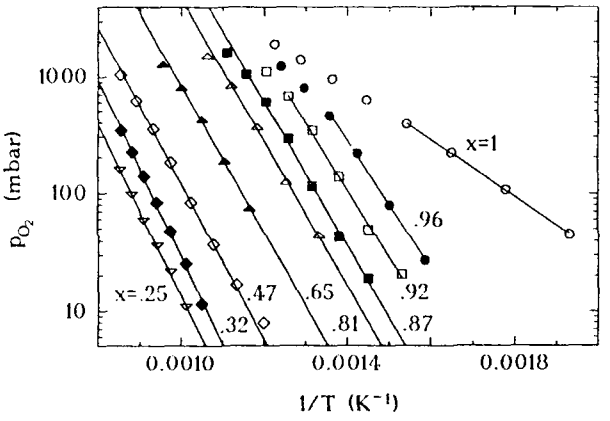

Fig. 1: Semilog. plot of oxygen partial pressure vs. 1/T for $YBa_2Cu_3O_{6+x}$ with various values of x. The curvatures at high pressure originate from the finite free volume (see text).

at high pressures, which becomes larger near x = 1. Straight lines were fitted to the data in the linear range. From the slopes 2 $\Delta\bar{H}$/ 2.303 k one obtains the partial enthalpy of oxygen $\Delta\bar{H}(x)$. It is depicted in Fig. 2 as function of composition.

$\Delta\bar{H}(x)$ varies moderately except near x = 1 where a drastic decrease is observed. This drop of $\Delta\bar{H}(x)$ close to the oxygen saturation content reflects a pronounced loss in stability towards oxygen desorption. Further measurements are needed in order to clarify whether the change in $\Delta\bar{H}(x)$ for x < 0.5 is caused by the orthorhombic-to-tetragonal transformation. The experimental errors of $\Delta\bar{H}(x)$ are conservatively estimated as < +/- 0.08 eV. Literature data on the partial enthalpy of oxygen are not available in this technologically most important range. To our knowledge, $\Delta\bar{H}(x)$ has been determined for x ≤ 0.9 only (Strobel et al 1987, Brabers et al. 1988, Verweij et al. 1989, Meuffels et al. 1989). Values are centered around 0.8 eV, but also enthalpies as high as 1.15 eV have been reported (Gallagher 1987). Most authors find a slight increase in $\Delta\bar{H}(x)$ with increasing x.

The data of Fig. 1 were used to calculate isothermal pressure-composition lines (Fig. 3). The change in oxygen concentration due to the dead volume was taken into account. At high temperatures and for x < 0.8 the slope of the log (p_{O_2}) vs. x lines is nearly constant. A strong increase is observed as x approaches 1, particularly at low temperatures.

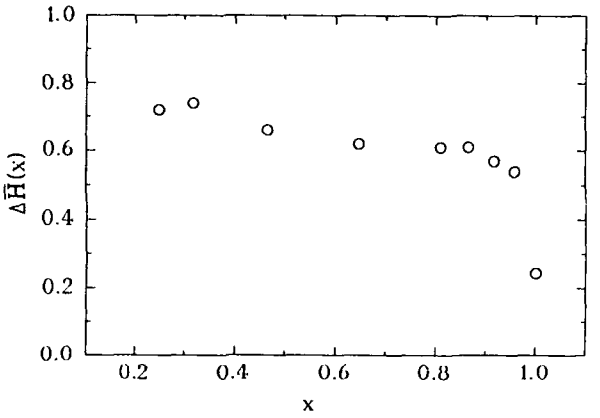

Fig. 2: Partial enthalpy for oxygen of $YBa_2Cu_3O_{6+x}$ as function of x.

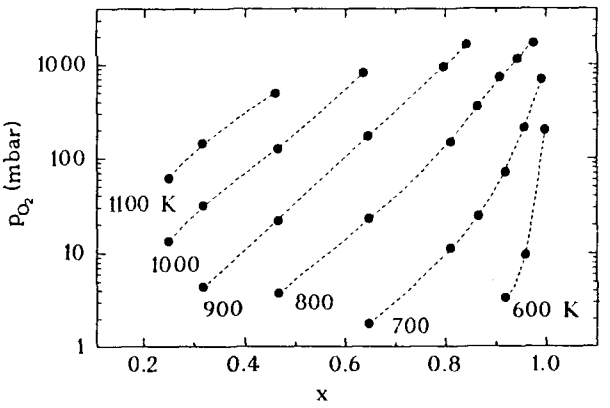

Fig. 3: Pressure-composition isotherms of $YBa_2Cu_3O_{6+x}$ between 600 and 1100 K.

The driving force in a chemical diffusion experiment is the gradient in the chemical potential, and not in the concentration. Hence, any concentration dependence of the oxygen pressure gives rise to an enhancement of the intrinsic diffusion coefficient according to (Manning 1968)

$$D_i = D^* \frac{d \ln a_O}{d \ln N} = D^* \frac{1}{2} \frac{d \ln p_{O_2}}{d \ln N} \qquad (1)$$

D^* is the oxygen tracer diffusivity and N the molar fraction of oxygen. The activity a_O is related to the partial pressure:

$$a_O = \left(\frac{p_{O_2}}{p^0_{O_2}} \right)^{1/2} \qquad (2)$$

$p^0_{O_2}$ is the reference pressure. The right-hand side of equation (1) was obtained from equation (2). It allows to calculate the thermodynamic factor $\Phi_O = d \ln a_O / d \ln N$ from the data shown in Fig. 3. The results are depicted in Fig. 4. On notes that Φ_O does not significantly depend on temperature and composition for $x < 0.8$. In this range Φ_O already causes a strong enhancement of the order of 100. As x approaches 1, Φ_O increases drastically, particularly at low temperatures.

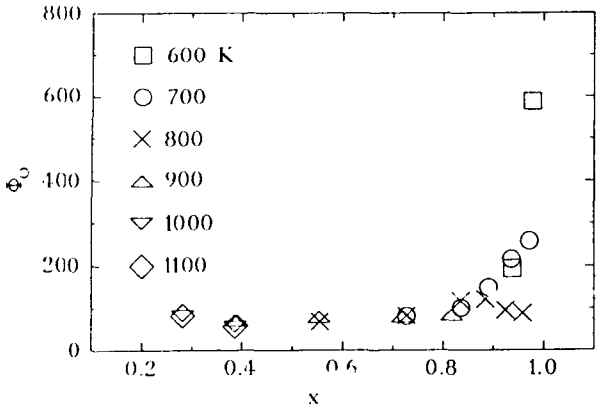

Fig. 4: Thermodynamic factor Φ_O of $YBa_2Cu_3O_{6+x}$ vs. oxygen content x for various temperatures.

In summary, it has been shown that in chemical diffusion experiments the diffusivity of oxygen can exceed the oxygen tracer diffusion coefficient by several orders of magnitude in the nearly saturated $YBa_2Cu_3O_{6+x}$ superconductor. In addition, a steep drop of the partial enthalpy for oxygen is observed in this range (Fig. 2). Apparently, $YBa_2Cu_3O_{6+x}$ close to $x = 1$ is much more prone to oxygen desorption at relatively low temperatures than has generally been assumed.

Acknowledgments

The authors are indebted to F. Neuß, who carried out most of the experimental work, H. Thomas from the laboratory of K. Winzer for sample preparation and K. Bente for x-ray diffraction. Sample material was also kindly provided by Hoechst company. This work has been supported by BMFT under grant No. 13 N 5493.

References

Brabers, V. A. M., de Jonge, W. J. M. , Bosch, L. A., Steen, C. v. d., de Groote, A. M. W., Verheyen, A. A. and Vennix, C. W. H. M. (1988): Mater. Res. Bull. 23, 197.

Chunlin, J., Chuanmeng, C., Kuihan, W., Sulan, L., Guiyi, Z., Guofan, Z., Cuenfu, Q., Weiming, B., Zhanguo, F. and Qian, X. (1988): Solid State Commun. 65, 859.

Engler, E. M., Lee, V. Y., Nazzai, A. I., Beyers, R. B., Lim, G., Grant, P. M., Parkin, S. S. P., Ramirez, M. L., Vasquez, J. E. and Savoy, R. J. (1987): Am. Chem. Soc. 109, 2848.

Faupel, F. and Hehenkamp, Th. (1990): Proc. ICMC, Topical Conf. High-Temp. Supercond. Mater. Aspects, Garmisch-Partenkirchen, FRG, in press.

Faupel, F., Hehenkamp, Th., Bente, K., Mariolakos, M. and Winzer, K. (1989): Physica C 162-164, 905.

Gallagher, P. K . (1987): Adv. Ceram. Mater. 2, 632.

Hazen, R. M., Finger, L. W., Angel, R. J., Prewitt, C. T., Ross, N. L., Mao, H. K., Hadidiacios, C. G., Hor, P. H., Menge, R. L. and Chu, C. W. (1987): Phys. Rev. B 35, 7238.

Manning, J. R. (1968): Diffusion Kinetics for Atoms in Crystals, Van Nostrand, Princeton, New Jersey.

Meuffels, P., Naeven, R. and Wenzel, H. (1989): Physica C 161, 539.

Musbah, O. A. and Chang, Y. A. (1989): Z. Metallkde. 80, 74.

Strobel, P., Capponi, J. J., Marezio, M. and Monod, P. (1987): Solid State Commun. 64, 51.

Verweij, H. and Bruggink, W. H. M. (1989): J. Phys. Chem. Solids 50, 75.

Experimental enthalpies of formation of some solid phases in the systems PtTi and PtZr

Najim SELHAOUI, Jean-Claude GACHON

Laboratoire de Thermodynamique Métallurgique U.R.A. C.N.R.S. 1108

Université de Nancy I, Faculté des Sciences B.P. 239

F 54506 VANDOEUVRE-LèS-NANCY CEDEX (FRANCE)

Abstract : Direct reaction calorimetry has been used to determine the enthalpies of formation of Pt_3Ti, PtTi, $PtTi_3$, Pt_3Zr and $PtZr_2$.
Results are given and compared to former literature values.

1 - Introduction

A systematic program of measurements was started, some ten years ago, in our laboratory to determine the enthalpies of formation of compounds made of a metal from the titanium column and a metal from the iron group (Gachon et al 1981). In addition to the industrial interest for transition metal alloys, such a program was motivated by the possibility to build theoretical models of transition metal and transition alloy cohesion based on d band and d electrons.

Our choice of components, with a d- electron poor metal and a d-electron rich metal allowed us to scan a wide range of d electron concentrations when varying the stoichiometries of compounds.

2 - Experimental method

We mix, in suitable proportions, at room temperature, fine powders of the two components, and compress the mixture in order to get small pellets, (typically 50 to 200 milligrams). These pellets are dropped into the calorimeter crucible which is kept at a temperature below the melting point of the compound but high enough to ensure a quick diffusion of both metals into each other. The most often we get reactions times of a few seconds. After cooling the calorimeter we check the products by X-rays and electron microprobe. The whole process of preparation and reaction is conducted under argon atmosphere in order to avoid oxidation of the transition metal powders.

From a thermodynamic point of view we start from one state : the two pure metals at room temperature, and we go to another state : the compound at the calorimeter temperature. The overall quantity of heat which is measured can be described as the sum of the pure metal enthalpy increments between room and calorimeter temperatures and of the enthalpy of formation at the calorimeter temperature. As enthalpy increments of pure metals are tabulated (e.g. Barin et al, 1973, 1977) and checked in our calorimeter, enthalpies of formation are found in a very simple manner.

3 - Results and discussion

Table 1 gives all our experimental results and compare them with literature data.

The first point to consider is the reliability of the phase diagrams we used as a base for our study : for PtTi two different ones are available :

- one from Kubaschewski et al (1983)
- one from Murray (1982)

There are disagreements between them on the platinum side and in the range 53 to 73 % at. of platinum. We selected for our study only the three compounds that are not to badly defined : $Ti_{0.75}Pt_{0.25}$ (Ti_3Pt), $Ti_{0.50}Pt_{0.50}$ (TiPt), and $Ti_{0.25}Pt_{0.75}$ ($TiPt_3$), using stoichiometric proportions to avoid the problem of ill-defined homogeneity ranges.

For Pt Zr one diagram is drawn in Elliott (1965) after a work by Kendal et al, another from Darling et al (1970) is nearly the same except for solid solubility of zirconium in platinum. Both agree on three different compounds : $Pt_{0.75}Zr_{0.25}$ (Pt_3Zr), $Pt_{0.50}Zr_{0.50}$ (PtZr), $Pt_{0.33}Zr_{0.67}$ ($PtZr_2$). Many other compounds have been suggested but never well confirmed. Existence of $Pt_{0.33}Zr_{0.67}$ ($PtZr_2$) is controversial, it could be stabilised by oxygen (Kleykamp 1990). We studied $Pt_{0.75}Zr_{0.25}$ (Pt_3Zr) and $Pt_{0.33}Zr_{0.67}$ ($PtZr_2$) since $Pt_{0.50}Zr_{0.50}$ has already

been studied (Gachon, 1988).

In the system PtTi, from a crystallographic point of view we found that $Pt_{0.75}Ti_{0.25}$ (Pt_3Ti) has a $AuCu_3$ structure like indicated in Murray (1982), while for $Pt_{0.50}Ti_{0.50}$ (PtTi) we got a mixture of CsCl and orthorhombic structures. Murray (1982) reported an allotropic transformation for $Pt_{0.50}Ti_{0.50}$ (PtTi) with a high temperature CsCl form and an orthorhombic low temperature form ($\leq$ 1000°C), so we think that our calorimetric result concerns the high temperature phase and that during cooling of the calorimeter a partial transformation into the low temperature form occurred. The last compound $Pt_{0.25}Ti_{0.75}$ ($PtTi_3$) was found cubic (βW) but with traces of another cubic phase, not reported in Murray (1982) or Kubaschewski et al (1983), possibly a metastable phase.

In the system PtZr we found $Pt_{0.75}Zr_{0.25}$ (Pt_3Zr) hexagonal (Ni_3Ti type), while for $Pt_{0.33}Zr_{0.67}$ ($PtZr_2$), in addition to the fcc Ni Ti_2 structure, traces of another phase appeared and it could be $Pt_{0.375}Zr_{0.625}$ (Pt_3Zr_5) as already proposed by Biswas and Schubert (1967).

From a thermodynamic point of view our values for 50/50 compounds can be compared to former results by Topor and Kleppa (1989) and there is a good agreement between them, within the uncertainty ranges. For the platinum rich compounds, Meschter and Worrel (1977) found, by derivation of

TABLE 1

EXPERIMENTAL RESULTS AND LITERATURE DATA

Pt Ti

Compounds	Structure literature experiment	References	Temperature (K)	Enthalpies of formation J/mole of atoms Experiment	literature*		
$Pt_{0.75}Ti_{0.25}$ (Pt_3Ti)	$AuCu_3$	Pt fcc	1673	**-94000**	exp	-85400	(MW)
	$AuCu_3$	Ti bcc		(σ = 4300)	comp	-70000	(N et al)
					comp	-78000	(CPH)
$Pt_{0.50}Ti_{0.50}$ (Pt Ti)	See discussion	Pt fcc	1673	**-77100**	exp	-79700	(TK)
		Ti bcc			exp	-75000	(G)
				(σ = 3100)	comp	-112000	(N et al)
					comp	-104000	(WB)
					comp	-94000	(CPH)
$Pt_{0.25}Ti_{0.75}$ ($PtTi_3$)	cubic	Pt fcc	1473	**-59000**	comp	-73000	(N et al)
	cubic + cubic	Ti bcc		(σ = 900)	comp	-72500	(CPH)

Pt Zr

Compounds	Structure literature experiment	References	Temperature (K)	Enthalpies of formation J/mole of atoms Experiment	literature*		
$Pt_{0.75}Zr_{0.25}$ (Pt_3Zr)	hexagonal Ni_3Ti	Pt fcc	1673	**-106000**	exp	-113000	(MW)
		Zr bcc		(σ = 3400)	exp	-128000	(SF)
					comp	-101000	(N et al)
					comp	-92000	(CPH)
$Pt_{0.33}Zr_{0.67}$ ($PtZr_2$)	fcc Ni Ti_2	Pt fcc	1500	**-84000**	comp	-118000	(N et al)
	fcc Ni Ti_2 + Pt_3Zr_5	Zr bcc		(σ = 3500)	comp	-74000	(CPH)
N.B. : 50/50 compound				- 90000(G) (σ = 10000)	exp	-96000	(TK)

* literature results : exp for experimental determination, comp for computation, (initials) in brackers refer to authors.

emf measurements, results relatively close to our own. For $Pt_{0.75}Zr_{0.25}$ (Pt_3Zr) Srikishnan and Ficarola (1974) gave a result too negative but it was got by combustion calorimetry and certainly not very accurate.

Model results by Miedema's group (Niessen et al, 1983), Colinet et al (1985) and Watson and Bennett (1984) are of the same order of magnitude as experimental results. The drawback of these values is that the experimental variations from one compound tc the other which follow the same trend as the melting points, as already mentionned by Kubaschewski and Alcook (1979), is not reproduced.

To conclude, this is the first set of experimental enthalpies of formation for compounds in the systems PtTi and PtZr. It confirms the tendency of enthalpies of formation and melting temperatures to vary in a same manner and shows that models are still not accurate enough.

References

- Barin L, Knacke O, Kubaschewski O. (1978) : Thermochemical Properties of inorganic substances, supplement (Berlin, Springer Verlag).
- Barin L., Knacke O. (1973) : Thermochemical Properties of inorganic substances, (Berlin, Springer Verlag).
- Biswas V.T.K., Schubert K (1967) : Zeitsch. Metallk., **58**, 558.
- Colinet C., Pasturel A., Hicter P., (1985) : Calphad, **9**, 77.
- Darling A.S., Selman G.L., Rushforth R, (1970) : Platinum Met. Rev., **14**, 124.
- Elliott R.P. (1965) : Constitution of binary alloys, 2d supplement, (New York, Mc Graw Hill).
- Gachon J.C. (1988) : J. Phys. Chem. Solids, **49**, 435.
- Gachon J.C., Giner J., Hertz J. (1981) : Scripta Metall., **15**, 981.
- Gachon J.C., Notin M., Hertz J. (1981) : Thermochemica acta, **48**, 155.
- Kleykamp H. (1990) : Private communication.
- Kubaschewski O., Alcock C.B., (1979) : Metallurgical Thermochemistry, 5th ed., (New York, Pergamon Press).
- Kubaschewsky O, Kubaschewski von Goldbeck O, Rogl P., Franzen H.F. (1983) : Ed. Komarek K.L. Atomic Energy Review, Special issue N° 9, Titanium, (Vienna, International atomic energye agency).
- Meschter P.J., Worrel W.L.(1977) : Met. Trans., **8A**, 503
- Murray J.L. (1982) : Bull. of Alloy Phase Diag., **3**, 329.
- Niessen A.K., De Boer F.R., Boom R., De Chatel P.F., Mattens W.C.M., Miedema A.R. (1983) : Calphad, **7**, 51.
- Srikrishnan V., Ficarola P.J. (1974) : Met. Trans., **5**,1471.
- Topor L., Kleppa O.J. (1989) : J. of the less Com. Met., **155**, 61.
- Watson R.E., Bennett L.H., (1984) : Calphad, **8**, 307.

THERMODYNAMIC INVESTIGATION OF THE SYSTEM Ag-Nb-Te

Angelika BRUNNER, Harald P. FRITZER and Werner SITTE

Institut für Physikalische und Theoretische Chemie
Technische Universität Graz, A-8010 Graz, Austria

Abstract.-

The tellurium rich part of the ternary system Ag-Nb-Te has been determined employing coulometric titrations in the solid state using solid silver ionic conductors in specially designed galvanic cells with mixtures of binary niobium tellurides as cathodes. In contrast to NbS_2 and $NbSe_2$ no silver intercalation of $NbTe_2$ could be observed. The results, confirmed by X-ray diffraction, indicate the coexistence of the binary silver tellurides Ag_2Te, $Ag_{1.9}Te$ and Ag_5Te_3 with $NbTe_4$. No ternary compounds could be found between 25 and 400°C. Finally, the advantages and limitations of the coulometric titration technique, regarding the simultaneous determination of thermodynamic parameters as well as the phase diagram with high stoichiometric resolution, are discussed.

1.- Introduction

The aim of this project was the investigation of the ternary system Ag-Nb-Te by solid state electrochemical methods using solid silver ionic conductors in proper galvanic cells. The title ternary system has not been subject to any analysis before, although binary and ternary chalcogenides of the IV., V. and VI. group of the transition metals are very interesting materials due to their tendency to form low dimensional compounds that might serve as cathode materials in solid state batteries.

In the system **silver-niobium** only a very slight solubility at high temperatures has been reported (Kieffer *et al.* 1963).

Up to now, four stable **niobium tellurides** have been characterized (Selte and Kjekshus 1964). $NbTe_4$, which coexists with metallic tellurium, is stable up to at least 900 °C (Böhm and von Schnering 1985, Böhm 1987, Mahy *et al.* 1984).

$NbTe_2$ is a member of the well known family of layered dichalcogenides. So far, no phase transitions or phase width are known. The layers separated by van der Waals gaps are somewhat buckled due to metal-metal-interactions that lead to the formation of Nb-triplets (Wilson and Yoffe 1969. Nb_3Te_4 has been successfully intercalated (Schöllhorn 1980, Huan and Greenblatt 1987a, 1987b). Finally, Nb_4Te_5 is the binary niobium telluride with the highest niobium concentration (Selte and Kjekshus 1963, Selte *et al.* 1966).

The binary **silver-tellurium** phase diagram has been investigated using the method of coulometric titration between 25 °C and 200 °C (Sitte and Brunner 1988). The results confirmed the established phase diagram (Kracek *et al.* 1966). The emf data of the binary system can be used as a basic set of information for comparison with the initial results of the tellurium rich part of the ternary system Ag-Nb-Te

In contrast to sulfides and selenides, only few examples of **ternary transition metal tellurides** are known that might give an insight into structure types which could be expected in this ternary system. The sulvanite type semiconductors (Hulliger 1961, 1968) exhibit a variety of compounds such as Cu_3NbX_4 (X = S, Se, Te), but no silver analogon is known. Ag_2NbTe_3 has been described by Brixner (1965) as a thermoelectric ternary alloy , but the author never denotes it to be a single phase compound. $AgSbTe_2$ could be found in the system Ag-Sb-Te; similar ternary compounds are known for sulfide and selenide systems. Liimatta and Ibers (1987) reported a layered ternary transition metal chalcogenide $NbNiTe_5$.

The selenides and sulfides of niobium are well known examples of intercalation. The only known intercalated tellurides have been prepared either by Li-intercalation in solution (Murphy *et al.* 1976) or by reaction of silver powder with the mixed layer-structure telluride $TiZrTe_4$ to give the intercalated compound $AgTiZrTe_4$ (Cybulski and Feltz 1989, Cybulski *et al.* 1989).

Huan and Greenblatt (1987a, 1987b) reported the preparation of intercalated Nb_3Te_4, where silver is incorporated by annealing of stoichiometric amounts of the elements to form $Ag_2Nb_6Te_8$.

2.- Coulometric titrations in the solid state

As has been shown by Kiukkola and Wagner (1957) and Sitte and Weppner (1985, 1987) the method of "coulometric titration" ("galvanostatic intermittent titration technique") in the solid state is a very useful tool in investigating binary and ternary phase diagrams with high stoichiometric resolution and obtaining thermodynamic parameters simultaneously. Of course, in order to achieve reliable emf data several conditions have to be fulfilled. At least one of the components of the system must exhibit high ionic mobility. An appropriate ionic conductor must be employed, which is stable in the desired temperature range. Additionally, the starting material incorporated in the working electrodes must exhibit mixed conduction and the compounds of the galvanic cell must not react with each other or the atmosphere.

In the case of the system Ag-Nb-Te the following galvanic cell has been used:

$$Pt\,|\,Ag\,|\,Ag^+\text{-ionic conductor}\,|\,Ag_xNb_yTe_z\,|\,Pt$$

(Ag^+-ionic conductor = AgI, $RbAg_4I_5$, Ag-ß"-Al_2O_3)

The silver concentration of the sample with the nominal composition "$Ag_xNb_yTe_z$" is varied by passing a constant current pulse through the sample according to

$$\Delta x = \frac{yM_{Nb} + zM_{Te}}{zFm_{Nb_yTe_z}} I\,\Delta t\,, \qquad (1)$$

if $m_{Nb_yTe_z}$, M_{Nb}, M_{Te} and F are the mass of the starting sample "Nb_yTe_z", the atomic mass of Nb and Te, and Faraday's constant, respectively.

A plot of the emf vs silver concentration is called a "titration curve" (fig.2). In addition to titrations at constant temperatures the variation of the emf with temperature yields entropy values and information on phase transitions (change of the slope in the E vs. T curve).

Fig.1 shows coulometric titration paths in the ternary system Ag-Nb-Te with binary (on the base line Nb-Te) and ternary starting samples. According to Gibbs' phase rule, emf plateaus reflect the existence of a three-phase regions (located between two- or one-phase regions). The correct phase diagram may be constructed from several titration curves with different starting samples.

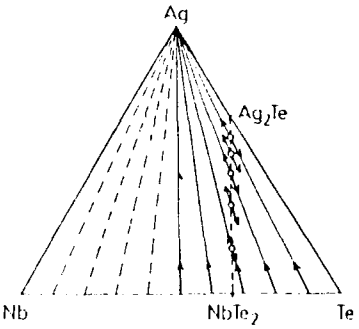

Fig.1 Coulometric titration paths with binary and ternary starting samples

3 Experimental

The starting samples were prepared by annealing stoichiometric amounts of the elements or binary precursors at temperatures between 700°C and 1000°C in evacuated silica tubes. The powders were finely ground and pressed into pellets of 50 to 500 mg. Problems in preparation were caused both by the easy sublimation of tellurium and the slow reaction of niobium under the given conditions. Usually the formation of the tellurium rich compound was favoured. In these cases the use of mixtures of finely ground single crystals (in the composition range from 20 to 33,33 mol-% niobium) proved to be very helpful. Single crystals of $NbTe_4$, $NbTe_2$ and Nb_3Te_4 have been grown by chemical vapor transport (using iodine as transport agent). In some cases Ag_2Te was added to those starting samples exhibiting low silver mobility and coexisting with Ag_2Te.

AgI was used between 150°C and 530°C (the softening of pressed AgI tablets well below the melting point and slight iodine evaporation limited the use of AgI to about 530°C). Additionally, $RbAg_4I_5$ covered the region between 25°C and 200°C, and Ag-β''-Al_2O_3 the region between 300°C and 550°C. All experiments were carried out under constant helium flow.

4 Results and discussion

Typical coulometric titration curves of the system Ag-Nb-Te are shown in fig.2. The starting compositions of the binary niobium tellurium mixtures varied between 10.00 and 31.15 mol-% Te.

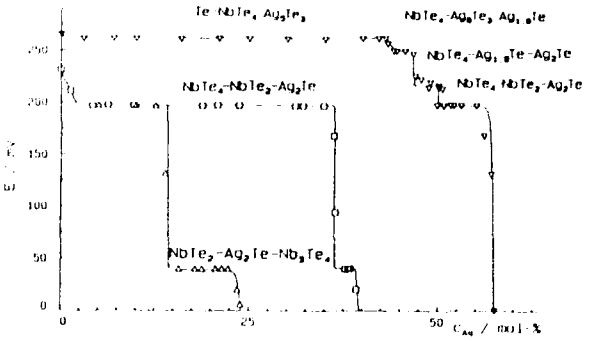

Fig.2 Coulometric titration curves for starting samples of various compositions
(Δ $Nb_{31.15}Te_{68.85}$, $Nb_{25.00}Te_{75.00}$, $Nb_{10.00}Te_{90.00}$)

The temperature dependence of the emf within the three phase regions of the ternary system Ag-Nb-Te is given in table 1.

Reaction	T / K	a / mV	b / mV/K
$NbTe_4(Ag) + 3\ Te + 5\ Ag \rightarrow$	450-520	127.6 ± 2.0	-0.225 ± 0.004
$NbTe_4(Ag) + Ag_2Te_3$	520-600	115.2 ± 1.0	-0.205 ± 0.002
$NbTe_4(Ag) + Ag_{1.63}Te \rightarrow$	450-530	54.3 ± 4.0	-0.062 ± 0.008
$NbTe_4(Ag) + Ag_{1.9}Te$	543-606	122.6 ± 4.2	-0.212 ± 0.007
$NbTe_4 + Ag_2Te + 4\ Ag \rightarrow$	500-630	115.4 ± 4.0	-0.142 ± 0.006
$NbTe_4 + 2\ Ag_2Te$	530-710	48.9 ± 4.0	-0.041 ± 0.006
$Nb_3Te_4(Ag) + 4\ Ag \rightarrow$	580-630	91.9 ± 4.0	-0.110 ± 0.006
$Nb_3Te_4 + 2\ Ag_2Te$	640-730	41.7 ± 4.0	-0.054 ± 0.006

Table 1. Temperature dependence of the emf of the galvanic cell
Ag|Ag^+-ionic-conductor|sample|P within the three phase regions of the ternary system Ag-Nb-Te; E = a + bT

The results indicate a coexistence of the binary silver tellurides Ag_2Te, $Ag_{1.9}Te$, and Ag_5Te_3 with $NbTe_4$. Additionally, Ag_2Te coexists with $NbTe_2$ and Nb_3Te_4. Especially for starting samples of 20 mol-% niobium the use of single crystal $NbTe_4$ was prefered to annealed powder materials, as residual (not reacted) tellurium in the case of powder materials gave misleading results, indicating a solubility of silver in $NbTe_4$, which could not be found if single crystals were used as starting materials for coulometric titrations. $NbTe_2$ could not be intercalated with silver, but instead, samples with high $NbTe_2$-contents decomposed during the coulometric titrations (tellurium crystals grew on the surface of the ionic conductor, the platinum leads, and even the counter electrode). After an amount of 30-50 weight-% of Ag_2Te had been added to the sample, coulometric titrations could be performed again with acceptable current densities (as Ag_2Te coexists with $NbTe_2$, only the silver migration had been improved and free tellurium had been trapped by the addition of Ag_2Te). Neither Ag_3NbTe_3 nor $Ag_2Nb_6Te_8$ could be found by coulometric titrations at temperatures up to 530°C. The results are supported by X-ray characterisation. Nb_3Te_4 showed a

remarkable silver solubility of approximately 4 mol-% silver between 450 °C and 530 °C, thus forming a two-phase region $Ag_{0.4}Nb_3Te_4$-Ag_2Te. In fig.3 the resulting ternary phase diagram is given for T=400 °C. At this temperature all three silver tellurides are present. The regimes of the eutectic and peritectic melts in the binary system Ag-Te (Kracek *et al.* 1966) are not governed by the present study and have to be left for modified experimental setups. The limitations of the method of coulometric titration in our case are mainly given by the upper temperature due to the melting point of AgI (555 °C) and the low reaction rates in the niobium rich part of the ternary system (niobium contents higher than 40 mol-%).

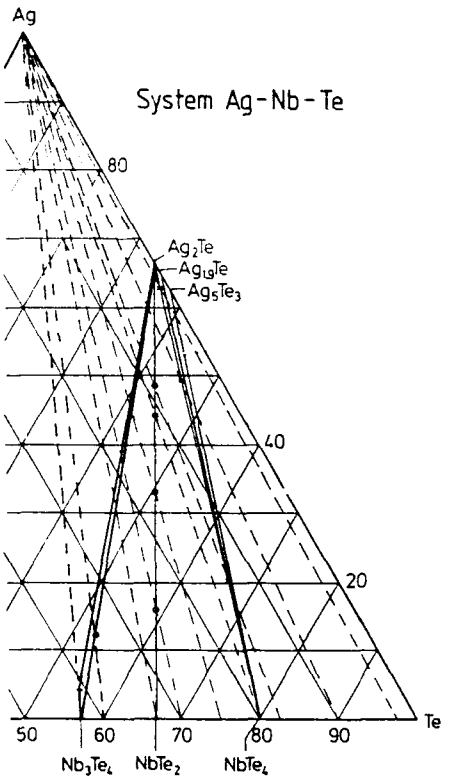

Fig.3 The tellurium-rich part of the ternary phase diagram Ag-Nb-Te at 400 °C.

By use of the emf values (see table 1) the Gibbs energy of formation of the coexisting phases of any of the three phase regions may be calculated by

$$E = (1/Fd) \sum_{i=1}^{3} (-1)^i d_{i1} \Delta_f G^{\ominus}(Ag_{xi}Nb_{yi}Te_{zi}) \qquad (2)$$

where $\Delta_f G^{\ominus}$, d, d_{i1} and F are the Gibbs energy of formation from the elements in their standard state (pure elements), the determinant formed by the stoichiometric coefficients of the three coexisting phases, the minor determinant (derived from d by eliminating the 1-th row (stoichiometric numbers of the electroactive component silver) and the first line), and the Faraday constant, respectively [30]. The temperature dependence of the emf values gives the values of the entropy of formation

$$\left(\frac{\partial E}{\partial T}\right)_p = - (1/Fd) \sum_{i=1}^{3} (-1)^i d_{i1} \Delta_f S^{\ominus}(Ag_{xi}Nb_{yi}Te_{zi}) \qquad (3)$$

whereas the enthalpy of formation results from the Gibbs-Helmholtz equation

$$\Delta_f H_i^{\ominus}(T) = \Delta_f G_i^{\ominus}(T) + T.\Delta_f H_i^{\ominus}(T). \qquad (4)$$

The activities of silver are related to the measured emf by

$$E = - \frac{1}{F} (\mu_{Ag} - \mu_{Ag}^{\ominus}) = - \frac{RT}{F} \ln a_{Ag}, \qquad (5)$$

whereas the activites of In and Sb may also be calculated according to eqn.(2) via the cell voltages of hypothetical In and Sb concentration cells (Sitte and Weppner, 1985, 1987). As no literature data regarding the thermodynamic properties of the niobium tellurides exist, a complete analysis of the thermodynamic properties of the ternary system Ag-Nb-Te can be given as soon as e.g. the enthalpy of formation of $NbTe_4$ is known by solution calorimetry.

Acknowledgments

The authors thank the Austrian Fonds zur Förderung der wissenschaftlichen Forschung for supporting this project (P5980) and Prof. Krischner for enabling X-ray measurements.

References

Böhm, H. und v.Sühnering, H.-G. (1985): Z. Kristall. 171, 41.
Böhm, H. (1987): Z. Kristall. 180, 113
Brixner, L.H. (1965): Ger. DE 1185825, 21st , 4
Cybulski, Z.and Feltz, A. (1989a): Z. anorg. allg. Chem. 569, 145
Cybulski, Z., Feltz, A. and Andratschke, M. (1989b): Mat. Res. Bull. 24, 157
Huan, G. and Greenblatt, M. (1987a): Mat. Res. Bull. 22, 943
Huan, R. and Greenblatt M. (1987b): Mat. Res. Bull. 22, 505
Hulliger, F.(1968): Struct. and Bonding 4, 83
Hulliger, F.(1961): Helv. Phys. Acta 34, 379
Kieffer, K., Windisch, St. und Nowotny, H.(1963): Metall 17, 669.
Kiukkola, K.and Wagner, C. (1957): J. Electrochem. Soc. 104, 379.
Kracek, F.C., Ksandra, C.J. and Cabri, L.J., Am. Mineral. 51, 14
Llimatta, E. and Ibers, J.A. (1987): J. Solid State Chem. 71, 384
Mahy, J ,Wiegers, G.A., Landuyt, J.Van and Amelinckx, S. (1984): Mat. Res. Soc. Symp. Proc. 21, 181
Murphy, D.W., Di Salvo, F.J., Hull, G.W. and Waszczak, J.V. (1976): Inorg. Chem. 15, 17
Schöllhorn, R. (1980): Angew. Chem. 92, 1015
Selte K. and Kjekshus, A. (1963): Acta. Chem. Scand. 17, 2560
Selte, K. and Kjekshus, A. (1964): Acta Chem. Scand. 18, 690.
Selte, K., Bjerkelund, E. and Kjekshus, A. (1966): J. Less-Common Met. 11, 14
Sitte, W. and Weppner, W. (1987): Z.Naturforsch.42a,1
Sitte, W. and Weppner, W. (1985): Appl.Phys. A38, 31.
Sitte, W. and Brunner, A. (1988): Solid State Ionics 27, 1324
Wilson, J.A.and Yoffe, A.D. (1969): Adv. Phys. 18, 193

Thermodynamic Study of Au-Pb-Pd Ternary Alloys by E.M.F Measurements

S.Spas, J.M. Miane, J.Riou, R. Baret,

Laboratoire de Chimie Générale,
Faculté de Pharmacie,
13385 Marseille CEDEX 5, France.

and J.P. Bros,

Laboratoire de Thermodynamique des Systèmes Métalliques,
Université de Provence,
13381 Marseille CEDEX 3, France.

Abstract:

An electrode potential study of the liquid Au-Pb-Pd system has been conducted with the cell

Pb / Pb^{2+} in LiCl+KCl / Pb-Pd-Au

in the temperature range 623-1200 K. Lead partial free energy and activity were determined for 33 alloys. Fifteen of them are gathered in this work. These measurements allow us to give a part of the liquidus surface of this system.

I Introduction:

In the course of the thermodynamic study carried out by our group concerning ternary metallic systems, we have measured by potentiometry the lead activity in a number of gold - lead - palladium liquid alloys.

The thermodynamic functions and the phase diagram of this ternary system have not been previously studied, except for $Au_xPd_{1-x}Pb_2$ by Havinga et al. (1972), by X-Ray diffraction to determine the lattice parameters of the f.c.c. solid solution.

II Bibliographic survey:

II.1. The gold - palladium system:

The phase diagram of this system, reported in Fig.1 from Okamoto et al. (1985) is very simple because of the complete solubility of gold and palladium at liquid and solid states at the whole composition. The liquid curve was determined by Ruer (1906) , and Miane et al. (1977).

Thermodynamic functions of this system were determined by Bartosik (1971) at 1373 K, Schmahl (1951) at 956 K, and Höhn et al. (1986) at 1200K, with the solid metals as reference. The integral enthalpy of mixing was determined by Miane (1979) at 1700 K for the liquid alloys.

II.2. The gold - lead system:

The phase diagram reported in Fig.2 is from Okamoto et al. (1985). The eutectic point coordinates are x_{Pb}= 0.848, T_{eut} = 485.5 K, and the peritectic temperatures are 701.1 K, 526.1 K, 494.6 K, corresponding to the decomposition of three intermetallic compounds Au_2Pb, $AuPb_2$ and $AuPb_3$ respectively.

Heats of mixing of this system were determined by Kleppa (1949 and 1956) and emf measurements were carried out by Hager et al. (1969), by Kameda et al. (1975) and by Rebouillon (1989). There is a serious desagreement among these authors about the heats of mixing.

II.3. The lead-palladium system:

There are four intermetallic compounds reported from Hultgren's et al. phase diagram in Fig.3: Pb_2Pd, $PbPd_3$ with congruent melting points at 727 K and 1493 K respectively; the peritectic decomposition of PbPd and Pb_2Pd_3 are at 768 K and 1103 K.

The thermodynamic functions of this system were determined by Sommer et al. (1978). Their lead activity values (determined by the effusion method) were in good agreement with those of Schwertfeger (1966) (potentiometry).

In this work, we report experimental values of lead activity in some Au-Pb, Pb-Pd, and Au-Pb-Pd alloys.

III Theory:

The formation of a binary or (ternary) alloy by a reaction of the type:

$$Pb + Pb_xAu_y \text{ -----> } Pb_{(1+x)}Au_y$$

may be investigated by a concentration cell represented schematically by Pb/ Pb^{2+} in molten LiCl-KCl / Pb in Au, Pb, or Au-Pd. Electric conduction across the phase boundaries metal/electrolyte is due to the transition of Pb^{2+} ions as the active charge carriers, exclusively, because this metal is more electropositive than gold and palladium; in effect, the standard electrode potentials in molten LiCl+KCl at 723 K, measured by Laitinen et al. (1958) are:

Au(I)-Au(0) = +0.205 V
Pd(II)-Pd(0) = -0.214 V
Pb(II)-Pb(0) = -1.10 V

From the knowledge of the emf value (E) at temperature T, the partial free energy and activity of lead in an alloy may be calculated by the following equation:

$$-zFE = \Delta_{mix} G_{Pb} = RT \ln a_{Pb}$$

The partial entropy and enthalpy of mixing of lead can be deduced from the potential variation versus temperature.

IV Experimental:

IV.1. Apparatus:

The experimental cell was described previously by Girard et al. (1980), and reported in Fig.4. The large external crucible (I), the lead wire sheath (D), and the thermocouple sheath (E) are in pure alumina. The pure lead alloys are also contained in pure alumina crucibles (A). The electrode crucibles are wedged in place on the bottom of the crucible (I) by several alumina tubes (C). Each cell contains ten electrodes; three with pure lead, and the others with alloys. The tungsten lead wires (D) for the electrodes and Pt-Pt 10% Rh thermocouple (E) are aligned by two covers (G and H). In the cover (G), suitable fittings permit a flowing argon.

The cell is heated by a cylindrical vertical furnace with two kanthal resistors; one of them is connected to an a-c supply, and the other to an electric regulator.
A more uniform temperature distribution is obtained by enclosing the cell inside the furnace within a concentric refractory steel cylinder (K) which also acts as an electric shield.

Emf values are measured with a digital scanner millivoltmeter (Prema 6000) with a large input impedance (10^{+12} ohms).

A program which has been described by Rebouillon (1989) allows the automation registration of data.

IV.2. Materiels:

99.9999 at.% gold and pallladium were provided by "La Compagnie Française des Métaux Précieux", and 99.999 at.% lead was a Prolabo.Soc . Product.

Lithium, potassium and lead chlorides were analytical grade salts (Carlo Erba and Koch-Light). The electrolytic salt was prepared by purging with gaseous chlorine from Messer Griesheim Comp.

The cell was supplied with pure argon (grade U-Air liquid Company).

IV.3. Cell preparation:

The molten electrolyte had to be carefully prepared to avoid considerable problems in experiments. The eutectic mixtures of lithium and potassium chlorides (44.2 weight percent LiCl; T_{fus}= 623 K) was dried at 523 K for 24 hours under dynamic vacuum. After heating at 650 K, 3 weight percent lead chlorine (kept under vacuum) was added. The decanted mixture of salts was also kept under gaseous chlorine (99.8%) for 30 minutes to improve the electrolytic preparation, and then transferred to the experimental cell after putting the metals in the crucibles.

The cell is heated up to about 1200 K and held for two hours at this temperature to stabilize. Potentials are then measured at intervals of about 50 K after stabilization of the cell.

IV.4. Accuracy:

During experiments, we took the following precautions : - attainment of equilibrium by alloys after each change in temperature was verified by observing the course of emf over a period of time - The emf between two reference electrodes was always lower than 10^{-4} V at each temperature.

Since lead vapor pressure becomes important above 1000 K (p= $1.65.10^{-5}$ Atm), all measurements were repeated on tne next day to check that measured voltages were constant for each composition.

Au-Pb, Pb-Pd alloys were studied in the same cells as ternary alloys. The results were compared with the published data to verify the smooth working of the cells.

V Experimental results and discussion:

V.1. Limiting binary systems:

- Au-Pb system:

The three alloys x_{Pb} = 0.10, 0.30, 0.50 were studied. In Table 1 we compared our lead activities values with those reported by Hager (1969) and by Rebouillon (1989), measured by the same method at 1200 K. The results are in good agreement, because the maximum of deviation between our values and Hager's (1969) is about 5%.

Table 1: Activities of lead in Au-Pb liquid alloys:

x_{Pb}	a_{Pb} /*/	a_{Pb} /**/	a_{Pb} /***/
0.10	0.030	0.032	0.037
0.20		0.105	0.093
0.30	0.176	0.197	0.176
0.40		0.261	0.281
0.50	0.410	0.400	0.400
0.60		0.524	0.512
0.70		0.623	0.628
0.80		0.766	0.753
0.90		0.883	0.889

* This work,
** Rebouillon (1989),
*** Hager (1969).

- Pb-Pd system:

For the six lead-palladium alloys studied, (x_{Pd} = 0.10, 0.20, 0.30, 0.40, 0.50, 0.60), we present the variation of potential versus temperature (see Fig. 5). The linear dependance corresponds to

liquid homeogeneous state, and the broken line for x_{Pd} = 0.60 and x_{Pd} = 0.50, at T = 1100 K and T = 900 K respectively are the limits of the liquid curve for these compositions in the phase diagram (Fig.3).

In Table 2, and Fig. 5, we have compared the lead activities measured by Schwertferger at 1273 K by potentiometry, and also measured by Sommer et al. (1978) by the effusion method. The lead activity in this binary system presents a large negative deviation from the Raoult's law, and our values tally with those of the precedent authors.

Table 2: Activities of lead in Pb-Pd liquid alloys:

x_{Pb}	a_{Pb} /*/	a_{Pb} /**/	a_{Pb} /***/
0.90	0.88	0.89	
0.80	0.72	0.7	
0.74		0.77	
0.70	0.58	0.553	
0.60	0.39	0.42	0.41
0.50	0.19	0.27	0.22
0.40	0.04	0.04	0.04

* This work,
** Sommer (1978),
*** Schwertfeger (1966).

The measurements concerning the Au-Pb and Pb-Pd systems let us expect to have access easely to the lead partial mixing functions of lead in the ternary Au-Pb-Pd.

- Au-Pb-Pd system:

We have studied fifteen ternary alloys with compositions as reported in Fig. 7-10.

The high temperature of Au-Pd liquid curve (Fig. 2) limited our investigation to the lead rich composition.

For the fifteen alloys, we have reported in table 3 the least squares regression coefficients E(mV)= a+bT (K). These coefficients are only available above the temperature indicated for number of alloys. In effect, we have obtained a few points of the liquidus of the ternary system Au-Pb-Pd by the break on E=f(T) graphs. In Fig.8 ,9 and 10, the potentials versus temperature are drawn for fifteen alloys with compositions:

x_{Au}/x_{Pd} = 4/1; x_{Pb} = 0.30; 0.40; 0.50; 0.60; 0.70;
x_{Au}/x_{Pd} = 1/1; x_{Pb} = 0.30; 0.40; 0.50; 0.60; 0.70;
x_{Au}/x_{Pd} = 1/4 ; x_{Pb} = 0.30; 0.40; 0.50; 0.60; 0.70;

The linear variation corresponds to the liquid monophase region and the curved part to the two-phase region. For both alloys, x_{Au}/x_{Pd} = 1/4; x_{Pb} = 0.30 and x_{Au}/x_{Pd} = 4/1; x_{Pb} = 0.30, the change of slope in the curve appears at 1030 K and 900 K respectively which corresponds to a two phase equilibrium. The liquidus temperatures determined in this way are shown in Fig.11.

For all the alloys studied, we have calculated the lead activity at 1200 K; corresponding values are reported in Table 3, and Fig.12 gives the general shape of the ΔG_{mix} function over the whole concentration range. The integral thermodynamic functions have been calculated by a thermodynamic model (Hoch-Arpshofen model (1984)) and will be published elsewhere.

Table 3: Regression coefficients E(mV)= a+bT(K) and lead activities for 15 Au-Pb-Pd liquid alloys

	a	b	a_{Pb}	T_{liq}
x_{Au}/x_{Pd}=1/4				
x_{Pb}=0.40	52.73	0.064	0.08	1000 K
x_{Pb}=0.50	20.18	0.043	0.24	
x_{Pb}=0.60	11.69	0.027	0.42	
x_{Pb}=0.70	5.87	0.015	0.62	
x_{Pb}=0.80	1.87	0.009	0.80	
x_{Au}/x_{Pd}=1/1				
x_{Pb}=0.30	78.82	0.073	0.04	820 K
x_{Pb}=0.40	33.18	0.055	0.14	
x_{Pb}=0.50	11.56	0.051	0.29	
x_{Pb}=0.60	9.59	0.025	0.46	
x_{Pb}=0.70	3.69	0.017	0.62	
x_{Au}/x_{Pd}=4/1				
x_{Pb}=0.30	28,58	0.068	0.12	900 K
x_{Pb}=0.40	13.41	0.047	0.26	
x_{Pb}=0.50	9.98	0.036	0.35	
x_{Pb}=0.60	7.15	0.024	0.49	
x_{Pb}=0.70	5.55	0.015	0.63	

VI Conclusion:

The activities of lead measured in fifteen Au-Pb-Pd alloys between 623 and 1200 K allowed us to propose the partial free enthalpy of mixing of lead. A number of points of the liquidus surface of the ternary system has been determined from the change of slope of E vs. T curves.

References:

Havinga E.E. Damsa H., Hokkeling P., (1972), J. Less-Common Met., 27, 2, p169.

Okamoto H., Massalski T.B., (1985), Bull. Alloy. Phas. Diagram, 6, 3, p 229.

Ruer R., (1906), Z. Anorg. Chem. 51, p 391.

Bartosik D.C.,
(1971), Thesis Northwest University Evanston, Illinois, USA.

Miane J.M., Gaune-Escard M., Bros J.P.,
(1977), High Temp.- High-Press., 9,
p 465.

Schmahl N.G.,
(1951), Z. Anorg. Allgm. Chem., 266, p1.

Höhn R., Herzig C,
(1986), Z.Metallkd., 77, 5, p 291.

Miane J.M.,
(1979), Thèse de Doctorat de 3ème cycle,
Université de Provence, France.

Okamoto H, Massalski T.B.,
(1984), Bull. Alloy. Phas. Diagr., 5, 3,
p 276.

Kleppa O,
(1956), J.Phys. Chem., 60, p 446.

Kleppa O,
(1949), J. Am. Chem. Soc., 71, 10,
p 3275.

Hager J.P., Walker R.A.,
(1969), Trans. Met. Soc. AIME, 245,
p 2307.

Kameda K., Sakairi S., Yoshida Y.,
(1975), J. Jap. Inst. Metals, 5, p 387.

Rebouillon P.,
(1989), Thèse de l'Université de
Provence.- Sciences, France.

Hultgren R., Desai P.D., Hawkins D.T.,
Gleiser M., Kelley K.K., Wagman D.,
(1973), "Selected values of the
thermodynamic properties of binary
alloys", Amer. Soc. Metals., Metals
Park.OH.

Sommer F., Suh Y.H., Predel B.,
(1978), Z. Metallkd, 69, p 401.

Schwertfeger K,
(1966), Trans. Met. Soc. AIME, 236, p 32.

Laitinen H.A., Liu C.H.,
(1958), J. Amer., Soc., 80, p 1015.

Girard C., Baret R., Riou J.,
Bros J.P.,
(1980), J. Electrochem. Soc., 127, 5,
p 1157.

Hoch M., Arpshofen I.,
(1984) Z., Metallkd, 75, p 23.

FIGURE 1

Au - Pd phase diagram

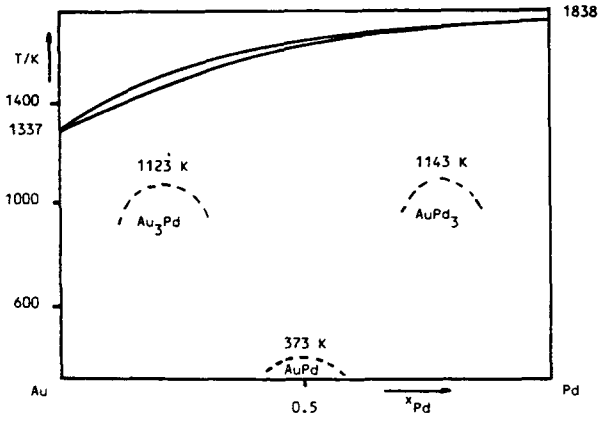

FIGURE 2

Au - Pb phase diagram

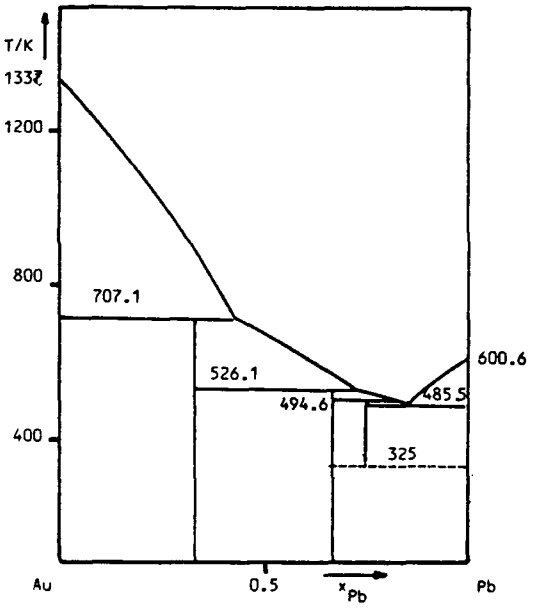

FIGURE 3

Pb - Pd phase diagram

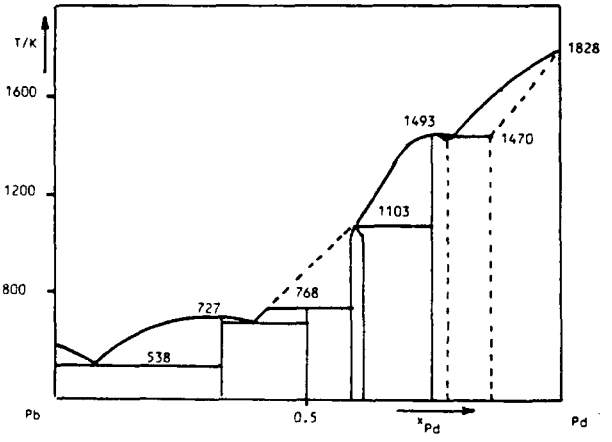

Figure 4; Schematic diagram of the apparatus

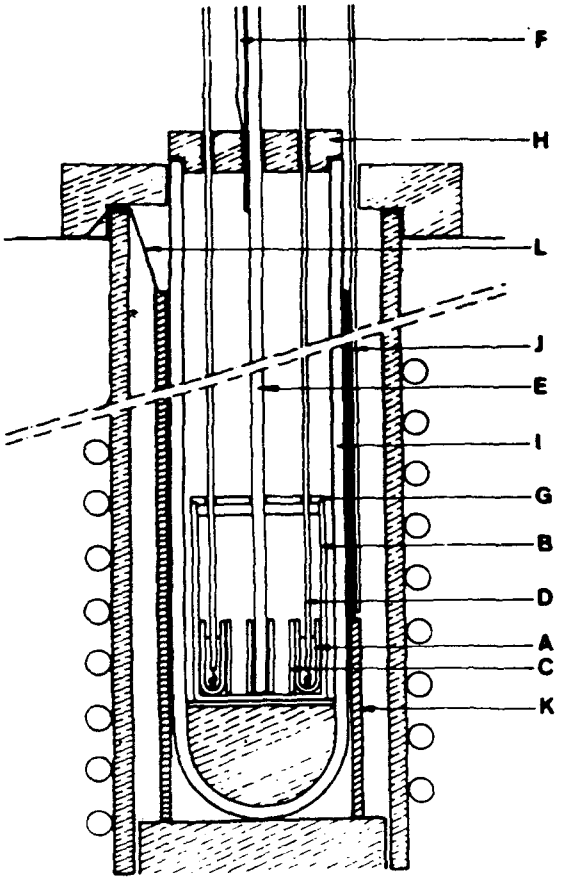

(A) Alumina crucible, (B) alumina crucible containing molten electrolyte, (C) alumina wedge, (D) lead wire sheath, (E) thermocouple sheath, (F) argon delivery pipe, (G) alumina cover, (H) alumina cover, (I) external alumina crucible, (J) thermocouple connected to the regulator, (K) refractory steel cylinder, (L) ground-wire.

FIGURE 5

Experimental values of emf plotted against temperature for 6 Pb-Pd liquid alloys

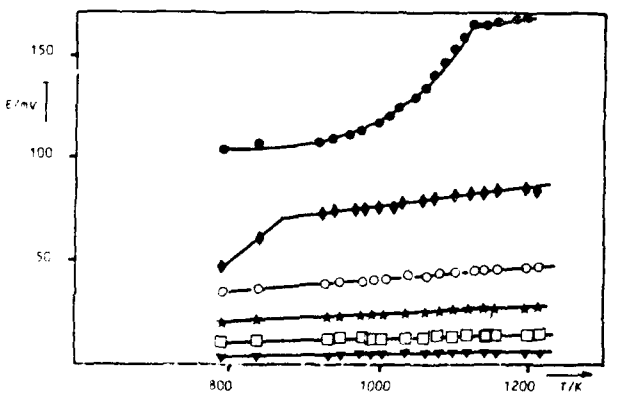

● x_{Pd} = 0.6 ; ♦ x_{Pd} = 0.5 ; ○ x_{Pd} = 0.4 ; ★ x_{Pd} = 0.3 ; □ x_{Pd} = 0.2 ; ▼ x_{Pd} = 0.1 ;

FIGURE 6

The activity of lead in Pb - Pd alloys

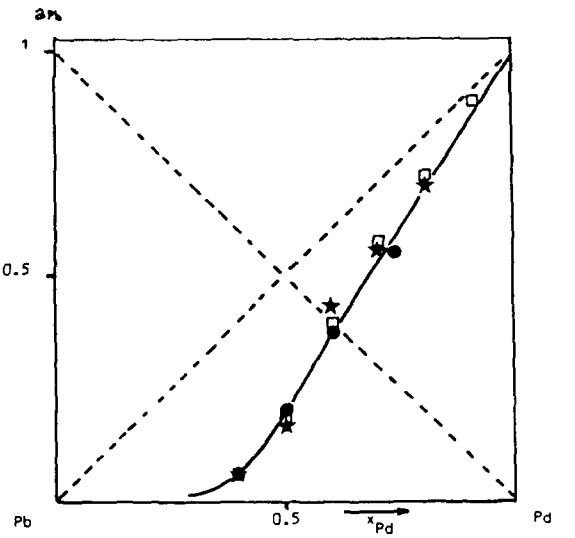

● Schwertfeger at 1173 K
★ Sommer at 1189 K
□ This work at 1100 K

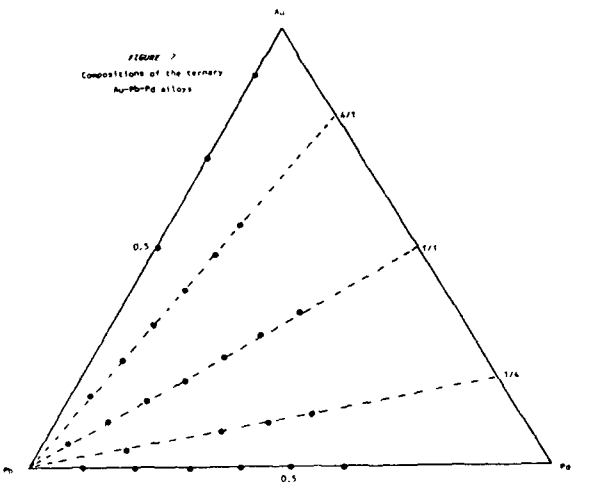

FIGURE 8

x_{Au} / x_{Pd} = 4/1

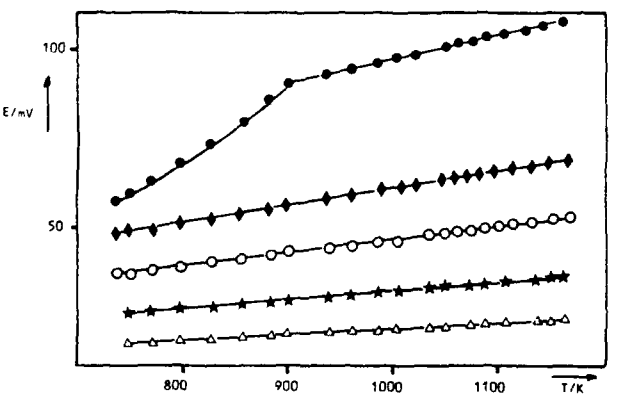

● x_{Pb} = 0.3; ♦ x_{Pb} = 0.4 ; ○ x_{Pb} = 0.5 ; ★ x_{Pb} = 0.6 ; △ x_{Pb} = 0.7

FIGURE 9

$x_{Au} / x_{Pd} = 1/4$

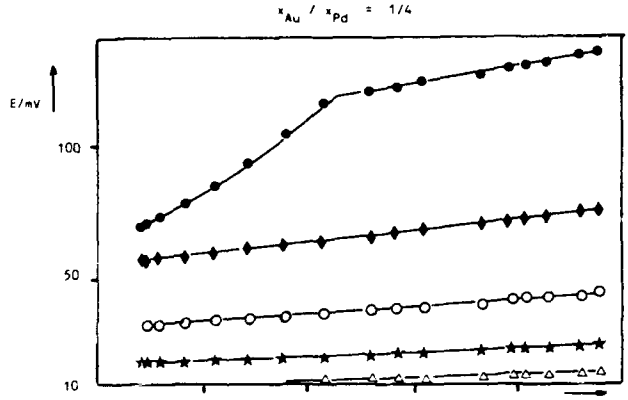

● x_{Pb} = 0,4 ; ♦ x_{Pb} = 0.5 ; ○ x_{Pb} = 0.6 ; ★ x_{Pb} = 0.7 ; △ x_{Pb} = 0.8

FIGURE 10

$x_{Au} / x_{Pd} = 1/1$

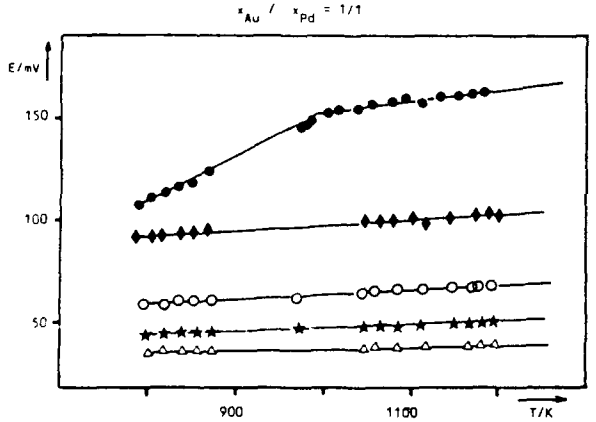

● x_{Pb} = 0.3 ; ♦ x_{Pb} = 0.4 ; ○ x_{Pb} = 0.5 ; ★ x_{Pb} = 0.6; △ x_{Pb} = 0.7

FIGURE 11

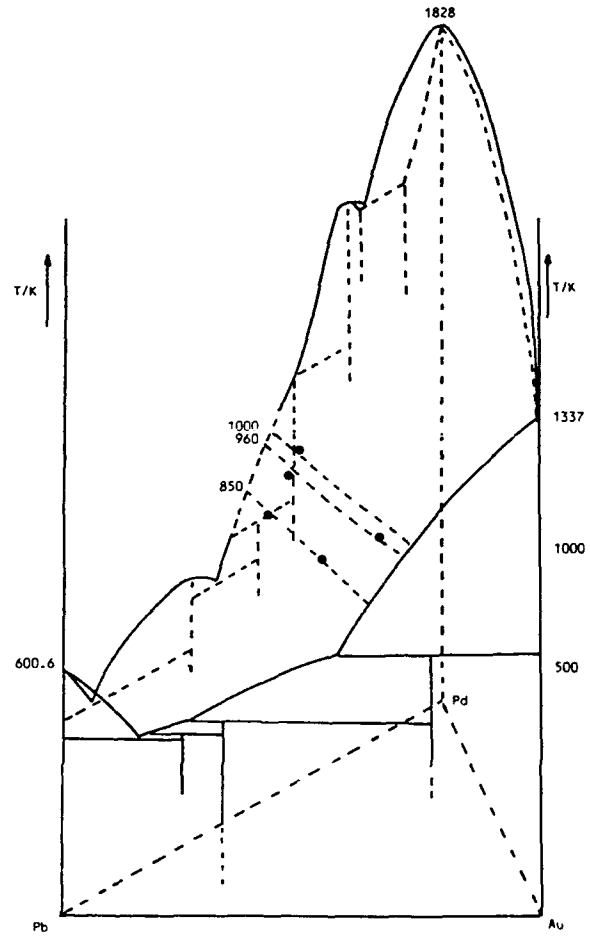

FIGURE 12

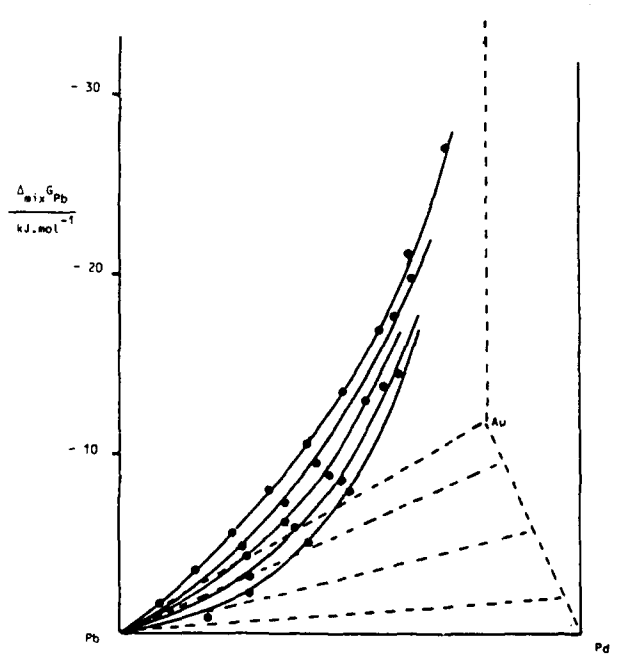

Review of Alloys Modelling

Bo Sundman

Division of Physical Metallurgy, Royal Institute of Technology, Stockholm, Sweden

Abstract

In order to calculate the thermodynamic equilibrium of a system one must have a mathematical model how the thermodynamic functions for each phase depend on temperature, pressure and composition. These types of models are useful for extrapolations to higher order systems or to higher temperatures where there are no data available. Thus these models may be called "models for extrapolation" in order to avoid confusion with models based on fundamental physical properties, like the electronic behaviour, which could be called "models for estimation". This paper will only discuss models for extrapolations which are useful for phase diagram calculations.

Introduction

The development of fast electronic computers have given a new dimension to the use of thermodynamic data. In the pre-computer age it was a tedious task to compute even very simple equilibria when solution phases were involved because it requires an iterative technique in order to solve nonlinear systems of equations. When restricted to pen and paper and maybe a mechanical multiplication machine it was necessary to introduce many simplification in the treatment of thermodynamic data. As many practical methods to solve problems involving thermodynamics were developed in the pen and paper times, these methods are still persisting and have a major influence on the teaching of thermodynamics today.

Some simplifications introduced in solving thermodynamic problems by pen and paper are still useful today. But sometimes these simplifications may be a problem because they tend to obscure the basic thermodynamic principles and instead keep the student busy with trivial tasks as changing reference states for the data. When most undergraduates have daily access to computers it is important to start to introduce thermodynamic methods that make use of such facilities.

Basic Thermodynamic relations

We need only very simple thermodynamics in order to describe the models. As most thermodynamic data are measured at known temperature, pressure and composition it is convenient to chose the thermodynamic function known as Gibbs energy, denoted G, as the basic modelling function. If the Gibbs energy is known one may derive other quantities from this in the following way

Entropy: $S = -(\partial G/\partial T)_P$ ...1

Enthalpy: $H = G + TS$ ...2

Volume: $V = (\partial G/\partial P)_T$ ...3

Heat capacity $C_P = -T(\partial^2 G/\partial T^2)_P$ ...4

Thermal expansivity: $\alpha = \frac{1}{V}(\partial^2 G/\partial P \partial T)$ ...5

Isothermal compressibility: $\kappa = -\frac{1}{V}(\partial^2 G/\partial P^2)_T$ ...6

The quantities introduced above are valid for all thermodynamic systems. If the system may vary in composition the composition must be constant. In solutions one may additionally define

Partial Gibbs energy for component i: $G_i = \partial G/\partial N_i$ ...7

where N_i is the amount in moles of component i.

In modelling we will use the Gibbs energy per formula unit,

$$G_m = \frac{G}{M} \quad ...8$$

where M is the total number of possible sites for constituents in the phase.

In modelling the thermodynamic properties of a system one must of course model each phase in the system separately. The properties of the system at equilibrium is then a function of the properties of the individual phases if surface effects can be negelected.

Models for phases with fixed composition

In real systems there are no phases which cannot vary in composition and in semiconductor system even very minute composition variations can be crucial for the properties. However, in many cases small variations can be ignored for simplicity. A phase that cannot vary in composition will have its Gibbs energy described as a function of temperature and pressure only.

Data for pure elements and compounds with fixed stoichiometry are the most readily available for modelling. As the amount of experimental information from measurements at constant pressure is much more abundant compared to that at constant volume it is reasonable to concentrate on models describing the data as functions of temperature and pressure.

In tables with data for compounds as in the book by Barin and Knacke (1973), the important thermodynamic quantities like C_p, H(T) - H(298), S and G are usually tabulated at given temperature intervals. In addition the values of ΔH_{298} and S_{298} are given. By convention H_{298} for the elements in their stable state at 298.15 K and 1 bar is assumed to be zero. The use of this reference for data is called Stable Element Reference and denoted SER.

The tabulated data can be expressed as a function the temperature in different ways. Sometimes the values of ΔH_{298}, S_{298} are given together with an expression of the C_p as a function of temperature from 298.15 K and up. A typical temperature dependence of C_p is shown in Fig. 1, which is for fcc-Cu. From the C_p and the other quantities it is possible to obtain all other thermochemical quantities because one may integrate the C_p function to a Gibbs energy function

$$G_m - \sum_i a_i H_i^{SER} = \Delta H_{298} - TS_{298} + \int_{298}^{T} C_p d\tau - T\int_{298}^{T} \frac{C_p}{\tau} d\tau \qquad ...9$$

where a_i is the stoichiometric factor for element i in the compound. For equilibrium calculations it is necessary to use data in the form of a Gibbs energy function in order to find the equilibrium. Another fact which supports the use of Gibbs energy is that for solutions, alloys and other mixtures, the Gibbs energy is the dominating quantity used for representing experimental information.

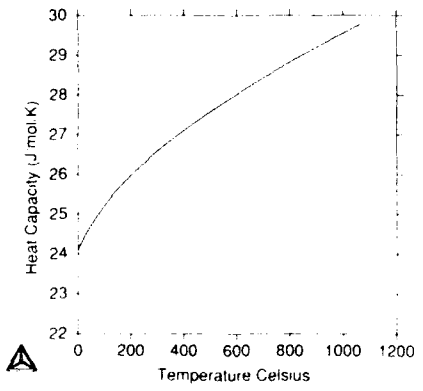

Fig. 1. The heat capacity at constant pressure, C_p, for fcc-Cu.

One may in some cases have to use the Helmholtz energy because it has the advantage that it can be used to calculate the critical point in gas/liquid equilibria. Of course it is always possible to compute the value of the Helmholtz energy using any representation of the temperature and pressure dependence. But one must realize that only in exceptional cases one may find a closed expression for the Helmholtz energy when starting from the Gibbs energy and vice versa.

Model for temperature dependence

The natural approach is to use a power series of T, including positive and negative integers as exponents, as a representation of the temperature dependence of the Gibbs energy of a compound. However, some temperature dependencies can be derived from a theoretical basis also.

In the present case one is only interested in temperatures above 298.15 K and this will in many cases be above the Debye temperature for most compounds. Thus there will be no explicit modelling of low temperature heat capacities included in the Gibbs energy function. The low temperature heat capacity can be sufficiently well modelled by including terms with negative powers of T. The first T^{-1} term can be related to the Debye temperature of the compound.

The heat capacity calculated from an expression for the Gibbs energy is given by eq. 4. Form this equation one finds that a temperature independent heat capacity would have the temperature dependence T*ln(T) in the Gibbs energy expression. As there are theoretical as well as experimental support for a temperature independent heat capacity at high temperatures one should include such a term in the Gibbs energy expression.

Non-integral powers have sometimes been used in the assessment of the temperature dependence of the Gibbs energy or heat capacity of compounds. As such powers have no support from physical interpretations of the heat capacity they should not be used. From these simple arguments the following formula should be recommended

$$G_m = \sum_i a_i T^i + bT\ln T \qquad ...10$$

In geochemistry one is interested to extrapolate to very high temperatures and thus geologists have a tendency to use mainly negative powers of T in eq. 10.

Temperature intervals

In the literature one often finds the following representation of the heat capacity of elements and compounds

$$Cp = a + bT + cT^2 + dT^{-2}$$

This can usually be applied in a limited temperature range only and instead of increasing the number of

coefficients one has used the same four coefficient expression but with different coefficients in two or more temperature regions. In such cases both the heat capacity and its derivative has been forced to be continuous at the break temperature. Except for cases when there are theoretical support for such temperature intervals they should not be used.

Second order transitions

A number of elements and compounds show second order transitions which can be due to magnetic ordering or other internal changes. At the magnetic transition temperature the heat capacity should become infinite and it would be impossible to represent the heat capacity in the vicinity of the critical point with eq. 10 unless many coefficients and maybe also temperature intervals were used. In such cases it is recommended that the contribution to the Gibbs energy due to the second order transition is modelled separately and added to eq. 10.

Eq. 10 can then be considered to be valid for a hypothetical element or compound that does not show the second order transition. For the magnetic transition the following model has been suggested by Inden (1975) and later modified by Hillert and Jarl (1978)

$$G_m^{mo} = RT\, f(\tau)\, \ln(\beta+1), \quad \tau = T/Tc \qquad ...11$$

for $\tau < 1$

$$f(\tau) = 1 - \left[\frac{79\tau^{-1}}{140p} + \frac{474}{497}\left(\frac{1}{p} - 1\right)\left(\frac{\tau^3}{6} + \frac{\tau^9}{135} + \frac{\tau^{15}}{600}\right)\right]/A \qquad ...12$$

and for $\tau > 1$

$$f(\tau) = -\left(\frac{\tau^{-5}}{10} + \frac{\tau^{-15}}{315} + \frac{\tau^{-25}}{1500}\right)/A$$

$$\text{where } A = \left(\frac{518}{1125}\right) + \left(\frac{11692}{15975}\right)\left[\left(\frac{1}{p}\right) - 1\right] \qquad ...13$$

and p depends on the structure. For the bcc structure p is 0.4 and for the fcc structure it is 0.28. Tc and β must be fitted to the experimental transition temperature and Bohr magneton number respectively.

The total Gibbs energy for an element or compound with a second order transition is thus

$$G_m = G_m^{hyp} + G_m^{mo}$$

where G_m^{hyp} is described by eq. 10. In Fig. 2 the C_p for Fe is shown for the stable modifications. The large effect of the ferromagnetic transition in bcc-Fe is clearly evident. When these values are integrated to a Gibbs energy one can obtain the curves in Fig. 3 which shows the value of the Gibbs energy relative to bcc-Fe extrapolated also into the metastable ranges. These curves are much more smooth but effect of the magnetic transition is shown by the increasing stability of bcc-Fe at lower temperatures.

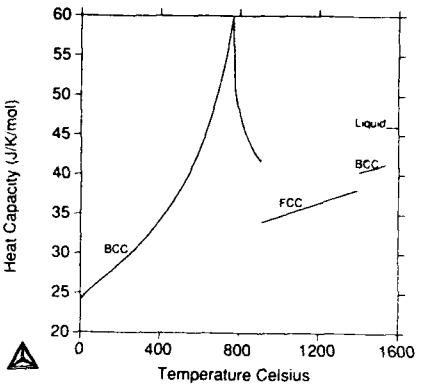

Fig. 2. The heat capacity at constant pressure, C_p, for the stable modifications of Fe showing the stong effect of the magnetic ordering on the bcc phase.

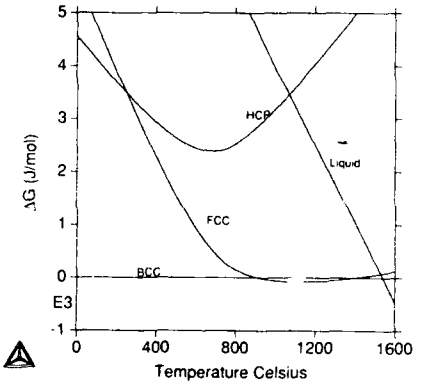

Fig. 3. Each curve represent the difference in Gibbs energy for the different modifications of pure Fe relative to bcc-Fe at a function of temperature. The curve with the lowest value at each temperature represent the stable modification.

Metastable extrapolations

In many cases it is interesting to know the properties of a compound or phase outside its range of stability in temperature, pressure or composition. In particular for the case of solution phase modelling described later it will turn out to be very important to estimate the Gibbs energy of elements and compounds outside their stable ranges.

The most important of this is extrapolation of the liquid phase below and the solid phase above the melting temperature. In this case one cannot use any experimental data but must use some assumption. In the development of a general solution database the Scientific Group Thermodata Europe (SGTE) (Ansara and Sundman, 1987) has employed the method that the heat capacity of the solid phases above the melting point should approach that for the liquid phase and the liquid phase below the melting point should approach that of the solid phase. This is a very crude method and it should only be used whenever one cannot find a better method. One advantage is that this method avoids the problem that the solid phases may become stable when extrapolating to very high temperatures. But this model cannot be used for the glass transition.

The extrapolation of data for a phase that is stable at least within a limited temperature range can thus be made with more or less crude methods. However, in solution modeling one is interested in the thermodynamic properties of pure Chromium with an fcc lattice for example. This has never been found in nature and thus such properties must be estimated by various methods and models (Sauders et al 1988; Kaufman and Bernstein, 1979). A recent recommendation of data for stable and metastable modifications of the elements have been compiled by Dinsdale (1989).

Model for pressure dependence

The pressure dependent properties like volume and thermal expansivity is often ignored in thermodynamic models. It is important only at very high pressures. For the gas phase, except close to the critical point or the boiling point, it is sufficient to describe the pressure dependence by one term, $RT\ln(P/P_0)$. For the condensed phases a model suggested by Murnaghan (1944) can be useful.

The isothermal compressibility, κ, is related to the Gibbs energy through eq. 6 and the thermal expansivity, α, through eq. 5. From this one can obtain the pressure dependent part of the Gibbs energy by integration, if α is pressure independent

$$G_V(T,P) = V_0 \exp\left[\int_{298}^{T} \alpha(T)dT\right] \int_0^P \exp\left[\int_0^P -\kappa dP\right] dP \qquad ...14$$

Here V_0 is the volume at 298 K and zero pressure. The pressure dependence for condensed phases are important only for pressures of several kbar and thus the lower integration limit can be set to zero rather than 1 bar. In the Murnaghan model one assumes that the bulk modulus can be expressed by a linear pressure dependence. As the compressibility is the inverse of the bulk modulus we have

$$\kappa(T,P) = \frac{1/n}{B_0(T)/n + P} \qquad ...15$$

where $B_0(T)$ is the bulk modulus at zero pressure and n is a constant independent of temperature and pressure. Experimentally n is found to be about 4 in many cases.

The thermal expansivity can usually be described as a power series in temperature and in order to make reasonable extrapolations from low temperature, where most measurements are made, one should use an expression

$$\alpha = \alpha_0 + \alpha_1 T + a_2 T^{-2} \qquad ...16$$

and avoid higher powers than one. This model was used in a recent assessment of pure iron (Fernandez Guillermet and Gustafson) and in Fig. 4 the phase diagram for iron is shown for varying temperatures and pressures. A great advantage with the Murnaghan model is that it can be inverted so that the pressure is expressed as a function of volume. This means that the same parameters can be used for a Helmholtz energy expression as well as a Gibbs energy expression. At very high pressures, for example in the core of the earth, the Murnaghan model may have to be augmented with several pressure terms. However, one then looses the possibility to invert the model.

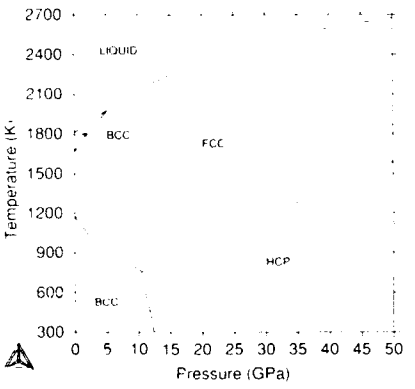

Fig. 4. The phase diagram for pure Fe.

Models for composition dependence

Most real systems contain one or more solution phases or mixtures. In a solution phase the composition may change, possibly restricted by some stoichiometric constraints. Each solution phase in a system must be modelled separately as well as each compound. As most solid solution phases are stable only within a limited composition range it is often necessary to make assumptions of the properties of some components of the phase outside its range of stability in order to assess the data for the phase.

In most cases models of the composition dependence is based on the mole fraction of the constituents as composition variable. However, in some cases other variables have been introduced in order to obtain simpler expression for the Gibbs energy model. For example when modelling chemical order/disorder one may use a variable describing the degree of order or one may use the fraction of lattice sites occupied by each

type of atom. In models for ordering the fraction of bonds or "clusters" are sometimes used as independent variables. Another example are the models used for organic liquids where a quantity related to the molar volume of the constituents are used.

In Fig. 5 a survey of models used for describing composition dependence is shown giving some idea of the relation between them. The basic model is the ideal and the term ideal should be reserved for the case when the constituents are real stable species like H2, CO2 etc. in a gas or H2O and OH^- in a liquid. If some fictitious species are added, the existence of which are not certain, these new species are a modelling aid and therefore the model is no longer ideal. In chemistry this is called a complex model if all species are non-interacting.

In order to describe miscibility gaps one must use a model which take into account the interaction between the elements. Such interaction terms are called excess Gibbs energy terms. There are many different such excess models suggested but for binary systems they are all identical. For a ternary system they may give different extrapolations.

If the interactive energy is negative, i.e. attractive, is possible to add fictitious species or "clusters" with or without a modification of the random mixing entropy expression. If the interaction parameter very negative it is probably a bad assumption that the constituents mix randomly. However, the fictitious species can be introduced in many different ways and there are several models making use of this method in order to describe ordering in crystalline phases and liquids.

A different method to modify the entropy of mixing is to take into account the existence of sublattices in crystalline phases. In each sublattice the entropy expression is assumed to be random. This model have successfully been used to describe interstitial solutions and intermetallic compounds with sites of different coordination number.

The essential property of the models is the ability to describe experimental information and allow extrapolations from these data. Thus the assessment of experimental data is crucial and in Fig. 6, from the Thesis by A. Fernandez Guillermet (1988), the normal assessment procedure is described.

A question commonly asked by those who are learning to do assessment work is when one can decide that the assessment is finished. Actually there are no finished assessments, all results presented from assessments represent the result when the assessor had to give up, either from lack of funding or interest.

Ideal solutions

The simplest description of a solution ase is that the constituents are noninteracting and that they mix randomly. This gives the following ideal solution model

$$G_m = \sum_i x_i {}^\circ G_i + RT \sum_i x_i \ln(x_i) \qquad ...17$$

A derivation of this expression using statistical mechanics and assuming non-interacting species in a gas can be found in any textbook on thermodynamics. It is interesting that one obtains the same formula assuming random distribution of atoms on fixed lattice sites. The quantities $^\circ G_i$ are the Gibbs energies of pure elements and compounds as function of temperature and pressure as discussed earlier.

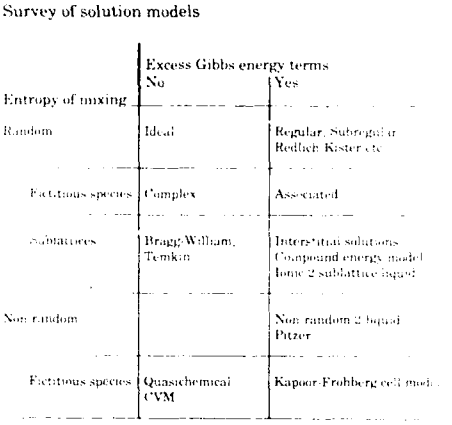

Fig. 5. Survey of models

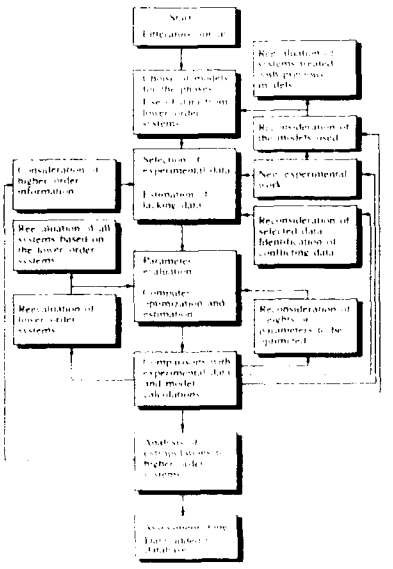

Fig. 6. A block diagram showing the procedure for assessing thermochemical data for solutions. Note the importance of models and estimated data for metastable states.

Complex models

In the expression for the ideal solution all real species formed in the phase should be included in the formula. If the solution phase shows a deviation from the ideal model this means that there is some interaction between the constituents which cannot be ignored. However, for negative interactions one may still retain the simple formula in eq. 17 and instead postulate the existence of more species. Such models are generally called "complex models" and are mainly used to describe the properties of the gas or liquid phase.

Excess Gibbs energy

Strong positive interaction means that the constituents do not like to mix and may lead to miscibility gaps. In order to describe a miscibility gap it is necessary to generalize eq. 17 in the following way.

$$G_m = {}^{ref}G_m + {}^{mix}G_m + {}^{E}G_m \qquad ...18$$

where ${}^{E}G_m$ is called the excess Gibbs energy. Substitutional regular solution models use ${}^{ref}G_m$ and ${}^{mix}G_m$ according to eq. 17 i.e.

$$\begin{aligned} {}^{ref}G_m &= \sum_i x_i {}^{\circ}G_i \\ {}^{mix}G_m &= RT \sum_i x_i \ln(x_i) \end{aligned} \qquad ...19$$

but other models, for example the sublattice model, use other expressions for ${}^{ref}G_m$ and ${}^{mix}G_m$. One should note the difference between the excess Gibbs energy and the Gibbs energy of mixing. The latter is

$${}^{M}G_m = G_m - \sum_i x_i {}^{\circ}G_i \qquad ...20$$

where the summation is made over the components of the system. The Gibbs energy of mixing is thus a model independent quantity whereas the excess Gibbs energy depends on the model.

Regular solution models

The regular solution models uses eqs. 18 and 19 as base and tries to account for the non-ideality of a phase by introducing terms in the excess Gibbs energy which depend on two or more fractions. In the simplest case one may estimate such terms from the heat of mixing.

When there are interactions between the two constituents of a binary phase the simplest modelling approach is this term

$${}^{E}G_m = x_1 x_2 L_{12} \qquad ...21$$

where x_1 and x_2 are the mole fractions of constituent 1 and 2 respectively. In multicomponent systems one can introduce an interaction between each pair of constituents

$${}^{E}G_m = \sum_{i} \sum_{j>i} x_i x_j L_{ij} \qquad ...22$$

One should note that the fractions x_i must be taken from the constitution of the multicomponent phase. In many cases it is not sufficient to have a single coefficient L_{ij} to describe the excess Gibbs energy of a binary system. One may then expand L_{ij} as a function of the fractions x_i and x_j. The following expansion is recommended for use when one wishes to extrapolate the binary excess Gibbs energy to a multicomponent system

$${}^{E}G_m^{ij} = x_i x_j \sum_n (x_i - x_j)^n L_{ij}^n \qquad ...23$$

The excess term expressed in the differences of the fractions in this way is usually called a Redlich-Kister polynomial. One great advantage with eq. 23 compared to other models like Margules or Legendre, is that one may use the fractions x_i from multicomponent system directly in eq. 23. This avoids any complicated extrapolation scheme like Kohler or Colinet in order to convert the multicomponent fractions into binary fractions before calculating the binary excess contribution. For ternary systems the method of using the ternary fractions in eq. 23 is called a Muggianu extrapolation scheme.

There are other excess models which use different forms of composition dependence but for binary system they are all equal. The advantage with eq. 23 is that the differences are invariant when there are three or more constituents and it is thus suitable for extrapolations to higher order systems because the compositions of i and j in the ternary or higher order system can be used directly in eq. 23. Note that eq. 23 must not be rewritten using the relation $x_i = 1 - x_j$ as this is valid only in the binary system.

The number of terms in a Redlich-Kister polynomial can be arbitrary high and of course the fit to experimental data is better the greater the number of coefficients. Therefore it is appropriate to point out that increasing the number of coefficients will decrease the significance of each coefficient and there is a limit which should not be exceeded especially if the assessment should be used for extrapolations to higher order systems. That limit is about 3 coefficients in metallic systems and 4 in non-metallic systems. If it is not possible to obtain fit within this limit one should reconsider the model used for the phase and try a sublattice model or an associated model. The reason for the restriction is that the experimental data in a binary system is usually limited and it is possible to obtain equally good agreement with the experiments using several different sets of coefficients. But these sets will give different extrapolations to higher order systems. The best way to decide which set is best is to try extrapolations into higher order systems where there might be more experimental information or include this information when assessing the binary system. This means that one often has to modify the binary subsystem when assessing a ternary system. But if a binary subsystem has been used in other ternary assessments one may not change it without reassessing also these systems if one is developing a general thermodynamic database.

Based on the binary interaction one may, for ternary phases which show deviation from the Gibbs energy extrapolated from the binary system, introduce a ternary interaction of the following form

$$^{E}G_{m}^{123} = x_1 x_2 x_3 L_{123} \qquad ...24$$

It is important to note that the strongest influence on the ternary properties will be the extrapolated binary excess Gibbs energies. When assessing ternary phases one should not simply add a ternary interaction but try to modify the binary interactions including the ternary information. If a single ternary interaction is not sufficient the following expression should be used

$$L_{123} = v_1 L^1_{123} + v_2 L^2_{123} + v_3 L^3_{123} \qquad ...25$$

where the v variables are defined as

$$v_1 = x_1 + (1 - x_1 - x_2 - x_3)/3$$

$$v_2 = x_2 + (1 - x_1 - x_2 - x_3)/3 \qquad ...26$$

$$v_3 = x_3 + (1 - x_1 - x_2 - x_3)/3$$

For the ternary system 1-2-3 the v and the x fractions are identical. However, in a higher order system the sum of v_i will always add up to unity whereas the sum of $x_1 + x_2 + x_3$ will be smaller. This term was first introduced by Hillert (1980).

Associated models

In modelling of condensed alloy phases one has traditionally used only the components as constituents. This is in contrast with the gas phase where there is usually many more constituents than there are components. The associated model is a mixture between the complex model and the regular solution model because it introduces fictitious species in order to describe short range order and allows interaction parameters between the real and fictitious constituents. The model thus have the same G_m equation as a regular solution model. But as the number of constituents have increased it can be used to describe more complicated Gibbs energy functions.

The associated model has successfully been used by Sharma and Chang (1980) to describe liquids where the activity of a component varies drastically within a small composition range. An example of this is shown in Fig. 7 for the Cu-S system. The associated model assumes that a species Cu_2S exists and thus the binary Cu-S system is transformed into a ternary as shown in Fig. 8. This means that one has an internal degree of freedom because the composition is the same along the dashed lines.

The curve inside the triangle shows a possible locus for the minimum Gibbs energy and it is clear that this model allows the system to be constructed as two almost independent binaries. In the phase diagram shown in Fig. 9 it is evident that this system has two miscibility gaps separated by a very stable liquid

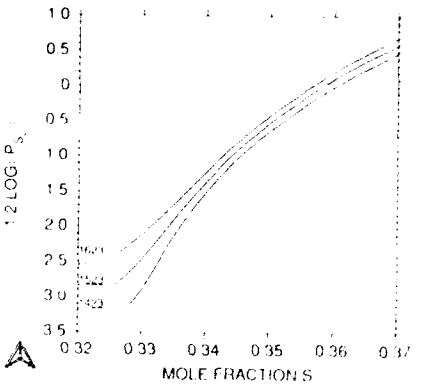

Fig. 7. The variation of sulphur activity in liquid Cu-S expressed as the partial pressure of S_2 with temperature and composition close to the Cu_2S composition.

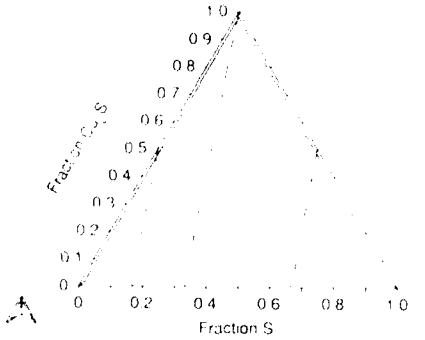

Fig. 8. The constitutional triangle for Cu-S modelled with an associate Cu_2S or, equivalently, modelled using the ionic two-sublattice liquid model with $(Cu^{+2})_P(S^{-2},Va,S^0)_2$.
Along the dashed lines the composition is constant.

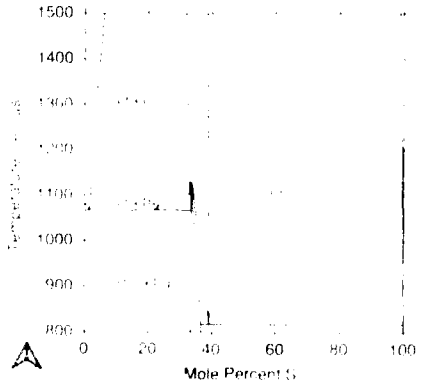

Fig. 9. The phase diagram for Cu-S showing the narrow range of stable liquid around Cu_2S.

phases. Any model used to describe this system must take into account the short range order in the liquid around the Cu_2S composition.

Sublattices

All crystalline phases have defined lattice sites for the atoms. In many cases the lattice sites have different coordination numbers and the distances to all nearest neighbours may not be constant. If there are different types of sites one should use this fact in modelling the thermodynamic properties of the phase. When using sublattices it is convenient to introduce a special fraction variable, called the site fraction, which gives the fraction of each component on each sublattice. The sum of the site fractions on each sublattice is thus unity.

The basic Gibbs energy expression for case with several sublattices is

$$G_m = \sum_I P_I(Y)^\circ G_I + RT\sum_s a_s \sum_i y_i^s \ln(y_i^s) + {}^E G_m \qquad ...27$$

where I is a "constituent array" specifying one constituent in each sublattice and Y is a matrix with all constituent fractions. $^\circ G_I$ is the Gibbs energy of formation of a compound with the constituents given by I. a_s is the (relative) number of sites on sublattice s and y_i^s is the fraction of constituent i on sublattice s. $^E G_m$ is the excess Gibbs energy. The term $P_I(Y)$ is the product of the site fractions of the constituents given by I, one from each sublattice,

$$P_I(Y) = \Pi_i y_i^s \qquad ...28$$

The excess Gibbs energy, $^E G_m$ consists of terms with two or more site fractions from the same sublattice and is thus similar to the excess Gibbs energy for a regular solution model.

The relation between the mole fraction and the site fractions are, assuming that each component enters only one sublattice and that there are no vacancies,

$$x_i = \frac{a_s y_i^s}{\sum a_s}$$

Sublattices have been used successfully to describe a number of different systems like interstitial solutions, intermetallic compounds, chemical ordering and oxides.

Sublattices for interstitial atoms

As an example of an interstitial solutions one may take for example C in fcc-Fe. In such a case one sublattice represent the substitutional sites for Fe and one the interstitial sites for C. As most of the interstitial sites are vacant it is convenient to introduce a new component, vacancies denoted Va, in order to simplify the mathematical expressions. At the same time it is required that the vacancies have their chemical potential equal to zero and thus one does not violate the Gibbs phase rule.

The Gibbs energy in this case is

$$G_m = y_{Va}\, {}^\circ G_{Fe:Va} + y_C\, {}^\circ G_{Fe:C} + RT(y_{Va}\ln(y_{Va}) + y_C\ln(y_C)) + {}^E G_m \qquad ...29$$

$^\circ G_{Fe:Va}$ is the Gibbs energy of formation of iron in the fcc state and $^\circ G_{Fe:C}$ is the Gibbs energy of formation of a fictitious fcc phase with all interstitial sites filled with carbon i.e. an fcc carbide.

The excess Gibbs energy, restricted to a single interaction term, can be written

$$^E G_m = y_{Va} y_C L_{Va,C} \qquad ...30$$

As the substitutional sublattice is completely filled with Fe the site fraction of Fe is unity and has been omitted. The relation between the site fractions, y_i^s and the mole fractions is

$$x_{Fe} = \frac{1}{1+y_C}$$

$$x_C = \frac{y_C}{1+y_C} \qquad ...31$$

In the Fe-C system there is no fcc carbide but there are many carbides with an fcc structure for example TiC and VC. In these phases the stoichiometric deviation is large towards the metal but it is usually very restricted towards carbon as shown in Fig. 10 for Ti-C. In order to demonstrate the effect of the restricted solubility due to the interstitial sublattice the Gibbs energy curves at 1500 K for the same system is shown in Fig. 11. The ration between interstitial sites and substitutional sites for the hcp phase is 0.5, for the fcc 1 and for the bcc 3.

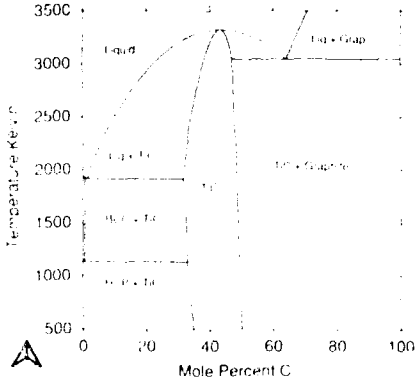

Fig. 10. The phase diagram for Ti-C showing the wide composition range of the fcc-carbide, modelled with a sublattice model.

It will lead to a less good description of the entropy of mixing for the phase if one ignores the fact that a phase has sublattices and this error will lead to more complicated excess Gibbs energy expressions. One reason why the sublattice model is not used more frequently is that it may not be obvious how to calculate the carbon potential using eq. 29. Therefore it is appropriate to give the basic equation how to derive the chemical potential for a phase with sublattices as derived by Sundman and Ågren (1981). One must first realize that one cannot calculate the chemical potential

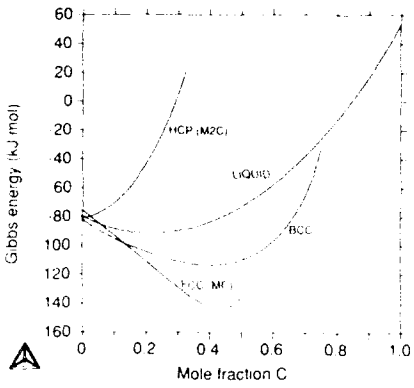

Fig. 11. The Gibbs energy curves for various phases in the Ti-C system at 1500 K. Note that the sublattice model ends at 1/3 for the hcp phase because there is 0.5 interstitial site per metallic site. The fcc phase ends at 0.5 and the bcc phase ends at 0.75.

for the components directly from eq. 27, but only for the constituent arrays, I. For any constituent array I we have the following chemical potential

$$G_I = G_m + \sum_i \frac{\partial G_m}{\partial y_i^s} - \sum_s \sum_j y_i^s \frac{\partial G_m}{\partial y_i^s} \quad ...32$$

Inserting eq. 29 we get for the Fe-C system

$$G_{Fe:Va} = G_m + \frac{\partial G_m}{\partial y_{Va}} - y_{Va}\frac{\partial G_m}{\partial y_{Va}} - y_C\frac{\partial G_m}{\partial y_C}$$

$$G_{Fe:C} = G_m + \frac{\partial G_m}{\partial y_C} - y_{Va}\frac{\partial G_m}{\partial y_{Va}} - y_C\frac{\partial G_m}{\partial y_C} \quad ...33$$

At equilibrium we also have

$$G_{Fe:Va} = G_{Fe} + G_{Va} \quad ...34a$$

$$G_{Fe:C} = G_{Fe} + G_C \quad ...34b$$

As G_{Va} is zero one may subtract eqs. 34a and 34b which gives after some rearrangement

$$G_C = G_{Fe:C} - G_{Fe:Va} \quad ...35$$

Inserting eq. 33 we get

$$G_C = \frac{\partial G_m}{\partial y_C} - \frac{\partial G_m}{\partial y_{Va}} =$$

$$^\circ G_{Fe:C} - {}^\circ G_{Fe:Va} + RT\ln\left(\frac{y_C}{y_{Va}}\right) + (y_{Va} - y_C)L_{Va:C} \quad ...36$$

It is straightforward to generalize to more sublattices and components starting from eq. 32 and generalizing eq. 34.

Sublattices for intermetallic phases

Phases with restricted solubilities are often found in alloy system. In the extreme case there is no solubility and the phase can be treated as a compound. But if the solubility is significant one should determine which sublattices there are in the crystalline structure. In many cases it would be to complicated to use the full structure so some of the sublattices may be treated as identical.

One unforseen complication with the use of sublattices for multicomponent systems might be that one must use the same sublattice model for the same phase in all systems. Thus if one makes simplifications of the real structure such simplifications must be valid in other systems as well. A particular example of this is the σ phase. σ phases appears in systems with bcc elements (A atoms) like Cr, Mo, V and fcc elements (B atoms) like Fe, Ni, Co. The unit cell of the σ phase has 30 sites divided on five sublattices. The first sublattice has two sites, the second four and the following three have eight sites each. The first sublattice is predominantly filled with B type atoms, the second with A type atoms, the third with B type atoms and the last two A and B are usually mixed. Thus three sublattices are sufficient for the modelling

$$(B)_{10}(A)_4(A,B)_{16}$$

However, there are some σ phases where this distinction is not so strong and in order to be able to handle such systems the following model has been adopted

$$(B)_8(A)_4(A,B)_{18}$$

Other intermetallic phases like μ, R and Laves phases can be treated accordingly. A system with many intermetallic phases is the Fe-Mo system and the calculated phase diagram from an assessment by A. Fernandez Guillermet (1982) is shown in Fig 12.

Sublattices are also very important in metal-nonmetallic compounds like oxides and sulphides. In some cases these phases have considerable compositional variation. In Fig 13 the

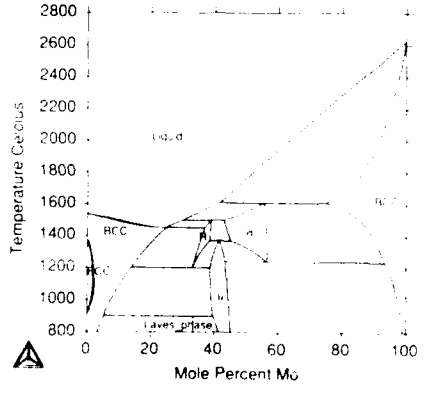

Fig. 12. The phase diagram for Fe-Mo showing several intermetallic phases modelled with the sublattice model.

wüstite phase region from the Fe-O system is shown. This has been modelled using a two-sublattice model with the fcllowing constituents

$(Fe^{+2}, Fe^{+3}, Va)_1 (O^{-2})_1$

At higher oxygen potential the fraction of Fe^{+3} increases in the wüstite. In order to maintain electroneutrality one must at the same time increase the number of vacant sites on the sublattice. The constitutional triangle for this system is shown in Fig 14. The line in the triangle represent the neutral combination of Fe^{+3} and Va.

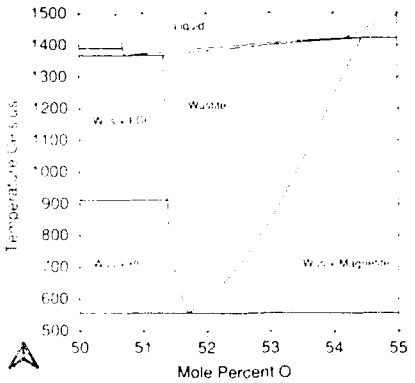

Fig. 13. The Wüstite phase field in the Fe-O system where the wüstite has been modelled with two sublattices, one with oxygen ions and on with Fe^{+2}, Fe^{+3} and Va.

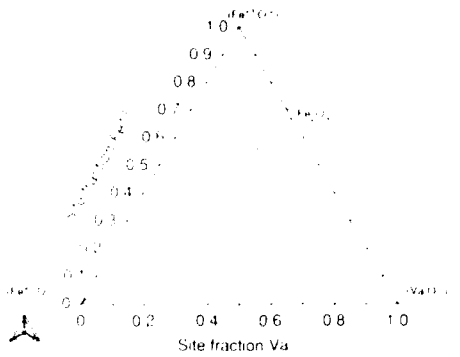

Fig. 14. The constitutional triangle for the wüstite phase. Note that only the line from FeO to Fe_2O_3 represent neutral combinations of Fe^{+3} and Va.

Sublattices for long range order

A final case where sublattices are useful is to describe chemical ordering. There is a significant difference between phases with sublattices of different types for example σ, and phases with ordering transformations for example fcc Au-Cu. The reason is that the σ phase the sites have different coordination numbers wheras the sites in the fcc phase are equivalent. If the interactions are negative in an fcc phase there will always be a transition between a state with a long range order (lro) and a disordered state, usually with some short range order (sro). The lro state can be modelled with the sublattice model for example the bcc phase in Fe-Si system as shown in Fig. 15 where the B2/A2 transition is shown as a dashed line.

The treatment of lro ordering presented by Bragg and Williams (1934) was identical to a sublattice model although they used an ordering parameter as independent variable.

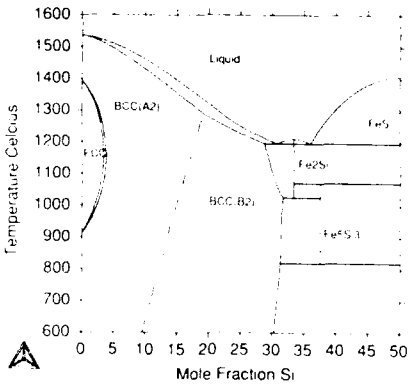

Fig. 15. The phase diagram for Fe-Si with the second order transition from A2 to B2 for BCC shown as a dashed line.

Quasichemical models

Systems with a strong negative interaction has a tendency for ordering i.e. unlike atoms like to be together. This has a significant influence on the entropy of mixing and the assumption of random distribution is no longer very good. Even without lro the negative interaction has a considerable influence on the sro contribution to the Gibbs energy for the phase.

A correction of the entropy of mixing called the quasichemical model was first suggested by Bethe (1935). In this model one assumes that the bonds between A and B atoms are distributed randomly. The bonds are related by a simple chemical reaction formula with a Gibbs energy of reaction

$$A\text{-}A + B\text{-}B = 2\ A\text{-}B \qquad \Delta G_{AB} \qquad ...37$$

This gives the following Gibbs energy expression

$$G_m = y_{AB}\Delta G_{AB} + RT(y_{AA}\ln(y_{AA}) + y_{BB}\ln(y_{BB}) + y_{AB}\ln(y_{AB}) + y_{BA}\ln(y_{BA})) \qquad ...38$$

where $y_{AB} = y_{BA}$. The mass balance conditions requires that the mole fractions of A and B are given by

$$x_A = y_{AA} + y_{AB}$$
$$x_B = y_{BA} + y_{BB} \qquad ...39$$

Eq. 38 can be generalized by introducing the number of bonds per atoms, z, but that is not important in this case. It is easily recognized that eq. 38 is identical to the Gibbs energy expression of a gas phase with AA, BB, BA and AB molecules (the Gibbs energy of formation of AB and BA molecules are the same). In a gas phase the molecules are independent but in a crystalline phase the nearest neighbours to a site must agree what atoms are placed in each site. In order to correct for the overestimation of the entropy in eq. 38 the following expression have been suggested

$$G_m = y_{AB}\Delta G_{AB} + RT(y_{AA}\ln(y_{AA}) + y_{BB}\ln(y_{BB}) + y_{AB}\ln(y_{AB}) + y_{BA}\ln(y_{BA})) - RT(x_A\ln(x_A) + x_B\ln(x_B)) \quad ...40$$

Even with this correction eq. 40 is valid only when the short range order is small. However, eq. 40 has one important property, if ΔG_{AB} is zero then there should be no sro and eq. 40 should be identical to an ideal model. In this case we have

$$y_{AA} = x_A^2$$

$$y_{AB} = y_{BA} = x_A x_B \quad ...41$$

$$y_{BB} = x_B^2$$

By inserting eq. 41 in eq. 40 we find that this becomes identical to eq. 17.

Cluster Variation Method

A more elaborate model for ordering, called the cluster variation method (CVM), has been developed by Kikuchi (1951). In this model one not only takes pairwise bonds into account but also "clusters" with three, four, five and more atoms. Each of these clusters will have a Gibbs energy of formation from the number of AB bonds it contains. And the entropy expression has a correction term in order to take into account the fact that the clusters share surfaces, edges and corners.

Indeed this model may seem very far from a model for a gas with molecules but actually it is not so. In Fig. 16 The Gibbs energy curves for three possible models for an ordered system is shown. The upper curve is for an ideal model with only the components A and B. The bottom curve is for an "associate" model or gas with the five clusters A_4, A_3B, A_2B_2, AB_3 and B_4. The intermediate curve is for a tetrahedron approximation of the CVM model with the same five clusters.

If the Gibbs energy curves are not very different the entropy curves may be. In Fig. 17 calculations of a prototype phase diagram for an fcc phase with $L1_2$ and $L1_0$ ordering is shown using three different models and the same nearest neighbour bond energy, from a paper by Sundman and Mohri (1990). It is very difficult to obtain the same diagram using only the sublattice model because this model ignores the short range order contribution and thus underestimates the stability of the disordered phase.

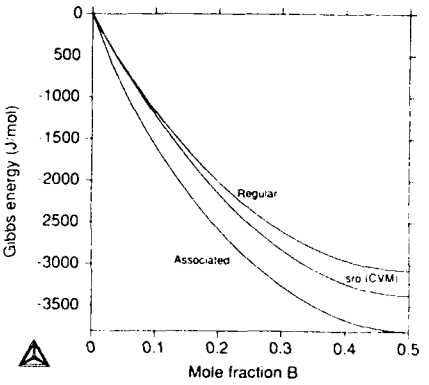

Fig. 16. The Gibbs energy for three different models using the same nearest neighbour bond energy. The regular solution model with just one interaction term is the highest curve. If one attempts to describe short range order by introducing associates, in this case the three associates A_3B, A_2B_2, AB_3 was assumed, the bottom curve is obtaind as the associates increase the entropy of mixing. Fially, if one corrects the entropy of mixing by considering that the associates will share corners and edges in the crystalline lattice one obtains the cluster variation method (CVM) and this is given by the intermediate curve.

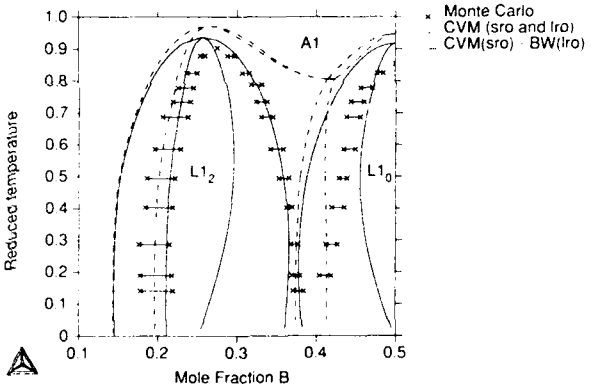

Fig. 17. This figure is a prototype phase diagram for an fcc phase with ordering. The dashed lines have been calculated using the CVM tetrahedron approximation for both the disordered phase and the ordered. The full lines show a calculation using CVM for the disordered phase and the sublattice model for the ordered phases. Finally the tie-lines are from a Monte-Carlo calculation by Binder.

Dilute models

The first application of thermodynamic calculations in metallurgy was made at a time when all calculations had to be made by pen and paper. At that time one could only handle dilute solutions and stoichiometric compounds and a number of simplified models as proposed, the most well known in metallurgy by Wagner (1952). In this ε-model the activity coefficient of a solute is assumed to be linearly dependent on its concentration whereas the solvent is assumed to obey Roults law.

Such a model may account for experimental information in the dilute range but the model is actually thermodynamically inconsistent as it violates the Gibbs-Duheim relation. Therefore one should not use such models in computer software for thermodynamic calculations, and in particular so when Bale and Pelton (1986) and Hillert (1986) have developed a method to incorporate the ε parameters into a regular solution model which actually extends the composition range for which they can be applied. Following Hillert the transformation is given by

$$^{\circ}G_i = RT\,\gamma_i^{\circ} + 0.5\,RT\,\varepsilon_{jj} \qquad ...42$$

$$L_{1i} = -0.5\,RT\,\varepsilon_{ii} \qquad ...43$$

$$L_{ij} = RT(\varepsilon_{ij} - 0.5(\varepsilon_{ii} + \varepsilon_{jj})) \qquad ...44$$

where 1 denotes the solvent and i and j solute atoms. Note that the terms $^{\circ}G_i$ are dependent upon the solvent. The parameters in eqs. 42-44 can be used in a substitutional regular solution model according to eq. 18.

Sublattice models for the liquid

Most liquids can be described fairly well with the substitutional regular solution model. However, in some cases sro is significant and this has lead to the use of the associate model in some systems.

In the liquid phase there are no sites like in a crystalline phase and thus the use of sublattice for liquids may seem artificial. However, already in 1945 Temkin (1945) showed that molten salts could be successfully described using a two-sublattice model with cations mixing on one set of sites and anions on another. In accordance with experience a liquid dominated by one cation and one anion would have very low entropy of mixing according to this model. The alternative model would be to assume that the ions formed "associates" in the liquid.

In particular when mixing four salts, A_cC_a, A_dD_a, B_cC_b, B_dD_b we obtain a reciprocal system as shown in Fig. 18, taken from Hillert and Staffanson (1970), with A and B in the first sublattice and C and D on the second.

$$(A^{+a},B^{+b})(C^{+c},D^{+d})$$

If all ions have the same valence the Gibbs energy expression for this liquid is identical to that for a crystalline two-sublattice model. However, if the valences of the cations or anions are not equal one must find some method to maintain electroneutrality in this liquid. one method is to use equivalent fractions defined by

$$z_A = \frac{N_A/a}{N_A/a + N_B/b}$$

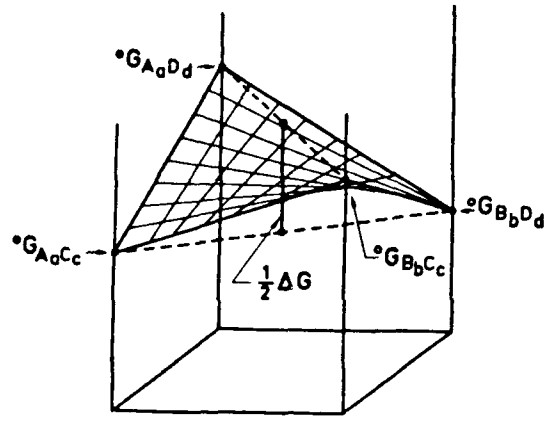

Fig. 18. The $^{ref}G_m$ surface for a reciprocal system showing the relation between the reciprocal energy, ΔG and the four corner compounds. In general the surface will be curved.

$$z_C = \frac{N_C/c}{N_C/c + N_D/d} \qquad ...45$$

where a, b, c and d are the valences of A, B, C and D respectively. However, the use of equivalent fractions has the drawback that it is impossible to extend the model to systems with neutral constituents. Therefore another model have been developed which can be extended both to systems with only cations (i.e. metallic systems) and also to the non-metallic liquids, for example liquid sulphur. This model is called the ionic two-sublattice liquid model (Hillert et al, 1985) and it uses site-fractions as constituent variables. In order to handle a liquid with only cations, i.e. metallic liquids, hypothetical vacancies are introduced on the anion sublattice and in order to extend the model to non-metallic systems one introduces neutral species on the anion sublattice. The model can be written as

$$(C_i^{v_i})_P(A_i^{v_i},Va,B_i^0)_Q$$

where each pair of parentheses surround a sublattice. C represents cations, A anions, Va hypothetical vacancies and B neutrals. The charge of an ion is denoted v_i and the index i is used to denote a specific constituent. The superscript v_i on cations and anions as well as 0 for the neutrals will not be included in the following text. The number of sites on the sublattices, P and Q, must vary with the composition in order to maintain electroneutrality. The values of P and Q are calculated from the following equations

$$P = \sum_i (-v_i)y_{A_i} + Qy_{Va} \qquad ...46$$

$$Q = \sum_i v_i y_{C_i} \qquad ...47$$

where y denotes the site fraction of a constituent. P and Q are simply the average charge on the opposite sublattice. The hypothetical vacancies have an induced charge equal to Q.

The ordinary mole fractions can be calculated from the site fractions in the following way for the components which behave like cations

$$x_{C_i} = \frac{Py_{C_i}}{P + Q(1-y_{Va})} \qquad ...48$$

and for the components which behave like anions or neutrals

$$x_{D_i} = \frac{Qy_{D_i}}{P + Q(1-y_{Va})} \qquad ...49$$

where D is used to denote any constituent on the anion sublattice. Eq. 49 cannot be applied to vacancies, however, because the mole fraction of vacancies is zero of course.

The integral Gibbs energy expression for this model is

$$G_m = \sum_i\sum_j y_{C_i}y_{A_j}{}^{\circ}G_{C_i:A_j} + Qy_{Va}\sum_i y_{C_i}{}^{\circ}G_{C_i} + Q\sum_i y_{B_i}{}^{\circ}G_{B_i} +$$

$$RT(P\sum_i y_{C_i}\ln(y_{C_i}) + Q(\sum_i y_{A_i}\ln(y_{A_i}) +$$

$$y_{Va}\ln(y_{Va}) + \sum_i y_{B_i}\ln(y_{B_i}))) + {}^{E}G_m \qquad ...50$$

where ${}^{\circ}G_{C_i:A_j}$ is the Gibbs energy of formation per $(v_i+(-v_j))$ moles of atoms of liquid C_iA_j, ${}^{\circ}G_{C_i}$ and ${}^{\circ}G_{B_i}$ are the Gibbs energies of formation per mole of atoms of liquid C_i and B_i respectively. The factor Q in front of the second and third sum comes from the variation of the number of sites with the composition. Note that G_m in eq. 50 is defined for $P + Q(1-y_{Va})$ moles of atoms. The term multiplied with RT is the ideal entropy of mixing and ${}^{E}G_m$ is the excess Gibbs energy.

Eq. 50 may look formidable in its complexity and one may wonder if simpler models cannot be equally useful. This criticism misses its point because eq. 50 is the general multicomponent expression and this model is indeed identical to simpler models in many special cases. The great advantage with eq. 50 is that it allows a continuous description of a liquid which changes in character with composition. Eq. 50 has successfully been used to describe oxide liquids, silicates, sulphides as well as liquid short range order, molten salts and ordinary metallic liquids.

A remarkable feature of eq. 50 is that is becomes identical to the associated model for some very simple systems, for example the Cu-S system with a Cu_2S associate. The assumptions behind the associate model and the ionic liquid model are very different and this shows clearly that one cannot make any statement about the true nature of a system just because a mathematical model, based on some physical picture of the system, gives good result. It may be possible that another physical picture of the system will yield exactly the same mathematical model.

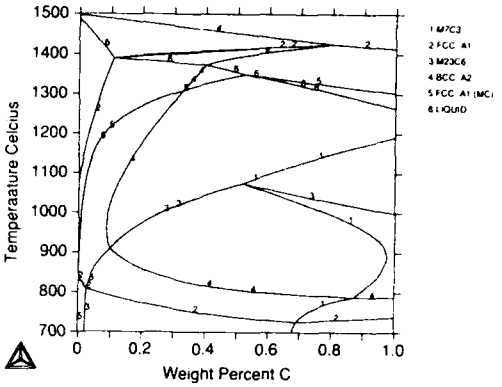

Fig. 19. A phase diagram for a multicomponent steel. The aim of the modelling described in this paper is to be able to make extrapolations into higher order system in order to predict the properties there. The curves are "zero phase fraction" lines and the digit on the curve indicate the phase that is stable with zero fraction along the curve.

Final remarks

A large number of thermodynamic models have been developed for alloys and related systems. However, on closer inspection most of these models are very similar with some minor differences. It thus seems possible that in the not to distant future the number of models used will be quite small which will improve the cooperation towards a generally applicable thermochemical database.

The importance of such a database is clearly evident if one knows what is currently possible even with a very limited database. With the use of phase diagrams like the isoplet shown in Fig. 19 for a steel with eight component, it is possible to develop new materials with better properties and at a lower cost.

References

I. Ansara and B. Sundman (1987): CODATA Report "Computer Handeling and Dissemination of Data", 154

I. Barin and O. Knacke (1973): "Thermochemical Properties of Inorganic Substances", Springer-Verlag, Berlin

H. A. Bethe (1935): Proc Royal Soc. A150, 552

W. L. Bragg and E. J. Williams (1934): Proc. Royal Soc. A145, 69

A. Dinsdale (1989): NPL Report DMA(A)195

A. Fernandez Guillermet (1982): Calphad Vol 6, 127

A. Fernandez Guillermet and P. Gustafson (1985): High Temp.-High Press. Vol 16, 591

A. Fernandez Guillermet (1988): Thesis, Royal Institute of Technology, Sweden

M. Hillert and L.-I. Staffanson (1970): Acta Chim. Scand. Vol 24, 3618

M. Hillert and M. Jarl (1978): Calphad Vol 2, 82

M. Hillert (1980), Calphad Vol 4, 1

M. Hillert, B. Jansson, B. Sundman and J. Ågren (1985): Met. Trans A, Vol 16A, 661

M. Hillert (1986): Met. Trans A, 17A, 1878

G. Inden (1975): Z. Metallkde, Vol 66, 725

L. Kaufman, H. Bernstein (1979): "Computer Calculations of Phase Diagrams", Academic Press, NY and London

R. Kikichi (1951): Phys. Rev., Vol 81, 998

F. D. Murnaghan (1944): Proc. Natl. Acad. Sci. (USA) Vol 30, 244

A. D. Pelton and C. W. Bale (1986): Met. Trans A, 17A, 1211

N. Saunders, A. P. Miodownik and T. T. Dinsdale (1988): Calphad Vol 12, 351

R. C. Sharma and Y. A. Chang (1980): Met. Trans B, Vol 11B, 575

B. Sundman and T. Mohri (1990): Z. Metallkde, Vol 81, 251

B. Sundman and J. Ågren (1981): J. Phys. Chem. Sol., Vol 42, 297

M. Temkin (1945): Acta Phys. Chim. USSR, Vol 20, 411

C. Wagner (1952): Thermodynamics of Alloys, Addison-Wesley Press, Cambridge, MA

NEW AND OLD TOOLS IN MARTENSITIC TRANSFORMATION STUDIES

A. Amengual(+), V. Torra(+), A. Isalgué(*), F. Marco(*)

(*) Dep. Física Aplicada U.P.C. Diagonal 649, 08028 Barcelona (Spain)
(+) Dep. Física Univ. Illes Balears, 07071 Palma Mallorca (Spain)

Abstract

We have developed a high resolution thermal analysis set-up that allows the accurate control and programmation of the temperature within a working space. In our experimental system, with a sample of less than 2 g in mass, it enables us to work cycling with a resolution and reproducibility about 0.005 K. The maximum amplitude used is near 70 K. The system has been built in a very simple way and the working domain lies around the room temperature. This controlled system has been applied to the study of the evolution of the martensitic transformation in Cu-based shape memory alloys. The available measurements are:
a) Acoustic emission (A.E.) observation. b) Optical microscopy (until 700x) and simultaneous video recording for further study (260-360 K). c) Resistance changes with a resolution near 0.1% for resistance values of 1 milliOhm. d) High resolution DSC (223-353 K). With suitable signal processing, it gives a resolution near 1 μV equivalent to 3 μW.
Multi-interface effects in resistance measurements (dependence of the resistance on both mass and number of interfaces) heve been observed.

1.-Introduction

Shape memory alloys are very interesting because of its possible technological applications and also because of basic scientific interest (see Delaey et al, 1989 and references therein). The change in shape is obtained from a martensitic transformation with a relatively low hysteresis in "thermoelastic" processes.

The martensitic transformation is a first order phase transformation between metastable phases and its behaviour is not ideal. There are many phenomena influencing the transformation: i) Thermoelasticity: the spontaneous transformation in a given sample -stress free- does not occur at a given temperature; it is necesary a continuous undercooling (overheating) to force the tranformation (retransformation) going on. ii) Stabilisation: Due to diffusive processes, the relative stability of the phases change with ageing time in one or other phase. This evolution depends on thermal treatements. iii) Pinning processes: The progression of the transformation is, in general, non-continuous or "burst-like". The position of the interphase remains stopped in some points, and then a sudden evolution may follow (burst-type transformation). In transforming and re-transforming, symmetric behaviour appears but, in local observations, an assymetrical behaviour is observed. iv) The width of the hysteresis cycle: Depends on thermomechanical treatment, on ageing time and on deffects concentration on the sample.

The mentioned phenomena are related to the main problems found in applications of the shape memory alloys. It is quite difficult to obtain reproducible results, in the production and training processes and in service (transformation seems stochastic). Then, it is necesary to have an accurate knowledge of the alloy behaviour in the transformation, including complete characterization, and to have also a good knowledge of the ageing effects after the production and training processes.

Diverse measurements can be done in order to characterise the martensitic transformation. These include: optical microscopy (thermomicroscopy), to monitor the interphase positions and changes in dimensions. Electron microscopy (SEM and/or TEM), with the same purpose, plus the ability to look at the crystallographic structures and not only to morphology. Electric resistance (resistivity) measurements, which may give also an indication of the degree of transformation achieved. Enthalpy changes, which give a change between different states of the sample. Accoustic emission, which measures the existence of burst-like processes in the sample during the transformation.

These techniques have different sensitivities respect to the detection of a certain degree of transformation. Then, care should be taken into account when different measurements realised with several techniques are to be compared. Our purpose is to have a system which allows different measurements to be performed together, in a controlled way, in order to get a better understanding of the transformation process in Cu-based shape memory alloys.

2.-Experimental set-up

The experimental set-up is a temperature controlled copper plate, on which it is possible to place the sample to be observed and characterised (see fig. 1). The sample size considered is relatively small (about 25mm * 3mm * 1mm), in order to obtain good response times in temperature (Heat diffusion is a limiting factor), enabling improved temperature control and reproducibility.

The copper plate is heated or cooled by use of the Peltier effect. The temperature is controlled by a computer, with a Pt-100 platinum resistance (resolution 1 mOhm). The temperature control

is done by using the transfer function of the system, together with a feed-back correction to account for room temperature changes during the measurements, as has been described elsewhere (Amengual and Torra, 1989; Amengual et al, 1989). The resolution and reproducibility of the temperature evolutions of the system are about 0.003 K. This has made possible to note that reproducibility in accoustic emission may be observed with a very rigurous temperature control (Amengual et al, 1987), suggesting that pseudo-random behaviour may be induced by non-reproducible external influences to the sample and mixed effects with histeretic behaviour of the surface martensite.

The optical microscopy is easily ecomplished with the system shown in fig. 1, enabling, in the 700x magnification, to observe small changes in the amount of the phases present in the martensitic transformation (resolution in Δx about 1 μm).

We determine resistance changes better than resistivity of a sample, because of shape changes and non-homogeneity during the martensitic transformation. We use the four-point method with appropiate contacts. The resistance of a standard sample (lenght 22 mm, width 2 mm, thickness 0.3 mm) is about 1 mOhm. The changes in resistance associated with the transformation are near 10 %. The intensity applied is about 0.1 A, which leads to an energy dissipation by Joule effect of about 0.01 mW, nominally enabling the obtention of simultaneous calorimetric information.

The resistence has been measured using two alternative methods (Amengual et al. 1989): The first one using an A/D board in the computer and a numeric phase-sensitive detection, with a resolution near to 0.1 % in the measured resistance values. In the second method, the computer devoted to the temperature control also produces a rectangular intensity wave: It switches a relay that changes the sense of the current supplied to the sample by a stabilised source, and triggers the measure of the potential across the sample and the current flowing realized by two digital multimeters (resolution 1% mV). The final resolution obtained is near to the one obtained with the lower-cost procedure (using the A/D board), but the temperature control can be better with a careful synchronism of the processes and the temperature rate is increased.

The DSC analysis is obtained by means of two plates of thermoelements MELCOR with 1 cm**2 of area connected in differential. Due to the imperfect differentiability of the system, the temperature program gives a continuous change in the base line. Also, the intensity fluctuations in the thermoelements heating/cooling the copper base induce predictible fluctuations in the output. The effect of the fluctuations in the intensity in the thermoelements can be removed by substracting the result of the convolution of this intensity fluctuations by using the initial calibration (obviously temperature dependent). After this correction and the corresponding to the ones induced by the fact that the sensitivity of the thermoelements depends on temperature, the uncertainty in the base line is estimated to be $\pm$0.001 mV which corresponds to an amount of heat power released in the sample area around 0.003 mW. This is one order of magnitude better than the resolution of standard DSC analyzers (see for instance, Perkin Elmer, Setaram and others).

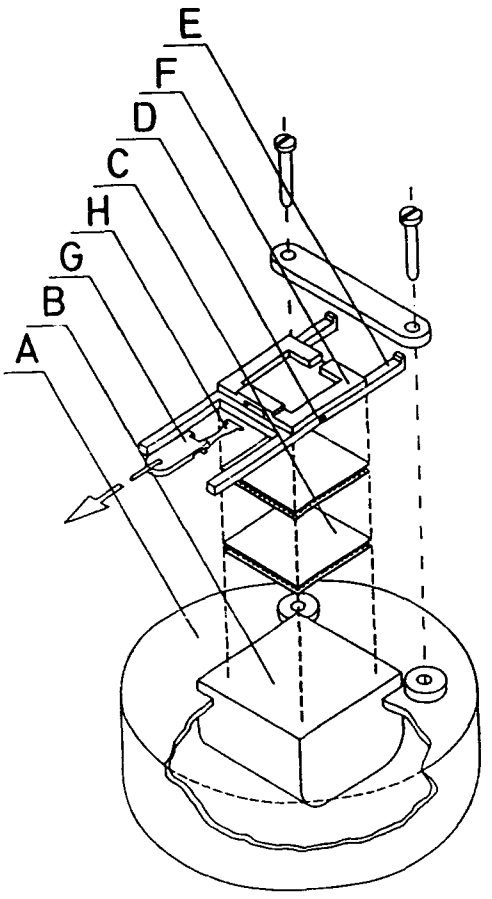

Fig. 1.- Experimental set-up used: A) thermal bath at room temperature. B) Brass block. C) Peltier effect elements (heating/cooling). D) Platinum resistance thermometer, Pt-100. E) Supports. F) Working area. at a programmed temperature T(t). G) Mechanical load (stress) applied to the sample. H) Sample.
To perform DSC, the sample is placed on one of two thermobatteries connected in differential, both placed on the controlled temperature area.

3.-Results

As an example, let us consider the results obtained regarding to optical

microscopy and simultaneous resistance measurements. A monocrystalline sample of Cu-16.7 Al- 14.1 Zn (weight %) stress-free and with a slightly stabilished, monovariant martensite plate, was thermally cycled with different amplitudes, recording both the resistance values and the image (dimensions of the martensite plate). In fig. (2) are shown the resistance versus temperature (fig. 2A) and the martensite plate width versus temperature (fig. 2B). Temperature amplitudes are 0.54 K and 0.30 K. From fig. (2), it can be concluded that, in single interphase single variant transformation the change in resistance is strictly proportional to the amount of material transformed.

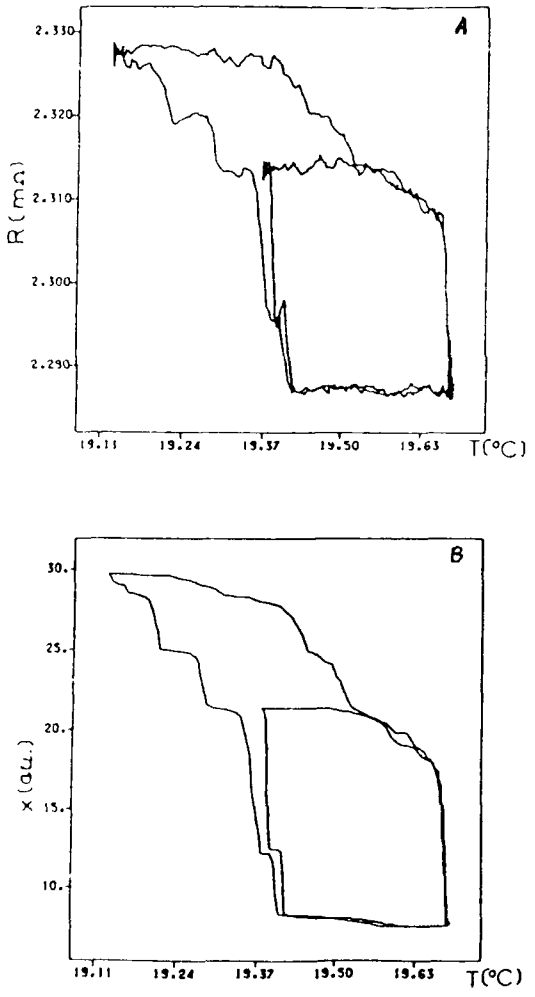

Fig. 2.- A) Resistance versus temperature for a monointerphase monovariant martensitic transformation. B) Interphase position equivalent to the martensite plate width for arbitrary units for the same processes represented in A).

However, if we consider multi-interphase transformations, the situation is more complicated and only mass-dependent in the statistical sense. In fig. (3) we show the evolution of the resistance and temperature with time for a sample with the same composition than the previous one. The sample is subjected to a small tensile force, but by cooling a martensite plate previously present grows, interacting with two self-accomodated microplates, and then growing to form two martensite plates linked by the microplate (fig. 4). As can be seen from the resistance evolution from cycle to cycle, the transformation produces a very complex pattern of the resistance behaviour.

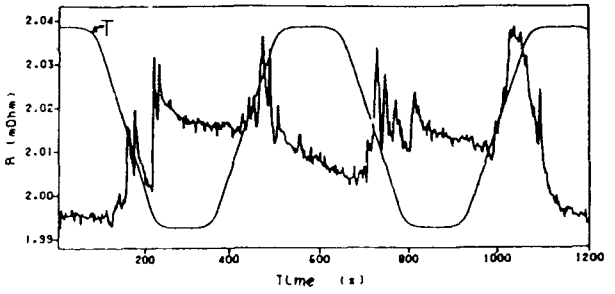

Fig. 3. Temperature and resistance values as a function of time for a complex transformation.

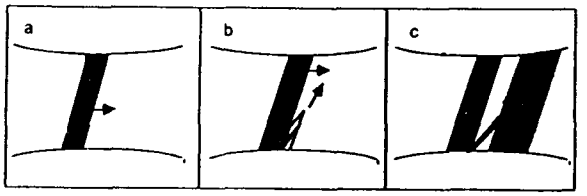

Fig. 4.-Schematic representation of the morphology in the transformation corresponding to the resistance values of fig. 4: in first place (a), one martensite plate grows. Then, two self-accomodating variants of martensite intercept the first plate (b), stopping the growth process. Finally, (c), the martensite continues growing, generating some beta-martensite interphases.

4.-Conclusions

We have developed a system that allows the accurate control and programmation of the temperature within a working space to study transformation cycles in shape memory alloys.

From this experimental set-up we have obtained results concerning multi-interphace effects in resistance measurements (dependence of the resistance on both mass and number of interfaces). Other possibilities appear in the high resolution thermal analysis: studies of transformation temperatures vs. time by ordering processes, defects production by cycling, intrinsic parameters studies (thermoelasticity in stress free processes) and the evolution of time scales with annealing in beta or martensite phases.

References

A. Amengual, V. Torra (1989): J. Phys. E: Sci. Instrum. 22 433.

A. Amengual, V. Torra, A. Isalgué, F. Marco (1989): Thermochim. Acta 115, 155.

A. Amengual, Ll. Mañosa, F. Marco, C. Stornell, C. Segui, V. Torra (1987): Thermochim. Acta 195, 116.

L. Delaey, K. Mukherjee, M. Chandrasekaran (1989): Proc. The Science and Technology of Shape Memory Alloys; V. Torra ed. (Univ. Illes Balears, Spain) p.117.

ELECTROCHEMICAL EXPERIMENTS WITH COMPOSITE ELECTROLYTES

C.B. Alcock
Freimann Chair Professor
University of Notre Dame
Notre Dame, IN 46556

Abstract

Following the review of solid electrolyte studies presented Prof. Pratt at the Vienna meeting, the present state of the art simple galvanic systems is briefly reviewed. It can be seen there are a number of shortcomings in the technique involving a composite of solid electrolyte with a sen dispersed phase wich enlarges the scope of the method is present. Examples are drawn from studies with stable oxides, sulphid carbides and hydrides.

Introduction

At the Vienna meeting, Prof. J. Pratt presented a comprehensive review of solid electrolyte systems which showed the potential for the determination of alloy thermodynamics using galvanic cells incorporating electrolytes in the solid state. Two alternative approaches which have been successfully applied are typified by the pioneering work of Rapp and Maak (1) who used a zirconia electrolyte

$$Ni/NiO \mid Zr_{0.85}Ca_{0.15}O_2 \mid Cu\text{-}Ni/NiO$$

and Aronson (2) who used a fluoride electrolyte

$$Th/ThF_4 \mid CaF_2 \mid ThF_4/ThC_2/C$$

The first cell measures an oxygen potential gradient, which in turn is related to the nickel chemical potential gradient. The second cell measures a fluorine potential gradient which is inversely related to the thorium potential gradient.. Since the carbon activity in the right hand electrode is unity, the results may be used to measure the Gibbs energy of formation of thorium dicarbide.

Extensive use of the fluoride electrolyte has been made in a number of other directions such as that used by Worrell (3) to measure the stabilities of sulphides, as typified by the cell.

$$Cu/Cu_2S/CaS \mid CaF_2 \mid Fe/FeS/CaS$$

In this cell the sulphur potential in each electrode establishes a calcium potential due to the presentce of an admixture of calcium sulphide, and the resulting calcium potential gradient between the electrodes establishes a fluorine potential gradient across the CaF_2 electrolyte in which the fluoride ion has unit transport number.

Jacob, Iwase and Waseda (4) extended this principle by using a sodium ion-conducting electrolyte β alumina for the measurement of a sulphur potential gradient. They used the cell

$$pH_2S/pH_2/Na_2S \mid Na/\beta\text{-}Al_2O_3 \mid Na_2S/p'H_2S/p'H_2$$

in which the sulphur potential gradient imposed a corresponding sodium potential gradient because of the presence of sodium sulphide at each electrode interface with the electrolyte.

Finally, these same authors (5) used a two-phase mixture of CaS and $ZrO_2(CaO)$ as the electrolyte between two gaseous mixtures with fixed sulphur potentials thus

$$Ar/H_2/H_2S \mid CaS+ZrO_2(CaO) \mid Ar'/H_2'/H_2S'$$

In each case the electrochemical circuit was completed via platinum contacts.

. There are a number of experimental difficulties associated with these schemes

for electrochemical measurement, amongst which must be numbered: (1) The appearance of a significant electon transport in stabilized zirconia at low oxygen potentials. Thus for systems as stable as Mn/MnO, it is necessary to use thoria-based electrolytes. These are not popular nowadays because of the radioactive hazard associated with the use of thorium. Also these latter have a lower conductivity than the corresponding zirconia-based electrolytes, and can only be used at low temperatures (less than about 500°C) with liquid electrodes. (2) The use of zirconia as a base for any other ionic species measurement than oxygen, presents the electron conductivity problem again. Despite the ingenious solution to the problem presented by Jacob et al., who used a secondary point elctrode with a catalytically active tip to avoid the effects of the oxygen atom flux through the electrolyte resulting from the low oxygen potential, it is desirable to find an alternative approach.

One other use of fluoride electrolytes which should be mentioned here, is the application of a BaF_2/BaC_2 mixture by Collters and Belton (6) who measured the stabilities of chromium carbides with cells such as:

$$Cr/Cr_{23}C_6 \mid BaF_2+BaC_2 \mid Cr_{23}C_6/Cr_7C_3$$

in which a carbon potential gradient in the electrodes establishes a barium potential gradient in the electolyte, and hence the inversely related fluorine potential gradient.

From the examples given above it will be clear that the fluoride electrolytes hold promise for a wide range of application in high temperature thermodynamics. It is also clear from those studies that the technique of imposing an alkaline earth potential gradient or a fluorine potential gradient by means of external electrodes produces cells which reach a steady potential only over a long period of time, in some instances several days.

The solid solutions formed by alkaline earth halides such as CaF_2-YF_3 and SrF_2-LaF_3 have considerably higher electrical conductivities than the corresponding pure fluorides. In electrochemical cells based on the SrF_2-LaF_3 electrolyte it has been found that the achievement of a steady potential in an electrochemical cell incorporating this material was much more rapid than when the pure fluoride was used. This electrolyte has formed the basis of the studies which are now presented.

Experimental Procedures

The preparation of polycrystalline SrF_2-LaF_3 solid solutions must be made under glove-box conditions because of the hygroscopic nature of these fluorides. In order to avoid the formation of surface oxides due to hydrolysis by moisture in the air, it is useful to mix some $(NH_4)HF_2$ with the fluoride mixture before pressing into pellet form and firing. The decomposition of the ammonium bifluoride leads to the evolution of HF gas during the firing procedure, and hence fluorination of contaminating oxides is achieved during fabrication. After firing at temperatures around 1100-1200°C, the material becomes quite insensitive to moisture in pellet form. This observation does not preclude the possibility that a very thin layer of oxide forms over the surface of the pellet immediately on removal from the furnace. In the present stuies a two phase mixture was prepared by adding either strontium or lanthanum oxides to the fluoride solid solution in order to use this dispersed mixture as an oxygen-sensing electrolyte. This dispersed phase does not significantly change the electrochemical or conduction properties of the electrolyte, unkike a dispersed phase of Al_2O_3, which is known to enhance the conductivity of CaF_2 (7). In this instance it serves to fix the strontium or lanthanum activity and hence fluorine, potential gradient across the electrolyte when it is in contact with electrodes which in turn impress an oxygen potential gradient as in the cell

$$Cu/Cu_2O \mid SrF_2\text{-}LaF_3,SrO \mid Ni/NiO$$

This electrolyte funtions as well as stabilized zirconia as the electrolyte in oxygen galvanic cells, and has been used with liquid electrodes down to 300°C, as in the cell

$$In(l)/In_2O_3 \mid SrF_2\text{-}LaF_3,SrO \mid Sn(l)/SnO_2$$

for which EMFs have been obtained in agreement with those calculated from thermochemical data. In fact, Japanese workers have recently demostrated that LaF_3 sigle crystal can be used to measure the oxygen content of water at room temperature (8).

After firing the electrolyte incorporating SrO or La_2O_3 the pellets should be stored in a vacuum desiccator, but this is not so critical as with other dispersed phases. The dispersed sulphide, SrS, which converts the SrF_2-LaF_3 electrolyte into a sulphur potential sensor was difficult to use satisfactorily until it was realized that after firing, the sulphide particles at the surface of the commposite electrolyte were hydrolyzed to yield a layer of oxide on the surface. When the fired SrF_2-LaF_3, SrS pellet was heated in a sealed quartz ampoule with a mixture of Ag, Ag_2S to re-convert any superficial oxide to sulphide, and subsequently stored in a desiccator, no difficulties were encountered.

A hydrogen sensign electrolyte has been described which is similar in operation to the fluoride systems described above by Gnanasekaran et al (9). This electrolyte was used to monitor hydrogen dissolved in liquid sodium, and uses a Li/LiH reference electrode. The $CaCl_2$-CaH_2 system has a crystal structure in which hydrogen and chloride ions occur in alternate layers, and has a hydrogen ion transport number close to unity. The hydrogen meter which was constructed using this electrolyte functioned at 450°C in liquid sodium for two to three months continuously. For such a practical application the meter must be rugged, and this was achieved by the use of thin-walled iron chambers to contain the reference electrode and electrolyte assemblies. Rapid chemical equilibrium for hydrogen potentials was obtained by diffusion of hydrogen through these iron containers. The cell construction could be described as

$$Na(H) \mid Fe \mid CaCl_2\text{-}CaH_2 \mid Li/LiH$$

Finally, a carbon sensing composite electrolyte has been prepared with a dispersion of LaC_2 in the fluoride base electrolyte, and this is best sintered in the composite pellet form surrounded by a layer of powder of the same composition to maintain the carbide dispersion.

In all of these composite electrolytes except the hydrogen electrolyte, the base electrolyte was chosen to be 70 mole % SrF_2 30 mole % LaF_3, as this was found to have the maximum conductivity in the solid solution range which extends up to at least 50 mole % LaF_3. The dispersed phase was usually present to the extent of 3-10 mole %. This prevents dispersoid-dispersoid contacts, and hence the intrinsic conduction properties of the dispersoid does not affect the conduction path of fluoride ions in the electrolyte.

RESULTS AND DISCUSSION

The Oxygen-Sensing System

The use of oxide-dispersed fluoride composite electrolytes can only be justifed if it can be shown that there is an experimental advantage over the well-established zirconia electrolyte. This advantage should be looked for either in the realm of lower temperature of operation, or in lower oxygen potential application. As far as the first criterion is concerned, there appears to be little advantage over zirconia, since it appears that the sluggish response of cells incorporating this electrolyte at low temperatures, i.e. below 500°C, is usually due to kinetic barriers at

the electrode/electrolyte interface(s), and not due to the performance of the electrolyte. However, at the low oxygen potential range there are distinct advantages over zirconia. The electronic properties of the dispersed oxide phase do not affect the performance because of the lack of continuity in the dispersoid. The fluorides are amongst the most stable fluorides and should thus be unaffected by a low oxygen potential.

As an initial test of this analysis, the EMF of the Cell

$$Cr/Cr_2O_3 \mid SrF_2\text{-}LaF_3,SrO \mid NbO/NbO_2$$

was measured and found to yield acceptable values in the temperature range 600-900°C. This contrasts with the values of Hoch, Iser and Nelken (10) which gave low EMFs because of semiconduction in the cell

$$Nb/NbO \mid ZrO_2\text{-}CaO \mid NbO/NbO_2$$

The cell used by Steele, employing a ThO_2-Y_2O_3 electrolyte (11) gave accurate EMFs but only above 850°C for the cell

$$NbO/NbO_2 \mid ThO_2\text{-}Y_2O_3 \mid Fe/FeO$$

In this case the fluoride composite has advantage both from the temperature and oxygen potential point of view. Preliminary results indicate that this electrolyte may be used successfully in the cell

$$Al/Al_2O_3 \mid SrF_2\text{-}LaF_3,SrO \mid Nb/NbO$$

which would make a wide new range of studies possible in, for example, the Ti-O,Zr-O systems at the metal-rich end.

The Sulphur-Sensing System

The dispersion of SrS in the fluoride electrolyte has been tested with only a few electrodes. Those used include Ag/Ag_2S,Cu/Cu_2S and Fe/FeS in the temperature range 425-725°C. The cells incorporating these electrodes displayed EMFs in good agrement with those calculated from literature data, but, at the higher sulphur potential generated by the Ag/Ag_2S system, there was evidence of short-circuiting after a few hours of operation at the highest temperatures due to vapour-pnase transport from one electrode to the other. The use of a two compartment cell incorportaing an electrolyte plug in an alumina tube, would seem preferable for cells with high sulphur potential electrodes.

Unfortunalely the sulphur-sensing electrolyte cannot be tested satisfactorily at low sulphur potentials because of the absence of accurate data from other sources with which to compare. This is principally because the H_2/H_2S gas-solid equilibrium technique can only be extended to partial pressures of H_2S down to about 10^{-6} atmos. Below these sulphur potentials the dissociation pressure of sulphur vapour is too low to measure by mass spectrometer, for example, unless the temperature is very high. There appears to be a large opportunity to exploit this new technique in the study of stable sulphides.

The Hydrogen-Sensing System

The example given above of a hydrogen meter for liquid sodium suggests that high temperature hydrogen sensors based on other halide electrolytes could be developed.

Apart from the measurement of the stabilities of metal hydrides, which this technique makes possible, the measurements of hydrogen solubilities in metal alloys might be valuable in connection with the Fermi surface variation with composition (12). This technique can also be applied in the measurement of integral Gibbs energies of formation of alloys (13).

The Carbon-Sensing System

Experimental work is in hand at the Center for the measurement of carbon potential by means of the electrochemical cells

$$C \mid SrF_2\text{-}LaF_3,LaC_2 \mid Mo/Mo_2C$$

$$C \mid SrF_2\text{-}LaF_3, LaC_2 \mid Cr/Cr_{23}C_6 \qquad II$$

$$Cr/Cr_{23}C_6 \mid SrF_2\text{-}LaF_3, LaC_2 \mid Mo/Mo_2C \qquad III$$

Clearly the IMF of cell III should be equal to the difference between those of cells I and II. Results are complete for cells I and II at the time of this discussion meeting, after overcoming a number of experimental difficulties. In such carbide cells it is imperative that the oxygen partial pressure be kept as low as possible so as to avoid carbon transport in the vapour phase by the Boudouard reaction

$$C + CO_2 \rightleftarrows 2CO$$

which can move carbon from one electrode to the other. At the present time, the use of titanium as a getter at 800°C for the argon stream which is to pass over the electrochemical cell, seems to have achieved this result. Tantalum foil mounted in the cell was found to be unoxidized after a few days of cell operation. The cell EMF responds rapidly to temperature change and thus the electrolyte holds promise as a carbon sensor. The complete results for the triad of cells shown above should be available for publication in the near future.

References

1. R.A. Rapp and F. Maak, Act Met., 10, 63 (1962).
2. S. Aronson, "Compounds of Interest in Nuclear Reactor Technology", (Boulder, CO:AIME 1964) 10, 247.
3. W.L. Worrell, Solid State Ionics, 3/4, 559 (1981).
4. K.T. Jacob, M. Iwase and Y. Waseda, Adv. Ceram. Mat., 1, 264 (1986).
5. K..T. Jacob, M. Iwase and Y. Waseda, J. App. Electrochem, 12, 55 (1982).
6. R.G. Coltters and G.R. Belton, Met. Trans., 15B, 517 (1984).
7. A. Khandar, V.B. Tare and J.B. Wagner, Jr., Rev. Chim. Mineral, 23, 274 (1986).
8. N. Yamazoe, J. Hisamoto, N. Miura and S. Kuwata, Sensors and Actuators, 12, 415 (1987).
9. V. Ganesan, T. Gnanasekaran, R. Sridharan, G. Periaswami and C.K. Mathews, Proc. 3rd Int. Conf. on Liquid Metal Engineering & Technology, British Nuclear Energy Society, Oxford (1984) Vol. 1, p. 369.
10. M. Hoch, A.S. Iyer and J. Nelken, J. Phys. Chem. Solids, 21, 280 (1961).
11. B.C.H. Steele, Ph. D. Thesis, University of London (1965).
12 W. Himmler, Z. Physik Chem., 195. 244, 253 (1950).
13. LS. Darken, J. Amer. Chem. Soc., 72, 2909 (1950).

Thermodynamic Criteria of Glass Formation in the As-Sb-Se System

M.T. Clavaguera-Mora , S. Suriñach , M.D. Baró and N. Clavaguera*

Física de Materials, Dept. Física, Universitat Autònoma de Barcelona, 08193-Bellaterra, Spain
***Dept. Estructura i Constituents de la Matèria, Fac. Física, Universitat de Barcelona, Diagonal 647, 08028- Barcelona, Spain**

Abstract.-

The Gibbs free energy of formation of an "ideal" glassy alloy relative to the stable crystalline phases at the same temperature can be deduced by use of thermodynamic arguments.This paper discusses the success of the Gibbs free energy of formation curves of the glassy alloy as a function of composition to describe the glass forming ability in the As_2Se_3-Se, Sb_2Se_3-Se and As_2Se_3-Sb_2Se_3 systems.

1.- Introduction

Glasses of the As_2Se_3-Sb_2Se_3-Se system have applications as photoconductive sensors and, in general, as semiconductor materials. The study of the liquid structure and its influence in the metastable states to which the undercooled liquid will evolve gives further insight on the formation of glasses in this system. The liquid structure of the elements and compounds is well known. Liquid Se can be described by an equilibrium between polymeric chains and ring molecules (Keezer and Bailey 1967). Liquid As_2Se_3 is formed mostly by bidimensional grouping of $AsSe_{3/2}$ (Lucovsky 1969). Finally, liquid Sb_2Se_3 contains associated complexes of Sb_2Se_3 (Satow 1978, Ghosh *et al.* 1989).

As a part of our general work on the study of the mechanisms responsible for glass-forming ability (GFA) and thermal stability of some chalcogenide melts, we report here on the Gibbs free energy of formation of the glass or Gibbs free energy difference between the "ideal" glass and the stable crystalline phases at the isentropic temperature as a measure of the driving force for eutectic crystallization (Clavaguera-Mora *et al.* 1989). The Gibbs free energy of formation of an alloy glass of any composition within the ternary system is calculated by taking into account the heat capacity difference between the liquid and the crystalline element or compound. For the solid phase we assume that there is no miscibility between Se, As_2Se_3 and/or Sb_2Se_3. For the liquid phase we assume that it can be treated as a strongly associated regular (SAR) solution (Clavaguera-Mora and Clavaguera 1982). The results obtained are correlated with the known glass forming region in the system.

2.- Thermodynamic approach

The goal of this study is to discuss and make reasonable predictions of glass formation in a simple eutectic system by calculating the Gibbs free energy of formation of a glassy alloy. The calculation needs a model for the liquid solution and its transformation into a glassy alloy. We will assume that the liquid phase is formed by $AsSe_{3/2}$ and/or Sb_2Se_3 complexes in thermodynamic equilibrium with the (uncombined) As, Sb and Se atoms. The assumption of the existence of complexes is not new as it was already stated by Berkes and Myers (1971). The equilibrium condition leads to the following equations

$$x_{AsSe_{3/2}} \; K_1 = x_{As} x_{Se}^{3/2}$$

$$x_{Sb_2Se_3} \; K_2 = x_{Sb}^2 x_{Se}^3$$

where x_j are the molar fractions of the different species j (j=$AsSe_{3/2}$, Sb_2Se_3, As, Sb, Se) and K_1 and K_2 the ideal dissociation equilibrium constants for the associated liquid solutions.

The values of these dissociation constants as well as of the interaction parameters between the main especies have been adjusted in order to reproduce correctly the experimental binary phase diagrams. The heat capacity difference, ΔC_p, between the liquid and the solid was estimated from direct measurement of the heat capacity jump at the glass transition (Mahadevan *et al.* 1986). The thermodynamic input data used for the calculations, apart from ΔC_p, are the melting point, T_m, and the enthalpy of fusion, ΔH_m, of each crystalline phase, reported in Table 1.

To calculate the Gibbs free energy of formation of the alloy glass we assume that the liquid alloy may exist in a metastable state down to the isentropic temperature Ts at which its entropy will be equal to that of the stable crystalline phases. At that temperature it will become an "ideal" glass with a heat capacity equal to that of the mixture of the stable crystalline phases (Clavaguera-Mora and Clavaguera 1989).

3.- Results

We will present successively the results of the calculations in the As_2Se_3-Se, Sb_2Se_3-Se and As_2Se_3-Sb_2Se_3 systems.

3.1.- As_2Se_3-Se system

The calculated phase diagram is shown in the upper part of Fig. 1 together with the experimental points (Dembovskii and Luzhnaya 1964; Myers and Felty 1967). Keeping the coordination numbers 3 for As and 2 for Se, the best fit is obtained taking $AsSe_{3/2}$ as the associated species for the liquid solution with an ideal dissociation constant K_1=.00001 and an interaction parameter between the main species $AsSe_{3/2}$ and Se of -1.0 kJ/mol. The calculated eutectic composition is 16 at.% As and the eutectic temperature is 414 K. The calculated isentropic T_s curve is shown in the lower part of Fig. 1. The Gibbs free energy of formation, ΔG_f, of the "ideal" glassy alloy (with respect to the stable mixture of As_2Se_3 and Se) is plotted as a function of composition in Figure 2. ΔG_f is independent of the temperature because as regards to the assumption we made the entropy of the "ideal" glass is equal to that of the crystal. According to a previous paper (Clavaguera-Mora and Clavaguera 1989), ΔG_f scales as ΔH_m and glass formation of stochiometric alloys from the liquid is expected if $0.2<\Delta G_f/\Delta H_m<0.3$. The broken lines in Fig. 2 correspond to these limiting values for ΔG_f. It can be concluded that GFA is thermodynamically favored in this system. This is in agreement with experimental findings. Flaschen *et al.* (1960) firstly reported that glasses are easily obtained by fusing the components in the entire glass formation range from elemental Se to alloys containing ~ 60 at.% As.

3.2.- Sb_2Se_3-Se system

The calculated phase diagram including the calculated values of T_s are shown in Fig. 3 together with the experimental phase diagram determinations (Parravano 1913; Myers and Berkes 1972). The best theoretical fit to the experimental results is obtained by taking K_2=.001 and a value of 4.0 kJ/mol for the interaction parameter between the main species Se and Sb_2Se_3. The Gibbs free energy of formation of the alloy glasses is shown in Fig. 4. The broken line in Fig. 4 relies the values of 0.3 times ΔH_m for the components Se and Sb_2Se_3. Therefore, the Gibbs free energy of formation is quite large compared to 0.3 times the melting enthalpies of the components. As expected from reported glass forming regions in the As-Sb-Se system (Borisova 1981) and other ternary systems (Bordas *et al.* 1990), GFA is thermodynamically very poor in this system.

3.3.- As_2Se_3-Sb_2Se_3 system

The experimental phase diagram was determined by Berkes and Myers (1971). According to these authors it is a simple eutectic diagram with an eutectic composition of 12.6 mol.% Sb_2Se_3 and

Table 1.- Enthalpies ΔH_m, and temperatures T_m, of melting and heat capacity difference ΔC_p, between the liquid and the solid.

	ΔH_m (kJ/g.at)	T_m (K)	ΔC_p (J/g.at)
Se	5.86	493	12.4[a]
As_2Se_3	8.16	650	14.6[b]
Sb_2Se_3	10.75	888	12.0[b]

a: Clavaguera-Mora *et al.* (1990)
b: Mahadevan *et al.* (1986)

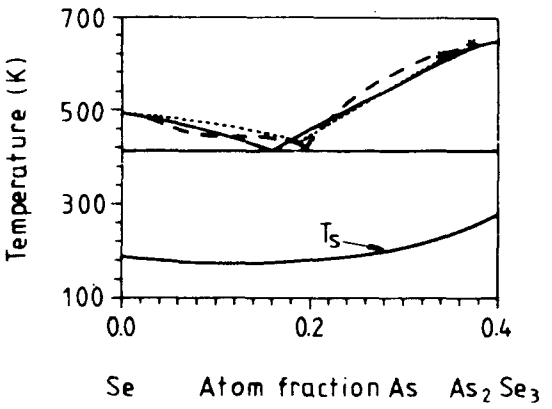

Fig. 1.- Full lines show the calculated phase diagram and T_s curves for the As_2Se_3-Se system. Dotted lines show the experimental phase diagram after Dembovskii and Luzhnaya (1964). Dashed lines correspond to experimental phase diagram after Myers and Felty (1967).

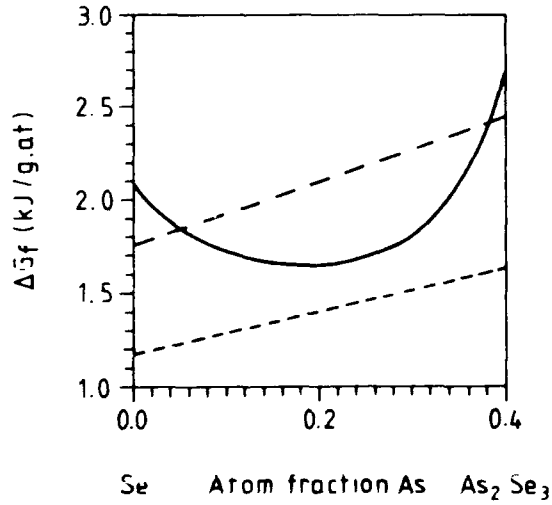

Fig. 2.- Calculated Gibbs free energy of formation of an alloy glass for the system As_2Se_3-Se. - -Line that relies the values corresponding to 0.3 ΔH_m for Se and As_2Se_3. --- Idem for the values of 0.2 ΔH_m.

eutectic temperature 636±5 K. Fig. 5 shows the experimental points, the calculated phase diagram and the Ts curve. Calculations were performed assuming an ideal association model behaviour for the liquid phase. The calculated eutectic composition and temperature are, respectively, 6.5 at.% Sb and 627 K. Association remains very strong for liquid alloys of the system as can be seen in figure 6 where the molar fractions of the main chemical species of the system are plotted as a function of composition. Fig. 7 gives the Gibbs free energy of formation of an "ideal" glassy alloy of the system. The broken line relies, as in fig. 4, the values corresponding to $0.3\Delta H_m$ for the two line compounds. Therefore, thermodynamically the best glass forming compositions in this binary lie in the nearby of 20 at.% Sb which is a composition rather far from the eutectic one. Experimental glass forming region as reported by Borisova (1981) and presented in Fig. 8 shows that glasses are easy to form when the Sb content is less than ~22 at.%. This result, compared to our calculations, reinforces the importance of the thermodynamic criteria on glass formation.

Conclusions

We have applied here the thermodynamic criteria of glass formation to systems in which the chemical ordering is very important in the liquid and glassy states. The main assumption introduced to obtain the Gibbs free energy of formation of an alloy glass was to treat the liquid as a SAR-solution. The parameters involved are the ideal equilibrium constants and the interaction energies between the main species. These parameters were adjusted to reproduce the experimental phase diagram. The values obtained for them are consistent with the main assumption we made. That is: (a) the equilibrium constants have values low enough to undertake strong associated treatment, and (b) the absolute values of the interaction energies are relatively low (<RT) for the regular approximation to be valid.

For the three binary systems considered the Gibbs free energy of formation has values in the nearby of those predicted for good glass forming systems (Clavaguera-Mora and Clavaguera 1989). Assuming that GFA is inversely proportional to ΔG_f, the trend of the Gibbs free energy curves versus composition agrees with experimental determination of GFA.

Acknowledgements

This work was supported by CICYT project No. MAT88-439 which is acknowledged.

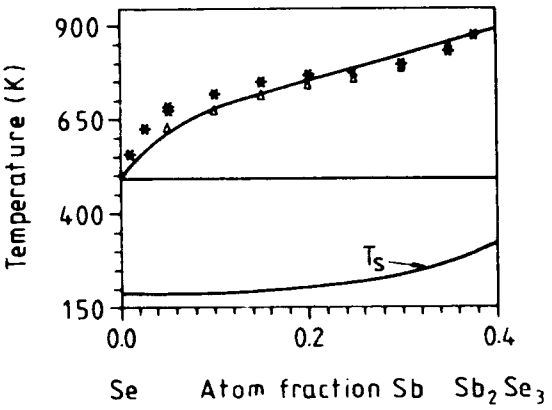

Fig. 3.- Calculated phase diagram and T_s curve for the Sb_2Se_3-Se system. (*) Experimental phase diagram data after Parravano (1913). (Δ) Experimental data after Myers and Berkes (1972).

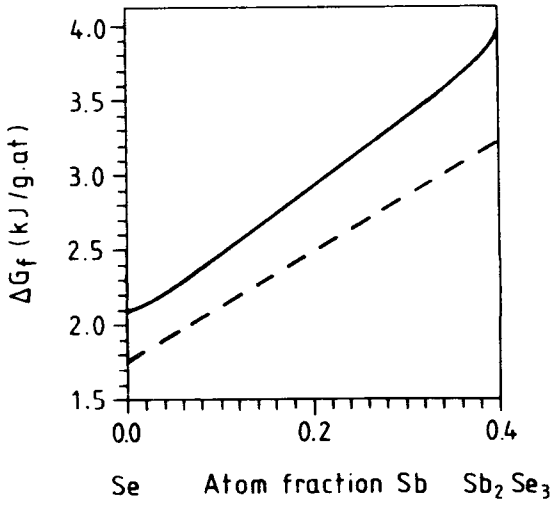

Fig. 4.- Gibbs free energy of formation of an alloy glass in the Sb_2Se_3-Se system.

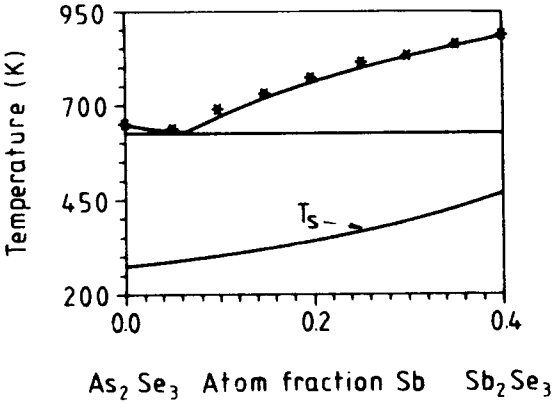

Fig. 5.- Calculated phase diagram and T_s curve for the As_2Se_3-Sb_2Se_3 system. (*) Experimental phase diagram data after Berkes and Myers (1971).

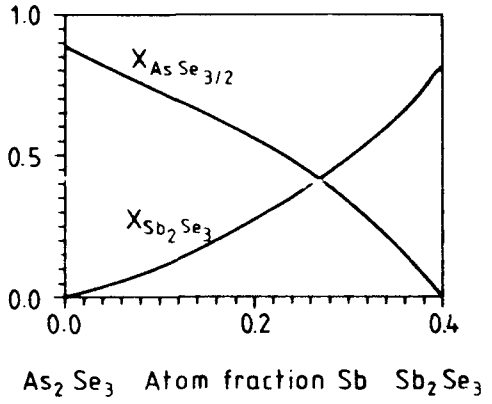

Fig. 6.- Molar fractions of the main chemical species $AsSe_{3/2}$ and Sb_2Se_3 of the liquid alloys of the As_2Se_3-Sb_2Se_3 system.

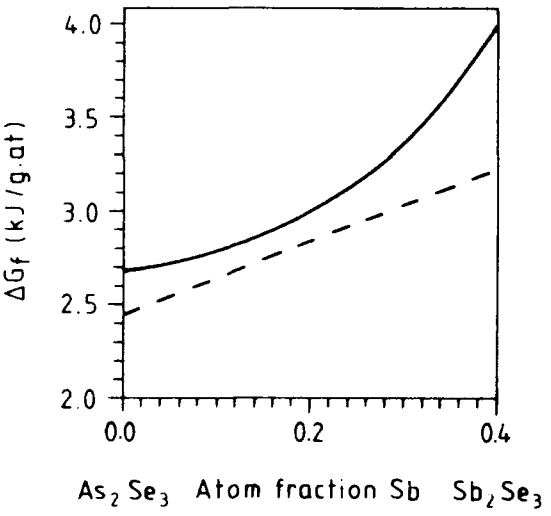

Fig. 7.- Gibbs free energy of formation of an alloy glass for the As_2Se_3-Sb_2Se_3 system.

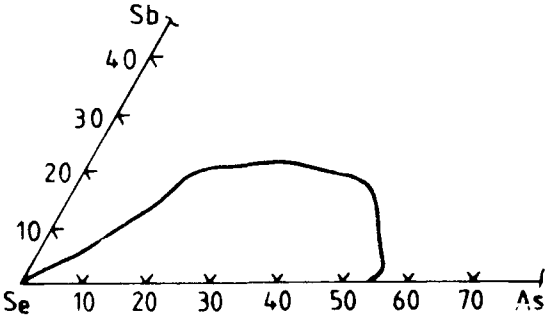

Fig. 8.- Glass forming region in the As-Sb-Se system after Borisova (1981).

References

Berkes, J.S. and Myers, M.B. (1971): J. Electrochem. Soc. Solid State Sci. 118, 1485.

Bordas, S., Clavaguera-Mora, M.T. and Clavaguera, N. (1990): J. Non-Cryst. Solids (in press)

Borisova Z.U. (1981): Glassy Semiconductors, (New York:Plenum Press) p. 16.

Clavaguera-Mora, M.T. and Clavaguera, N. (1982): J. Phys. Chem. Solids 43, 963.

Clavaguera-Mora, M.T. and Clavaguera, N. (1989): J. Mater. Res. 4, 906.

Clavaguera-Mora, M.T., Baró, M.D., Suriñach, S., Bordas, S. and Clavaguera, N. (1989): Advanced Solid State Chemistry (Eds. Frumar, M., Cerny, V. and Tichy, L.) Elsevier, p. 372.

Clavaguera-Mora, M.T., Baró, M.D., Suriñach, S., Saurina, J. and Clavaguera, N., (1990): in Basic Features of the Glassy State (Ed. J. Colmenero) World Scientific, Singapore

Dembovskii, S.A. and Luzhnaya, N.P. (1964): Zh. Neorg. Khim. 9, 660.

Flaschen, S.S., Pearson, A.D. and Northover, W.R. (1960): J. Am. Ceram. Soc. 43, 274.

Ghosh, G., Lucas, H.-L. and Delaey, L. (1989): Z. Metallkde. 80, 663.

Keezer, R.C. and Bailey, M.W. (1967): Mat. Res. Bull. 2, 185.

Lucovsky, G. (1969): Mat. Res. Bull. 4, 505.

Mahadevan, S., Giridhar, A., and Singh, A.K. (1986): J. Non-Cryst. Solids 88, 11.

Mills, K.C. (1974),Thermodynamic Data for Inorganic Sulphides, Selenides and Tellurides, Butterworths, London.

Myers, M.B. and Berkes, J.S. (1972): J. Non-Cryst. Solids 8-10, 804.

Myers, M.B. and Felty, E.J. (1967): Mat Res. Bull. 2, 535.

Parravano, N. (1913): Gazz. Chim. Ital. 43, 210.

Satow, T., Uemura, O., Akaike, S. and Tamaki, S. (1978): J. Non-Cryst. Solids 29, 215.

C.A.D. Solid-modeling for the Representation of Three and Four Component Phase Diagrams: A User's Approach

J. D. DeLa'O and A. Hellawell
Department of Metallurgical and Materials Engineering
Michigan Technological University
Houghton, MI 49931, U.S.A.

Abstract. -

Materials which must be described in terms of three or four chemical components are common today in nearly all areas of materials science and technology. Unfortunately, the three dimensional nature of isobaric ternary and isobaric, isothermal quaternary phase diagrams has limited the effective use of such diagrams. In the present work the authors explored the utilization of the "solid-modeling" capabilities of a Computer Aided Design (CAD) system to address the problem of three-dimensional phase diagram representation for phase diagram users.

Relevant 3-D, isobaric phase diagrams for a hypothetical quaternary eutectic system were constructed (using input data similar, in kind and amount, to experimental data commonly found in the literature), displayed in various ways intended to aid visual comprehension, and manipulated to extract numerical information and create planar sections.

The authors concluded that CAD systems offer many advantages relative to computer programs which have been developed specifically for phase diagram representation. These advantages include: powerful and versatile geometrical entity generation methods, sophisticated display features, ease of use, and wide availability. However, it is also pointed out that only through the use of solid-modeling can the full advantages of CAD system representations of 3-D phase diagrams be realized.

1. - Introduction.

In the preface to the 1964 English translation of "Phase Equilibria in Multicomponent Systems", the authors noted "It would be hard today to find a single branch of industry and technology that does not make extensive use of multicomponent alloys and other multicomponent materials" (Palatnik and Landau 1964). During the ensuing 26 years, intense research activities involving "super alloys", ceramics for structural or electronic applications and geological materials, to name but a few examples, have increased the scientific and technological relevance of multicomponent phase equilibria. However, in spite of a well documented understanding of the "rules" governing the topology of phase diagrams for three and four component systems (the simplest of multicomponent systems), the unwieldiness of the necessary three-dimensional (3-D) representations has often diminished the effectiveness and discouraged the use of such diagrams.

2. - Background.

Phase equilibria in binary systems at constant pressure, may be fully expressed as a function of 2 independent macroscopic variables (i.e., composition and temperature), thus allowing two dimensional graphical representation. With each additional chemical component, an independent composition variable is added to the system. thus, ternary phase diagrams consist of two independent composition variables (usually plotted in "Gibbsian" coordinates within an equilateral triangle) and the temperature variable (typically represented on an axis normal to the plane of the triangle). In such a ternary diagram, phase equilibria for the pure components are depicted at the vertices of the Gibbs triangle, the three binary subsystems along the sides of the triangle and the ternary system within the interior volume. For quaternary phase equilibria, the three independent composition variables are typically plotted within a regular tetrahedron (the "Roozeboom tetrahedron"). A fourth dimension would be required to explicitly display temperature information, therefore each tetrahedron represents isothermal quaternary phase equilibria. Analogous to the ternary diagram, each vertex, edge and side represents, respectively, isothermal sections through unary, binary and ternary subsystems.

The difficulties of working with three dimensional diagrams have prompted the development of several alternative representations. For example, polythermal projections of both ternary and quaternary diagrams are commonly used (Prince 1966) as well as two dimensional schematic representations of quaternary monovariant paths (Schairer 1942). Such techniques are quite useful (as evidenced by their wide acceptance), however, they are simplifications and by their nature contain only a subset of the useful information available in the explicit three dimensional representations.

Faced with the obvious difficulties of visualization and conceptualization of three dimensional phase diagrams, workers have presented such diagrams using a variety of media including wire models,

clay or plastic sculptures, and multi-colored line drawings which produce a '3-D effect' when viewed through special eye-glasses. Notis and Tarby (1986) have presented a more complete list of these techniques, including references.

It should be realized, however, that visual representation is only one of three major problems which often confront researchers who would apply 3-D phase diagrams to their work. In may cases, reliable thermodynamic models for a particular sys em are unavailable, and workers must construct" the phase diagrams from experimentally determined data. Furthermore, experimental data are usually incomplete; various quasi-binary or quasi-ternary sections along with polythermal projections may be all the information that is available for quaternary systems. Construction of 3-D phase diagrams from this information requires the use of interpolation. Hc ever, standard graphical interpolation, which works simply and directly in two dimensions, becomes overwhelmingly difficult in three-dimensional space. Thus, construction of 3-D phase diagrams from available data can be a major obstacle for those who would make use of such diagrams. Finally, after construction and display have been suitably managed, there remain the obvious difficulties associated with extracting information, both numerical and geometrical, from 3-D phase diagrams.

In order to address these difficulties and thereby facilitate the use of three-dimensional phase diagrams, the present work explores the use of a commercially available computer aided design (CAD) software package in the construction, display, and manipulation of ternary and quaternary phase diagrams. It should be noted that the use of computers for phase diagram representation is not new, but dates back nearly 30 years. An excellent overview of such work is provided by Massalski (1989). It is not the authors' intention to provide a review of the literature on this subject, although the results of the present work will be discussed partly in terms of these previous efforts.

3. - Procedure.

In order to determine the usefulness of the CAD system for the representation of 3-D phase diagrams and to develop efficient techniques for utilizing the capabilities of the system, a hypothetical, symmetrical quaternary eutectic diagram was constructed and manipulated.

3.1 - Equipment.

The computer hardware chosen for this work consisted solely of a SUN 4 workstation (aka, SPARC). The workstation was comprised of a central processor, external hard drive, high resolution graphics monitor and a conventional "mouse". It is similar in size to a personal computer, sells for approximately twice the cost of a high quality PC, but has tremendously greater capabilities. The software chosen was I-DEAS (Integrated Design Engineering Analysis Software) level 4.0 created by Structural Dynamics Research Corporation and released in 1988. I-DEAS was chosen largely because of its solid-modeling capabilities and powerful display features.

3.2 - Overall Approach.

Experimental data for phase equilibria in four component systems are hierarchical, that is, the data are most certain and complete for the binary subsystems with reliability and availability of data progressively decreasing as additional chemical components are added to the system. In order to develop a technique that would be applicable to real systems, input data to be used for the hypothetical system constructed in the present work were chosen to be similar to data which are typically available in the literature. Binary subsystems were assumed to be completely described. Data for the ternary subsystems consisted of the information typically available from two dimensional polythermal liquidus projections of ternary space models, supplemented by minimal subsolidus information. Finally, data for the interior of the quaternary system consisted only of points along the monovariant reaction paths.

The overall procedure for constructing the 3-D quaternary isotherms was designed to take advantage of the more completely determined low-order systems. The binary systems were constructed first. Data points were entered and displayed in the binary composition-temperature plane. Points were spline fit to form the phase boundaries (curves). Binary subsystems were then combined to define the sides of the ternary space models. Data points for the interior of the space models were entered and curves were fitted to these points, thus completing the wireframe (i.e., curves in 3-D space) representations of the ternary diagrams. The relatively more complete information for the binary subsystems was in this way used to aid in the construction of the ternary diagrams. The ternary space models were subsequently completed by utilizing a variety of surface generation techniques available with the I-DEAS software. In many cases (e.g., 3-phase regions and liquidus surfaces) the available data were sufficient to precisely define the surfaces. In other cases (e.g., solvus surfaces), where only the surface edges and a few internal points were known, surfaces were generated using least squares or interpolation fits. Isothermal sections were then taken through the completed ternary diagrams. These cross-sections were subsequently combined to form the

exterior surfaces of the quaternary isothermal tetrahedra. Analogous to the procedure used to build the ternary space models, interior data points were entered, curves fitted to form wireframes, and surfaces created over the curves.

It should be noted that three short programs were written, using a high level programming language (Ideal) provided in the I-DEAS environment. These programs converted between the temperature/composition coordinates of phase diagram space and the internal, Cartesian coordinates of the CAD system, as well as calculating phase fractions present in monovariant regions, given bulk composition and temperature as input information.

4. - Results.

Solid models representing three quaternary isotherms (Fig. 1) and the ternary subsystems were created. For any given diagram, each phase region was created and stored as a separate solid object with an appropriate name (e.g., Alpha + Liquid, for the 2-phase alpha-liquid region). The complete phase diagram was created by defining a "system" composed of the individual phase regions (each having associated with it a spatial orientation). Figure 2 shows a "system" composed of the stored phase regions for a ternary subsystem. However, in this figure, the system was defined to include translation vectors for each phase region, thus moving the regions apart to create the "exploded" configuration shown. Each surface is described by facets (used for shaded image displays and for defining cross-sections during cutting operations) as well as having a mathematical representation (nonuniform rational B-spline surface modeling is used). The faceted display can be refined, almost instantaneously, producing facets (up to 7500 facets per phase region) which deviate only negligibly from the mathematical surface. This dual representation allows efficiency of file storage yet highly precise representations for display and manipulation

Visual comprehension of the complex 3-D diagrams was aided by a number of sophisticated display features. "Dynamic viewing" allows rotation of diagrams (in 3-D space) zooming, and diagram translation to be accomplished continuously, interactively, and in real time, by movement of the "mouse" about its pad. These same view changes can be accomplished non-continuously simply by entering appropriate values from the keyboard (e.g., degrees of rotation about each axis). As already alluded to, displays which include shaded surfaces were created to aid in visual comprehension. A wide variety of attributes can be assigned individually for each shaded surface. The most useful among these attributes proved to be surface color and degree of transparency. Furthermore, line-drawings (e.g., composition coordinate grids) can be combined and superimposed upon shaded images to create a variety of useful displays.

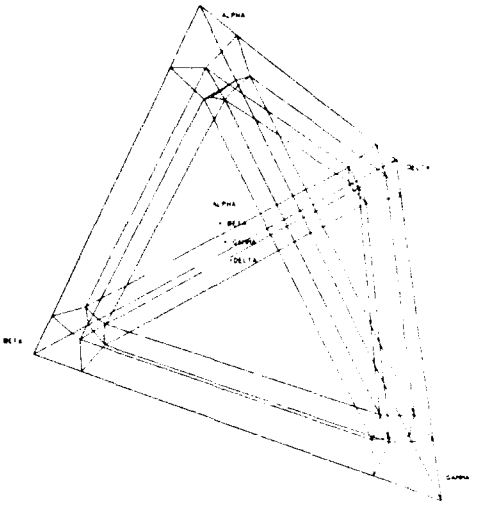

Fig. 1. A subsolidus quaternary isotherm.

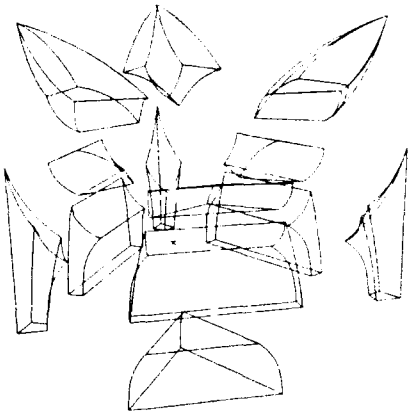

Fig. 2. An 'exploded' view of the solid-model for a ternary eutectic diagram.

Extraction of information from the 3-D phase diagrams was facilitated by a number of capabilities of the CAD system, many of which have already been mentioned. The composition and temperature of any point on a surface or curve can easily be accessed. Given a temperature and a bulk composition lying within a monovariant reaction region, the fraction of each phase present can also be easily accessed. Furthermore, tie-lines were stored as line drawings and superimposed upon the appropriate phase regions to aid in phase fraction determination in multivariant phase regions. Finally, planar sections through the 3-D diagrams were quickly and conveniently generated using a variety of input information to orient the "cutting plane" as desired.

5. - Discussion.

As mentioned above, various computer methods for the representation of phase diagrams have been proposed and used. Much of the work in this area has been aimed at creating computer programs which would be dedicated to one or more aspects of phase diagram representation. Although, to the author's knowledge, none have been intended primarily to assist researchers working with multicomponent materials in the efficient development (from available experimental data) and use of 3-D phase diagrams. Furthermore, the wide availability and reasonable cost of CAD systems have provided researchers with powerful new tools; tremendous resources have been devoted to the development of these systems, thus providing several advantages for the user. These often include (as is true for the CAD system used in the present work): dynamic viewing, the ability to create shaded surface displays using a variety of sophisticated display attributes (including translucency), the capability to utilize nonuniformly spaced input data, faceted representations of surfaces which can be nonuniformly spaced (allowing finer facets in more complex areas), the use of nonuniform rational B-spline curves and surfaces (allowing complex areas to be modeled without introducing unwanted inflection points), and the immediate display of data entered and geometry generated to allow interaction on the part of the user. Moreover, CAD programs are high level, menu-driven programs which do not require the user to possess advanced programming skills.

In spite of the merits of CAD systems for phase diagram applications, very few researchers have attempted to utilize CAD systems for this work. To the authors' knowledge, previous work using CAD systems (e.g., Roeder et al (1986) was limited largely or entirely to wireframe representations. Unfortunately, without solid-modeling, many of the advantages of CAD representations of 3-D phase diagrams are sacrificed. The lost capabilities include: shaded surface displays, efficient and self-consistent generation of planar sections through diagrams, and self consistent determination of composition-temperature coordinates for phase boundary surfaces.

6. - Conclusions.

The results obtained using the hypothetical quaternary eutectic system indicate the potential usefulness of this procedure. Given the successful results of the procedure with the type of input data used, it is reasonable to expect that the process should be applicable to many real systems. Currently, this procedure is being applied to a real quaternary system (CaO-Al_2O_3-MgO-SiO_2) which is relevant to the authors' study of solidification phenomena in geological materials.

It is envisioned that the use of this technique (or similar techniques which could be developed utilizing other CAD systems with solid-modeling) could allow researchers to make use of ternary and quaternary phase diagrams with something approaching the facility which has heretofore only been attainable with binary phase diagrams.

References

Massalski, T. B. (1989): Met. Trans. A 20A, p. 1295.

Notis, M. R. and Farby, S. K. (1986): in "Computer Modeling of Phase Diagrams", ed. Bennett, L. H., (TMS), Warrendale, PA, p. 355.

Palatnik, L. S. and Landau, A. I. (1964): "Phase Equilibria in Multicomponent Systems" (Holt, Rinehart and Winston, Inc.).

Prince, A. (1966): "Alloy Phase Equilibria" (Elsevier).

Roeder, J. F. (1986): in "Computer Modeling of Phase Diagrams", ed. Bennett, L. H., (TMS), p. 385.

Schairer, J. F. (1942): J. Am. Ceram. Soc. 25, p. 241.

A TIGHT BINDING ANALYSIS OF THE COHESIVE PROPERTIES IN TRANSITION METAL CARBIDES.

Duc Hiep LE, Catherine COLINET and Alain PASTUREL
Laboratoire de Thermodynamique et Physico-Chimie Métallurgiques, ENSEEG,
BP 75, 38402 SAINT MARTIN D'HERES Cédex, France.

Abstract :
The electronic structure and cohesive properties of transition metal carbides in NaCl structure are studied on the basis of a tight-binding recursion method. The electronic structure is analyzed in terms of a p-d interaction between the p orbitals of carbon and the d orbitals of the transition metal. A good agreement is found with the most sophisticated calculations like the ones based on the APW method. Concerning the cohesive properties of these compounds we have calculated the heats of formation of (Ti, Zr, Hf, V, Nb, Ta)-C and compared with the experimental values. We are able to interpret the evolution of the experimental values when we go through a column or a row in Mendeleiev's table.

I. - Introduction

Transition metal carbides which crystallize in the NaCl structure have long been of special interest because of their unusual combination of properties such as high melting point, ultrahardness and metallic conductivity. These compounds usually present important deviations from stoechiometry, due to a high concentration of metalloid vacancies, these vacancies having a strong influence on the measured values of all physical properties of the compounds. To attempt to explain all these properties, extensive experimental and theoretical studies on the electronic properties as well as on the phonon spectra have been performed over the past several years. The binding mechanism has been investigated by Schwarz (1977) and the calculated densities of states show a low energy narrow band due to the s electrons of the carbon and a higher conduction band mainly due to the hybridization between the p states of the carbon and the d states of the metal. This p-d hybridization has been shown to be of great importance in the interpretation of the energies of formation of the transition metal-aluminium or silicon compounds (Pasturel et al 1982,1984). In this paper, we propose to use this simple scheme to explain the thermodynamic behaviour of (Ti, Zr, Hf, V, Nb, Ta)-C compounds crystallizing in the NaCl structure, or in other terms, how the energy of formation of a transition metal carbide varies when we go through a column or a row. To investigate the energy of formation, we have chosen to use the recursion method of Haydock et al. (1972) within the tight-binding approach to describe the p-d hybridization ; the method allows one to analyze the local density of states, a basic "physical" quantity of the electronic structure of a solid. Within the tight-binding scheme, one can change easily interactions in order to study their influence on the local density of states, as it is done in the present study by "switching off" the nearest neighbour interactions between p- and d- electrons.

II. - Model

To describe the energetic interactions in the carbide, we start from the tight-binding Hamiltonian which can be written :

$$H = \sum_n \sum_i \sum_{\lambda_i} p_n^i \, |n,\lambda_i\rangle \, \varepsilon_i^{\lambda_i} \, \langle n,\lambda_i| + \sum_{n,m} \sum_{i,j} \sum_{\lambda_i \mu_j} p_n^i \, |n,\lambda_i\rangle \, \beta_{nm}^{\lambda_i \mu_j} \, \langle m,\mu_j| \, p_n^j \quad (1)$$

where the indices i, j label the chemical nature of the atoms. $p_n^i = 1$ if the site n is occupied by an atom of type i and $p_n^i = 0$ otherwise. $|n,\lambda_i\rangle$ is the atomic orbital λ_i (2 p for C and 3d, 4d or 5d for M) centred on site n and $\varepsilon_i^{\lambda_i}$ is the atomic energy level corresponding to the orbital λ_i at site n. Finally, $\beta_{nm}^{\lambda_i \mu_j}$ is the hopping integral between the λ_i orbital at site n and the μ_j orbital at site m. Since, $\beta_{nm}^{\lambda_i \mu_j}$ decreases very rapidly with the distance between sites n and m, we will consider three types of hopping orbitals only, corresponding to first ($\beta_{MC}^{\lambda_M \mu_C}$) and second ($\beta_{MM}^{\lambda_M \mu_M}$ and $\beta_{CC}^{\lambda_C \mu_C}$) neighbour distances. As usual, these hopping integrals can be expressed in terms of two centre integrals {ddσ, ddπ, ddδ} for β_{MM}, {ppσ, ppπ} for β_{CC} and {pdσ, pdπ} for β_{MC}

From this Hamiltonian, it is then easy to calculate the partial density of states of symmetry λ at site 0, $n_0^\lambda(E)$, as the imaginary part of the projection, on the atomic

orbital $|0,\lambda>$, of the Green function G(E) :

$$G(E) = \frac{1}{E-H} \tag{2}$$

$$n_0^{\lambda}(E) = -\frac{Im}{\pi} <0,\lambda| G(E + i0)|0,\lambda> \tag{3}$$

$n_0^{\lambda}(E)$ can be calculated as a continued fraction, the coefficients of which will be computed within the recursion method (Haydock et al. 1972). The energy of formation can be written in the Hartree-Fock approximation :

$$\Delta E = \int^{E_F} E\, n(E)\, dE - \frac{1}{2} \sum_{i=M,C} \int^{E_{Fi}} E\, n_i(E)\, dE$$

$$-\frac{1}{4} \sum_{i=M,C} U_i\, \Delta(N_i^2) \tag{4}$$

where the first and second terms represent the change in the one-electron band energy in alloying (Pasturel et al. 1984). Half the associated electron-electron interaction is substracted to correct for double counting in the first term of (4). $n_i(E)$ and N_i are the density of states and total number of electrons, respectively, associated with atom i ; E_{Fi} is the corresponding Fermi energy. In presence of charge transfers, we take into account intraatomic charge transfer effects in a Hartree-Fock scheme :

$$\varepsilon_i = \varepsilon_i^0 + U_i\, \Delta N_i \tag{5}$$

in which the reference state is equal to the pure metallic value ε_i^0, U_i is the Coulomb integral and ΔN_i is the variation of the number of electrons of i species during alloying (Pasturel et al. 1984).

We shall use here the standard Slater-Koster parameters deduced by Pecheur et al. (1984) from APW band structure calculations for NbC, with the previous simplification of keeping only the first (metal-carbon, which couples the two sublattices) and second (metal-metal and carbon-carbon, on each sublattice) nearest neighbour hopping integrals. Only the metal d and metalloid p bands have been considered since APW results show that metalloid s-band does not participate to cohesive properties [1]. For the other carbides, these seven hopping parameters have been corrected using Harrison's (1980) scaling law to take into account the variation of the lattice parameter from a carbide to another one. Besides these hopping parameters, we have to consider, two atomic levels, ε_p for the p orbitals on a C atom and ε_d for a M atom. We have used the values of the tables of Herman and Skillman (1963). Indeed, to perform the self-consistent calculations of charge transfer, we have used $U_{dd} = 3$ eV and $U_{pp} = 1$eV in agreement with previous calculations (Nguyen Manh et al. 1985). All the parameters are gathered in table I.

Table I : Tight-binding parameters for the carbides in the NaCl structure (in eV).

	ddσ	ddπ	ddδ	ppσ	ppπ	pdσ	pdπ
TiC	-0.8285	0.2898	0	0.6972	0.1537	-2.1979	1.0695
ZrC	1.0927	0.3822	0	0.5914	-0.1304	-2.3247	1.1312
HfC	-1.2254	0.4287	0	0.6063	-0.1337	-2.4926	1.2129
VC	-0.6499	0.2273	0	0.7521	-0.1658	-2.0218	0.9838
NbC	-1.0120	0.3540	0	0.6530	-0.1440	-2.3508	1.1439
TaC	-1.1516	0.4028	0	0.6577	-0.1450	-2.5167	1.2246

III - Results and discussion

We start by discussing the electronic density of states (DOS) obtained in our simplified tight-binding Hamiltonian. In figure 1, we show the density of states of NbC compound, calculated with a continued fraction exact up to the 10th level. It is clear from the partial p and d densities of states of figure 1 that the electronic density of states of the compound results from a strong mixing between the d and p states ; this strong mixing is characterized by the formation of bonding and antibonding states well separated by the occurrence of a pseudogap. We shall see that it explains the stability of these compounds. We have shown also the ab-initio results proposed by Schwarz (1977) ; one can see that our results are in qualitative agreement with these calculations. The densities of states of the other carbides are very similar to the one of NbC, the only main difference is the location of the Fermi level for TiC, ZrC and HfC compounds since Ti, Zr and Hf have one d electron less.

The importance of the p-d interaction is illustrated by a second calculation setting the p-d parameters of table I to zero. All other parameters remained unchanged. In this case, the p- and d- bands decouple as demonstrated clearly by figure 2. The bandwidth is now reduced by a factor 2-3 caused by switching off the p-d hybridization. There is also no characteristic minimum between two peaks as seen in figure 1.

Let us consider now the cohesive properties of the carbides. Using our simple p-d Hamiltonian, eqn.(4) can be rewritten as :

$$\Delta E = \int^{E_F} E\, .\, n(E)\, dE - \frac{1}{4} \sum_{i=M,C} U_i\, \Delta(N_i^2)$$

$$-\frac{1}{2} \int^{E_{FM}} E\, n_{sd}(E)\, dE + X \tag{6}$$

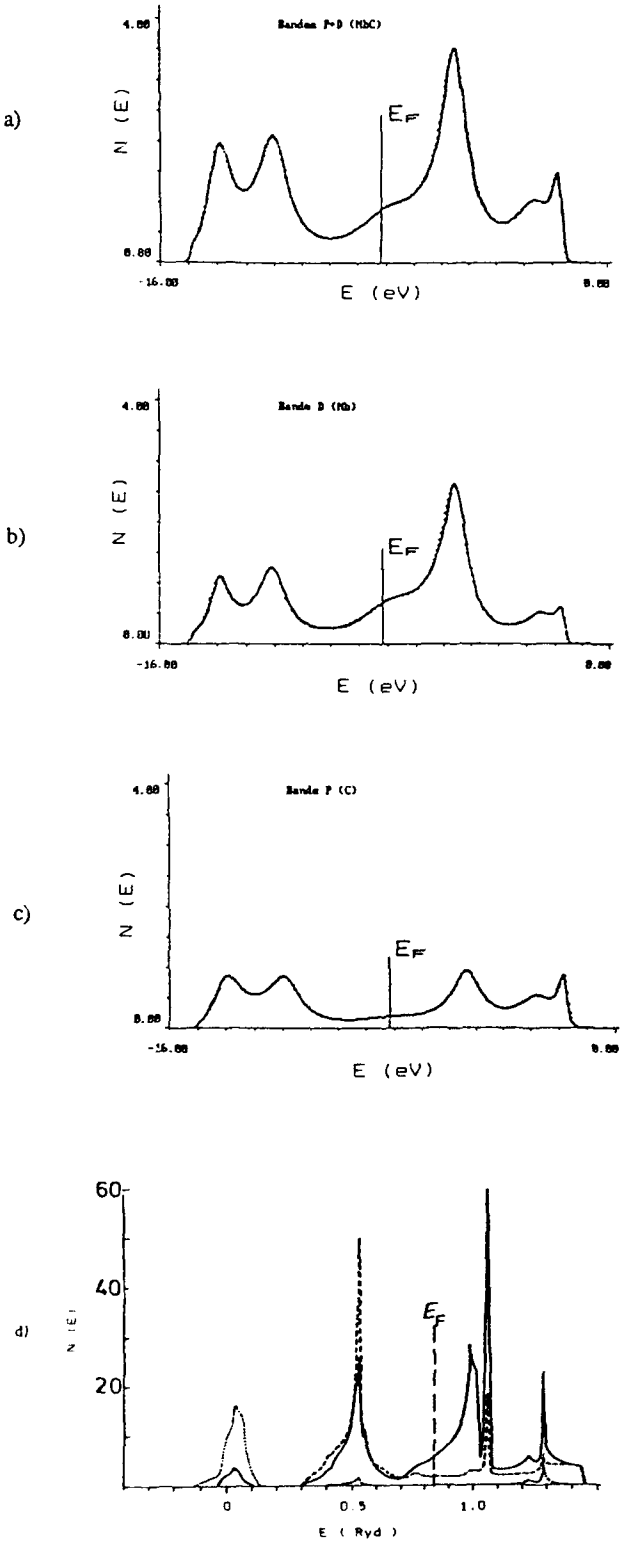

Figure 1 : Total (a) and partial (b-c) p and d electronic density of states of NbC compound in the NaCl structure ; (d) ab-initio results of Schwarz (1977).

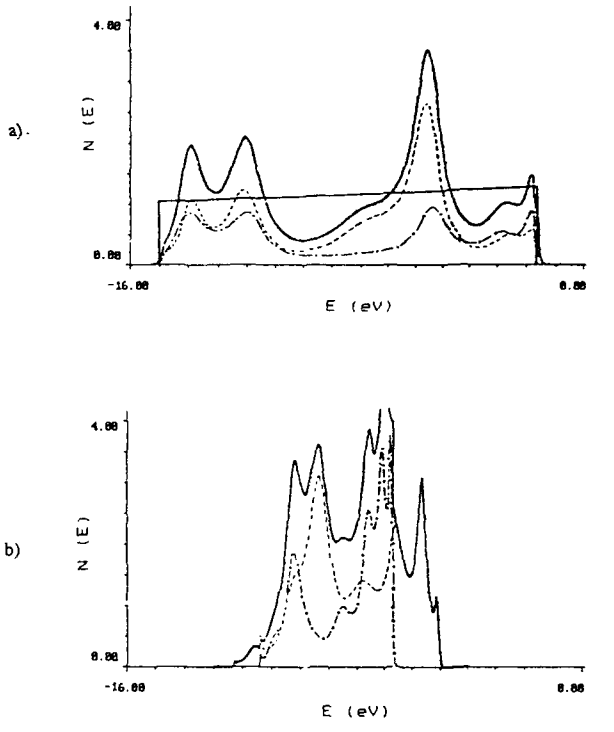

Figure 2 : Terminated continued fraction DOS for 10 levels with (a) and without (b) p-d hybridization (thin full line : background DOS with first 4 moments equal to those of the DOS). (14,8)

X being a constant equal to :

$$X = -\frac{1}{2} \int^{E_{F\,c}} E\, n_{s,p}(E)\, dE + \int^{E_F} E\, n_s(E)\, dE \qquad (7)$$

X can be considered as a contribution to account for transformation of carbon from a semiconducting reference state into an hypothetical metallic state. It has already been used by several authors (Pasturel et al. 1982, 1984 and Niessen and De Boer, 1981) to describe the heats of formation of carbides, silicides, nitrides or phosphides. Here, to obtain a quantitative description of the energies of formation of the carbides as a function of the transition element, we have chosen to fit the value of X on the energy of formation of NbC compound. In table II, we present our results for all the studied carbides and compare these values with the experimental ones. One can see that our values reproduce the experimental trend : the heats of formation become more and more negative when one goes down a column and more and more positive when one moves from IVB column to VB column. This latter behaviour can be easily understood from the location of the Fermi level in the electronic density of states.

Table II.: Comparison between experimental (*) (Hultgren et al. 1973 and Wagman et al. 1982) and calculated energies of formation of the carbides in the NaCl structure (in eV/at).

TiC	VC	ZrC	NbC	HfC	TaC
-0.89	+0.10	-1.05	-0.73	-1.23	-0.81
-0.96*		-1.02*	-0.73*	-1.13*	-0.77*

For VB column, the Fermi level is shifted due to an extra d electron of the transition metal. The most favourable situation is for IVB elements for which the Fermi level is located in the pseudogap, all the bonding states being filled and all the antibonding states being empty ; in this case, the cohesive energy of the carbide is the most important and explains the more negative values for the carbides based on the IVB column.

The evolution of the energies of formation of the carbides when we go down a column, can be explained from the values of the p-d hopping parameters which become stronger and stronger ; the pseudogap is then more pronounced and leads to more negative values for the heats of formation.

To show the influence of this pseudogap and the position of the Fermi level in relation to it, figure 3 displays the difference of the bond energy calculated with

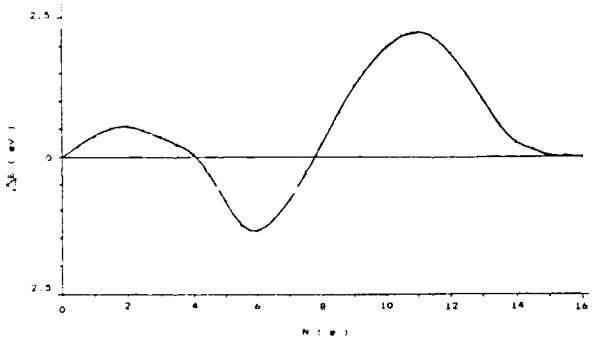

Figure 3 : Difference of structural energy of the terminated-continued fraction DOS for 10 levels minus background DOS with the first 4 moments equal.

10 levels minus a rectangular skew background ; the first four moments of the background DOS are equal to those of the actual DOS of the NaCl structure, necessarily leading to at least two zeros of the difference curve according to Ducastelle and Cyrot-Lackmann (1971). This curve presents 2 maxima at about 2 and 11 electrons and a pronounced minimum at 6 electrons. The minimum at 6 electrons occurs because the Fermi level falls into the pseudogap of the NaCl structure-DOS. It explains the stability of IVB and VB based carbides since these carbides correspond to a total filling of 6 and 7 electrons at the Fermi level.

IV. Conclusion

The application of the recursion method coupled with a simple p-d Hamiltonian enables an interpretation of the stability of IVB and VB based carbides in the NaCl structure. The density of states of these carbides is characterized by the occurrence of a pseudogap due to the strong coupling between the p-orbitals of the carbon and the d orbitals of the transition element. For the studied carbides, the Fermi level falls into the pseudogap, leading to the filling of all the bonding states, the antibonding states being empty : from the point of view of the cohesive properties it is the ideal situation.

REFERENCES

Ducastelle, F. and Cyrot-Lackmann, F. (1971) : J. Phys. Chem. Solids 32, 285.
Harrisson, W.A., (1980) : Electronic Structure and the Properties of Solids", ed. by W.H. Freeman and Company, San Francisco .
Haydock, R. Heine, V. and Kelly, M. J. (1972) : Phys. C.5, 2845.
Herman, F. and Skillman, S. (1963) : "Atomic Structure Calculations", Prentice Hall, New York .
Hultgren, P. Desai, P.D. Hawkins, D.T. Gleiser, M. Kelley, K.K. (1973) : "Selected Values of the Thermodynamic Properties of Binary Alloys", A.S.M., Metals Park, Ohio (1973).
Nguyen Manh, D. Mayou, D. Pasturel, A.and Cyrot-Lackmann, F. (1985) : J. Phys. F. 15, 1911.
Niessen, A.K. and de Boer, F.R. (1981) J. Less-Common Met. 82, 75.
Pasturel, A. Hicter P. and Cyrot-Lackmann, F. (1982) J. Less-Common Metals, 86, 181 ;
Pasturel, A. Hicter P. and Cyrot-Lackmann, F. (1984) Physica (B+C) 124, 247.
Pasturel, A. Colinet, C. and Hicter, P. : (1984) Acta Metall. 32, 1061.
Pécheur, P. Toussaint, G. and Kauffer, E. : (1984) : Phys; Rev. B. 29, 6606.
Schwarz, K. (1977) : J. Phys. C.10, 195.
Wagman, D.D. Evans, W.H. Parker, V.B. Schumm, R.H. Halow, I. Bailey, S.M. Churney, K.L. and Nuttall, L. J. Phys. Chem. Ref. Data, Vol. 11, Suppl. 2, (1982).

A SOLUTION MODEL FOR THE RELATION BETWEEN ENTHALPY OF MIXING AND EXCESS ENTROPY IN LIQUID BINARY ALLOYS

Toshihiro TANAKA*, Nev A. Gokcen**, Zen-ichiro MORITA* and Philip J. SPENCER***

* Dept. of Materials Science & Processing, Osaka Univ., 2-1 Yamadaoka, Suita, Osaka, Japan.
** United States Department of the Interior, Bureau of Mines, 1450 Queen Avenue SW, Albany, Oregon 97321-2198, U.S.A.
*** Lehrstuhl für Theoretische Hüttenkunde u. Metallurgie der Kernbrennstoffe, RWTH Aachen, Kopernikusstr. 16, 5100 Aachen, West-Germany.

Abstract.-

The relation between $\Delta\bar{H}_B$ and $\Delta\bar{S}_B^{Ex}$ in infinite dilution in liquid binary alloys of A and B, which depends on the melting points of the components, has been obtained on the basis of free volume theory.

1.- Introduction.

Several empirical attempts have been made to correlate the enthalpy of mixing and excess entropy in liquid binary alloys. For example, Kubaschewski (1981) obtained the following relationship between the partial enthalpy of mixing $\Delta\bar{H}_B$ and the partial excess entropy $\Delta\bar{S}_B^{Ex}$ of solute elements in infinite dilution of liquid binary alloys.

$$\Delta\bar{H}_B = 3400\ \Delta\bar{S}_B^{Ex} \qquad (1)$$

Lupis and Elliott (1967) proposed the following similar relationship :

$$\Delta\bar{H}_B = \tau\cdot\Delta\bar{S}_B^{Ex} \qquad (2)$$

In this equation, τ is a constant and a value of 3000 ± 1000 for this parameter has been proposed for ordinary metallic solutions. However, they suggested that τ is not always constant for all types of alloys and might be dependent upon the nature of the alloy components.

Recently, the authors have derived a solution model for the relationship between the enthalpy of mixing and the excess entropy in liquid binary alloys. In this paper, an outline of the model as applied to infinite dilution of liquid binary alloys is presented with some new results.

2.- Derivation of Thermodynamic Equations.

The derivation of the solution model has already been described in detail in our previous publications (Tanaka et al. 1990 "A" & "B"). Only a summary of the model will therefore be presented here. In this model, the equations for the enthalpy of mixing and excess entropy have been derived on the basis of the free volume theory advanced by Shimoji and Niwa (1957) and the first approximation of the regular solution model proposed by Gokcen (1986), by considering configuration and vibration of atoms in alloys. Assuming that an atom vibrates harmonically in its cell surrounded by its nearest-neighbours, the excess Gibbs energy of mixing ΔG_{mix}^{Ex} is expressed by the following equations:

$$\Delta G_{mix}^{Ex} = \Delta H_{mix} - T\,\Delta S^{Ex} \qquad (3)$$

$$\Delta H_{mix} = N_{AB}\,\Omega_{AB} / Z \qquad (4)$$

$$N_{AB} = ZN_0X_AX_B(1-X_AX_B\Omega_{AB} / kT) \qquad (5)$$

$$\Delta S^{Ex} = \Delta S_{CONF}^{Ex} + \Delta S_{NONCONF}^{Ex} \qquad (6)$$

$$\Delta S_{CONF}^{Ex} = -X_A^2X_B^2\Omega_{AB}^2 / 2kT^2 \qquad (7)$$

$$\Delta S_{NONCONF}^{Ex}$$
$$= 3/2kN_0\{X_A\ln(v_A/v_{AA}) + X_B\ln(v_B/v_{BB})\}$$
$$= 3/2kN_0\{2X_A\ln(L_A/L_{AA}) + 2X_B\ln(L_B/L_{BB})$$
$$+ X_A\ln(U_{AA}/U_A) + X_B\ln(U_{BB}/U_B)\} \qquad (8)$$

where N_{AB} is the number of A-B pairs; Z, coordination number; Ω_{AB}, exchange energy; k, Boltzmann constant; T, temperature in K; N_0, Avogadro number; X_A, X_B, mol-fraction; v_A, v_B, v_{AA} & v_{BB}, free volume; L_A, L_B, L_{AA} & L_{BB}, distance which interatomic potential extend in a cell, as shown in Fig.1; U_A, U_B, U_{AA} & U_{BB}, depths of the potential energy in a cell, as shown in Fig.1. In the above equations, the suffices AA & BB indicate pure elements and A & B indicate the states of A and B atoms in an A-B alloy. In Eq.(8), if the free volumes of A and B in an A-B alloy are larger than those in the pure states, i.e., $v_A>v_{AA}$ and $v_B>v_{BB}$, the region in which an atom moves randomly in its cell surrounded by its nearest-neighbours increases, and consequently $\Delta\bar{S}_{NONCONF}^{Ex}$ becomes positive. On the other hand, if $v_A<v_{AA}$ & $v_B<v_{BB}$, the reverse is true.

When the concentration of B in liquid A-B alloy is infinitely small, the following equations for $\Delta\bar{H}_B$ and $\Delta\bar{S}_B^{Ex}$ can be obtained by differentiation and rearrangement:

$$\Delta\bar{H}_B = \Omega_{AB} \qquad (9)$$

$$\Delta\bar{S}_B^{Ex} = \Delta\bar{S}_{B,\ NONCONF}^{Ex}$$
$$= 3/2kN_O[(L_{AA}-L_{BB})^2/L_{AA}L_{BB}$$
$$+\{4U_{AA}U_{BB} - 2\Omega_{AB}(U_{AA} + U_{BB})$$
$$- (U_{AA} + U_{BB})^2\}/2U_{AA}U_{BB}] \qquad (10)$$

U_{AA} and U_{BB} in Eq.(10) can be obtained from the following equations. (Tanaka et al. 1990"A").

$$U_{ii} = -2\pi^2 L_{ii}^2 M_{ii} \nu_{ii}^2 / N_O \qquad (i=A \text{ or } B) \quad (11)$$

In Eq.(11), M_{ii} is the atomic weight. L_{ii} is assumed to be half of the nearest-neighbour distance and this can be obtained from

$$L_{ii} = 1/2(2^{1/2}V_{ii}/N_O)^{1/3} \qquad (i=A \text{ or } B) \quad (12)$$

where V_{ii} is the molar volume. ν_{ii} in Eq. (11) is the frequency of an atom, which can be evaluated by the following equation proposed by Iida and Guthrie (1988).

$$\nu_{ii} = 2.8\ 10^{12}\beta_{ii}(Tm,_{ii}/M_{ii}V_{ii}^{2/3})^{1/2} \qquad (13)$$

(i=A or B)

where $Tm,_{ii}$ is the melting point and β_{ii} is the coefficient to transform the frequency in the solid state into that in the liquid state at the melting point. Values of β_{ii} were obtained from the experimental data for the surface tension of the pure elements in the liquid state.

Consequently, the following relationship between $\Delta\bar{H}_B$ and $\Delta\bar{S}_B^{Ex}$ can be derived from Eqs.(9) and (10).

$$\Delta\bar{S}_B^{Ex} = 3/2kN_O[(L_{AA}-L_{BB})^2/L_{AA}L_{BB}$$
$$+\{4U_{AA}U_{BB}-2\Delta\bar{H}_B(U_{AA}+U_{BB})$$
$$-(U_{AA}+U_{BB})^2\}/2U_{AA}U_{BB}] \qquad (14)$$

As shown in Eqs.(9)-(14), the partial excess entropy and also the partial excess Gibbs energy $\Delta\bar{G}_B^{Ex}$ can be obtained from the physical properties listed in Table 1 for pure elements when the value of the partial enthalpy of mixing is known.

3.- Calculation of $\Delta\bar{S}_B^{Ex}$ and $\Delta\bar{G}_B^{Ex}$.

In this work, the values of $\Delta\bar{H}_B$ were obtained using Miedema's semi-empirical method (Niessen et al. 1983). U_{AA} and U_{BB} in Eq. (14) can be calculated from Eqs.(11)-(13) with the physical properties shown in Table 1 (Iida and Guthrie 1988, Niessen et al. 1983). They then have the units erg·atom^{-1} and must therefore be transformed into J·mol^{-1} to obtain the same unit of $\Delta\bar{H}_B$ as that corresponding to Eq.(14). In this case, the following equation for U_{AA} and U_{BB} can be derived from Eqs.(11)-(13).

$$U_{ii} = -685.3\beta_{ii}^2 Tm,_{ii} \quad / \text{ J mol}^{-1} \qquad (15)$$

(i=A or B)

Calculations of $\Delta\bar{S}_B^{Ex}$ and $\Delta\bar{G}_B^{Ex}$ were carried out for the 60 alloy systems presented in Table 2. Experimental values of $\Delta\bar{G}_B^{Ex}$ (Hultgren et al. 1973, The 19th Committee on Steelmaking 1988) are also shown in Table 2.

4.- Relationship between $\Delta\bar{H}_B$ and $\Delta\bar{S}_B^{Ex}$.

Figure 2 shows the relationship between $\Delta\bar{H}_B$ and $\Delta\bar{S}_B^{Ex}$, both calculated as in the preceding section. As can be seen from this figure, the relationship is dependent upon temperature.

When A and B in an A-B alloy have nearly the same values of molar volume and atomic weight, the following approximate relation can be derived from Eqs.(11)-(14).

$$\Delta\bar{H}_B = \{14.0/(1/Tm,_A+1/Tm,_B)\}\Delta\bar{S}_B^{Ex} \qquad (16)$$

Plots of $\Delta\bar{H}_B(1/Tm,_A+Tm,_B)$ against $\Delta\bar{S}_B^{Ex}$ are shown in Fig.3. It is evident from this figure that $\Delta\bar{H}_B(1/Tm,_A+1/Tm,_B)$ is proportional to $\Delta\bar{S}_B^{Ex}$ as proposed in Eq.(16). Hence, the relationship between $\Delta\bar{H}_B$ and $\Delta\bar{S}_B^{Ex}$ depends on the melting points $Tm,_A$ and $Tm,_B$ of the components of the alloy and the ratio of $\Delta\bar{H}_B$ to $\Delta\bar{S}_B^{Ex}$ becomes larger when the alloy is composed of the components with higher melting points.

5.- Conclusion.

The relationship between $\Delta\bar{H}_B$ and $\Delta\bar{S}_B^{Ex}$ in infinite dilution of liquid binary alloys has been discussed on the basis of the free volume theory. It is shown that the relationship is dependent upon the melting points of the components.

References.

Hultgren, R., Desai, P.D., Hawkins, D.T., Gleiser, M. and Kelley, K.K. (1973): Selected Values of the Thermodynamic Properties of Binary Alloys, ASM, Metals Park, Ohio.

Gokcen, N.A. (1986): Statistical Thermodynamics of Alloys, Plenum Press, New York.

Iida, T. and Guthrie, R.L. (1988): The Physical Properties of Liquid Metals, Oxford Science Pub.

Kubaschewski, O. (1981): High Temp.- High Press., 13, 435.

Lupis, C.H.P. and Elliott, J.F. (1967): Acta Metall., 15, 277.

Niessen, A.K., de Boer, F.R., Boom, R., de Chatel, P.F., Mattens, W.C.M. and Miedema, A.R. (1983): CALPHAD 7, 51. See Gokcen (1986) for a comprehensive summary.

Shimoji, M. and Niwa, K. (1957): Acta Metall 5, 496.

Tanaka, T., Gokcen, N.A., and Morita, Z. (1990)"A": Z. Metallkde., 81, 49.

Tanaka. T., Gokcen. N.A., and Morita, Z. (1990)"B": Z. Metallkde., 81, (in press)

The 19th Committee on Steelmaking in The Japan Society for the Promotion of Science (1988): Steelmaking Data Sourcebook, Gordon and Breach Sci. Pub., New York.

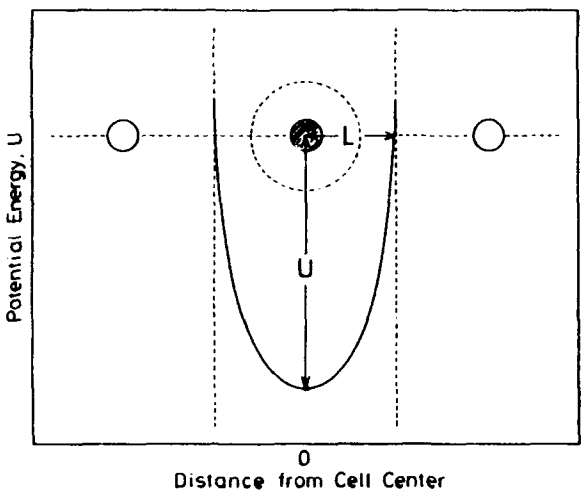

Fig.1 Interatomic potential in a cell.

Table 1 Physical properties used in the calculation of $\Delta\bar{S}_B^{Ex}$, V_{ii}/cm^3mol^{-1}, $Tm_{,ii}/K$, $\beta_{ii}/-$.

i	V_{ii}	$Tm_{,ii}$	β_{ii}	i	V_{ii}	$Tm_{,ii}$	β_{ii}
Ag	10.25	1234	0.47	Mo	9.39	2903	0.50
Al	9.99	933	0.52	Na	23.78	371	0.49
Au	10.19	1336	0.49	Nb	10.81	2793	0.50
Bi	19.32	544	0.54	Ni	6.60	1728	0.50
Cd	13.00	594	0.56	Pb	18.28	601	0.55
Co	6.69	1765	0.50	Sb	16.96	904	0.40
Cr	7.23	2178	0.50	Si	8.61	1687	0.38
Cu	7.12	1356	0.46	Sn	16.30	505	0.64
Fe	7.09	1808	0.48	Ta	10.81	3263	0.50
Hg	14.08	234	0.84	Ti	10.58	1998	0.50
In	15.74	430	0.68	Tl	17.23	576	0.55
K	45.63	337	0.50	V	8.36	1973	0.50
La	22.54	1193	0.50	W	9.54	3653	0.50
Mg	14.00	923	0.45	Zn	9.17	693	0.54
Mn	7.35	1517	0.50	Zr	14.00	2130	0.50

Table 2 Values of $\Delta\bar{H}_B/kJmol^{-1}$ by Miedema's semi-empirical method and calculated results for $\Delta\bar{S}_B^{Ex}/JK^{-1}mol^{-1}$ and $\Delta\bar{G}_B^{Ex}/kJmol^{-1}$. Values in parenthesis are experimental values: *-Hultgren et al. (1973), **-The 19th Committee on Steelmaking (1988).

System A	B	Temp.	$\Delta\bar{H}_B$	$\Delta\bar{S}_B^{Ex}$	$\Delta\bar{G}_B^{Ex}$
Al	Au	1338	-92	-12.2	-76(-140)*
Al	Cu	1373	-28	-3.7	-23(-36)*
Al	Fe	1873	-41	-6.2	-29(-56)*
Al	In	1173	30	4.8	25(23)*
Al	Sn	973	19	3.1	16(15)*
Al	Zn	1000	2	0.1	2(6)*
Cu	Ag	1423	10	1.4	8(14)*
Cu	Al	1373	-34	-4.5	-27(-36)*
Cu	Au	1550	-42	-4.8	-34(-24)*
Cu	Fe	1823	52	4.7	44(36)*
Cu	Pb	1473	41	6.6	32(20)*
Cu	Sn	1400	-6	-0.6	-5(-57)*
Cu	Tl	1573	43	6.6	33(26)*
Fe	Ag	1873	123	12.6	99(83)**
Fe	Al	1873	-48	-7.0	-35(-47)**
Fe	Co	1873	-2	-0.2	-2(-9)**
Fe	Cr	1873	-6	-0.9	-4(2)**
Fe	Cu	1873	50	4.5	42(34)**
Fe	La	1873	25	3.8	18(35)**
Fe	Mn	1873	1	0.0	1(6)**
Fe	Mo	1873	-9	-2.5	-4(0)**
Fe	Nb	1873	-70	-6.3	-58(-25)**
Fe	Ni	1873	-6	-0.6	-5(-7)**
Fe	Pb	1873	160	19.7	123(105)**
Fe	Si	1873	-75	-10.7	-55(-103)**
Fe	Sn	1873	56	5.2	46(15)**
Fe	Ta	1873	-67	-7.1	-54(-50)**
Fe	Ti	1873	-74	-5.9	-63(-73)**
Fe	V	1873	-29	-2.5	-24(-36)**
Fe	W	1873	0	-3.9	7(0)**
Fe	Zr	1873	-118	-8.9	-101(-51)**
Na	Hg	673	-42	-15.3	-31(-34)*
Na	In	713	-20	-10.0	-13(-1)*
Na	K	384	6	3.1	5(3)*
Na	Pb	700	-70	-24.4	-53(-48)*
Na	Tl	673	-43	-16.1	-32(-21)*
Pb	Ag	1273	9	0.9	8(8)*
Pb	Al	1200	33	5.5	27(31)*
Pb	Bi	700	0	-0.1	0(-4)*
Pb	Cd	773	5	1.2	4(8)*
Pb	Cu	1473	23	3.6	18(19)*
Pb	In	676	-3	-0.5	-2(2)*
Pb	K	848	-89	-31.7	-63(-36)*
Pb	Mg	973	-28	-5.3	-23(-17)*
Pb	Na	700	-63	-22.5	-48(-34)*
Pb	Sn	1050	6	1.0	5(17)*
Pb	Tl	773	-3	-0.5	-2(-1)*
Pb	Zn	923	16	3.5	12(16)*
Tl	Ag	975	10	0.7	9(11)*
Tl	Cd	750	8	1.7	7(4)*
Tl	Cu	1573	26	3.7	20(16)*
Tl	K	798	-55	-20.6	-39(-34)*
Tl	Mg	923	-12	-2.3	-10(-21)*
Tl	Na	673	-41	-15.5	-31(-32)*
Tl	Pb	773	-3	-0.5	-2(-2)*
Tl	Sn	723	6	0.9	5(4)*
Zn	Al	1000	2	0.1	2(8)*
Zn	Au	1080	-73	-12.0	-60(-67)*
Zn	In	700	14	2.9	12(14)*
Zn	Pb	923	25	5.2	20(27)*

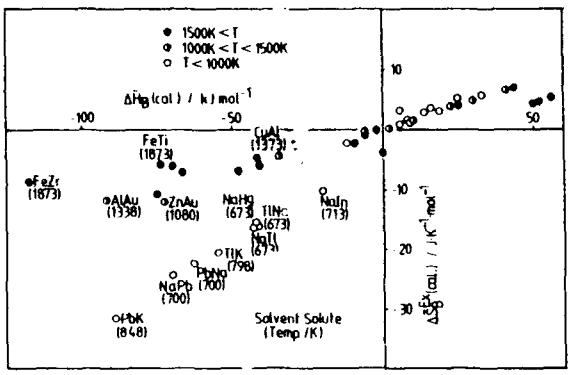

Fig.2 Calculated results for the relationship between $\Delta\bar{H}_B$ and $\Delta\bar{S}^{Ex}_B$ in infinite dilution of liquid binary alloys.

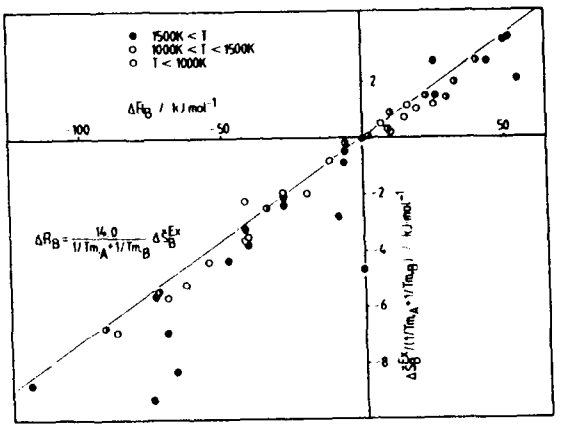

Fig.3 Calculated results for the relationship between $\Delta\bar{H}_B$ and $\Delta\bar{S}^{Ex}_B/(1/Tm_{,A} + 1/Tm_{,B})$ in infinite dilution of liquid binary alloys.

Thermodynamic Effects, Seen on the Atomic Sites, in Strongly Bound Liquid Alloys

K. Ott*, B. Balschun, M. Dürrwächter, M.A. Haghani, M. von Hartrott* and D. Quitmann

Institut für Experimentalphysik, Freie Universität Berlin, Arnimallee 14, D–1000 Berlin 33, FRG

*BESSY, Lentzeallee 100, D–1000 Berlin 33, FRG

Abstract

The importance of local, i.e. atomic scale information for the understanding of liquid metal alloys with strong A–B bonding and compound forming tendency is stressed. Within a model of chemical reaction $A+B \rightleftharpoons AB$ which is well established for thermodynamics we discuss the NMR observables Knight shift K and quadrupolar relaxation rate R_q. The hyperfine interaction selects the atom (A or B) and then differentiates between left hand and right hand side states (A,B vs. AB). This model was applied successfully to K and R_q in liquid alloys of s–p–metals. Using additional data (electric and magnetic field fluctuations) it appears possible to derive a measure of bond character (ionic/ covalent/metallic) in liquid alloys.

1. Introduction

In many binary liquid melts $A_{1-x}B_x$ from metallic components A,B the A–B interaction is much stronger than the A–A, B–B interactions, as shown by considerable exothermic heat of mixing $\Delta H(x)$ which for very strong interactions assumes a "V" shape. It is generally found that when the minimum of $\Delta H(x)$ is sharp, the minimum composition x_s corresponds to a rather low stoichiometry $x_s/(1-x_s)=1:1$, 1:2, 2:3 etc.. Also the entropy of mixing falls below the ideal value and shows, for some cases, a sharp local minimum at x_s. Among the many cases known (see e.g. Hultgren et al. 1973) we refer to the pairs of s–p metals, where the stoichiometry follows chemical expectations: IA–IIIA, –IVA, –VA; IIIA–VA; IIIA–, IVA–VIA etc.. In almost (but not strictly) every case, there exists in the solid A–B system a crystalline intermetallic compound which has the same stoichiometry and an elevated melting point T_m, i.e. increased stability. One may ask: How much of "the bonding effects" is still present in the liquid alloy? Which influence does it have on the various properties of the liquid alloy?

Additional signs of strong A–B bonding in liquid alloys of s–p metals are the strong deviations of electronic properties (electrical conductivity $\sigma(x,T)$, magnetic susceptibility $\chi(x,T)$) from their expected free electron or nearly free electron behaviour, viz. semiconducting or diamagnetic behaviour near x_s, T_m. For reviews, see Mott (1987), Cutler (1977), Glazov et al. (1969), Warren (1977). These anomalies prove that the bonding energy gain is accompanied by a modulation of the electron density up to the point of electron localization (Mott 1987), and certainly accompanied by a corresponding deviation of the A–B density distribution from a random mixture; for a well studied case see Li–Pb (Chieux and Ruppersberg 1980). One is thus forced to reconcile in a model these seemingly contradictory requirements: bonding like in the crystalline phase, yet long (and probably intermediate) range disorder since the system is liquid.

2. Model of association

One way of modeling these combined requests is to think in terms of bonds within very small groups of neighbouring atoms (e.g. 2,3,5 atoms for $x_s/(1-x_s)=1:1,1:2,2:3$), considering this group of bonds (1,2,6 bonds) as largely uncorrelated with other bonds. It is this last qualifier which distinguishes the liquid from the bond concept in crystals. The independence between groups of bonds may be justified qualitatively for metallic bonds by the strong screening, and for ionic bonds (not quite as well) by the averaging effect of the long range Coulomb interaction. Covalent bonds can apparently also exist under these conditions: it is known from amorphous semiconductors and covalent glasses or melts (see e.g. Elliott 1990) that there remain basically only the steric restrictions if one goes further than the second nearest neighbour.

A description of the enthalpy and entropy of mixing for metallic alloys in terms of bonds has been developped in detail and applied very successfully (see Guggenheim 1952, Bhatia and Hargrove 1974, Sommer 1982, Brebrick et al.1983, Terzieff et al. 1986, Ott et al. 1989). It is based on an assumed exothermic reaction between "free" atoms A,B, which leads to an "associate" $A_\mu B_\nu$

$$\mu A + \nu B \rightleftharpoons A_\mu B_\nu \qquad (1)$$

with $x_s=\mu/(\mu+\nu)$. Introducing interaction parameters for the reaction to the right hand side (ΔH^0, ΔS^0) and also between the three species A=1,B=2 and $A\mu B\nu=3$ (W_{12},W_{13},W_{23}), the concentrations of these species, n_1,n_2 and n_3 respectively, can be worked out in a standard procedure (see Ott et al. 1989). The important point for the following is that the atoms A, B are considered to be in two states corresponding to the left or right hand side of eq.(1): "free" or metallic A and B on the lhs., associated or "bound" on the rhs. The dynamic equilibrium (see (1)) gives the probabilities of any individual A or B atom to be "free" or "associated" as

$$P_{1free}=\frac{n_1}{n_1+\mu\, n_3};\quad P_{2free}=\frac{n_2}{n_2+\nu\, n_3};\quad P_{1ass}=1-P_{1free};$$

$$P_{2ass}=1-P_{2ass}. \qquad (2)$$

An important property of the associate $A\mu B\nu$ will be its excess volume $\Delta V=V_3-\mu V_1-\nu V_2$, or its structure (Bhatia and Hargrove 1974). However, the former is not measurable microscopically, and the latter is difficult to derive uniquely from the experimental two–point scattering functions S(q). We shall therefore turn to other measurable effects of the bonding which can be identified as signs of the bonding locally, i.e. on the atoms A and B.

3. Connection between bonding and microscopic observables: Knight shift

Extremely local observables, specific to the site of A or B, are the NMR properties Knight shift, magnetic and quadrupolar relaxation rate (see e.g. Abragam 1978). The Knight shift K is produced by conduction electrons (at the Fermi energy ϵ_f) which are polarized by the external magnetic field and which transfer this polarization to the site of the nucleus as an additional hyperfine field; for s– and p–elements, the main contribution is generally assumed to come from spin polarization of those conduction electrons at ϵ_f which have s–character, so that essentially

$$K=\frac{8\pi}{3}\chi_p <|\psi(0)|^2>_{\epsilon_f} \Omega \qquad (3)$$

with χ_p=Pauli spin susceptibility, Ω=atomic volume, $<|\psi(0)|^2>_{\epsilon_f}$ = average density of electrons at the nuclear site and with Fermi energie ϵ_f.

In those liquid alloys where the A–B bonding and electron localization is strong enough to make them liquid semiconductors ($\gamma(x_s) << x_s\sigma_1+(1-x_s)\sigma_2$), a strong decrease of the Knight shift around x_s has been observed (e.g. Au–Cs: Dupree et al 1980, Cu–Te: Warren 1973; Ga–Te: Warren 1971). This is in full agreement with the decrease near $x \rightarrow x_s$ of conduction electrons. Starting from eq.(1), conduction electrons are supplied by the metallic lhs. atoms A and B, with concentrations $n_1(x)$ and $n_2(x)$. Since $n_1,n_2 \rightarrow 0$ as $x \rightarrow x_s$, there occurs a reduction of χ_i which may be roughly estimated using the free electron model

$$\chi_i \sim [(Z_1 n_1 + Z_2 n_2)/V_{mol}]^{1/3} \qquad (4)$$

with the valencies Z_1,Z_2 of A and B, and the molar volume V_{mol}. In fig.1a we show the calculated dependence of n_1,n_2 and n_3 on x for the case Cu–Te (thermodynamical data from Blachnik and Gather, 1983).

The Knight shifts (from Warren 1973) are presented in fig.1b. It is seen that Cu– und Te–Knight shift both drop from their pure liquid values as $x \rightarrow x_s$, as expected. However, the Cu shift stays low on the Te side! Qualitatively the same occurs for K(Ga) in Ga–Te (Warren 1971), K(Cs) in Au–Cs (Dupree et al. 1980), K(Cs) in Cs–Sb (Dupree et al. 1982), and from measurements of our group also for Te on the metal side in Sn–Te (Ott et al. 1989a).

There is thus an asymmetry in K versus x: $K << K_{metal}$ near x_s and on the minority side for either constituent A or B. Since $\chi_i(x)$ behaves symmetrically, see fig. 1a and eq.(4), the asymmetry has to be ascribed to the factor $<|\psi(0)|^2>_{\epsilon_f}$ of eq. (3): it must be small on the minority side.

This is, in fact, exactly what one expects if bond formation occurs and the system behaves according to eq.(1): On the minority side of A (i.e $x_1<(x_s)_1$) virtually all A atoms are bound in associates, $P_{1free} \rightarrow 0$. The outer electrons which atom A used to contribute as conduction electrons, when A was in the pure liquid metal A or was the majority component ($x_1>(x_s)_1$), are now engaged in bonds. They are no longer at ϵ_f, i.e. no longer polarizable, and thus do not contribute to the shift K (A):

$$<|\psi(0)|^2>_{\epsilon_f} \approx 0 \quad \text{for } A_\mu B_\nu \qquad (5)$$

The same argument works for B on its minority side. The shape of the curves K(A), K(B) vs. x,T is then fully determined by the thermodynamic parameters (ΔH^0, W_{ij} etc.) which are obtained independently from the thermodynamic data $\Delta H(x)$ etc.. For a more detailed description of the calculation we refer to Ott et al. (1989).

This quantitative connection between thermodynamic data ($\Delta H(x)$ etc.) and microscopic observables (K(A), K(B)) has become possible by the two–step parametrization occuring for eqs.(1), (2), (3) and (4). For the case of Cu–Te this approach reproduces the experimental Knight shift data over the whole composition range (see fig. 1b). Equally good agreement is achieved for Sn–Te (Ott et al. 1989b), Au–Cs and Cs–Sb (Ott et al. 1990a). For the case Au–Cs see fig.2. – It should be noted however, that two similar tight binding approaches including local densities of states (Geertsma 1982, and particular for Au–Cs Franz et al. 1980) have also produced an asymmetric curve K vs.x. While there is qualitative agreement in the calculations, the differences may well be within the accuracy achievable in future experiments.

4. Other observables

A similar chain of arguments as was just explained for the Knight shift K, has been given earlier for another NMR–, "local" quantity, viz. for the quadrupolar part of the nuclear spin relaxation rate R_q (see Ott et al. 1989). There the decisive conclusion drawn from eq. (1) was that one can derive a prediction for the decay time of electric field fluctuations since a most important contribution to the decay time comes from the back reaction. The latter slows down as $x \rightarrow x_s$ and $n_1,n_2 << n_3$, in order to fulfill the dynamic equilibrium. It was found necessary to include also the exchange reaction, schematically $A'+AB \leftrightarrows A+A'B$. This rate, like that of the back reaction, is determined by the parameters of the thermodynamics. Application of this ansatz to some 20 binary and ternary

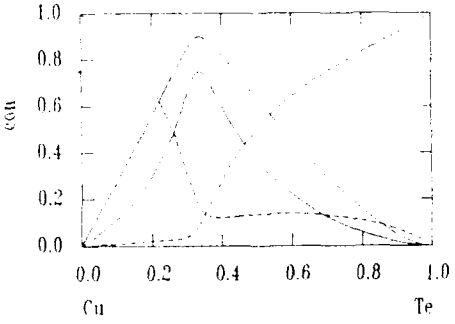

Fig.1a: Liquid Cu–Te: Concentrations n_1,n_2,n_3 of free species Cu, Te, (dashed lines) and associates Cu_2Te, (lower full line) from thermodynamic model eq.(1).Interaction parameters: W_{12}=–30, W_{13}=+10, W_{23}=0, $\Delta H^0_{Cu_2Te}$=–66, ΔS^0=0; in KJ/mol, T=1400 K. Upper full line: fraction of associated atoms, $(\mu+\nu)\cdot n_3/[(\mu+\nu)n_3+n_1+n_2]$.

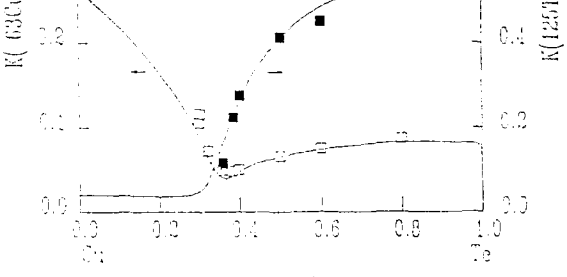

Fig.1b: Knight shifts of Cu, K(Cu) and of Te, K(Te) in liquid Cu–Te, with experimental points from Warren (1973); T=1400 K. The curves are calculated as described in the text.

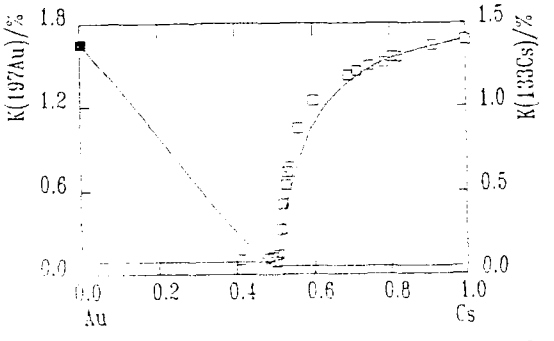

Fig.2: Knight shift of Cs in liquid Au–Cs alloys, data from Dupree et al. (1980) T=873 K.. Full square: K(Au), from Carter et al., 1977; T=4 K. Model calculation based on eq.(1) –(4), from Ott et al. (1989).

liquid metallic alloys gave for the first time a possibility to understand the very large increases which R_q displays when a liquid metal A is alloyed with a bonding partner B, like e.g. In with Sb. For details, we have to refer to Ott et al. (1989); the binary systems considered there are Au–Ga, Au–In, Bi–In, Bi–Te, Ga–Sb, Hg–In, Hg–Na, In–Sb, Sb–Te. Note that liquid semiconducting alloys were not included, for a reason discussed there. If the interpretation of R_q offered in Ott et al. (1989) due to compound forming tendency is correct, it may constitute a rather strong support for using eq.(1) in metallic alloys with bonding, because this analysis is based on the dynamics of the bonds, a property which is often more sensitive to the modelling than e.g. the structure. – Note, however, that there are also liquid alloy systems with bonding effects, where these effects are better described within the nearly free electron model, see Paulick at al. (1990).

Even though a proof of the bimodal distribution of states implied by eq.(1) is to our knowledge lacking at present, one may tentatively proceed one more step: Assuming the concept of bonds in a liquid alloy to be useful, can they be classified as to their metallic, covalent or ionic character? This question has been addressed in a general fashion by Robertson (1983a) and for specific cases e.g. by Gay et al. (1982), Tsuchiya et al. (1982), Fischer and Güntherodt (1977). Brinkmann et al. (1985) have analyzed quadrupolar nuclear spin relaxation as measured on an inert gas atom (Xe) in liquid metal–tellurium alloys; they ascribe the main contribution to electric field fluctuations seen on the Xe nucleus to effective ionic charges on the neighbour atoms and from that infer an amount of charge transfer metal–tellurium which defines in turn the ionic character of the bonds. Thus they arrive at a covalent–ionic scale for liquid metal–Te alloys. In this work, Tl–Te was taken as the reference point for a strongly ionic case from Gay et al. (1982). The latter assumption is in full agreement with a model calculation by Robertson (1983b) who finds liquid Tl_2Te to be 89% ionic. Similarly, the occurence of charged states is important in liquid Se–Te alloys (Cutler et al. 1990), and in fact a considerable increase of R_q for Xe had been observed in liquid Se–Te (Maxim). In fig.3 we show the placement of liquid Te–alloys in a bond– character chart (from Brinkmann et al. 1985).

In order to explain the strong differences in magnetic susceptibility between crystalline semiconductors, Chadi and White (1975) have used the concept of bond character. This reasoning can be applied to liquid semiconducting metal–tellurium alloys; for a description in terms of the (assumed) aggregates, their probability of occurence (from thermodynamics) and their bond character see Ott et al. (1990b). The observed magnetic susceptibility then leads again to an estimate of the bond character for each alloy (Ott et al. 1990b). The agreement with the bond character chart fig.3 is rather satisfactory.

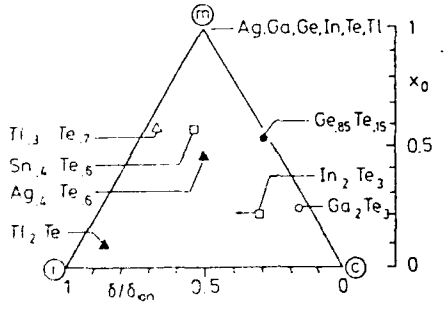

Fig 3: Bond character chart for liquid metal–tellurium alloys from Brinkmann et al. (1985). Metallic character is derived from the electrical conductivity. Ionic character is derived from R_q, i.e. from electric field fluctuations, observed at nuclei of Xe impurity atoms embedded in the liquid alloys.

Acknowledgements
This work is supported by Bundesministerium für Forschung und Technologie.

References

Abragam, A. (1978): The Principles of Nuclear Magnetism, Oxford University Press, Oxford
Bhatia, A.B. and Hargrove, W.H. (1974): Phys. Rev. B10, 3186
Blachnik, R., Gather, B. (1983): J. Chem. Therm. 15, 401
Brebrick, R.F., Ching–Hua Su, and Pok–Kai Liao (1983): Semiconductors and Semimetals, 19, 171
Brinkmann, R., Paulick, C.A., Elwenspoek, M., v. Hartrott, M., Kiehl, M., Maxim, P , Quitmann, D. (1985): Physics Letters, Vol. 111A; No.8,9 435
Carter, G.C., Bennett, L.H., Kahan, D.J. (1977): Metallic Shifts in NMR, Progr. Mat. Sci., Pergamon Press
Chadi, B.J., White, R.M., Harrison, W.A. (1975): Phys. Rev. Lett. 35, 1372
Chieux, P and Ruppersberg, H. (1980): J. de Phys. 41, C8–145
Cutler, M. (1977): Liquid Semiconductors, Academic Press, New York
Cutler, M., Kao, S.S., Silva, L.A. (1990): Phys. Rev. B, 41, 3339
Dupree, R., Kirby, D.J., and Freyland, W. (1982): Phil. Mag., B46, 595
Dupree, R., Kirby, D.J., and Freyland, W., and Warren, W.W. (1980): J. de Phys. 41, C8–16
Elliott, S.R. (1990): Physics of Amorphous Materials, Longman Scientific and Technical, Essex
Fischer, M., Güntherodt, H.J. (1977): Intern. Conf. on Amorphous on Liquid Semiconductors, Edinburgh, 889
Franz, J.R., Brouers, F., and Holzhey, C. (1980): J. Phys. F, 10, 235
Gay, M. Enderby, J.C., Copestake, A.P. (1982): J. Phys. C15, 4641
Geertsma, W. (1982): ed. in Lecture Notes in Physics 172, Springer, p. 111
Glazov, V.M., Chizhevskaja, S.N., Glagoleva, N.N. (1969): Liquid Semiconductors, Plenum Press, New York
Guggenheim, E.A. (1952): Mixtures, Clarendon Press, Oxford
Hultgren, R., Orr, R.L., Anderson, P.D., Kelley, K.K. (1973): Selected Values of Thermodynamic Properties of Metals and Alloys, Wiley, New York
Maxim, P: private communication
Mott, N. (1987): Conduction in Non–Crystalline Materials, Clarendon Press, Oxford
Ott, K., Haghani, M.A., Paulick, C.A., and Quitmann, D. (1989): Progress in NMR Spectroscopy, 21, 203
Ott, K., Dürrwächter, M., Haghani, M.A., v. Hartrott, M., Sauer, B., Quitmann, D. (1989a): J. of Non–Crystalline Solids, 114, 828
Ott, K., Dürrwächter, M., Haghani, M.A., Sauer, B. Quitmann, D. (1989b): Europhysics Letters, 10, 757
Ott, K., Dürrwächter, M., Haghani, M.A., Quitmann, D. (1990a): J. of Non–Crystalline Solids, 117/118, 646
Ott, K., Dürrwächter, M., Haghani, M.A., Quitmann, D. (1990b): to be published
Paulick, C.A., Rubinstein, M., Gasser, J.G., Senel, I. and Quitmann, D., contribution to this conference
Robertson, J. (1983a): Adv. Phys. 32, 362
Robertson, J. (1983b): Phil. Mag. B, Vol. 47, L1–L3
Sommer, F. (1982): Z. Metallkunde 73; 72, 77
Terzieff, P., Komarek, K.L., Wachtel, E. (1986): J. Phys. F, 16, 1071
Tschuchiya, Y., Takeda, S., Tamaki, S., Seymour, E.F.W. (1982): Sol. State Phys. 15, 6497
Warren, W.W. (1971): Phys. Rev. B3, 3708
Warren, W.W. (1973): Proc. Prop. Liq. Met. Taylor and Francis, London, p. 395
Warren, W.W. (1977): Inst. Phys. Conf. Ser., No 30, 436

LIQUID ALLOYS WITH STRONG INTERACTIONS

Marie-Louise Saboungi, D. L. Price, G. K. Johnson, and H. T. J. Reijers[†]

Argonne National Laboratory, 9700 South Cass Avenue, Argonne, IL 60439 U.S.A.

[†]On leave from Solid State Physics Laboratory, University of Groningen, Groningen, The Netherlands.

Abstract. -

Liquid alkali metals alloyed with either Pb or Sn show remarkable features in the electronic, thermodynamic, and structural properties at the "octet" composition and/or the equiatomic composition. A review of these properties will be presented, with special emphasis on the complementarity of information obtained from different experimental results. Recent molecular dynamics simulations of the structure and dynamics of the equiatomic alloys reveal interesting insights into the atomic structure and explain results obtained from inelastic neutron scattering.

1. - Introduction. -

In a recent review, Saboungi *et al.* (1990) have discussed ordering in liquid alloys with a special emphasis on experimental methods of characterizing the nature and extent of such ordering. Indeed, liquid alloys display a rich variety of atomic and electronic structures. At one extreme are alloys with chemically similar constituents, which undergo relatively small changes on mixing; in these cases, the local structure is not too different from that of the pure elements, and the changes in transport and thermodynamic properties can be described in terms of small deviations from ideal behavior. When the constituents are chemically dissimilar, e.g., as characterized by electronegativity, charge transfer becomes possible and the structure and properties of the alloys display features analogous to those observed in molten salts. In the extreme case when the chemical interactions become especially strong, complex ionic species can be formed on alloying, characterized by remarkable geometric arrangements of the atoms, dramatic changes in the electrical behavior, and large anomalies in the temperature dependence of the thermodynamic functions, such as specific heat.

Equiatomic liquid alloys of the form AM, where A is an alkali metal and M a Group-IV element, such as Pb, Sn, Ge, or Si, provide fascinating examples of the extreme behavior associated with strong interactions and complex ion formation. Extensive work on these alloys has been carried out with electrical transport measurements, calorimetry, neutron diffraction, inelastic neutron scattering, and computer simulation. The remarkable properties observed in each case can be ascribed to the formation of complex ions M_4^{4-} first proposed by Zintl. In this picture, the M atoms acquire a fifth valence electron from the alkali metal and form tetrahedral complexes with threefold coordination according to the (8-N) rule.

In what follows, we will review experimental results, along with molecular dynamics simulations.

2. - Experiments. -

A battery of experimental techniques have been used to define the physicochemical properties of these systems. The electrical conductivity apparatus has been described in detail by van der Marel *et al.* (1980), Meijer (1988), and Calaway and Saboungi (1983). The thermodynamic properties have been derived from a combination of electromotive force (emf) measurements and calorimetry. In the emf setup, both liquid electrolytes, such as LiCl-KCl or LiCl-LiF eutectics, and solid electrolytes, such as Na, K, or Rb-substituted β-Al_2O_3, have been used. In the latter case, a coulometric titration technique was followed to oxidize or reduce the alkali metal at the reference and working electrodes. High-temperature drop calorimetry was used to confirm the anomalously large values of the heat capacities derived from emf measurements. This

technique, which was proven (Fredrickson *et al.*, 1966) to yield data of extremely high quality, was used to measure the melting points, related thermodynamic functions, and temperature dependence of the heat capacity. Finally, the static and dynamic structure was measured using pulsed neutrons at the Intense Pulsed Neutron Source at Argonne National Laboratory. To complement these measurements and fully exploit the data, molecular dynamics simulations of equiatomic liquid alkali-lead alloys were carried out to calculate the structure and atomic motions.

3. Results. -

3.1 Electrical Transport Properties. -

The electrical conductivity of the alkali-Pb alloys and its temperature dependence have been measured as a function of composition by Meijer *et al.* (1985, 1988, 1989), Nguyen and Enderby (1977), and Calaway and Saboungi (1983); the results for the electrical resistivity ρ and the derivative ($d\rho/dT$) are shown in Fig. 1. In the case of Li-Pb and Na-Pb, a peak in ρ and $d\rho/dT$ is observed at the "octet" composition, A_4Pb, which corresponds to a charge transfer of one electron from each of the alkali atoms to a Pb atom, leading to a closed shell configuration on both ions, as in a molten salt. In the case of Na-Pb, an additional feature, a shoulder at the equiatomic composition appears, which becomes the main peak for KPb, RbPb, and CsPb. The electrical conductivity for these two latter alloys (not shown in Fig. 1) reaches a maximum value of 2200 ± 100 and 7000 ± 200 $\mu\Omega$cm, with $d\rho/dT = -18$ and -115 $\mu\Omega$cm K^{-1}, respectively, which are characteristic of liquid semiconductors according to Mott and Davis' (1979) classification of liquid alloys. Geertsma *et al.* (1984) have interpreted the behavior of the alkali-lead alloys by suggesting the formation of Zintl ions (Busmann, 1961) for which charge transport takes place within the ions rather than through the metal as a whole. Each Zintl ion is formed by a Pb tetrahedron surrounded by an alkali-metal tetrahedron oriented in the opposite direction.

3.2. - Thermodynamic Properties. -

As mentioned earlier, both emf measurements and calorimetry have been used to derive, as accurately as possible, the thermodynamic properties of these liquid alloys. Perhaps the most illustrative function is the excess stability, ES, advanced first by Darken to characterize ordering in solutions, $ES = (d^2\ \Delta G^E_m/dX_i^2) = \frac{RT}{1-X_i}(\sigma\ \ln\gamma_i/\gamma X_i)$, where γ_i and X_i are the activity coefficient and atomic fraction, respectively. Figure 2 shows the excess stability as a function of composition for four alloys A-Pb with A = Li, Na, K, and Rb (Saboungi *et al*, 1985, 1986; Tumidajski *et al.*, 1990). The behavior of ES parallels that of the electrical resistivity; however, the shoulder observed in NaPb becomes more prominent in the ES function. Note that no data are available for Cs-Pb, due mostly to experimental difficulties; the unavailability of either a solid electrolyte, such as Cs-substituted β-alumina, the fact that Cs and its alloys have a high solubility in the cesium halides (Bredig, 1964), and a high vapor pressure render the thermodynamic investigation of such a system by emf measurement techniques almost impossible. The high accuracy of the measurements shown in Fig. 2 stems from the fact that (i) the coulometric titration technique was used, and (ii) the cells were operated at constant temperature.

When the composition of the alloy was kept constant and the temperature cycled randomly, entropies ΔS_m and excess entropies ΔS^E_m were derived. Figure 3 gives the variations of these functions with composition for K-Pb and Rb-Pb. Two remarks are in order. First, the negative values taken by ΔS_m are unusual for metallic alloys, but more common for ionic systems (Blander, 1964); second, the V-like shape of ΔS^E_m and the cusp-like shape of ΔS_m are typical of ordered solutions. So far, the conclusions reached from these thermodynamic measurements are in full agreement with those deduced from the electrical transport measurements, showing the presence of ordering in these alloys.

At an average temperature, the excess heat capacity ΔCp was evaluated and is shown in Fig. 4 for K-Pb and Rb-Pb. The dramatic increase of ΔCp around the equiatomic alloy has been observed for the first time in an alloy. An interpretation of this unusual composition dependence of ΔCp was advanced, based on the dissociation of structural entities. The magnitude of the heat capacity at the equiatomic composition and its

temperature dependence have been confirmed by independent calorimetric measurements (Johnson and Saboungi, 1987; Saboungi *et al.*, 1988a). Figure 5 shows the heat capacities for the four liquid alloys. Both the large values of C_p and its rapid decrease with temperature above the melting point give strong support to the formation of structural entities in the liquid. A quantitative model prepared by Geertsma (private communication), based on the reactions

$$M_4^{4-} \rightleftarrows 4M^-$$

$$M_4^{4-} \rightleftarrows 4M + 4e^-,$$

make it possible to explain the curves of ΔCp versus temperature and estimate the fractions of dissociated tetrahedra as a function of temperature. The results are similar to those of the phenomenological model proposed by Saboungi *et al.*

3.3. - Neutron Diffraction Results. -

The existence of complex ions, e.g., polyvalently charged anions, has been demonstrated on the atomic scale by several neutron diffraction experiments. Figure 6 shows the measured total structure factor S(Q) for the alkali-metal-lead alloys. The pronounced first sharp diffraction peak at low scattering vector ($Q \sim 1$ A^{-1}) is indicative of relatively long-range order associated with the formation of structural units. The results of model calculations, based on units consisting of a Pb_4^{4-} Zintl ion with a larger compensating tetrahedron of 4 A^+ ions and arranged according to the structure found in the crystalline phase, are shown by continuous solid and dashed lines in Fig. 6 and seen to give an excellent representation of the data. The height of the first peak measured as a function of temperature in KPb falls with increasing temperature, consistent with the dissociation of the Zintl ions deduced from the emf and calorimetric measurements (Saboungi, 1987; Fig. 7). Finally, measurements of S(Q) for various K-Pb composition by Reijers *et al.* (1989) show that the first sharp peak decays with departure from the 50:50 composition, giving support to the concept of ordering in solution as evidenced from the variations of ES and ΔCp with composition. A powerful method for distinguishing between these different kinds of ordering is provided by the structure factors measured by neutron or x-ray diffraction, where the value of the scattering vector of the first peak in the structure factor scaled by the nearest-neighbor distance and the mean atomic spacing falls into a certain range characteristic of the type of ordering involved (Price *et al.*, 1989, Saboungi *et al.*, 1990, Fig. 8).

It should be mentioned that inelastic neutron scattering measurements, coupled with calculations of atomic motions by molecular dynamics simulations, have been performed recently. The results, which are beyond the scope of this review, are reported in Toukan *et al.* (1990).

3.4 - Molecular Dynamics Simulations. -

A wealth of information on the atomic distribution of any binary alloy system can be derived from a knowledge of the partial functions, e.g., the three partial structure functions and their corresponding radial distribution functions in real space. Since isotopically substituted samples are not readily available for these systems, molecular dynamics simulation of the structure was carried out by Reijers *et al.* (1990). The system consisted of alkali atoms and Pb_4^{4-} Zintl ions, interacting according to a simplified Tosi-Fumi potential (Tosi and Fumi, 1964). The lead atoms were taken to exist as preformed tetrahedral units with the Pb atoms held together by harmonic springs. For further details, the reader is referred to the works of Reijers *et al.* (1990) and Saboungi *et al.* (1988b). The partial structure factors show that the Pb-Pb system contributes most to the FSDP with minor contributions from the A-Pb system. The structure of NaPb could not be reproduced unless a significant amount of dissociation of the Pb_4^{4-} ions was assumed. Finally, triplet angular correlations of the A, Pb, and CM (CM being the center of mass of the Pb_4^{4-} tetrahedron) were calculated; the results confirm the tendency for A^+ atoms to lie opposite the faces of the Pb_4^{4-} tetrahedra in a fashion similar to that observed in the crystalline phase.

4. - Conclusion. -

In this review, we have summarized the physicochemical properties of a special class of liquid alloys. The behavior of the liquid alkali-metal-lead alloys is mimicked to a great extent by liquid alkali-metal-tin alloys, where it was shown that the Sn_4^{4-} ions form and are even more chemically

stable than the $PbTe_4^{4-}$ ions. The systems formed by the alkali-metal-Si and -Ge alloys are presently under investigation and the stability of the Si_4^{4-} and Ge_4^{4-} ions are expected to be enhanced. It is hoped that measurements of the lifetime and dynamics of polyanions could be performed by a diversity of techniques such as Raman spectroscopy, NMR, inelastic, and elastic diffraction. An improvement of the anomalous x-ray diffraction technique (Ludwig *et al.*, 1987) is badly needed for handling liquids. Many questions still remain unanswered, especially dealing with the CsPb and CsSn systems, where the FSDP is abnormally narrow, signaling a long range for the atomic correlations. Quasi-elastic measurements are being performed to study transitions in the systems occurring prior to melting. Similarly, the study of subcooled NaPb or NaSn should help in understanding these systems, which appear to be intermediate between the Li and the K, Rb, and Cs alloys.

Acknowledgments. -

This work is supported by the U.S. Department of Energy, Division of Materials Sciences, Office of Basic Energy Sciences, under Contract No. W-31-109-ENG-38.

References. -

Blander, M. (1964): *Molten Salt Chemistry* (Wiley, Interscience, New York).

Bredig, M. A. (1964): *Molten Salt Chemistry*, ed. M. Blander (Wiley, Interscience, New York).

Busmann, E. (1961): Z. Anorg. (Allg.) Chem. 313, 90.

Calaway, W. F. and Saboungi, M.-L. (1983): J. Phys. F: Metal Phys. 13, 1213.

Fredrickson, D. R., Barnes, R. D., Chasanov, M. G., Nutall, R. L., Kleb, R., and Hubbard, W. N. (1969): High Temp. Science 1, 373.

Geertsma, W., Dijkstra, J., and van der Lugt, W. (1984): J. Phys. F: Metal Phys. 14, 1833.

Johnson, G. K. and Saboungi, M.-L. (1987): J. Chem. Phys. 87, 6376.

Ludwig, K. F., Jr., Warburton, W. K., Wilson, L., and Bienenstock, A. I. (1987): J. Chem. Phys. 87, 604.

Marsh, R. E. and Shoemaker, D. P. (1953): Acta Crystallogr. 6, 197.

Meijer, J. A., Geertsma, W., and van der Lugt, W. (1985): J. Phys. F: Metal Physics 15, 899.

Meijer, J. A. (1988): Ph.D. thesis, University of Groningen, The Netherlands.

Meijer, J. A. and van der Lugt, W. (1989): J. Phys.: Condens. Matter 1, 9779.

Moss, S. C. and Price, D. L. (1987): in *Physics of Disordered Materials*, eds. D. Adler, H. Fritzsche, and S. R. Ovshinsky (Plenum, New York) p 77.

Mott, N. F. and Davis, E. A. (1979): *Electronic Processes in Non-Crystalline Materials* (Clarendon Press, Oxford).

Nguyen, V. T. and Enderby J. E. (1977): Phil. Mag. 35, 1013.

Price, D. L., Moss, S. C., Reijers, R., Saboungi, M.-L., and Susman, S. (1989): J. Phys.: Condens. Matter 1, 1005.

Reijers, H. T. J., van der Lugt, W., van Dijk, C., and Saboungi, M.-L. (1989a): J. Phys.: Condens. Matter 1, 5229.

Reijers, H. T. J., Saboungi, M.-L. Price, D. L., Richardson, J. W., Jr., Volin, K. J., and van der Lugt, W. (1989b): Phys. Rev. B 40, 6018.

Reijers, H. T. J., Saboungi, M.-L., Price, D. L., and van der Lugt, W. (1989c): Phys. Rev. B 41(9), 5661.

Reijers, H. T. J., van der Lugt, W., and Saboungi, M.-L. (1990): accepted for publication Phys. Rev. B.

Reijers, H. T. J (1990): Formation of Polyanions in Liquid Alloys, Ph.D. Thesis, University of Groningen, The Netherlands.

Saar, J. and Ruppersberg, H. (1988): Z. Phys. Chem. Neue Folge (LAM VI Proc.) 156, 587.

Saboungi, M.-L., Herron, S. J., and Kumar, R. (1985): Ber. Bunsenges. Phys. Chem. 89, 375.

Saboungi, M.-L., Leonard, S. R., and Ellefson, J. (1986): J. Chem. Phys. 85, 6072.

Saboungi, M.-L., Blomquist, R., Volin, K. J., and Price, D. L. (1987): J. Chem. Phys. 87, 2278.

Saboungi. M.-L., Reijers, H. T. J., Blander, M., and Johnson G. K. (1988a): J. Chem. Phys. 89, 5869.

Saboungi, M.-L., Rahman, A., Halley, J. W., and Blander, M. (1988b): J. Chem. Phys. 88, 5818.

Saboungi, M.-L., Geertsma, W., and Price, D. L. (1990): Ann. Rev. Phys. Chem. 40, 207.

Tosi, M. P. and Fumi, F. G. (1964): J. Phys. Chem. Solids 25, 31 and 45.

Toukan, K., Reijers, H. T. J., Price, D. L., and Saboungi, M.-L. (1990): Phys. Rev. B 41, 11739.

Tumidajski, P. J., Petric, A., Takenaka, T., Saboungi, M.-L., and Pelton, A. D. (1990): J. Phys.: Condens. Matter 2, 209.

van der Lugt, W. and Geertsma, W. (1987): Can. J. Phys. 65, 326.

van der Marel, C., Geertsma, W., and van der Lugt, W. (1980): J. Phys. F: Metal Phys. 10, 2305.

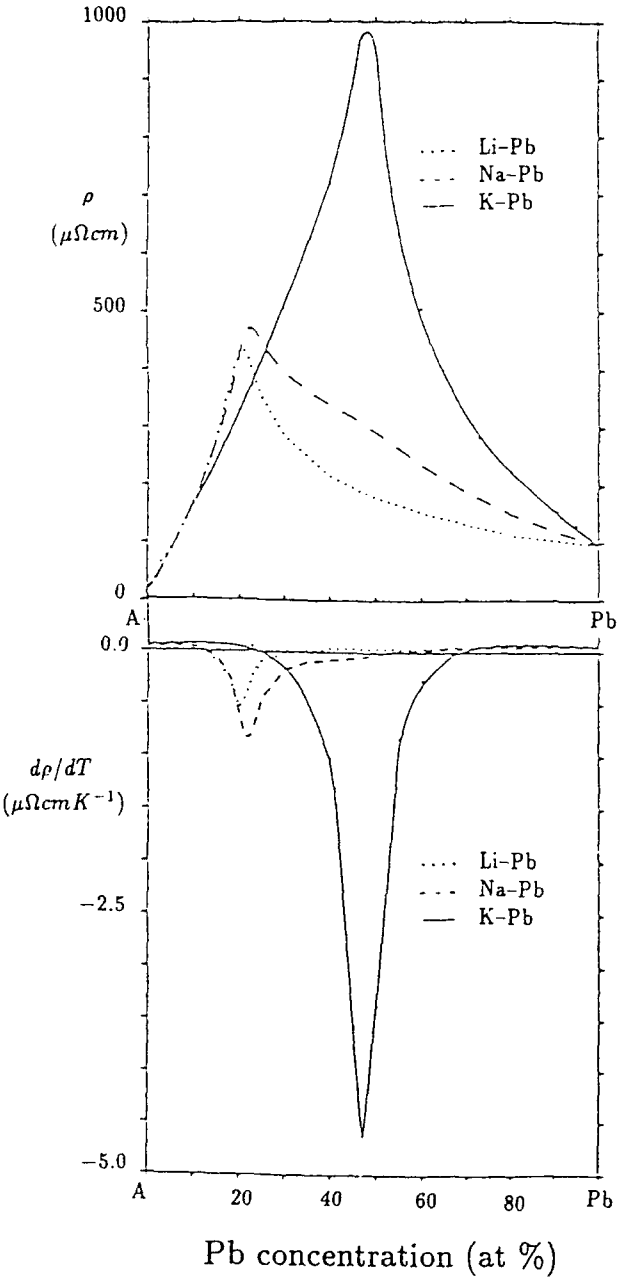

Fig. 1. Electrical resistivity and its temperature dependence in alkali-metal lead alloys as a function of composition (Meijer *et al.*, 1985).

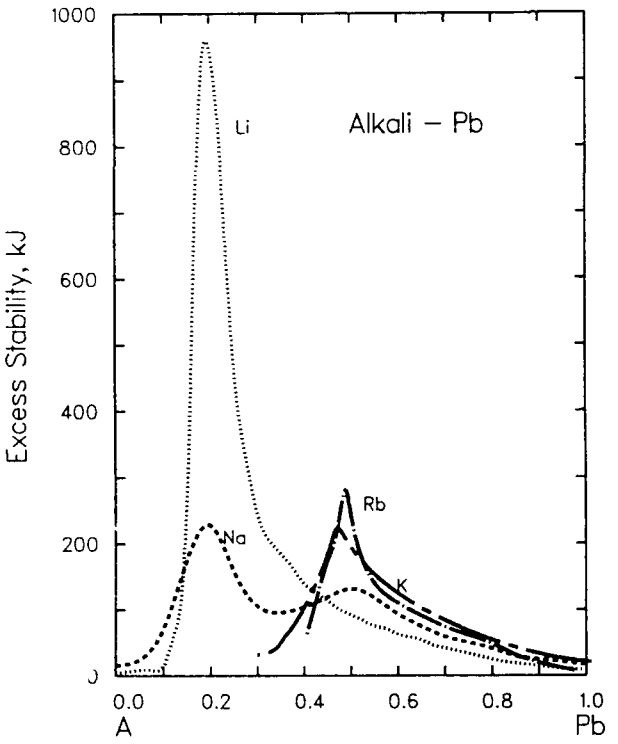

Fig. 2. Darken excess stability for A-Pb alloys from emf measurements (Tumidajski *et al.*, 1990).

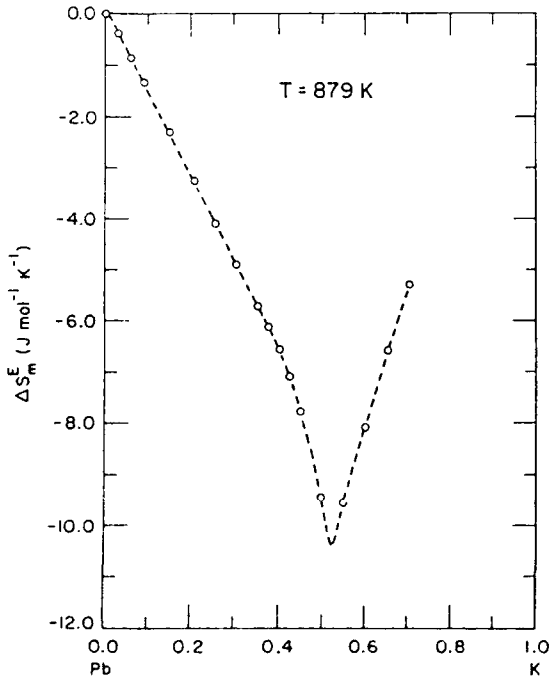

Fig. 3. Variations of the excess entropy of mixing for liquid K-Pb alloys (Saboungi *et al.*, 1986).

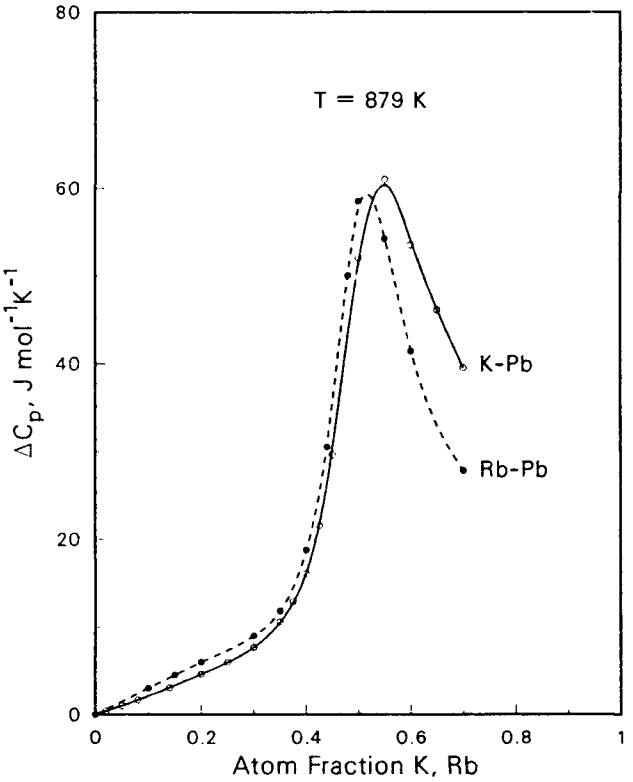

Fig. 4. Heat capacity of alkali-metal lead alloys as a function of composition (Tumidajski *et al.*, 1990).

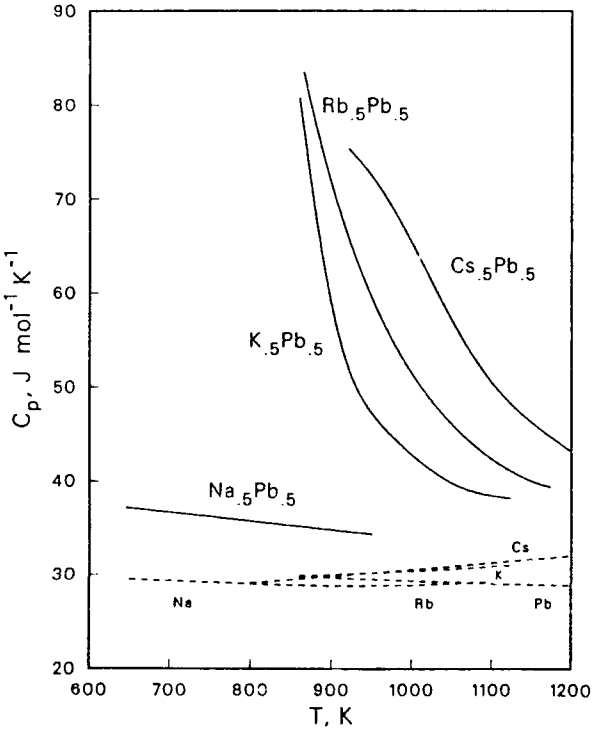

Fig. 5. Heat capacity of alkali-metal lead alloys as a function of temperature (Saboungi *et al.*, 1988a).

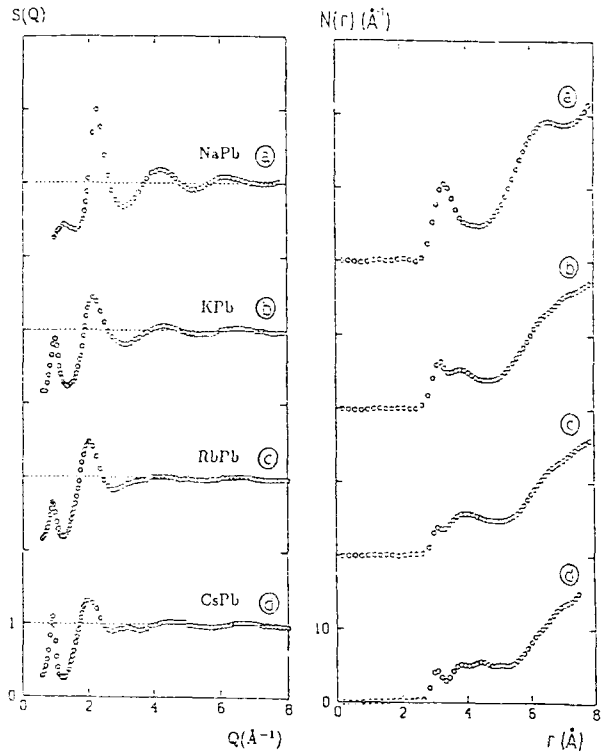

Fig. 6. Measured total structure factors for APb alloys (Reijers *et al.*, 1989b).

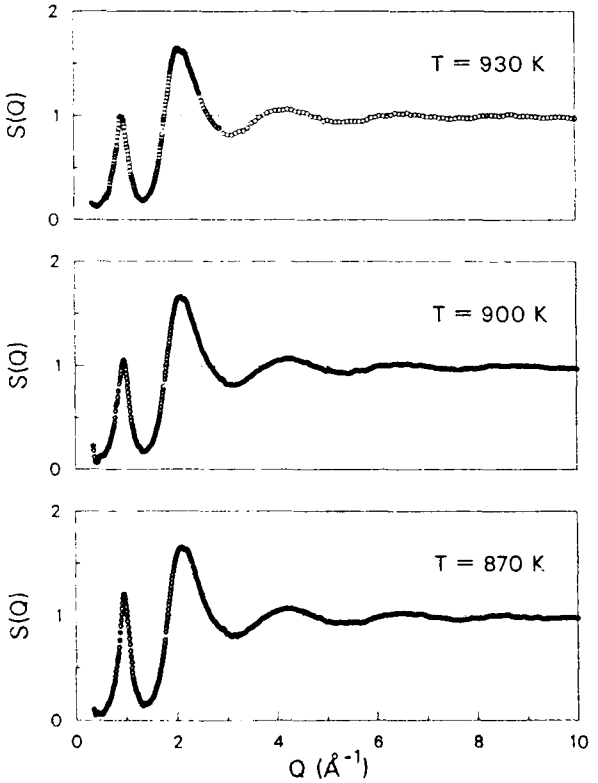

Fig. 7. Variations of the structure factor S(Q) of liquid KPb with temperature (Saboungi *et al.*, 1987).

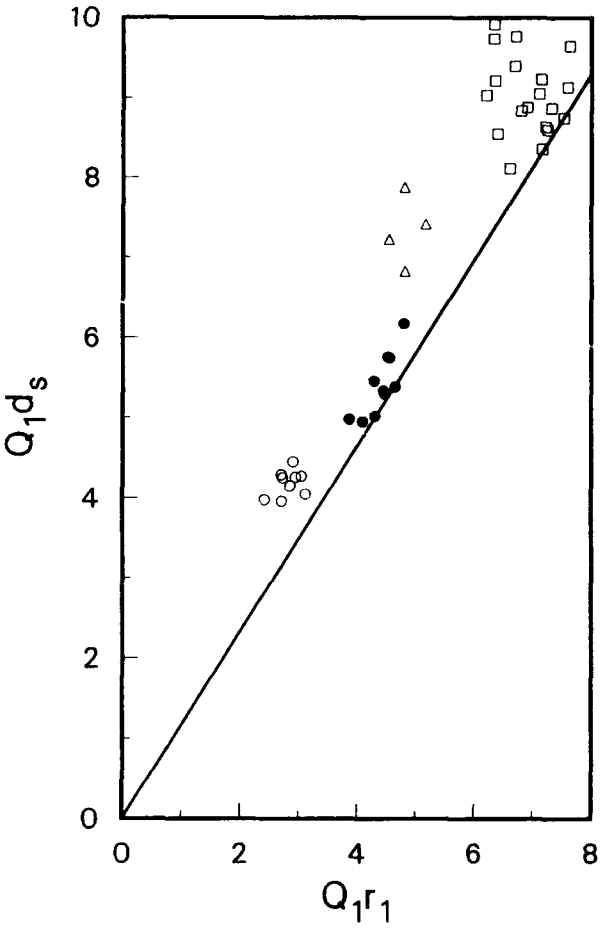

Fig. 8. Wave vectors Q_1 of first peaks in the structure factors of several liquid metals and alloys, scaled by the nearest-neighbor distance r_1 and the mean atomic spacing $d_s = (6/\pi\rho)^{1/3}$: first sharp diffraction peaks (o), prepeaks (•), peaks in network-forming liquids (△) and hard-sphere peaks (□) (Saboungi *et al.*, 1990).

SOLUTE-SOLVENT DROP CALORIMETRY OF TRANSITION METAL INTERMETALLIC COMPOUNDS

O.J. Kleppa† and L. Topor*

**†The James Franck Institute and The Department of Chemistry
The University of Chicago, Chicago, Illinois 60637, USA**

***Department of Geology, Princeton University
Princeton, New Jersey 08544, USA**

Abstract -

The authors have developed a new calorimetric method, "solute-solvent drop calorimetry", which has proved useful in the study of intermetallic and other refractory compounds. This method involves the dropping of small capsules which contain a solid mixture of solute and solvent from room temperature into a high-temperature calorimeter, where they generate a homogeneous liquid mixture. The "solute" is either the refractory compound or a mechanical mixture of its constituent elements. In our studies of intermetallic compounds the "solvent" was usually a mixture of platinum or palladium with germanium. The development of this method will be outlined and its application to intermetallic compounds of Group IVA metals with platinum group metals will be reviewed.

1. - Introduction

It is well known that the available information on the standard enthalpies of formation of intermetallic and related compounds leaves much to be desired. An important reason for this is that the thermochemistry of most of these compounds cannot be studied effectively by the classical methods of combustion and room-temperature solution calorimetry. In alloy thermodynamics high-temperature liquid metal solution calorimetry has to some extent improved this picture. However, this approach, which has been very useful for non-refractory alloy phases, has had little impact in the area of transition metal intermetallics. For such compounds most of the reported thermochemical information has been obtained either calorimetrically by direct synthesis from the elements or has been derived indirectly from high temperature e.m.f. or vapor pressure measurements.

In direct synthesis calorimetry one usually first prepares a compressed pellet of the desired composition from powders of the two elements. This pellet is brought to chemical reaction by raising its temperature so that a reaction is initiated; the heat effect is then measured calorimetrically. Such measurements may be carried out either at or near room temperature by heating the sample in a furnace which is completely enclosed in a calorimeter (see e.g. Capelli *et al.* (1974)) or by dropping the pellet from a lower temperature (often 298K) into a high-temperature calorimeter (see e.g., Gachon and Hertz (1983)). In either case, unless the reaction product is a congruent melting compound, which is melted in the course of the experiment, there are often questions regarding the completeness of the reaction and hence about the significance of the results. It is for this reason that Gachon and Hertz, in their early work on intermetallic compounds, characterized some of their values as "indicative".

Our research group in Chicago has a long-standing interest in the thermodynamics of refractory meterials and intermetallic compounds. About 10 years ago we initiated a research program in the thermochemistry of refractory borides based on solution calorimetry in a liquid copper solvent. In this way we succeeded in measuring the enthalpies of formation of a number of late transition metal borides with good precision and accuracy (Kleppa and Sato, 1982; Sato and Kleppa, 1982). However, when we attempted to extend such measurements to borides of some of the early transition metals, we did not succeed. Among the borides of interest was LaB_6, a well-known electron emitter which is frequently used in high current density cathodes. Unfortunately, this compound did not dissolve in liquid copper at 1400 K or in any of the other liquid alloys that we had tried using regular solution calorimetry. Furthermore, since LaB_6 is very refractory and has a melting point near 3000 K, this compound was not a good candidate for direct synthesis calorimetry at our operating temperature of 1400 K.

In 1983, while we were working with LaB_6 in our Calvet-type high temperature calorimeter near 1400 K, we discovered by accident that at this temperature LaB_6 readily forms a liquid alloy with platinum. This suggested to us a possible new approach to the thermochemistry of refractory borides. We proceeded to use this approach to measure the standard enthalpies of formation of LaB_6 (Topor and Kleppa, 1984) and of several other refractory borides (Topor and Kleppa, 1985 a,b; 1986 a).

The physical basis of this new method, "solute-solvent drop calorimetry", is very simple. It rests on the fact that the binary system boron plus platinum has an extensive liquid range near 1400 K, and that these liquid alloys may act as solvents for many refractory metals. In each experiment these "solvents" are generated in the high temperature calorimeter by dropping the components in from room temperature. The "solute" consists of the refractory compound which is being studied or of a mechanical mixture of the two elements. While this method originally was developed for refractory borides, it has also been used for silicides (Topor and Kleppa, 1986 b; 1987 a; 1988 d; 1989 b) and most recently for intermetallic compounds (Topor and Kleppa, 1986 c; 1987 b,c; 1988 a,b,c,e). For silicides our solvent usually has been an alloy of platinum or palladium with silicon, while for intermetallic compounds we now prefer platinum, palladium or nickel with germanium. There is a distinct advantage in the fact that pure germanium is liquid at our calorimetric temperature of 1400 to 1500 K.

2. - Experimental

2.1 - Calvet-Type calorimeter

Our early measurements of transition metal borides were all carried out in our Calvet-type twin calorimeter near 1400 K. This unit, which was constructed some 15 years ago has been used nearly continuously since that time. The crucial calorimetric jacket is constructed from a number of 2.5 cm thick alumina discs, each about 19 cm in diameter, which together generate two cylindrical wells which house two nearly identical Calvet-type calorimeters. The two calorimeters each has a thermopile built from 64 Pt-Pt13%Rh thermocouples; these measure the temperature difference between the calorimeter proper and the surrounding alumina jacket. The whole cylindrical unit is completely enclosed in a furnace with three independently controlled heaters: top, bottom and main heater; all heaters are constructed from Pt 40% Rh wire.

The two thermopiles are connected in series, but bucked against each other. Therefore a minor change in the overall temperature of the alumina jacket should influence the two twin calorimeters in the same way, but with the opposite sign. Hence theory indicates that minor temperature disturbances of the calorimeter jacket should give rise to little drift in the overall calorimeter system. This is the theory. For Calvet-type twin calorimeters operating at room temperature, or at moderately elevated temperatures, with jackets constructed from high thermal conductivity metals such as copper, silver or aluminum, this condition is frequently realized. However, our jacket is constructed from sintered alumina; hence the ideal conditions assumed in theory are not realized. Furthermore, "at high temperature everything reacts with everything else and they also become electrically conducting". In fact, our twin alumina calorimeter, when operated at high sensitivity at 1400 K frequently would not have adequate base-line stability to yield the desired precision and accuracy. This prompted us to develop a new high-temperature calorimeter specifically intended for use in solute-solvent drop calorimetry.

2.2 - Setaram-type calorimeter

At the present time it is possible to purchase, at very considerable cost, a differential high temperature integrated heat flux calorimeter which allows calorimetric measurements at temperatures up to about 1800 K. This calorimeter is produced by Setaram in France, and has been available commercially for many years. In this unit the thermal effects are measured differentially along the axis of the cylindrical calorimeter, rather than radially as in the Calvet-type apparatus. The 'working' junctions of the differential thermopile surround the crucible in which the reaction takes place, while the 'reference' junctions are maintained in a constant temperature environment some distance removed from the crucible. Unfortunately, most investigators who have used this equipment have complained about difficulties associated with precise calibration, and the number of scientific publications which have resulted from its use is small. The reasons for this are now fairly well understood: the construction of the differential thermopile in the Setaram calorimeter does not satisfactorily integrate the heat flux over the surface of the crucible in which the reaction is carried out. The calibration factor of the calorimeter therefore depends critically on the amount of material contained in the crucible. Investigators active in this area have recognized this, and have made modifications to the Setaram design. We are familiar with at least two French groups which have addressed these problems (Hatem *et al.* 1981; Gachon and Hertz, 1983). However, even in these modified versions of the Setaram calorimeter there is still poor thermal coupling between the crucible in which the reaction takes place, and the thermopile.

During the past three years we have experimented with a new high temperature calorimeter which represents a modification of the improved versions of the Setaram design. This new calorimeter has been used extensively in our work on intermetallic compounds. The apparatus was described in some detail in a publication which appeared last year (Kleppa and Topor, 1989 a). We will limit ourselves here to describe its principal features. The "heart" of the new calorimeter is shown in Fig. 1 which gives an overall view of the "working section" and the "reference section" of the unit. The calorimeter is constructed from a tube of recrystallized alumina, about 29 mm O.D., 23 mm I.D. and 76 cm long, one end closed. On the outside surface of this tube have been ground 40 shallow vertical grooves to allow the placement of a 20 couple thermopile shown schematically in Fig. 1 (only half the junctions are shown).

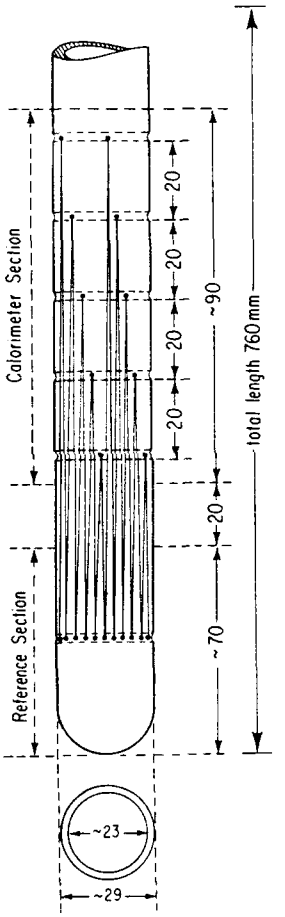

Fig. 1. Schematic view of calorimeter section ('working section') and 'reference section' of the new calorimeter.

Twenty thermocouple junctions are distributed over the 'working section' of the calorimeter, located at five different levels, about 20 mm apart. The other 20 junctions are placed at the same level near the closed end of the calorimeter tube, forming the 'reference section'. The couples were made from 0.5 mm diameter Pt-Pt 13% Rh wire, purchased from Engelhard, and were cemented into the grooves with morganite cement. Two long platinum wires, cemented into two parallel grooves in the alumina tube, carry the differential e.m.f. to a constant temperature Dewar. Here junctions are made to copper wires connected to the amplifier. The output of the amplifier is fed in parallel circuits to the recorder, and through a voltage-to-frequency converter to an Apple IIe computer.

All calorimetric experiments are performed inside a special calorimeter 'liner' of 20 mm I.D. The lower part of this liner is constructed from Pt-20% Rh tubing about 0.5 mm wall thickness, total length about 80 cm, one end of which is closed. The upper end of the liner is connected to a thin-walled stainless steel tube, and has a standard ground joint. The lower end of the liner contains the BN crucible assembly in which experiments are carried out. Details of this arrangement are shown in Fig. 2. The actual location of the liner is adjusted so as to maximize the e.m.f. generated by the calorimeter thermopile.

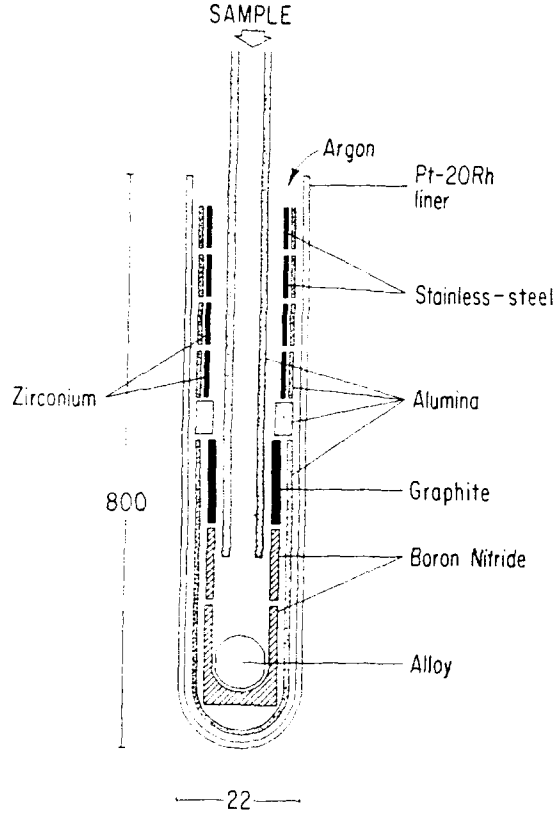

Fig. 2. Schematic diagram of the calorimetric cell assembly, showing part of the Pt-20Rh liner, the boron nitride crucible, the boron nitride protective cylinder and stirrer, and the alumina protective crucible and protective cylinders, as well as parts of the final gettering system for the argon gas.

Calibration of the calorimeter is achieved by dropping weighed pieces of 3 mm diameter pure copper wire from room temperature into the BN crucible (see Fig. 3). The calibration is based on the heat content of the copper at the operating temperatures of the calorimeter and is generally reproducible within ± 1%.

Example of application

We first used the new single unit differential calorimeter to determine the enthalpies of formation of PtMe (Topor and Kleppa, 1988 b) and IrMe (Topor and Kleppa, 1988 c) at 1473 ± 2 K (Me = Ti, Zr, Hf). The three Pt compounds had recently been studied by Gachon *et al.* (1985), who used direct reaction calorimetry. In our calorimeter we measured heat effects which ranged from 80 J to 200 J. For example, in our investigation of the intermetallic compounds PtHf, the following two reactions were carried out in the calorimeter

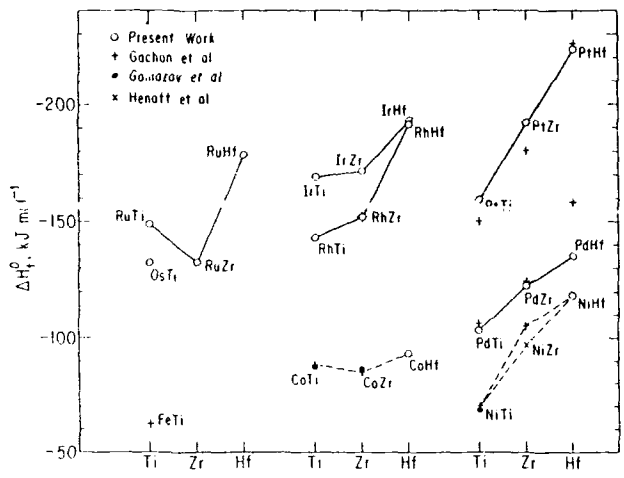

Fig. 3. Systematically based plot of standard enthalpies of formation considered in the present paper. Gachon *et al.*, 1985, 1986; Gomozov *et al.*, 1986; Henaff *et al.*, 1984.

$$0.05\ \mathrm{PtHf(s, 298)} + 0.26\ \mathrm{Pt(s, 298)} + 0.64\ \mathrm{Ge(s, 298)} = \mathrm{Hf_{0.05}Pt_{0.31}Ge_{0.64}(1, 1473)} \quad (1)$$

and

$$0.05\ \mathrm{Hf(s, 298)} + 0.31\ \mathrm{Pt(2, 298)} + 0.64\ \mathrm{Ge(s, 298)} = \mathrm{Hf_{0.05}Pt_{0.31}Ge_{0.64}(1, 1473)} \quad (2)$$

On the basis of six measurements for each of these reactions we derive the following enthalpy changes, with reference to one mole of PtHf

$$\Delta H_m(1) = 624.3 \pm 11.0\ \mathrm{kJ\ mol^{-1}}$$

$$\Delta H_m(2) = 397.0 \pm 7.3\ \mathrm{kJ\ mol^{-1}}$$

combining eqns. (1) and (2), we obtain

$$\Delta H_f^0(\mathrm{PtHf}) = \Delta H_m(2) - \Delta H_m(1) = -227.3 \pm 13.2\ \mathrm{kJ\ mol^{-1}}.$$

Note that the mean values of $\Delta H_m(1)$ and $\Delta H_m(2)$ are associated with errors (standard deviations) of about 1.8%. The corresponding uncertainty in ΔH_f^0(PfHf) obtained from $(\delta_1^2 + \delta_1^2)^{1/2}$ was 5.8%. In comparison, the corresponding value for this compound quoted by Gachon *et al.* (1985) was −226 kJ mol^{-1}. However, these authors were uncertain about the probable error in this value, which was quoted as "indicative".

3. - Results

A summary of all the experimental results obtained in the course of the present investigations is given in Table 1. For each intermetallic compound studied this table shows the composition of the liquid alloy formed in each series of measurements, the average values of ΔH_f^0 with the standard deviations calculated from measurements corresponding to eqs. (1) and (2) above, and finally the weighted mean values of ΔH_f^0 with the calculated standard deviations of the weighted mean. The last column of the table give the percent relative error indicated for each reported mean value of ΔH_f^0. It will be seen that for most compounds the relative errors are about ± 5% to ± 6%.

A systematically based graph of our experimental enthalpy values is presented in Fig. 3; this figure also shows earlier reported data taken from Gachon *et al.* (1985), from Gomozov *et al.* (1986) and from Henaff *et al. (1984).*

We first take note of the general agreement between our new results and the earlier values of Gachon *et al;* this agreement ranges from excellent for RhZr, PdTi, PdZr and PtHf, to fair for PtTi and PtZr; however, the agreement is not satisfactory for PdHf. It is also true that the agreement between Gachon *et al.* and Gomozov *et al.* for CoTi, CoZr and NiTi is very good, while that between Gachon *et al.* and Henaff *et al.* for NiZr is only fair. In conclusion, Fig. 3 shows extensive agreements among the earlier studies, and between the results of the earlier studies and our own; this strongly suggests that the enthalpy information displayed in Fig. 3 on the whole is correct. Hence the data in this figure may, with confidence, be used as the basis for a general discussion of the thermochemistry of the families of intermetallic compounds under consideration.

Acknowledgements

This work was supported by N.S.F. We are also grateful to Alcoa Foundation for an unrestricted grant.

References

Capelli, R., Ferro, R. and Borsese, A. (1974): Thermochimica Acta 10, 13.

Gachon, J.C. and Hertz, J. (1983): Calphad 7, 1.

Gachon, J.C., Charles, J. and Hertz, J. (1985): Calphad 9, 29.

Gachon, J.C., Jorda, J.L., Charles, J. and Hertz, J. (1986): Calphad 10, 217.

Gomozov, P.A., Zasipalov, Yu. V. and Mogutnov, B.M. (1986): Zh. Fiz. Khim 60, 1865.

Hatem, G., Gaune, P. and Bros, J.P. (1981): Rev. Sci. Instrum. 52, 585.

Henaff, M.P., Colinet, C., Pasturel, A. and Bushow, K.H.J. (1984): J. Appl. Phys. 56, 307.

Topor, L. and Kleppa, O.J. (1984): J. Chem. Thermodyn. 16, 993.

Topor, L. and Kleppa, O.J. (1985a): J. Chem. Thermodyn. 17, 109; (1985b): J. Chem. Thermodyn. 17, 1003.

Topor, L. and Kleppa, O.J. (1986a): High Temp. Sci. 22, 139; (1986b): Met. Trans. 17A, 1217; (1986c): Z. Metallk. 77, 633.

Topor, L. and Kleppa, O.J. (1987a): J. Chem. Thermodyn. 19, 69; (1987b): Met. Trans. 18A, 1989.

Topor, L. and Kleppa, O.J. (1988a): Met. Trans. 19A, 1061; (1988b): Met. Trans. 19A, 1827; (1988c): J. Chem. Thermodyn. 20, 1271; (1988d): Z. Metallk. 79, 623; (1988e): High Temp. Sci. 25, 163.

Kleppa, O.J. and Topor, L. (1989a): Thermochimica Acta 139, 291; (1989b): Met. Trans. 20B, 879; (1989c): J. Less-Common Metals 155, 61.

TABLE 1

Summary of Experimental Data for the Intermetallic Compounds MeTi, MeZr, MeHf (Me = Pd, Rh, Ru, Pt, Ir), OsTi, CoHf, NiHf

Compound	Melting Temp. °C	Liquid Alloy Composition	$-\Delta H_f^\circ$ kJ mol^{-1}	$-\Delta H_f^\circ$ (mean) kJ mol^{-1}	Error %
PdTi	1400	$Ti_{0.04}Pd_{0.04}Cu_{0.67}Si_{0.25}$ $Ti_{0.05}Pd_{0.05}Cu_{0.65}Si_{0.25}$	102.5±22.9 103.1±14.6	102.8±12.7	12.3
PdZr	1600	$Zr_{0.05}Pd_{0.05}Cu_{0.60}Ge_{0.30}$ $Zr_{0.05}Pd_{0.05}Cu_{0.65}Ge_{0.25}$	117.9±15.4 123.7± 7.4	122.6± 7.0	5.7
PdHf	1610(p)	$Hf_{0.05}Pd_{0.05}Cu_{0.60}Ge_{0.30}$ $Hf_{0.05}Pd_{0.05}Cu_{0.65}Ge_{0.25}$	135.3± 8.8 132.7±17.0	134.8± 7.8	5.8
RhTi	1940	$Ti_{0.05}Rh_{0.05}Cu_{0.45}Ge_{0.45}$		143.0± 9.8	6.9
RhZr	~1900	$Zr_{0.05}Rh_{0.05}Cu_{0.45}Ge_{0.45}$		151.8± 7.1	4.7
RhHf	~2290	$Hf_{0.05}Rh_{0.05}Cu_{0.45}Ge_{0.45}$ $Hf_{0.05}Rh_{0.05}Cu_{0.25}Ge_{0.65}$	190.7± 4.5 199.8±14.1	191.6± 4.3	2.2
RuTi	2130	$Ti_{0.05}Ru_{0.05}Pt_{0.26}Ge_{0.64}$ $Ti_{0.05}Ru_{0.05}Pd_{0.26}Ge_{0.64}$ $Ti_{0.07}Ru_{0.07}Pd_{0.25}Ge_{0.61}$	158.3±15.7 153.1±17.4 152.5± 9.6	153.9± 7.4	4.8
RuZr	~2100	$Zr_{0.05}Ru_{0.05}Pt_{0.26}Ge_{0.64}$ $Zr_{0.05}Ru_{0.05}Pt_{0.26}Ge_{0.64}$	139.1± 9.6 135.5± 9.5	137.3± 6.8	5.0
RuHf	~2400	$Hf_{0.05}Ru_{0.05}Pt_{0.15}Ge_{0.75}$ $Hf_{0.05}Ru_{0.05}Pd_{0.26}Ge_{0.64}$	173.3±21.6 186.6±11.8	183.5±10.4	5.7
PtTi	1830	$Ti_{0.05}Pt_{0.31}Ge_{0.64}$		159.3±12.9	8.1
PtZr	2100	$Zr_{0.05}Pt_{0.31}Ge_{0.64}$		191.9±12.4	6.5
PtHf	–	$Hf_{0.05}Pt_{0.31}Ge_{0.64}$		227.3±13.2	5.8
IrTi	2120	$Ti_{0.05}Ir_{0.05}Pd_{0.26}Ge_{0.64}$ $Ti_{0.05}Ir_{0.05}Pt_{0.20}Ge_{0.70}$	168.9±11.8 168.4± 9.8	168.6± 7.5	4.4
IrZr	2050	$Zr_{0.05}Ir_{0.05}Pd_{0.26}Ge_{0.64}$ $Zr_{0.05}Ir_{0.05}Pt_{0.20}Ge_{0.70}$	171.9± 8.8 169.3±15.6	171.3± 7.7	4.5
IrHf	2440	$Hf_{0.05}Ir_{0.05}Pt_{0.20}Ge_{0.70}$ $Hf_{0.05}Ir_{0.05}Pt_{0.30}Ge_{0.60}$	187.0±16.0 196.8±12.0	193.3± 9.6	5.0
OsTi	2160	$Ti_{0.05}Os_{0.05}Pt_{0.20}Ge_{0.70}$ $Ti_{0.05}Os_{0.05}Pt_{0.26}Ge_{0.64}$	138.8±10.7 135.3± 9.8	136.9± 7.2	5.3
CoHf	~1470	$Hf_{0.05}Co_{0.05}Pt_{0.20}Ge_{0.70}$ $Hf_{0.05}Co_{0.05}Pt_{0.26}Ge_{0.64}$	99.2± 7.6 87.1±10.3	94.9± 6.1	6.4
NiHf	1530	$Hf_{0.05}Ni_{0.05}Pt_{0.20}Ge_{0.70}$ $Hf_{0.05}Ni_{0.05}Pt_{0.24}Ge_{0.66}$	115.4± 6.9 121.5± 6.9	118.5± 4.9	4.1

Some Relations Between the Enthalpy of Mixing and Deviations from Free Electron Behaviour Observed in Liquid Ternary Cu-Ag-Ge Alloys

C.PAULICK[1], M.RUBINSTEIN[3], J.G.GASSER[2],, I.SENEL[1,4] and D.QUITMANN[1]

[1] Institut für Experimentalphysik, FU Berlin,D-1000 Berlin 33
[2] Faculté des Sciences,Université de Metz,F-57045 Metz Cédex 1
[3] Naval Research Laboratory, Code 6340, Washington D.C 20375, U.S.A.
[4] Now at Ondokuz Mayis Unversity, Samsun, Turkey

Abstract.-

N.M.R. experiments in liquid Cu-Ge and $Cu_{50}Ag_{50}$-Ge alloys show values for the Knight shift (**K**) which are substantially lower than expected for free electron behavior. These deviations are largest around x(Ge)=0.25 where also the enthalpy of mixing (Castanet 1984) has a minimum. The observed changes in the Cu-Knight shift indicate a reduction in the density of states (**DOS**) at E_F of nearly 30% with respect to pure copper and an even bigger reduction if one takes the interpolated free-electron **DOS** for comparison. If part of the occupied states at E_F are shifted downward by an appreciable amount the corresponding reduction in **DOS** at E_F would account for the observed ΔH_{mix}.

1.-Introduction.-

There is an increasing amount of data on electronic anomalies in amorphous and liquid alloys of group I or II elements with polyvalent elements (Häussler 1983,1990, Terzieff 1989). As a general rule most pronounced deviations from free electron behavior occur when the Fermi momentum matches the wave vector introduced by structural features of the liquid, i.e. $2k_F \approx q_{max}$ of the interference function a(q).

To our knowledge no one has tried to derive the structure induced minimum in the density of states **DOS** which has been proposed by Nagel and Tauc (1975) from N.M.R. measurements, and to relate it to thermodynamic properties.

A rather straightforward way of investigating the **DOS** is to measure the shift of the N.M.R. line which is for an s-element proportional to the extra magnetic field caused by polarized conduction electrons (Knight shift).

$$K = C^{*}\langle|\psi(0)|^2\rangle_F{}^{*}\mathbf{DOS} \qquad (1)$$

From an analysis of existing data (Carter et al 1977) for the Cu-Al system there is evidence that the observed minimum in the Knight shift can not be attributed to changes of $\langle|\psi(0)|^2\rangle$ because it is seen in the same way on both nuclei, ^{27}Al and ^{63}Cu.

In order to study whether there is a systematic trend in **K** and the heat of mixing ΔH_{mix} we have studied the ternary Cu-Ag-Ge system . These alloys offer as an other advantage that the role of a possible s-d hybridization can be studied, by changing the Cu to Ag ratio.

In order to compare our alloys with other noble-metal polyvalent alloys investigations of the electrical conductivity as a function of concentration and temperature have also been performed. An analysis with the extended Zimann theory (Dreirach et al 1972) shows satisfactory agreement.

2.-Experiment.-

The N.M.R.experiments have been done on finely dispersed samples because of skin depth problems. First the samples were alloyed in quartz ampules of metals with 5N purity. Then the homogeneity of the samples was checked by metallographic analysis before they were ground to 40 µm powder. Finally the metal powder was mixed with about 3/2 the volume of Al_2O_3 and sealed under vacuum in quartz ampules.

The frequency shifts were measured with respect to solid CuJ and corrected for the small chemical shift of CuJ as given by Carter et al (1977).

We used a commercial N.M.R. spectrometer (Matec) for pulsed N.M.R.in a field of 4-6 T, together with a homemade tank which allowed tuning and matching from 33 to 62 MHz. The N.M.R. coil (7 turns, 11mm dia.) was made from platinum ribbon of 3 mm width and welded into a quartz tube which helped to prevent ringing. To achieve a faster ringdown time the tank was used in an overcoupled mode. The coil with the sample is placed inside a furnace which carries a non inductive winding (NiCr-wire). The maximum temperature which could be reached was 1440 K. The temperatures are measured using an electrical shielded thermocouple in contact with the sample.

Fig.1 shows a typical free induction decay for $Cu_{64}Ge_{36}$. The trace is the average of 2000 "shots" (about 2 min.measuring time). For each frequency point 6 to 9 different carrier frequencies around the resonance have been measured and the respective beats evaluated. The accuracy of the derived resonance frequency is ±0.5 kHz which results in a relative accuracy for the Knight shift values of ± 1%.

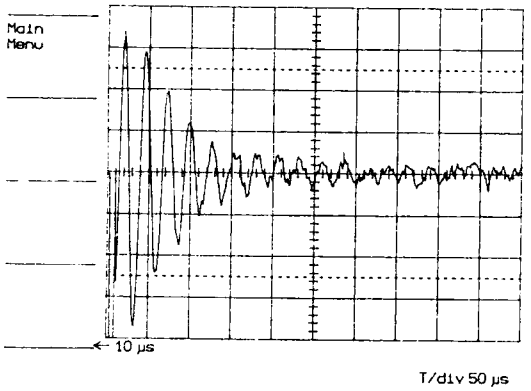

Fig.1:
Cu-N.M.R.signal (FID) of $Cu_{64}Ge_{36}$, 1356 K

Resistivity measurements have been performed by the method described by Gasser (1982) from the corresponding liquidus temperature to 1470 K.

3. Results and Discussion.

Before we turn to the results let us mention that one expects a different behaviour for the resistivity if the double Fermi momentum $2k_F$ is smaller, about equal or larger than q_{max} of the interference function, according to the theory of Faber and Zimann; for a review see e.g.Güntherodt (1977).

Fig. 2 shows the concentration dependence of K at fixed temperature for three alloy systems, Cu-Ag (our measurements), Cu-Al and Al-Ge (Carter et al 1977), which correspond to the above mentioned cases.

It is seen that significant deviations from free electron behavior are found when $2k_F$ equals approximately q_{max}.

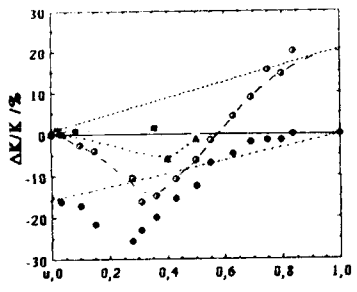

Fig.2: Relative changes of the Knight shift as function of concentration:
full circles: ^{27}Al
half circles: ^{63}Cu in Cu-Al, $x=x_{Al}$
squares: ^{27}Al in Al-Ge, $x=x_{Ge}$
triangles: ^{63}Cu in Cu-Ag, $x=x_{Ag}$

Fig. 3 presents the results for Cu-Ge and $(Cu_{50}Ag_{50})$-Ge. Due to problems in the production of sufficiently microcrystalline samples the N.M.R.measurements were limited to Ge-concentrations < 0.36 ; the continuation to concentrations where the curve is expected to approach again the interpolated free electron value (dashed line) as in the Al-Cu case, remains for future work.

Furthermore fig.3 compares the thermodynamic data for the ternary Cu-Ag-Ge system with data for resistivity and Knight shift. The enthalpy of mixing ΔH_{mix} (Castanet 1984, Beja 1969, Predel and Stein 1971) shows three characteristic features:

a) demixing tendency for the binary Cu-Ag
b) an asymmetric shape with the minimum at about x(Ge)=0.25 independent of the Cu/Ag ratio
c) the absolute value of this ΔH_{mix} minimum shows a decrease as Cu is replaced by Ag

Of these effects, the second is the corollary of the Knight shift minimum, and of the resistivity maximum.

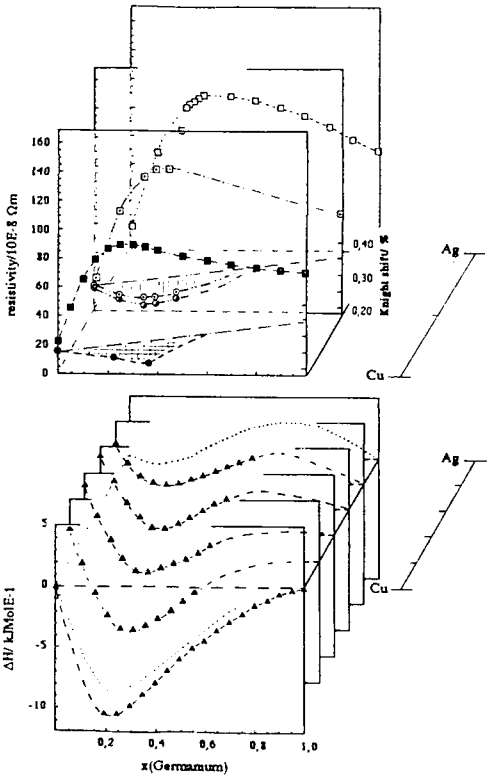

Fig.3: Resistivity, Knight shift and enthalpy of mixing in the ternary Cu-Ag-Ge system: *open squares*: ρ(Ag-Ge),1273 K; *dotted squares*: $\rho(Cu_{50}Ag_{50}$-Ge),1273 K; *full squares*:ρ(Cu-Ge), 1373 K; *dotted circles*: K$(Cu_{50}Ag_{50}$-Ge),1373 K; *half circles*: K$(Cu_{50}Ag_{50}$-Ge) at the liquidus Temp.; ΔH_{mix} (*triangles*) from Castanet (1984) at 1348 K;dotted lines Predel and Stein (1971)

For the resistivity as a function of concentration all three measured systems behave in a similar manner. This shape agrees with resistivities as calculated with the extended Faber-Zimann theory using the same procedure as in (Gasser 1982). The data for Cu-Ge are in agreement with earlier data of Günterodt et al.(1977).

It may be noted that for the magnetic susceptibility deviations from the additivity rule had been found in a series of gold alloys: Au-In, Au-Ge and Au-Sb (Terzieff 1989). There the maximum deviation is shifted to lower concentrations of the polyvalent elements as their valence increases. For many alloys the $2k_F = q_{max}$ condition corresponds to an conduction electrons per atom ratio e/a of about 1.8 (Häussler 1983) which explains the systematic shift.

Fig. 4 demonstrates that the same tendency is found also for Cu-Al and $(Cu_{50}Ag_{50})$-Ge in the **K** (x) and **ΔHmix** curves.

At the present stage, a clear correlation can thus be demonstrated between the observed deviations from free electron behaviour of resistivity , Knight shift and enthalpy of mixing on the one hand, and expected deviations of the density of states on the other hand. For a quantitative discussion of s- and p-elements, the electron matrix interaction may be treated in the pseudopotential approximation, using the structure factors of the alloys together with the Fermi wave number; these two ingredients will place the largest deviations at $2k_F=q_{max}$ (Nagel and Tauc 1975). Such calculations have not yet been done for alloys with d-elements where the t-matrix formalism replaces the pseudopotential formalism Therefore we have arbitrarily normalized the curves **K**(x) and **ΔHmix**(x) in fig 4. such that the correspondence is easily seen.

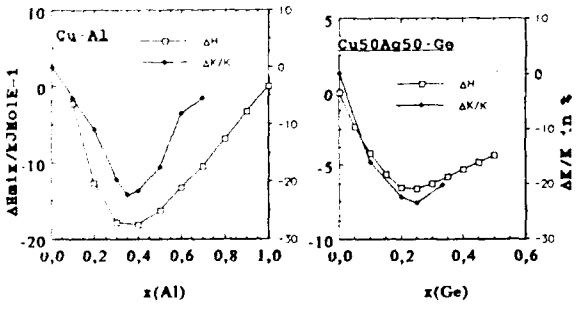

Fig.4:Enthalpy of mixing and deviation from free electron behaviour.The values **ΔK/K** represent the difference between the measured **K** values and the free electron value as in fig.1. The data for **ΔHmix** are from Beja (1969)

From Knight shift data it is also evident that the idea of a local **DOS** connected with compound forming tendency, which has been elaborated by Ott et al. (1990) for liquid semiconductors, cannot be applied to our case because the assumed associates would cause different Knight shift trends in the concentration dependence of the two nuclei, particulay on their respective minority sides.

From the discussion just given, one would not expect any difference between Cu-Ge and e.g. $Cu_{50}Ag_{50}$-Ge. Indeed **K** and the conductivity show negligible differences. However the systematic decrease of ΔHmix is of a considerable magnitude, see fig.3. It appears most logical to attribute it to the energy shift of the d-band with respect to E_F. Note that the energy gain which appears as ΔH_{mix} , would correspond for the (Cu/Ag)-Ge systems to an average downward shift of the occupied s-conduction electron states by about 0.05 - 0.1 eV

Acknowledgements

We want to thank P. Häussler for comunicating unpublished material to us, and Mrs. M.Dämmrich for the metallographic analysis of the N.M.R. samples. For making the quartz resistivity cells we are obliged to J.-C. Humbert and N. Zimmermann.
This work is supported in part by "Deutsche Forschungsgemeinschaft"

References

Beja, R. (1969), Thesis Université d'Aix Marsaille,France
Carter, G.C. et al (1977), Metallic shifts in NMR, in Prog.in Mater.Science, Pergamon Press, New York
Castanet, R. (1984), Z.Metallkunde **75**,H1 (1984),41
Dreirach, O.et al (1972),J.Phys.**F2**,709,
Gasser, J.-G.(1982),Habilitation Université de Metz, France [the calculations do not include deviations from a free electron DOS]
Güntherodt H.J. (1977),Adv. in Sol. State Phys. XVII, Vieweg
Häussler, P.(1983),Z.Physik B53,15
Häussler, P (1990) in glassy metals III, Eds. H.Beck and H.J.Güntherodt, Springer
Nagel, S.R. and J. Tauc (1975), PRL 35,380
Ott,K et al. (1990) contribution to this conference
Predel and Stein (1971), Z.Naturforsch.**A**,26 722
Terzieff,P (1989),priv. communication

ORDERING OF $L1_2$, Cu_4Pt DISORDERED BY COLD-ROLLING AND BY MELT-SPINNING

A.R.YAVARI+,M.D. BARO*, S. SURINACH*

+ LTPCM-CNRS UA29 Institut National Polytechnique de Grenoble, BP 75, Domaine Universitaire 38402 St Martin d'Hères, France.

* Departament de Fisica, Universitat Autonoma de Barcelona, 08193, Bellaterra, Spain

Abstract

Ordering kinetics of disordered Cu4 Pt have been reexamined. Such reordering occurs in two stages with stage I attributed to the mobility of excess defects and stage II to that of equilibrium vacancies. It is found that mobile excess defects populations are higher in Cu4 Pt disordered by cold-rolling as opposed to samples disordered by melt-spinning.The order-disorder enthalpy $\Delta H_{o\text{-}d}$ is found to be ≈ 0.1 k T_c compared to $\Delta H_{o\text{-}d} \approx 0.5$ k T_c predicted by CVM.

1. Introduction

In the framework of a european research program, we study the re-ordering kinetics in $L1_2$ type alloys disordered by various thermomechanical processes. Mitsui et al (1989) previously studied ordering in Cu_4 Pt disordered by quenching from the solid-state. In this note we compare ordering of Cu_4 Pt disordered both by cold-rolling and by rapid quenching from the liquid state.

We also report on the ordering energy $\Delta H_{o\text{-}d}$ and compare it to the disordering energy $\Delta H_{d\text{-}o}$ as measured by calorimetry

2. Experimental procedure

A Cu_4 Pt alloy was prepared by melting together appropriate amounts of pure components in a cold crucible under purified argon gas. The ingot was then divided into two parts. One part was cold-rolled down to a thickness reduction of 90 % and the other part was melt-spun from a quartz tube onto a copper wheel in a helium chamber. Ordered and disordered states were then characterised by differential scanning calorimetry (DSC) and X-ray diffraction.

3. Experimental results

X-ray intensities of fundamental Bragg peaks in $L1_2$ type AB_3 alloys are proportional to $(f_A + 3 f_B)^2$ while those of the superlattice peaks scale with $(f_A - f_B)^2$ and the latter are by consequence lower than the former (f_i are the atomic scatttering factors).

Since f_i scale with the atomic number, the superlattice intensity contrast increases with the square of the difference in the constituents' atomic numbers. As such, while quite weak for Ni_3 (Al-Fe) as reported earlier (Yavari and Bochu 1989), it is very strong for Cu_4 Pt alloys. Figure 1 shows the X-ray diffraction patterns of ordered $L1_2$ states of these two alloys.

The strong intensity of the Cu_4 Pt superlattice lines allows accurate detection of the degree of order from X-ray diffraction . Figure 2 shows the diffraction patterns for samples of the same ingot disordered by moderate cold-rolling and by melt-spinning. It shows a total disappearance of the superlattice Bragg peaks indicating the absence of $L1_2$ order and the γ' phase in these samples . The pattern for the cold-rolled sample also shows a strong <200> texture.

We next studied the re-establishment of ordering in these samples by calorimetry (DSC). Figure 3 shows the thermogram for the sample disordered by cold-rolling. The curve with the double arrows is the second heating cycle. Consistent with the work of Mitsui et al (1989), ordering occurs in two stages (corresponding first to heterogeneous, then homogeneous nucleation and growth of γ' phase), producing exotherms with maxima at T $\approx$ 640 K and 800 K. Subsequently, at T > 900 K equilibrium disordering produces the expected endothermic effect with a maximum at T $\approx$ 956 K ($T_c \approx$ 1000 K). The sample is then cooled in-situ at 320 K/min and then reheated to produce the double-arrow curve which shows. a weak endothermic effect occurs near T $\approx$ 800 K indicating that the rapid cooling in the DSC has retained a small degree of disorder which disappears in this stage II reordering regime.

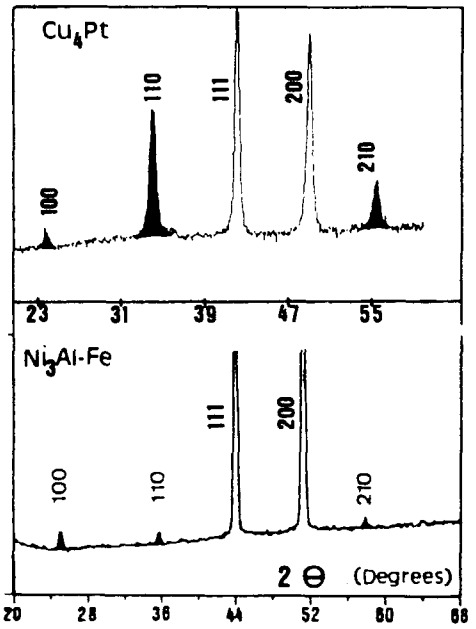

Figure 1 :
X-ray diffraction patterns of ordered $L1_2$ states of Cu_4 Pt (top) and Ni_3 Al-Fe (bottom, from Yavari and Bochu 1989). Superlattice peaks are in black (Cu K_α radiation).

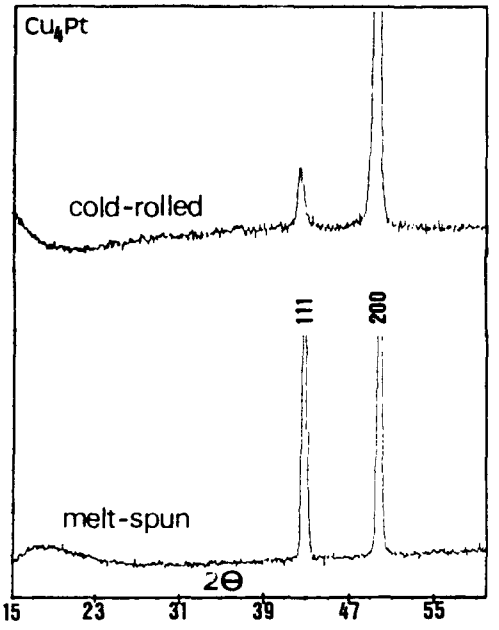

Figure 2 :
X-ray diffraction patterns of cold-rolled (top) and melt-spun (bottom) Cu_4 Pt showing total absence of superlattice peaks (Cu K_α radiation).

Figure 4 shows similar results for the melt-spun sample. One significant difference with figure 3 is that stage II ordering is stronger in the melt-spun sample indicating that stage I ordering has left more disordered regions to be ordered at higher temperature. Conversely one can say that stage I ordering in the cold-rolled sample has resulted in near complete ordering. Stage I ordering is generally thought to occur at low temperatures when vacancy defect supersaturated populations become mobile. As they anneal out to dislocations and grain boundaries or cluster to form large immobile defects such as voids and stacking fault tetrahedra, they help order the surrounding regions with the nucleation of order occuring at vacancy sinks (Mitsui et al 1989). Any disordered zones remaining after the annealing-out of the quenched-in defects must then await stage II temperatures at which equilibrium vacancies become mobile and of sufficient numbers.

4. Discussion

The fact that stage I ordering in cold-rolled samples results in more ordering than in melt-spun samples can be due to one or both of the following two reasons : either the mobile defect supersaturations are higher in the cold-worked sample than in the liquid-quenched sample, or the effective vacancy sink density is lower in the former thus requiring longer diffusion distances for vacancy defects to reach the sinks. The vacancy supersaturation in micro-crystalline metals obtained by rapid quenching is expected to be very high (Van Mourik et al, 1985)but the expected small grain size implies a large sink density. In the cold-rolled sample the dislocation density is expected to be high, at least of the order of $\rho = 10^{11}/cm^2$ giving intersink distances of the order of $1/(\rho)^{1/2} \approx$ 30 nm which is lower than the grain size in melt-spun samples. Thus sinks are just as numerous if not more. It would therefore appear then that mobile vacancy defect densities are higher in the cold-rolled sample. This can be understood as follows : since these vacancies are generated during deformation at room- temperature via forced motion of certain dislocation kinks and jogs, they are not sufficiently mobile to move to meet each other at 300 K and to form large immobile vacancy clusters, but in the melt-spun sample such diffusion is possible during cooling from high temperature.

Assuming single constant activation energies E_I and E_{II} for atomic migration resulting in the heat release of each of the two ordering stages I

and II, and using thermograms obtained at different heating rates, from the displacement of the peak maxima with the heating rate (Damask and Dienes 1963) we have obtained $E_I \approx 1.0$ eV and $E_{II} \approx 2.2$ eV in agreement with Mitsui et al (1986).

The activition energy E for atomic diffusion via equilibrium vacancy jumps is $E = \Delta H_v + \Delta H_m$ where ΔH_v and ΔH_m are respectively the formation and migration energies of vacancies (see for example Shewmon 1963). Various empirical relations can be used to relate these quantities to the cohesive energy, melting temperature, bulk modulus and other physical properties. For Cu, $E_I \approx 2$ eV and for Pt, $E \approx 3$ eV. such that our value $E_{II} \approx 2.2$ eV is within the right range for $\Delta H_m + \Delta H_v$ in a disordered fcc CuPt alloy. Generally, $\Delta H_v > \Delta H_m$ and if we take as experimentally determined for gold (Bauerle and Koehler, 1957), $\Delta H_m \approx 0.8\ \Delta H_v$, we obtain $\Delta H_m \approx 0.98$ eV for stage II ordering with $E = \Delta H_v + \Delta H_m \approx 2.2$ eV. When the kinetics are controlled by the mobility of large supersaturated vacancy populations as postulated for stage I ordering, $E = \Delta H_m$ and ΔH_v is omitted as the diffusive jump attempt frequency is no longer multiplied by the vacancy formation probability. The fact that $\Delta E_I = \Delta H_m = 1.0$ eV for stage I is in very good agreement with our estimation of ΔH_m from stage II kinetics confirms the present interpretation and excludes any major role for divacancies as reported elsewhere (Mitsui et al 1989). The enthalpy released on ordering (stage I + stage II) ΔH_{d-o} and the enthalpy ΔH_{o-d} absorbed upon disordering below $T_c \approx 1000$ K have also been measured with $\Delta H_{d-o} > -\Delta H_{o-d}$ because of the exothermic contribution from the annealing-out of excess defects. $\Delta H_{o-d} \approx 730$ kJ / g.at. Theoretical estimates relating ΔH_{o-d} to T_c for AB_3 alloys predict $\Delta H_{o-d} \approx 0.25\ k\ T_c$ and $\Delta H_{o-d} = 0.5\ k\ T_c$ for Bragg-Williams theory and cluster variation method (CVM) respectively (see discussion in Cahn et al. 1987).

These values are to be compared with the present experimental relation $\Delta H_{o-d} \leq 0.1\ k\ T_c$ for Cu_4 Pt. A low -T tail occurs on the disordering endotherms of the DSC thermograms (see figure 4) which does not reappear on the second heating cycle but creates

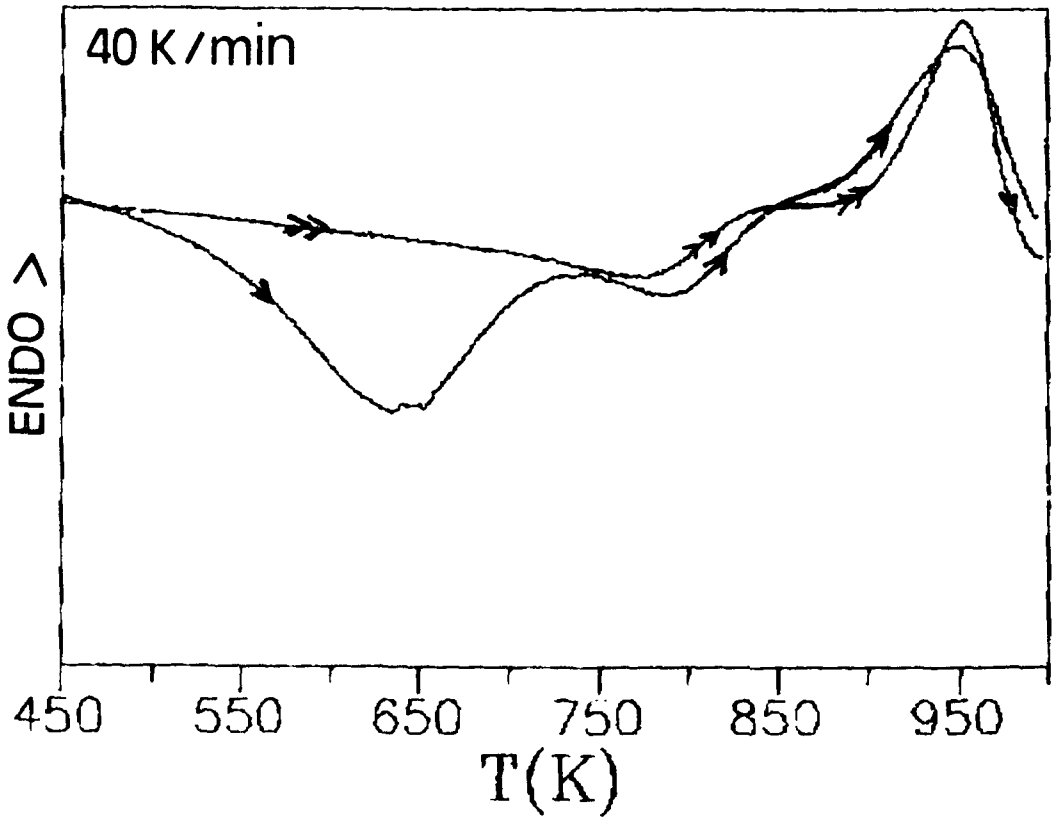

Figure 3 : DSC thermogram of cold-rolled Cu_4 Pt (→) and second passage after quenching in the calorimeter (→→).

a shoulder on the endotherm ; this shows that disordering (γ nucleation) which peaks at 956 K at our heating rate occurs more easily in the anti-phase domain structure of the reordered sample, that is likely to have a complex microstructure of microdomains, compared to he larger domains expected in the sample heated in the calorimeter to $T > T_c$. it implies that like in the case of heterogeneous nucleation of ordering on defects as reported by Mitsui et al (1989), disordering also nucleates heterogeneous, in this case on the remaining anti-phase domain boundaries.

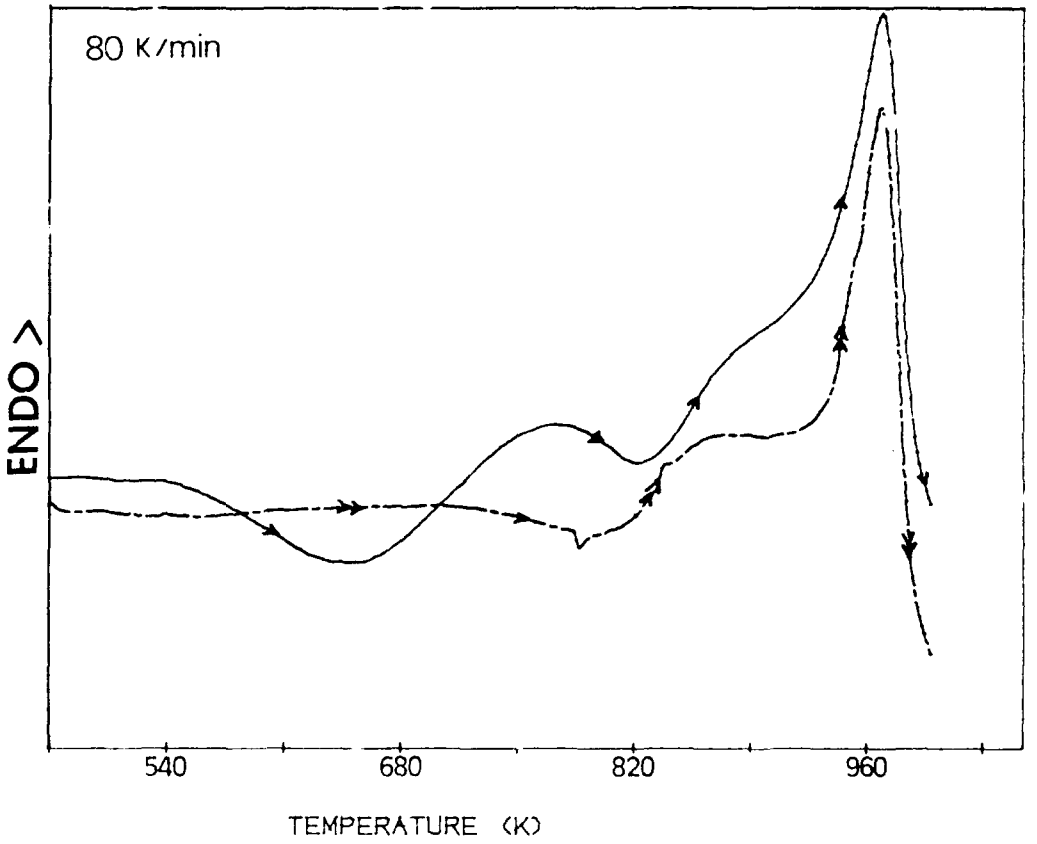

Figure 4 : DSC thermogram of melt-spun Cu_4 Pt (→) and second passage after quenching in the calorimeter (→→).

Acknowledgement : This work was financed by the EEC under the SCIENCE contract "Ordering Kinetics".

References

-J. Bauerle and J. Koehler, (1957) Phys. Rev. 107 , 1043
- R.W. Cahn, P.A. Siemens, J.E. Geiger and P. Bardhan. (1987) Acta Metall. 35, 2737
- A.C. Damask and G.J. Dienes, (1963), "Point Defects in Metal", Gordon and Breach, London.
- K.Mitsui, Y. Mishima and T. Suzuki, (1986) Philo. Mag. A 54, 501
- K.Mitsui, Y. Mishima and T. Suzuki, (1989) Philo. Mag. A 59, 123
- P.G. Shewmon,"Diffusion in Solids" (1963), Mc Graw Hill.
- P. Van Mourik, F.H. de Keijer and E.J. Mittemeijer (1985), Rapidly Quenched Metals, S. Steeb and H. Warlimont (eds.), Elsevier Science Publishers, p. 899.
- A.R. Yavari and B. Bochu, (1990), Phio. Mag. A 59, 697

SHORT-RANGE ORDER-DISORDER TRANSITION IN LIQUID ALLOYS ACCORDING TO THE ASSOCIATED MODEL.

R.CASTANET

Centre de Thermodynamique et de Microcalorimétrie du C.N.R.S, 26 rue du 141eme R.I.A. , F-13003, Marseille, France

1. INTRODUCTION.

In the last two decades, many careful investigations on liquid alloys showed that in many cases their thermodynamic behaviours are very sensitive to temperature. We pointed out as early as 1969 (Castanet, 1969) that compound-forming tendency of melts with negative deviations to ideality is the rule rather than the exception. These melts have strong negative values of the enthalpy of formation, positive excess C_P^{xs} of formation and the entropy of formation often shows a minimum with respect to composition. Application of the regular associated model to this class of binary alloys shows that such a behaviour can be attributed to the temperature dependence of their chemical short-range order and demonstrates that this dependence, due to the destruction of associated species, takes place in a more or less narrow temperature range according to the value of the standard parameters of formation of the associates (Castanet et al., 1984) . The aim of this paper is to show that such a change of structure can be ascribed in many drastic cases to a genuine second order transition.

2. ASSOCIATED SOLUTION MODEL.

In its well-suited form to metallic liquids the associated solution model was mainly developed by Jordan (1970), Bhatia et al., (1974), Sommer, (1982), Clavaguera and al., (1982) and Castanet et al., (1982 and 1984). The models developed by these workers are fundamentally similar but we used a definition of the entropy of configuration in which the size difference between the associates and the pure components are taken into account and where the associations are assumed sufficiently stable to be regarded as persistent (The A and B atoms in the associates cannot be exchanged with monoatomic species). Indeed, the correct determination of the configurational entropy is a necessary condition for the assignement of a physical meaning to the other contributions to the thermodynamic functions. In particular the entropy of formation of the associations and the temperature dependence of their stability are strongly related to the configurational entropy. Then we used here the regular associated model developed in Marseille (Bergman et al. 1982). The basic assumptions of the model are the following :

(i) The binary A-B melt is condidered as a ternary one where the species in equilibrium are pure A and B and $A_a B_b$. $A_a B_b$ are the suspected associated species mainly responsible of the negative deviations to thermodynamic ideality according to :

$$aA + bB \rightleftharpoons A_a B_b \equiv C \qquad [0]$$

(ii) The interactions between the three species are assumed as independent with respect to temperature and composition (strictly regular associated model).

(iii) The standard enthalpy H^0 and entropy S^0 of formation of the $A_a B_b$ associates are also assumed to be temperature independent i.e. the standard heat capacity of formation $C_P^0=0$.

(iv) Finally the atomic volumes of A and B are to be taken the same (V) and we assumed the additivity law for the volume of the associates $[V(A_a B_b)=aV_a+bV_b=(a+b)V]$.

From a practical point of view, starting from experimental determinations of the enthalpy and free enthalpy of formation of the melt, we resolve numerically a set of three equations for each value of the nominal mole fraction x of the alloy :

$$h^f(x,T) = N_C H^0 + [1-(a+b-1)N_C]\,[w_{AB}X_AX_B + w_{BC}X_BX_C + w_{CA}X_CX_A] \qquad [1]$$

$$g^f(x,T) = N_C H^0 + [1-(a+b-1)N_C]\,[w_{AB}X_AX_B + w_{BC}X_BX_C + w_{CA}X_CX_A] - TN_C S^0 - TN_C S^{conf} \qquad [2]$$

$$G^0 = H^0 - TS^0 = RT\,\mathrm{Ln}\left(\frac{\alpha_C}{\alpha_A^{\,a}\,\alpha_B^{\,b}}\right) = -RT\,\mathrm{Ln}K \qquad [3]$$

where s^{conf} is the entropy of configuration as defined later and K is the equilibrium constant for reaction [0].

Replacing α_i by γ_i/x_i equation [3] can be rewritten :

$$H^0 + TS^0 + RT\,[\ln\gamma_C - a\ln\gamma_A - b\ln\gamma_B] + RT\,\ln\left(\frac{X_C}{X_A^{\,a}X_B^{\,b}}\right) = 0 \qquad [4]$$

where $RT\ln\gamma_A = g_A^{f,xs} = h_A^{f,xs} - Ts_A^{f,xs} = w_{AB}X_B + w_{AC}X_C - \Sigma wX - Ts_A^{f,xs}$

and $\Sigma wX = w_{AB}X_AX_B + w_{BC}X_BX_C + w_{CA}X_CX_A$

$g_i^{f,xs}$, $h_i^{f,xs}$ and $s_i^{f,xs}$ are respectively the partial molar free enthalpy, the enthalpy and the entropy of i.

Then equation [4] becomes :

$$H^0 - TS^0 + w_{AC}(X_A - aX_C) + w_{BC}(X_B - bX_C) - w_{AB}(aX_B + bX_A) + (a+b-1)\Sigma wX + RT\left(\frac{X_C}{X_A^{\,a}\,X_B^{\,b}}\right) - T(s_C^{f,xs} - as_A^{f,xs} - bs_B^{f,xs}) = 0 \qquad [5]$$

3. SHORT-RANGE ORDER-DISORDER TRANSITION.

In order to simplify the problem we assumed here that the binary interaction coefficients $w_{ij} = 0$ (ideal associated model). Then we neglected the regular contributions to the heat capacity of the melt. Indeed, even in the case of $dw_{ij}/dT=0$, these contributions take values different from zero since the terms $w_{ij}X_iX_j$ in equation [1] depend on the degree of aggregation of the solution i.e. on the temperature.

In this case equations [1], [2] and [3] become :

$$h^f(x_A,T) = N_c H^0 \qquad [6]$$

with $\quad C_P^{xs} = H^0 dN_c/dT$

$$g^f(x_A,T) = N_c H^0 - T\{N_c S^0 + [1-(a+b-1)N_c]s^{conf}\} \qquad [7]$$

$$\frac{N_c[1-(a+b-1)N_c]^{a+b-1}}{(x_A-aN_c)^a(1-x_A-bN_c)^b} = \exp\left\{-\frac{H^0}{RT}+\frac{S^0}{R}+\frac{1}{R}\left(s_c^{f,xs}-as_A^{f,xs}-bs_B^{f,xs}\right)\right\} \qquad [8]$$

where the partial excess entropies of A_aB_b, A and B depend obviously on the definition used for the configurational entropy.

We used three different definitions

$$s^I/R = -\Sigma_i x_i \mathrm{Ln}x_i$$

i.e. assuming that A_aB_b occupy only one site of the quasi-lattice and that the permutations between free A or B atoms and A or B atoms engaged in the associates are forbidden. In this case, the partial excess entropies are equal to zero.

$$s^{II}/R = -\Sigma_i x_i \mathrm{Ln}\phi_i$$

where $\phi_i = r_iN_i/\Sigma_i r_iN_i$ and r_i is the number of atoms of the i specie. Such a definition proposed by Flory (1942), as the first one, allows the permutations between free and linked atoms but takes into account the difference of volumes.

Finally, the definition s^{III} :

$$s_c^{f,xs} = R\left\{\frac{a+b}{1+(a+b-1)X_c}\right\}$$

and $\quad s_A^{f,xs} = s_B^{f,xs}$

$$= R\,\mathrm{Ln}(1-X_c) - \frac{R}{a+b}\mathrm{Ln}\left\{\frac{1-X_c}{1+(a+b-1)X_c}\right\}$$

taking into account the difference of volume between free atoms and associates and considering the associates as permanent clusters.

From typical values of H^0 and S^0, we calculated the enthalpy of formation of hypothetical binary systems in order to follow their variations temperature and compare the influence of the three definitions of the entropy of configuration.

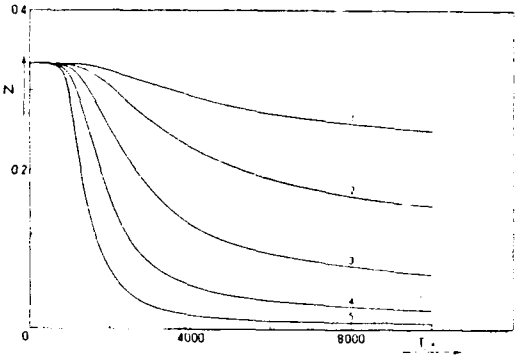

Fig. 1. Quantity of associates A_2B, N_C, with respect to temperature for x=2/3, H^0 = -50 kJ.mol^{-1}, s^{conf} = sIII, S^0/J.K^{-1}.mol^{-1} = (1) : +20 ; (2) : +10 , (3) : 0 ; (4) : -10, and (5) : -20.

Fig.1 shows the evolution of N_c with respect to temperature for an hypothetical ideal associated system A_2B (a=2 and b=1). It is obvious that the example given here is unrealistic since N_c is shown up to 10 000 K i.e. in a temperature range where the alloy became totally vaporized. The different curves were obtained for $s^{conf}=s^{III}$, $H^0=-50$ kJ per mole of associates and four typical values of S^0. The calculation was performed for $x_A=2/3$ i.e. for the stoichiometry of the associations. The quantity of associates, N_c, (that is h^f/H^0), decreases when the temperature increases. More negative is the value of S^0 and more drastic is the destruction of the associates. It is in the case of $S^0 = -20$ J.K^{-1}.mol^{-1} that the temperature range where h^f increases drastically is the smallest and that the quantity of high-temperature remaining associates are the smallest. In this case, the excess heat capacity of the alloy exhibits a sharp peak in a narrow range of temperature similar to a second-order transition. Such a peak has been shown experimentally by Geffken et al.(1967) in the case of the Cd-Sb melts.

The dependence on temperature of h^f and g^f for $S^0 = -20$ and +10 J.K^{-1}.mol^{-1} is shown on Fig.2. At T=0, N_c=1/3, $h^f = g^f = -50/3$ kJ mol^{-1}. g^f first increases strongly

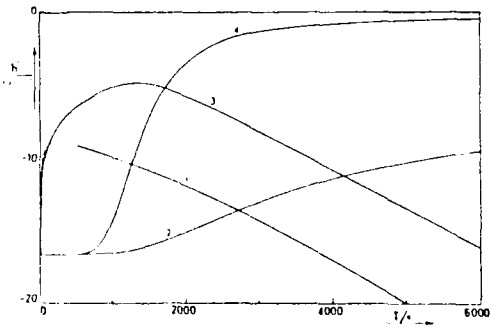

Fig. 2. Molar enthalpy and free enthalpy of formation of the alloy with respect to temperature for x=2/3, H^0 -50 kJ mol^{-1}, s^{conf} = sIII, a = 2 and b = 1. S^0/J.K^{-1}.mol^{-1} = 10 (curves 1 and 2) and -20 (curves 3 and 4) ; g^f : curves 1 and 3 , h^f : curves 2 and 4.

then decreases when T increases. Such a behaviour corresponds at low temperature to negative values of the entropy of formation of the alloys, $s^f=-dg^f/dT$, then to positive values at high temperature. It is the case of the Au-Si alloys as shown by Castanet et al. (1978) and Allen et al. (1980).

In many cases it is not possible to measure the enthalpy of formation in the whole range of temperature where the transformation takes place because (i) the

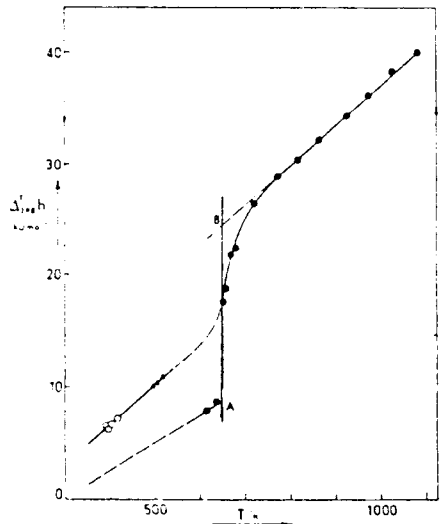

Fig. 3. Molar enthalpy variation, $\overline{T}_{298}h$, from 298 to T of the Te-rich eutectic of Ge-Te alloys in the crystalline supercooled and stable liquid states with respect to T. ● stable states (drop method). o supercooled liquid (drop method). ▲ supercooled liquid (differential scanning calorimetry).

low temperature part is located below the liquidus temperature (ii) the high vapor pressure of the components prevents any experimental determinations at high temperature. However we succeeded in such measurements for Ge-Te eutectic alloys starting at low temperature from glassy alloys and deriving the enthalpy of formation from D.T.A. The results obtained in this way

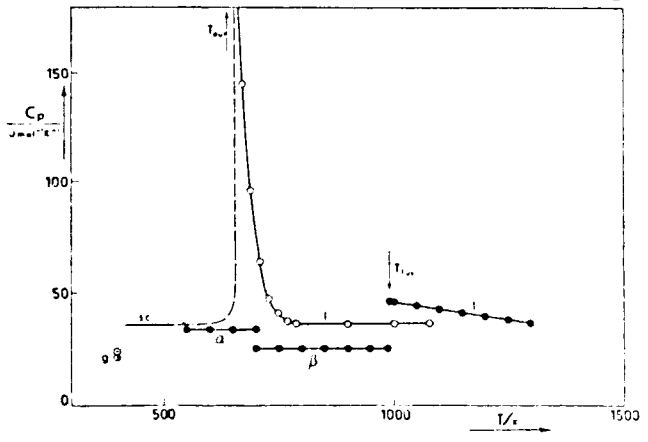

Fig. 4. Molar heat capacity, C_p, of the Te-rich eutectic (o, ⊕) and $Ge_{0,5}Te_{0,5}$ compound (●) in the crystalline, glassy, supercooled and liquid states with respect to T. ● $Ge_{0,5}Te_{0,5}$ (α, β and liquid). o Te-rich eutectic. ◑ glassy alloy. ⊕ glassy alloy.

are given in Figs.3 and 4 (Castanet and Bergman, 1985). They definitely show a transition in the melt near the eutectic temperature. Unfortunately we could not apply the associated model to the system since there is no available Gibbs energy data concerning the Ge-Te liquid phase.

In the Ge-Te alloys there is probably only one kind of association, namely Ge_2Te. On the contrary application of the model to the Cu-Sb alloys (Hayer et al., 1977; Saïd et al., 1984) stated that there are two kinds of associates (Cu_3Sb with $H^0=-28.6$ kJ.mol^{-1} and $S^0=19.6$ J.K^{-1}.mol^{-1} and CuSb with $H^0=-0.22$ kJ.mol^{-1} and $S^0=14.2$ J.K^{-1}.mol^{-1}). Then the behaviour of these alloys is more complicated (Fig.5 and 6).

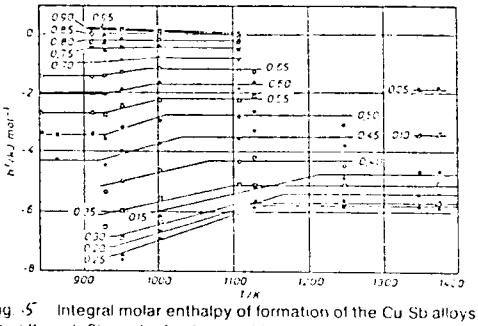

Fig. 5. Integral molar enthalpy of formation of the Cu Sb alloys at different Sb mole fractions with respect to temperature

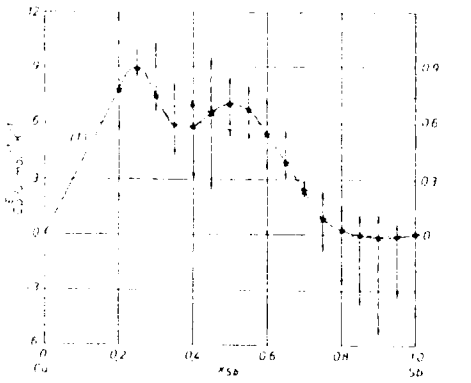

Fig. 6. Excess heat capacities, C_p^E/J.mol^{-1}.K^{-1}, of liquid Cu-Sb alloys referred to the pure liquid components as a function of composition (curve 1). The points signify the linear interpolated value. The arrows mark the maximum deviation.

The transition takes place entirely in the stable liquid phase on the Sb-rich side but not on the other side. The results of the calorimetric measurements with respect to temperature (Fig.5) clearly show the existence of two transitions which differ by their enthalpy and by the temperature range where they take place.

Finally, as a last example, we show the enthalpy of formation (Fig.7) and the excess heat capacity (Fig.8) of the In-Te alloys (Castanet, 1989). The application of the model lead to the existence of two kinds of associations (In_2Te_3 and InTe). We measured the enthalpy of formation of the

melt (Saïd et Castanet., 1978) at 9 temperatures between 737 and 1340 K. Up to

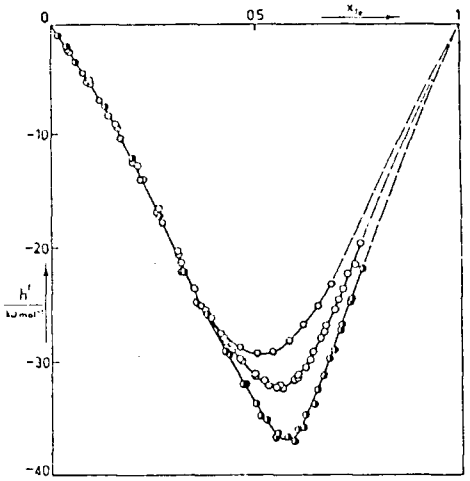

Fig. 7 Integral molar enthalpy of formation of the In-Te liquid alloys referred to both pure liquid components at 1340 K (O), 1123 K (●) and 987 K (◑).

987 K we did not observe any variation of h^f with temperature. The results obtained at high temperature are shown on Fig.8. They state a strong temperature dependence on the Te-rich side. We pointed out that when the temperature increases the minimum decreases and its location is shifted towards the In-rich side. Such a behaviour is in agreement with the density measurements of Thurn and Ruska (1976) who pointed out that the maximum of the volume of mixing decreases also when temperature increases and is also shifted towards the In-rich part.

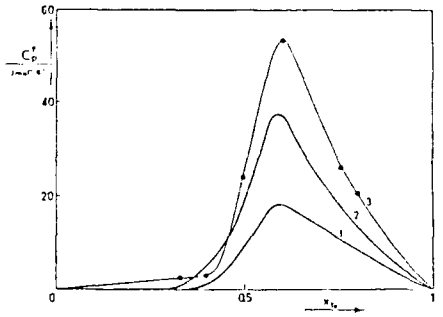

Fig. 8 Excess heat capacity of the In-Te liquid alloys referred to pure liquid components. Curve 1 (1123 to 1340 K) and curve 2 (987 to 1123 K) from direct reaction calorimetry. Curve 3: from adiabatic calorimetry.

The previous results were obtained for $s^{conf}=s^{III}$ i.e. using our definition of entropy of configuration for strongly associated alloys. The same calculations were performed with $s^{conf}=s^{I}$ and s^{II}. The evolution of the enthalpy of formation as a function of T is plotted on Fig.9 for $S^0=-20$ and +10 $J.K^{-1}.mole^{-1}$ using the three definitions of s^{conf}. As can be seen, our definition is better suited to very strongly associated systems since the transition begins later and takes place in a more restricted temperature range. The residual short-range order at high temperature is the smallest i.e. the value of the "enthalpy of

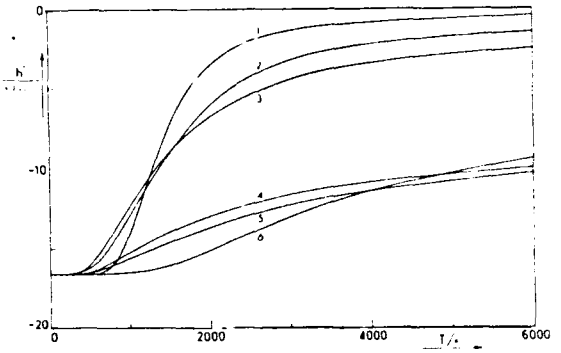

Fig. 9. Molar enthalpy of formation of the liquid alloy with respect to temperature for x = 2/3, H^0 = 50 kJ mol^{-1}, a = 2 and b = 1, $s^{conf} = s^{III}$ (curve 1 and 6), $s^{conf} = s^{II}$ (curve 3 and 4), $s^{conf} = s^{I}$ (curve 2 and 5), $S^0/J.K^{-1}.mol^{-1}$ = -20 (curves 1, 2 and 3) and +10 (curves 4, 5 and 6).

transition" :

$$h^{tr} = H^0 \ [N_c(T=\infty) - N_c(T=0)]$$

is maximum as shown also by Fig.10 for usual values of S^0 (from -20 to +20 $J.K^{-1}.mol^{-1}$).

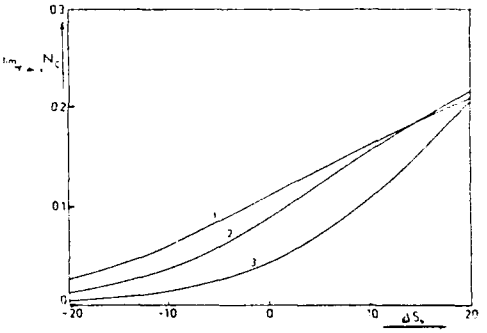

Fig. 10. $\lim N_C(T\to\infty)$ with respect to S^0 for x = 2/3, H^0 = - 50 kJ.mol^{-1}, a = 2 and b = 1, $s^{conf} = s^{II}$ (curve 1), s^{I} (curve 2) and s^{III} (curve 3).

The more negative is S^0 and the higher is h^{tr} but even at high temperature there is an unnegligible residual short-range order. These observations allow us to a better understanding of the behaviour of the Cu-Sb melts. We pointed out experimentally that the destruction by heating of the two kinds of associates lead to a very weak increase of the enthalpy of formation of the liquid : 0.9 $kJ.mol^{-1}$ maximum (x_{Sb} = 0.35) i.e. only 16% of the value at low temperature. Then it appears that 84% of residual enthalpy can be due mainly to undestroyed associates and not to the interactions between the different species.

4. CONCLUSION.

In conclusion we have to point out that the thermodynamic behaviour of an associated liquid cannot be understood from investigation in a too restricted temperature range only. Indeed the dependence on

temperature can be divided into three domains :

a) A low temperature region where the enthalpy of formation is strongly negative due to a high degree of association and where there is a very weak variation with T. This range in many cases lies below the liquidus temperature and is not available for experimentation.

b) A middle range where associates are very sensible to thermal agitation. The melt undergoes a drastic change of heat capacity which can be considered as a genuine short-range order transition. The more negative the standard entropy of formation of the associates, the more restricted the temperature range of the transition and the less important the residual enthalpy of formation at high temperature.

c) Finally a high temperature region where the main part of the associates are destroyed and where excess C_P is nearly constant and close to zero (Kopp and Neumann law). Even at high temperature, associated liquids do not become completely disorderd. Still at high temperature there is some residual negative enthalpy of formation due to the persistence of non-negligible quantities of associates.

REFERENCES

Allen J.W., Wright A.C. and Connell G.A.N., J.Non-Cryst.Solids, 42(1980)509.

Bergman C., Castanet R., Said H., Gilbert M and Mathieu J.-C., J.Less-Comm.Metals, 85(1982)121.

Bhatia A.B. and Hargrove W.H., Phys.Rev.B, 10(1974)3186.

Castanet R., State thesis, Marseille, France, 1969.

Castanet R., Chastel R. and Bergman C., Mater.Sci.Engng., 32(1978)93.

Castanet R., Gilbert M. and Mathieu J.-C., J.Less-Comm.Metals, 96(1984)1.

Castanet R. and Bergman C., Phys.Chem.Liquids, 14(1985)219.

Castanet R., Z.f.Metallkde, 80(1989)737.

Clavaguera-Mora M.T. and Clavaguera N., J.Phys.Chem.Solids, 43(1982)129.

Flory P.J., J.Chem.Phys., 10(1942)51.

Geffken R., Komarek K.L. and Miller E., Trans. Met.Soc.AIME, 239(1967)1151.

Hayer E., Komarek K.L. and Castanet R., Z.f.Metallkde, 68(1977)688.

Jordan A.S., Metall.Trans., 1(1970)239.

Said H.and Castanet R., High-Temp., High-Pressure, 10(1978)681.

Said H., Castanet R., Gilbert M. and Mathieu J.-C., J.Less-Comm.Metals, 96(1984)79.

Sommer F., Z.f.Metallkde, 73(1882) 72 and 77.

Thurn H and Ruska J., Z.Anorg.Allg.Chem., 426(1976)237.

Glass Forming Ability in Chalcogen Rich Ge-Se-Te Glasses

Y. Calventus, M.D. Baró, S. Suriñach, S. Bordas, M.T. Clavaguera-Mora, and N. Clavaguera*

Física de Materials, Dept. Física, Universitat Autònoma de Barcelona, 08193-Bellaterra, Spain
*Dept. Estructura i Constituents de la Matèria, Fac. Física, Universitat de Barcelona, Diagonal 647, 08028- Barcelona, Spain

Abstract.-
The empiric parametrization of glass forming ability by use of thermal, kinetic and thermodynamic information is discussed for a binary and a ternary chalcogenide glasses. A triple parametrization is proposed. The first one comes from the temperatures of the transitions inherent to the glassy state and includes as parameters the reduced glass transition temperature, the second one uses the time needed, at the glass transition temperature, to obtain a certain amount of crystalline phase. The third one comes from the comparison between the Gibbs free energy of formation of the glass and the melting enthalpy.

1.- Introduction

The glass forming ability (GFA) of alloys produced by the application of rapid solidification from the melt has been discussed extensively from various viewpoints (Turnbull 1969, Uhlmann 1972). It appears to be established that only a limited range of multicomponent systems can be solidified into an amorphous glassy state by the rapid solidification technique. Among them, those that can be solidified into a glassy phase at rather low cooling rates include the chalcogenide alloys.

The aim of this work is to look into the GFA of pure Se-Te alloys as compared to that obtained with some small additions of Ge on them. The empirical parametrization of the GFA is obtained as well from thermal and crystallization kinetic results as from thermodynamic considerations.

In order to estimate the GFA various thermal empirical parameters have been used by several authors. The first one is the reduced glass temperature $T_{rg}=T_g/T_l$, where T_g is the glass transition temperature and T_l the liquidus temperature. This parameter (T_{rg}) ranges in general between 1/2 and 2/3, the last value being obtained for very good glass formers (Sakka and Mckenzie 1971). Another parameter used is the Hruby (1972) parameter $K_{gl}=(T_p-T_g)/(T_l-T_p)$, where T_p is the temperature of the crystallization peak. Good glass formers would have high K_{gl} values.

Other parameters are fundamentally kinetic like, for instance, the change in Gibbs free energy, ΔG, in the crystallization of the bulk liquid or driven force for crystallization (Thompson and Spaepen 1983, Saunders and Miodownik 1983, Greer 1988). The thermodynamical approach is used to calculate the Gibbs free energy of formation of the alloy glass relative to the stable crystalline solid solution (Bormann *et al.* 1988).

Parametrization of GFA from kinetic data comes from the assumption that under isothermal conditions the fraction x of crystallized material at a given time t follows an equation of the type

$$g(x) = k(T)\, t \qquad (1)$$

where g(x) is a function which depends on the mechanism of crystallization and k(T) is given by the Arrhenius expression

$$k(T) = k_o \exp(-E/RT) \qquad (2)$$

were k_o is a pre-exponential factor and E the effective activation energy.

In the Johnson-Mehl-Avrami-Erofe'ev model we have

$$g(x) = [-\ln(1-x)]^{1/n} \qquad (3)$$

were n is the kinetic exponent.

According to equation (1) the lower value of k(T) at a given temperature the longer the time needed to crystallize the glass at this temperature. Assuming further that all glasses are in corresponding states at T_g, the following empirical parameter was defined (Suriñach *et al.* 1984)

$$\bar{A} = k_o \exp(-E/RT_g) \qquad (4)$$

then $1/\bar{A}$ represents the time necessary at the glass transition temperature to get a value of x that conforms to g(x)=1. According to that and to the previous discussion, low values of $\bar{A}$ are indicative of high GFA.

2.- Experimental

Glasses of the two following compositions were prepared by air quenching:

$Se_{85}Te_{15}$ and $(Se_{85}Te_{15})_{98}Ge_2$. The alloy glasses were obtained by melting weighed amounts of the elements (5N purity) in evacuated and sealed quartz ampoules. The molten alloys were held at 1275 K for 12 hours and constantly agitated to ensure homogeneity; subsequently they were quenched in air at room temperature. The estimated quenching rate at 600 K is about 10^2 K/s. The glassy state of the sample was checked by X-ray powder diffraction.

Differential scanning calorimetry (DSC) was carried out in about 10 mg of powdered material in a Perkin Elmer DSC II under pure dynamic argon atmosphere. Constant heating rate experiments were recorded at scan rates β varying from 1.25 to 40 K/min. Isothermal experiments were performed at temperatures in the range 350-420 K. The systematic exploitation of experimental data is described by Suriñach *et al.* (1983).

3.- Results and discussion

The DSC curves of the glassy samples for a heating rate of 20 K/min are shown in Fig. 1. The glass transition and the crystallization exotherm occur prior to the melting transformation. The experimentally determined temperatures T_g, of the glass transition, T_p, of the crystallization peak, and T_l, of the liquidus are reported in Table 1.

The detailed study of the crystallization kinetics is reported in a separate paper by Suriñach *et al.* (1990). The activation energy E, was deduced from non-isothermal measurements by the peak method (Kissinger 1956). The Kissinger plot of $\ln(\beta/T_p^2)$ versus $1/T_p$ is shown in Fig. 2. The pre-exponential factor k_o, was deduced from isothermal measurements by the plot of $\ln[-\ln(1-x)]$ versus $\ln t$ as shown in Fig. 3.

The Gibbs free energy of formation ΔG_f of the binary Se-Te alloy glass was calculated using the assessed values of Ghosh *et al.* (1988) who also give the melting enthalpy ΔH_m, as a function of the composition of the alloy. For a $Se_{85}Te_{15}$ alloy, from the calculation, the value of the Gibbs free energy of formation at the glass transition temperature is ΔG_f=2.04 kJ/g-at while ΔH_m=7.3 kJ/g-at. Therefore, for the Se-Te glass we obtain $\Delta G_f/\Delta H_m$=0.27.

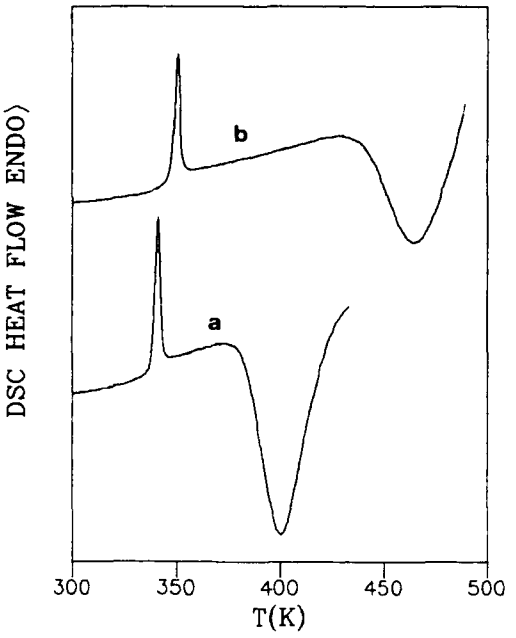

Fig. 1.- DSC plots at a heating rate of 20 K/min:
a) Se-Te glass; b) Se-Te-Ge glass.

As explained by Clavaguera-Mora and Clavaguera (1989) a good glass former system would have a value of $\Delta G_f/\Delta H_m$ in the range 0.2-0.3. Therefore, this ratio was used to characterize GFA. Due to the lack of assessed thermodynamical data in the Se-Te-Ge system no Gibbs free energy of formation was calculated for the Se-Te-Ge alloy glass.

Table 2 presents the values of the several empirical parameters T_{rg}, k_{gl}, $\bar{A}$ and $\Delta G_f/\Delta H_m$ used to estimate GFA in both chalcogenide glasses. The parameter T_{rg} is rather insensitive to small composition changes but all the rest of the parameters calculated are quite sensitive to the introduction of Ge in the Se-Te alloy. The glass forming parameter k_{gl} increases to about twice its value with small Ge addition in the Se-Te alloy. Following the same trend, the time $(1/\bar{A})$ needed to crystallize the alloy at the glass transition temperature increases from 9×10^4 to 2×10^5 s.

Table 1.- Temperatures T_g, of the glass transition, T_p of the crystallization peak and T_l of the liquidus and effective activation energy E, and logarithm of the pre-exponential factor $\ln(k_o)$, for the two alloy glasses studied.

	T_g^* (K)	T_p^* (K)	T_l (K)	E (eV)	$\ln(k_o)_1$ k_o in s^{-1}
$Se_{85}Te_{15}$	330	385	540	1.2	31.0
$(Se_{85}Te_{15})_{98}Ge_2$	338	446	550	0.8	15.6

*At a heating rate of 5 K/min

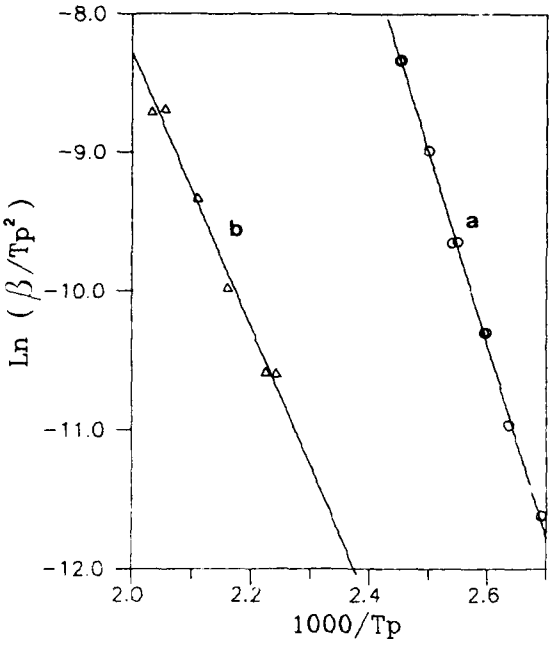

Fig. 2.- Plots of $ln(\beta/T_p^2)$ against $1/T_p$ for: a) Se-Te glass; b) Se-Te-Ge glass.

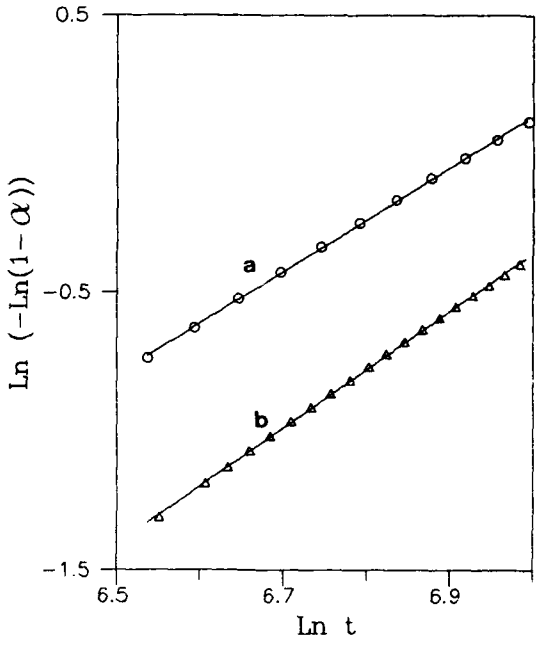

Fig. 3.- Plots of $ln[-ln(1-x)]$ as a function of lnt from the isothermal results: a) Se-Te glass; b) Se-Te-Ge glass.

Table 2.- Values of the empirical parameters used to characterize GFA in the two alloy glasses studied.

	T_{rg}	k_{gl}*	$\bar{A}(s^{-1})$	$\Delta G_f/\Delta H_m$
$Se_{85}Te_{15}$	0.63	0.31	1.1×10^{-5}	0.27
$(Se_{85}Te_{15})_{98}Ge_2$	0.66	0.70	6.2×10^{-6}	

*At a heating rate of 5 K/min

4.- Conclusions

An approximate evaluation of the glass forming ability in Se rich glasses of the Se-Te system with or without small addition of Ge on them has been presented.

A triple parametrization of GFA has been done. The first one comes from thermal data related to the transformations induced on heating the glass and includes parameters such as the reduced glass transition temperature, T_{rg}, and the Hruby k_{gl} parameter. The second one comes from the crystallization kinetic data and reflects the time needed to obtain a certain fraction of crystallized material at the glass transition temperature. Finally, the third one comes from thermodynamic quantities which were only evaluated for the Se-Te glass. The one used here is the Gibbs free energy of formation of the glass at the glass transition temperature compared to the melting enthalpy.

As expected, whatever was the parameter used to measure GFA, the Se rich glasses are good glass formers, their GFA increasing with the Ge addition.

Acknowledgements

This work was supported by CICYT project No. MAT88-439 which is acknowledged.

References

Bormann, R., Gärtner F., and Zöltzer, K. (1988): J. Less-Common Met. 145, 19.

Clavaguera-Mora, M.T. and Clavaguera, N. (1989): J. Mater. Res. 4, 906.

Ghosh, G., Lucas, H.L. and Delaey, L. (1988): CALPHAD 12, 295.

Greer, A.L. (1988): J. Less-Common Met. 145, 131.

Hruby, A. (1972): Czech. J. Phys. B22, 1187.

Kissinger, H.E (1956): J. Res. Nat. Bur. Stand. 57, 217.

Sakka, S. and Mckenzie, J.D. (1971): J. Non-Cryst. Solids 6, 145.

Saunders, N. and Miodownik, A.P. (1983): Ber. Bunsenges. Phys. Chem. 87, 830.

Suriñach, S, Baró, M.D., Clavaguera-Mora, M.T. and Clavaguera, N. (1983): J. Non-Cryst. Solids 58, 209.

Suriñach, S., Baró, M.D., Clavaguera-Mora, M.T. and Clavaguera, N. (1984): J. Mater. Sci. 19, 3005.

Suriñach, S., Calventús, Y., Baró, M.D., Clavaguera-Mora, M.T. and Clavaguera, N. (1990): to be published.

Thompson, C.V. and Spaepen, F. (1983): Acta Metall. 31, 2021.

Turnbull, D. (1969): Contemp. Phys. 10, 473.

Uhlmann, D.R. (1972): J. Non-Cryst. Solids 7, 337.

STRUCTURAL AND THERMODYNAMIC PROPERTIES OF LIQUID ALLOYS AT THE EUTECTIC COMPOSITION CASE OF THE GOLD-SILICON AND GERMANIUM-TELLURIUM SYSTEMS .

C.BERGMAN, C.BICHARA, R.BELLISSENT*, R.CEOLIN**, J.P. GASPARD*** and P.CHIEUX****

*LLB, CEA-CNRS - F-91191 Gif-sur-Yvette, France
**Faculté de Pharmacie - F-37042 Tours, France
***Université de Liège, Institut de Physique B-4000 Sart-Tilman, Belgium
****Institut Laue-Langevin, B.P.156X, F-38042 Grenoble, France

C.T.M., C.N.R.S., 26 rue du 141e R.I.A., F-13003 Marseille,France.

Abstract

Neutron diffraction measurements have been performed on the D4B and D20 spectrometers at the ILL (Grenoble), on gold-silicon and germanium-tellurium alloys, in the liquid state, at the eutectic composition. In the Au-Si case, the total structure factor shows the behavior of a liquid metal without variation with temperature ; for Ge-Te, the total structure factor shows a prepeak followed by three main peaks of quite similar amplitude at low temperature, presenting a remarkable evolution when increasing temperature. These results are brought together with the relative heat capacities data previously measured at the laboratory.

1 - Introduction

In a review (Bergman and Komarek,1985), the importance of the relative heat capacity of a liquid alloy has been emphasized and presented as a sensitive indicator of the chemical short-range order (CSRO). The word "chemical" is usually associated to distinguish the ordering (here tendency for heterocoordination) from the topological effects. Obviously, the diffraction experiments which yield the liquid structure factor, S(Q), related by Fourier transform to the pair correlation function, G(r), which describes the probability of finding another atom at a distance r from an origin atom, are very attractive for this purpose.

The aim of this study is to bring together the experimental informations obtained from both methods of investigation. Two different systems have been selected, the gold-silicon and the germanium-tellurium systems for the following reasons :
- both phase diagrams present an eutectic ($x_{Au} = 0.80$ in the first case and $x_{Te} = 0.85$ in the second one) for which the existence of CSRO is often correlated to the higher stability of the corresponding liquid phase.
- both systems have been investigated by calorimetry in the laboratory in order to obtain the relative heat capacity in a large temperature range above the eutectic temperature.

2 - Calorimetric study -

2.1 - Experimental

In both cases, the experimental procedure was the same ; the measurements were carried out with a high-temperature Calvet calorimeter. The determination of the enthalpy difference $\Delta^{T}_{298}h = h(T)-h(298)$ was performed by dropping solid samples (100 mg) at 298 K into the calorimetric cell at T under pure argon atmosphere. For each value of T, the measurements were repeated about ten times.

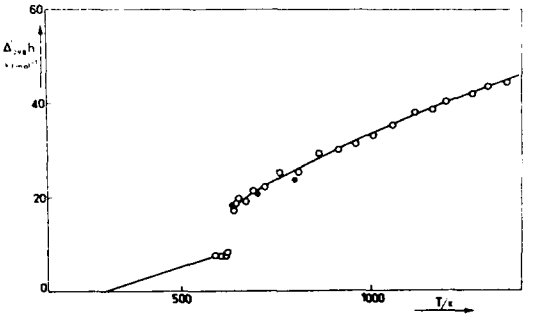

Fig. 1 - Molar enthalpy variation, $\Delta^{T}_{298}h$, of the $Au_{0.80}Si_{0.20}$ eutectic alloy with respect to T. o Castanet and Bergman, 1979 ; • Chen and Turnbull, 1967.

The calorimeter was calibrated by adding small quantities of National Bureau of Standards α-alumina into the melt after each series of measurements. These results have been reported in more details in previous papers (Castanet and Bergman,1979 and 1985) (resp. for Au-Si and Ge-Te.)

2.2 - Results

The measured variation of the heat-content, $\Delta^{T}_{298}h = h(T)-h(298)$ of the $Au_{0.80}Si_{0.20}$ liquid alloy (resp. $Ge_{0.15}Te_{0.85}$) is shown in the figure 1 (resp.figure 2) versus the temperature. The values of the heat capacity, C_p, of the liquid phase obtained by derivation and the values of the relative heat capacity (or excess heat capacity), ΔC_p, calculated as the deviation from the Kopp-Neumann rule are given in table 1 (resp. table 2) for the Au-Si liquid alloys (resp. the Ge-Te liquid alloys). These later values are calculated from the following relation :

$$\Delta C_p = C_p - \Sigma\, x_i C_{p,i} \qquad (1)$$

where x_i and $C_{p,i}$ refer respectively to the molar fraction in the corresponding alloy and to the heat capacity of the pure elements.

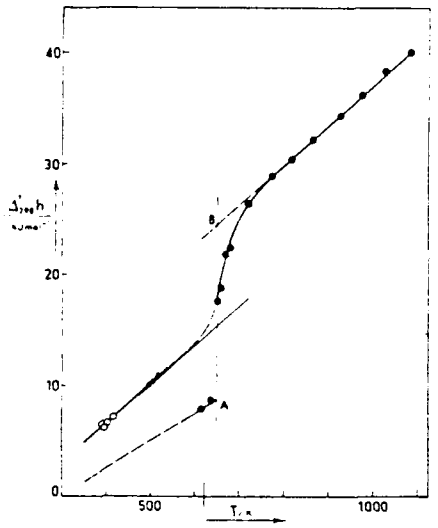

Fig. 2 - Molar enthalpy variation, $\Delta_{298}^{T}h$, of the $Ge_{0.15}Te_{0.85}$ alloy in the crystalline, supercooled and liquid states with respect to T. ● liquid state (drop method) ; o supercooled liquid (drop method) ; ▲ supercooled liquid (DSC).

In both cases, it can be seen that C_p is not constant with temperature, presenting a maximum value of 18.0 J.mol^{-1} K^{-1} (resp.183 J.mol^{-1} K$_{-1}$) at the eutectic composition of Au-Si alloys (resp. Ge-Te alloys). When increasing temperature, C_p falls and vanishes 500 °C above the eutectic temperature in the Au-Si alloys whereas in the case of the Ge-Te alloys, C_p reaches 0 less than 150 °C above the corresponding eutectic temperature.

Table 2.

Heat capacity, C_p, and relative heat capacity, ΔC_p, of the liquid eutectic alloy $Ge_{0.15}Te_{0.85}$

T/K	C_p/J mol^{-1}K^{-1}	ΔC_p/J mol^{-1}K^{-1}
650	219	183
670	155	119
690	96	60
710	64	28
730	47	11
750	41	5
770	37	1
790	36	0

Table 1.

Smoothed values of the enthalpy variation from 298 K to temperature T, of the heat capacity and the relative heat capacity of the $Au_{0.80}Si_{0.20}$

T/K	$\Delta_{298}^{T}h$ kJ mol^{-1}	Cp J K^{-1} mol^{-1}	ΔCp J K^{-1} mol^{-1}
625	17.74	48.7	18.8
650	18.95	47.9	18.0
700	21.30	46.2	16.3
750	23.57	44.5	14.6
800	25.75	42.8	12.9
850	27.85	41.1	11.2
900	29.87	39.5	9.6
950	31.80	37.8	7.9
1000	33.65	36.1	6.2
1050	35.41	34.4	4.5
1100	37.09	32.7	2.8
1150	38.68	31.0	1.1
1200	40.19	29.3	-0.6
1250	41.62	27.7	-2.2
1300	42.96	26.0	-3.9
1350	44.22	24.3	-5.5

Most often, such a variation of the relative heat capacity has been attributed to the presence of preferential interactions between unlike atoms (see for example Chen and Turnbull, 1967) and its evolution with temperature. However, in the case of tellurium-based alloys, the peculiar behavior of pure tellurium in the liquid state should definitely be taken into account in the interpretation.

3 - Neutron diffraction measurements

The samples were prepared by heating pure elements until the lowest melting temperature was reached, by levitation in the case of Au-Si and in a quartz container under vacuum for Ge-Te ; the alloys were then filled into cylindrical containers which were made from a Φ 6.10-8.14 mm (resp. Φ 5.94-7.10 mm) quartz tube in the case of Au-Si (resp. Ge-Te).

The neutron diffraction measurements were performed on the neutron diffraction spectrometers D20 and D4B located at the Institut Max Von Laue-Paul Langevin, Grenoble, France, operating respectively at a wavelength λ = 0.82 and 0.703 Å. The data were corrected for the quartz container, the 0.1 mm thick vanadium foil heater and the sample self absorption in the usual way. The corrections for inelasticity effects, multiple scattering and incoherent scattering were made according to Eisenberg et al.(1982).

3.1 - Au-Si alloys

3.1.1 - Structure factor S(Q)

The measurements were performed at three different temperatures, T/K = 680, 780

and 880, that is 50, 150 and 250°C above the eutectic point.

The structure factors measured at the two extreme temperatures, 680 and 880 K for $Q \leq 14$ A^{-1} are shown in the figure 3.

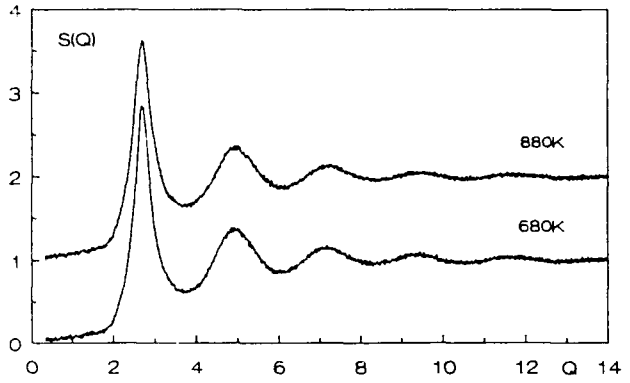

Fig. 3 - Structure factors, S(Q), of the liquid $Au_{0.80}Si_{0.20}$ eutectic alloy versus Q in $\AA^{-1}$, at two temperatures (the zero of the ordinate has been shifted by +1).

The first peak at $Q_1 = 2.70$ A^{-1} is relatively sharp followed by small peaks at $Q_2 = 4.95$, $Q_3 = 7.15$ and $Q_4 = 9.34$ A. The ratio Q_2/Q_1 is equal to 1.83, a value observed in many liquid structures. The structure factors measured at different temperatures compare very well as far as peak positions are concerned, suggesting no important change in the local order with increasing temperature. The lower amplitude of the first peak at 880 K shows nothing more than increasing thermal disorder.

3.1.2 - Thermodynamic limit

As the thermodynamic properties were measured by Knudsen-cell mass spectrometry (Bergman et al, 1978), the thermodynamic limit can be used to scale the data for the value Q = 0. Including also estimated values of the isothermal compressibilities and the densities, the following data were calculated :
S(0) = 0.030, 0.034 and 0.039 at T = 680, 780 and 880 K.
The densities values measured in the liquid state by Filonenko (1969) were discarded because they are not coherent with the observed volume expansion on solidification. Thus we estimated d = 15.6 g/cm³ from the densities of the pure solid elements adding 2% to take into account the volume variation.

3.1.3 - Pair correlation function

We have reported the two pair correlation functions, $G(r) = 4\Pi r\rho_0 [g(r)-1]$ obtained by Fourier transform of the structure factors, in the figure 4 at T = 680 and 880 K ; the peak positions at 680 K are $r_1 = 2.82$, $r_2 = 5.21$ and $r_3 = 7.40$ A followed by small oscillations up to 20 A which is the normal behavior in compact structures. Increasing the temperature by 200° does not affect the pair correlation functions. The number density ,as mentionned above, has been taken equal to 0.057 constant with respect to temperature and the

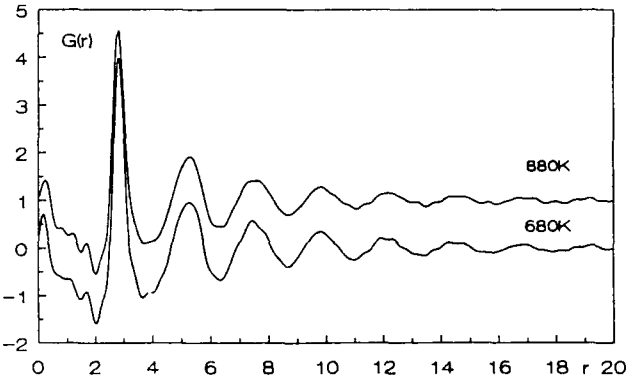

Fig. 4 - Pair correlation functions, G(r) , of the liquid $Au_{0.80}Si_{0.20}$ eutectic alloy, versus the distance r in Å at two temperatures (the zero of the ordinate has been shifted by + 1).

coordination number corresponding to the first neighbours shell is 11.8.

In the figure 5, the functions g(r) of the eutectic alloy at 880 K and of pure liquid Au (Waseda,1980) are reported and can be compared. It can be seen that they are quite similar, the main differences being a small shift in the peak positions (at shorter distances in the alloy) and the existence of a small hump effect on the left of the first peak in the eutectic alloy. Using the same method of calculation, the coordination number in pure liquid Au is found to be 10.8.

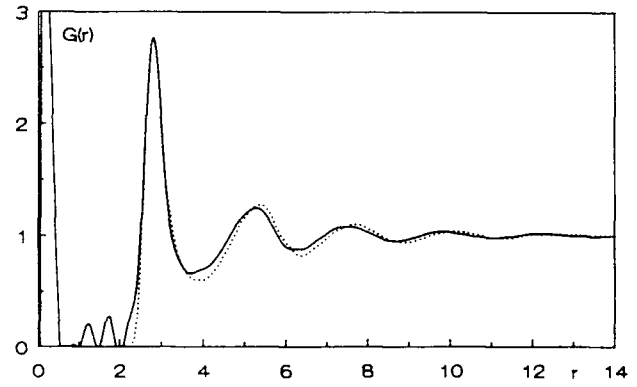

Fig. 5 - Comparison of the pair correlation functions, g(r), of the liquid $Au_{0.80}Si_{0.20}$ alloy at T/K = 880 (—) and of pure liquid Au at T/K = 1420 (---).

These results can be compared to those obtained by Waghorne et al (1976) from X-Ray diffraction measurements who have found the following values : r_1 = 2.73 and r_2 = 4.73 A.

3.2 - Ge-Te alloys

Neutron diffraction measurements have been performed on eutectic Ge-Te alloys by Nicotera et al (1972) and Neumann et al (1985,1987). The comparison with amorphous Ge-Te sample allowed the former authors to conclude that the transition from the liquid to the amorphous state is accompanied by a change of the coordination number (3.25 to 2.43). The combination of neutron and X-ray diffraction measurements performed by Neumann et al leads to the determination of the partial pair correlation functions and they propose a scheme where α-GeTe-like associates and pure Te-regions are coexisting in the low temperature liquid .

3.2.1 - Structure factor S(Q)

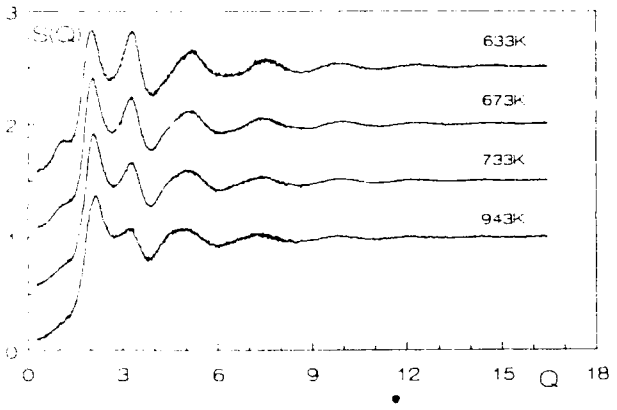

Fig. 6 - Structure factors, S(Q), of the liquid $Ge_{0.15}Te_{0.85}$ eutectic alloy versus Q in $Å^{-1}$, at different temperatures (the zero of the ordinate has been shifted by + 2).

Table 3.

Characteristics of the structure factor, S(Q), in $Å^{-1}$, for the eutectic $Ge_{0.15}Te_{0.85}$ alloys at different temperatures.

T (K)	Q_0	Q'_1	Q_1	Q_2	Q_3	Q_4
633	1.13	2.23	3.30	5.20	7.53	9.74
673	1.09	2.29	3.30	5.07	7.41	9.66
733	1.03	2.13	3.30	4.99	7.33	9.54
943	0.98	2.17	3.30	4.91	7.29	9.50

The measurements were performed at four different temperatures T = 943, 733, 673 and 633 K by decreasing the temperature in order to obtain supercooled liquid (T_{melt} = 648K) where CSRO is expected to be important. The structure factors measured for Q ≤ 17 $Å^{-1}$ at the different temperatures are represented in the figure 6 and the values of Q at which the maxima of S(Q) arise are given in the table 3. Three main observations can be made :
- the presence of a pre-peak, at Q_0, which vanishes with increasing temperature
- this small prepeak is followed by five peaks whose positions slightly shift towards small Q by increasing temperature, except the second one noted Q'_1 (cf table 3) whose maximum is located at the value 3.30 $Å^{-1}$ independent on T
- the intensity of this peak Q'_1 is strongly temperature dependent by opposite to the others which only show increasing thermal disorder.

3.2.2 - Thermodynamic limit

The estimation of the different thermodynamic data used in calculating the limit was made from the knowledge of the enthalpies of mixing measured by calorimetry at 1150 K, the densities measured by Nicotera et al (1972) and the isothermal compressibilities of the pure liquid elements. The following values were obtained : S(0) = 0.070, 0.073, 0.078 and 0.094 at T = 633, 673, 733 and 943 K.

3.2.3 - Pair correlation function

The four pair correlation functions $G(r) = 4\pi r\rho_0 [g(r)-1]$ are reported in the figure 7 ; the peak positions of the functions G(r), as well as the coordination number are given in the table 4. The main features are the following :

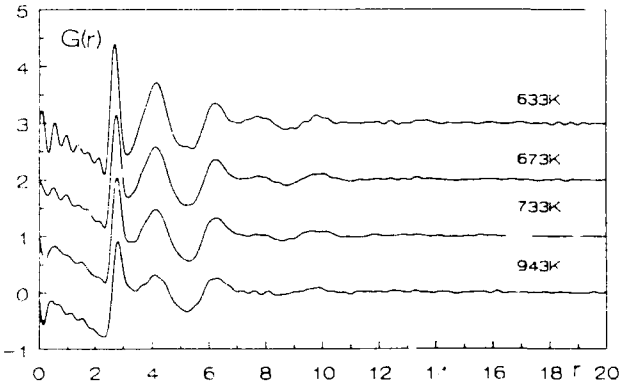

Fig. 7 - Pair correlation functions, G(r), of the liquid $Ge_{0.15}Te_{0.85}$ eutectic alloy versus r Q in $Å^{-1}$, at different temperature (the zero of the ordinate has been shifted by + 1).

-three main peaks are observed and the shape of the second peak smoothly changes with T up to the highest temperature where a sub-peak appears on the left side.
-the corresponding r_2 and r_3 values of the second and the third maximum (cf table 4) are constant while r_1 is varying from 2.68 to 2.86 in the temperature range investigated.

The number density determined by Nicotera et al (1972) takes the values : 0.0298, 0.0296, 0.0294 and 0.0298 at.A^{-3} by increasing T from 633 to 943 K . The corresponding coordination numbers given in the table 4 are obtained in the integration range $2.30 \leq r \leq 3.15$; the variation from 2.83 to 2.96 with increasing temperature is rather weak.

Table 4.

Peak positions of the pair correlation fonction $g(r)$ in Å and the coordination number n of the first shell for the eutectic $Ge_{0.15}Te_{0.85}$ alloy at different temperatures.

T/K	r_1	r'_2	r_2	r_3	n_1
633	2.68		4.12	6.17	2.83
673	2.67		4.12	6.17	2.89
733	2.67	(3.70)	4.12	6.17	2.95
943	2.86	3.67	4.12	6.29	2.96

3.2.4 - Comparison with pure tellurium

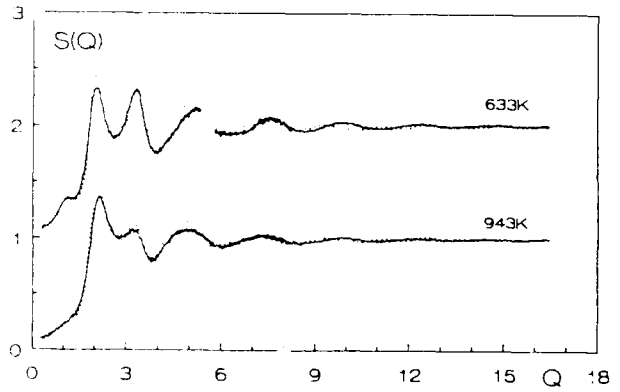

Fig. 8 - Comparison at two temperatures of the structure factors, S(Q), of the liquid eutectic Ge-Te alloy (—) and pure liquid Te at T/K = 740 (- -) (the origin of the ordinate has been shifted by + 1).

The figure 8 presents the total structure factors of the eutectic alloys at the two extreme temperatures as well as S(Q) of pure liquid tellurium given in Waseda (1980) at T/K = 740. It can be seen that the spectra differ much more at low than at high temperature. More recent measurements performed at different temperatures in supercooled and liquid tellurium (Menelle et al,1987) should also be compared in order to improve the analysis.

3.3 - Conclusion

At the present time, this study concerns essentially experimental results and allows us to present preliminary conclusions .

The structural and thermodynamic investigations of Au-Si and Ge-Te liquid eutectic alloys clearly show strongly different behaviors. If for both systems, the relative heat capacities are different from zero, the maximum value observed in the Ge-Te system is ten times higher than that of the Au-Si one ; furthermore, the temperature range in which the variation can be observed is 150 ° for Ge-Te and more than 450° for Au-Si, probably involving different mechanisms.

The structure factors and the pair distribution functions are very different too. The structure factor of the Au-Si eutectic alloy compares well with that of a liquid metal, characteristic of compact structures and does not show any significant variation with the temperature. It is very similar to that of pure gold. On the contrary, the structure factor of the Ge-Te eutectic alloy presents some characteristics of the liquid semiconductors with a prepeak vanishing at high temperature and three other peaks relatively temperature-insensitive in amplitude, slightly shifting towards low Q, within the investigated temperature range. However, the second peak which is located at Q'_2 (cf table 3) strongly varies as far as the intensity is concerned but is located at a constant Q value. A rough comparison with pure tellurium shows a tendency for the S(Q) of Ge-Te to become closer to pure Te at high temperature.

In conclusion, the thermodynamic study (especially the measurement of the relative heat capacity) can point out a peculiar temperature dependence even if no significant variation can be inferred from the stuctural study. Obviously, the development of simulation models is definitely necessary to go further in the interpretation of these results.

References

Bergman C., Chastel R., Gilbert M. and Castanet R., (1978) : High Temp. High Pressure, **10**, 581. 1
Bergman C. and .Komarek K.L., (1985) : Calphad, **9**, 1, 1.
Castanet R. and Bergman C., (1979) : Ann.Chim.Fr., **4**, 419.
Castanet R. and Bergman C., (1985) : Phys.Chem.Liq., **14**, 219.
Chen H.S. and Turnbull D., (1967) : J.Appl.Phys., **38**, 3646.
Eisenberg S., Jal J.F., Dupuy J., Chieux P. and Knoll W., (1982):Phil.Mag.A, **46**, 2, 195.
Filonenko V.A., (1969) : Russ.J.Phys.Chem., **43**, 874.
Menelle A., Bellissent R. and Flank A.M., (1987) : Europhys.Lett., **4**, 6, 705.
Neumann H., Matz W., Hoyer W. and Wobst M., (1985) : Phys.Stat.Sol.(a), **90**, 489.
Neumann H., Hoyer W., Matz W. and Wobst M., (1987):J.Non-Crystalline Solids. **97-98**,1251.
Nicotera E., Corchia M., De Giorgi G., Villa F. and Antonini M., (1972) : J.Non-crystalline Solids, **11**, 417.
Waghorne R.M., Rivlin V.G. and Williams G.I., (1976) : J.Phys.F., **6**, 147.
Waseda Y.,(1980 "The structure of non-crystalline materials", MGraw-Hill Ed.,253.

RELATIVE SOLID SOLUBILITY IN BINARY ALLOYS OF TRANSITION METALS

J.A. Somoza[+], J.A. Alonso[*] and L.J. Gallego[+]

[+]Departamento de Fisica de la Materia Condensada, Facultad de Fisica, Universidad de Santiago de Compostela, Spain

[*]Departamento de Fisica Teórica, Facultad de Ciencias, Universidad de Valladolid, Valladolid, Spain

Abstract.-

Predictions of relative solid solubility in binary alloys of transition metals are made using the semiempirical theory of Miedema. In this treatment the heat of solution of a solute metal S in a matrix metal M includes a chemical contribution, an atomic size mismatch contribution and a structural contribution. For low temperature phases the model's predictions are in good agreement with the available experimental information. We also calculate relative solid solubilities in some high temperature phases containing Zr and Hf, whose shear moduli are expected to be much smaller in this region than at low temperatures. Although these latter calculations are only approximate, the model's predictions are also encouraging in this case.

1.- Introduction

Relative solid solubility at the ends of the concentration range in the phase diagram of binary alloys has interested metallurgists ever since Hume-Rothery proposed his "relative valence rule" (Hume-Rothery et al. 1969). According to this rule a higher-valent metal is more soluble in a lower-valent metal than vice versa. Later work has clarified the situation a good deal. Gschneidner (1980) examined 300 systems formed by two metals of different valency and for which the terminal solid solubilities are known at both ends of the phase diagram; the result was that 55% of the systems do not obey the rule. Watson et al. (1983) found that the trends in TM-TM alloys (TM=transition metal) can be correlated with band theory concepts: in admittedly simplified terms, their observation is that the metal with a d-band closer to half-filled prefers to be the solute rather than the solvent.

Prediction of the correct trends in relative solid solubilities is a strong test for theories of alloy formation. Pettifor (1987) and Watson et al. (1983) extended to TM-TM alloys the successful d-band bonding model of the cohesive energies of transition metals (Friedel 1969). Then Watson et al. (1983) calculated the heats of solution of one transition metal in another and vice versa and found that the trend in the calculated heats of solution parallels that observed in the experimental relative solid solubilities.

A semiempirical model of alloy formation developed by Miedema and coworkers which was originally devised to describe liquid alloys and ordered solid compounds (Miedema et al. 1980) has recently been extended to handle terminal solid solutions (Niessen and Miedema 1983, López and Alonso 1985). As far as we know, the predictions of this model concerning relative solubilities have not been explicitly tested. This is the main objective of the present paper. Since in this model the heat of solution is the sum of three distinct components, a chemical contribution, an atomic size mismatch contribution, and a structural contribution, we have also looked at the relevance of each of these to the problem in hand. One of our objetives is, in fact, to propose a modification of the structural contribution which leads to an improved agreement with experiment concerning relative solubilities.

As shown elsewhere (Gallego et al. 1988, Van der Kolk et al. 1988) an accurate description of terminal solid solubilities is needed for theories which aim to predict the concentration range in which amorphous alloys can be obtained.

2.- A model for the heat of solution in substitutional alloys

Since the description of the heat of solution Δh (S in M) of a solute metal S in a matrix metal M is well documented elsewhere (Niessen and Miedema 1983), we only give here a brief account, with emphasis on the parts of the model which are relevant to our discussion below. Our work will be restricted to TM-TM alloys. For these, Δh (S in M) can be written as the sum of three terms

$$\Delta h\ (S \text{ in } M) = \Delta h^{chem} + \Delta h^{size} + \Delta h^{struct} \quad (1)$$

Δh^{chem} is a chemical term, equal to the heat of solution of liquid S in liquid M. The precise expression for Δh^{chem} is the core of Miedema's model (Miedema et al. 1980).

Δh^{size} is the elastic energy generated when a solute atom of volume V_S is forced into a hole of volume V_M in the matrix. Classical elasticity theory leads to the expression

$$\Delta h^{size} = \frac{2K_S G_M}{3K_S V_M^* + 4G_M V_S^*} (V_M^* - V_S^*)^2 \quad , \quad (2)$$

where K_S is the bulk modulus of the solute metal and G_M is the shear modulus of the matrix. V_M^* and V_S^* are effective volumes corrected for charge transfer effects (Niessen and Miedema 1983).

Finally, Δh^{struct} reflects the fact that in the transition metal series there is a well known correlation between the number Z of valence (s+d) electrons and the equilibrium crystal structure. This trend has been quantified by Niessen and Miedema (1983), who have derived the variation of absolute stability $E_\sigma(Z)$ (σ=bcc, fcc, hcp) of each of the main crystal structures in the transition metal series. In view of this correlation, it is reasonable to assume that structure dependent energies in TM-TM solid solutions also vary systematically with the average number of valence electrons per atom when the two metals form a common d-band. Consequently, dissolving metal S in a host M changes the energy that stabilizes the crystal structure of the host. The structural energy change upon dissolving metal S (with crystal structure σ) in the matrix M (with structure σ') can be written as

$$\Delta h^{struct}(S_\sigma \text{ in } M_{\sigma'}) = [E_{\sigma'}(Z(M)) - E_\sigma(Z(S))] + (Z(S) - Z(M))\left[\frac{dE_{\sigma'}(Z)}{dZ}\right]_{Z=Z(M)} \quad , \quad (3)$$

where the first term corresponds to the difference in structural energy of the pure metals and the second is the change in structural stability of the σ' structure due to the change in average valency. Evidently, Δh^{struct} can be easily computed from the stability functions $E_\sigma(Z)$.

In the following sections we employ the model described here to study the relative solubilities of systems whose phase diagrams present different degrees of complexity.

3.- Alloys without intermediate compounds

The experimental information on terminal solid solubilities is contained in phase diagram compilations (Hansen and Anderko 1986, Elliot 1986, Shunk 1986, Moffatt 1984). When intermediate phases do not exist, the only competitive phases are the terminal solid solutions of A in B and of B in A. In this case the relative solubilities will be controlled by the relative values of the heat of solution since the partial entropy of a phase is usually a small fraction of the partial enthalpy (Watson et al. 1983, Kubaschewski 1981). That is, the solubility of A in B will be larger than that of B in A if Δh (A in B) is more negative (less positive) than Δh (B in A), and both solubilities will be about equal if the two heats of solution have similar values.

Table 1 shows, for 39 alloys of 4d and 5d metals for which the above references give solubility data, whether there is agreement (Y) or not (N) between these data and the theoretical predictions based on comparison of values of Δh (A in B) and Δh (B in A) calculated using the model of Section 2 (alloys containing Y or La have not been included because it is expected that the solute atoms prefer to be interstitial in several systems based on those two metals). In the case of alloys containing Zr or Hf, the theoretical and experimental results considered are for temperatures at which the low temperature hcp phase of these two metals is the stable one.

Table 1. Comparison of predictions and experimental observations of relative solid solubilities in binary alloys without intermediate compounds. Agreement is indicated by Y and disagreement by N. Theoretical predictions are based on Δh of equation (1) with Δh^{struct} obtained from the unmodified stability functions of Niessen and Miedema (1983).

B	Zr	Nb	Mo	Tc	Ru	Rh	Pd	Hf	Ta	W	Re	Os	Ir	Pt
A														
Zr	Y							Y	Y					
Nb		Y						Y	Y	Y				
Mo									Y	Y				
Tc				Y	N	Y					Y	Y	N	N
Ru					Y	Y					Y	Y	Y	N
Rh						Y					N	N	Y	Y
Pd										Y		Y	Y	Y
Hf									Y					
Ta										Y				
W														
Re												Y	N	Y
Os													Y	N
Ir														Y
Pt														

Agreement with the heat of solution criterion is obtained in 31 cases (79%), and disagreement in 8 cases (21%): TcRh, TcIr, TcPt, RuPt, RhRe, RhOs, ReIr and OsPt. We think that the main source of the discrepancies lies in the theoretical predictions, for the following reason. The structural stability functions of Niessen and Miedema (1983) have been "smoothed" somehow. For σ=bcc, a minimum was introduced in $E_\sigma(Z)$ at Z=5.5 and a maximun at Z=8.5, and vice versa for σ=fcc and σ=hcp curves. Although this procedure seems reasonable it is not evident that it is better than just drawing straight lines between Z=4 and Z=5, and between Z=8 and at Z=9. In fact, the structural stability functions plotted by Skriver (1985), obtained from density functional calcula-

tions for the pure metals, do not display such "smoothed" behaviour.

Figure 1 shows the result of deleting the maxima and minima at Z=5.5 and Z=8.5. This change can obviously affect Δh^{struct} through the derivative $[dE_\sigma(Z)/dZ]$. When applied to the alloys of table 1 the modified heats of solution lead to agreement with experimental relative solubilities in 35 cases (90%) and discrepancy in only 4 (10%): TcPt, RuPd, RhOs and PdOs, two of which are common to table 1. The improvement obtained is significant.

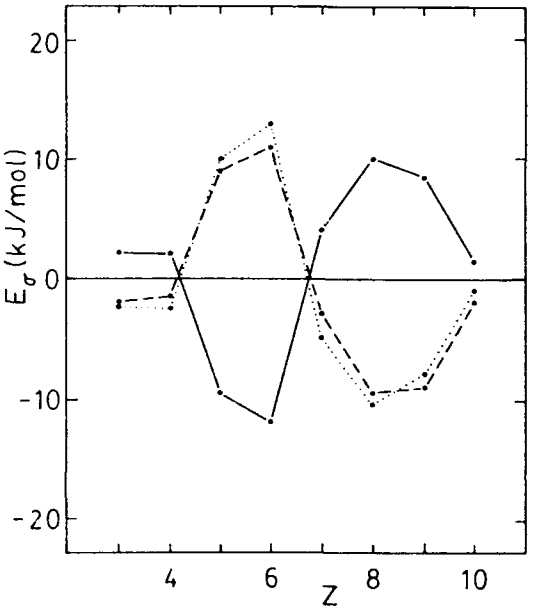

Fig.1. The structural stability E_σ of paramagnetic transition metals with bcc (——), fcc (- - -) and hcp (· · · · ·) structures as a function of the number Z of valence electrons per atom. These have been obtained after Niessen and Miedema (1983), but interpolating linearly between Z=4 and Z=5, and between Z=8 and Z=9.

4.- Alloys with intermediate phases

When intermediate phases are present, the dilute solution competes with its neighbouring compound and not with the other terminal solution. This question has been explored by Ansara (1979) and by López and Alonso (1985). The work of these authors illustrates the role played by line compounds in lowering the solubility limits. Nevertheless, it is appropriate, in first approximation, to follow the traditional route of making comparison between calculated heats of solution and relative solubilities (Watson et al. 1983, Ansara 1979).

Table 2 lists the results of comparing experimental relative solubilities with values of Δh, using the corrected values of Δh^{struct} calculated from fig. 1. The results for Zr or Hf alloys again correspond to temperatures at which the hcp phase of these two metals is the stable one. Of the 34 systems for which experimental data were found we obtained wrong predictions for only 5 cases (15%). When the uncorrected Δh^{struct} is used, 8 wrong predictions are obtained (24%).

Table 2. Comparison of predictions and experimental observations of relative solid solubilities in binary alloys with intermediate compounds. Agreement is indicated by Y and disagreement by N. Theoretical predictions are based on Δh of equation (1) with the corrected values of Δh^{struct} obtained from fig. 1.

B	Zr	Nb	Mo	Tc	Ru	Rh	Pd	Hf	Ta	W	Re	Os	Ir	Pt
A														
Zr		Y				Y	Y					Y	Y	
Nb				Y	Y	N	N				Y	N	N	Y
Mo			Y	Y	N	Y	Y				Y	Y	Y	Y
Tc														
Ru									Y	Y				
Rh									Y	Y				
Pd								Y	Y					
Hf										Y				
Ta											Y			Y
W											Y	Y	Y	Y
Re														
Os														
Ir														
Pt														

5.- Solid solubility in high-temperature phases

To calculate high temperature solid solubility it is necessary to know the temperature dependence of the elastic moduli K and G (see equation(2)). For several metals, such as Zr and Hf, it is known (Niessen and Miedema 1983) that at ΔT=1000 K, ΔG/G is about 50%, which is exceptionally large. Consequently the size mismatch contribution to the heat of solution in these metals will fall considerably with rising temperature.

We have compared the theoretical high temperature relative solid solubilities with the experimental information for some Zr and Hf alloys without intermediate compounds: ZrNb, ZrHf, ZrTa, NbHf and HfTa. The predictions were based on equation (1), with the corrected Δh^{struct} calculated for the high temperature bcc structures of Zr and Hf. As far as we know, the elastic constants of bcc-Zr and bcc-Hf are not available, so that we have taken for the bulk moduli the values corresponding to the low temperature hcp phases, and have assumed that the shear moduli are reduced by half. The values of the elastic constants of the other metals have been considered as independent of temperature. Of the 5 systems considered (all those for which sufficient experimental data are available), predictions and experiment agree in 4 (80%) and disagree in only

one, ZrTa, (20%). Given the simplicity of the approximation made concerning the elastic constants, these results can be considered successful.

An analogous study was finally performed for systems with intermediate compounds. The theoretical predictions were based on the same assumptions as above about the temperature dependence of the elastic constants of the various metals. Of the 13 systems considered (ZrMo, ZrRu, ZrRh, ZrPd, ZrW, ZrOs, ZrIr, ZrPt, MoHf, RuHf, PdHf, HfW and HfRe) we obtained correct prediction in only 7 cases: ZrMo, ZrRh, ZrPd, ZrIr, RuHf, PdHf and HfRe. Better results are nevertheless to be expected when more accurate estimates of the temperature dependence of the elastic constants become available.

The poorer quality of our predictions for alloys with intermediate compounds with respect to those for the case when intermediate phases are absent, reveals that a fully satisfactory theory of the relative terminal solubilities requires going beyond the simple comparison of heats of solution. Explicit consideration of the effect of intermediate compounds, as done for instance in our exploratory calculations (López and Alonso 1985), is then needed for this purpose.

6.- Conclusion

The semi-empirical model for the heat of solution of binary alloys developed by Miedema and coworkers provides a useful framework for studying the relative solid solubilities of transition metal systems. The predictions of the model are very successful for low temperature phases, especially when the correction that we have proposed for calculating the structural contribution is introduced. For high temperature Zr- and Hf-based alloys we have made an approximate estimation of the size mismatch contribution to the heat of solution by considering that the change in this quantity is mainly due to the known large reduction in the shear moduli of Hf and Zr with respect to the low temperature values. Although the results obtained with this assumption can be considered encouraging, it is expected that agreement with experiment will be better when a more accurate estimation of the temperature dependence of the elastic constants of the various metals is available.

Our results also suggest that the effect of intermediate compounds on the solubility of terminal phases should be taken into account for quantitative purposes when those compounds exist.

Acknowledgements

We acknowledge support by the DGICYT (Grant PB86-0654-C02).

References

Ansara, I. (1979): Int. Metall. Rev. 24, 20.

Elliot, R.P. (1986): Constitution of Binary Alloys, First Supplement (Schenectady, NY: Genium).

Friedel, J. (1969): The Physics of Metals, ed. J.M. Ziman (Cambridge: Cambridge Univ. Press) p 1.

Gallego, L.J., Somoza, J.A., Alonso, J.A. and López, J.M. (1988): J. Phys. F 18, 2149.

Gschneidner, K.A. (1980): Theory of Alloy Phase Formation, ed. L.H. Bennett (Warrendale, Pa.: Metall. Soc. AIME) p 1.

Hansen, M. and Anderko, K. (1986): Constitution of Binary Alloys, 2nd edn (Schenectady, NY: Genium).

Hume-Rothery, W., Smallman, R.E. and Haworth, C.W. (1969): The Structure of Metals and Alloys (London:The Institute of Metals).

Kubaschewski, O. (1981): High Temp.-High Pressures 13, 435.

López, J.M. and Alonso, J.A.(1985):Z. Naturforsch. a 40, 1199.

Miedema, A.R., de Châtel, P.F. and de Boer, F.R. (1980): Physica B 100, 1.

Moffatt, W.G. (1984): The Handbook of Binary Phase Diagrams (Schenectady, NY: Genium).

Niessen, A.K. and Miedema, A.R. (1983): Ber. Bunsenges. Phys. Chem. 87, 717.

Pettifor, D.G. (1987): Solid State Phys. 40, 43.

Shunk, F.A. (1986): Constitution of Binary Alloys, Second Supplement (Schenectady, NY: Genium).

Skriver, H.L. (1985): Phys. Rev. B 31, 1909.

Van der Kolk, G.J., Miedema, A.R. and Niessen, A.K. (1988):J. Less-Common Met. 145, 1.

Watson, R.E., Bennett, L.H. and Goodman, D.A. (1983): Acta Metall. 31, 1285.

THE INFLUENCE OF CRYSTALLINE ORIENTATION OF Cu-Zn-Al SHAPE MEMORY SINGLE CRYSTALS ON THERMAL EFFICIENCY.

J.M.GUILEMANY• and F.J.GIL+

•Metalurgia Física. Facultad de Química. Universidad de Barcelona. C/ Martí i Franqués 1. 08028.Barcelona. Spain.

+Ciencia de los Materiales e Ingeniería Metalúrgica. E.T.S.I.I.B. Universidad Politécnica de Catalunya. Avda.Diagonal 647. 08028 Barcelona. Spain.

Abstract.-

The thermal efficiency of three single crystals of identical chemical composition and different crystalline orientation has been determined. Due to the shape memory effect, these single crystals can convert heat produced by temperature differences into mechanical energy. It can be seen than the single crystals of lesser interplanar distance in relation to compression axes have greater thermal efficiency.

1. Introduction.-

The possibility of converting thermal energy into mechanical energy through memory effect materials has been studied by authors such as (Ahlers 1975)(Tong et al. 1974), who have built various prototypes of solid state engines with Cu-Zn-Al and Ni-Ti alloys.

These prototypes are based on two way memory effect in which the material can be made to remember successively and cycles both the β and martensite form; despite being submitted to up to 70 Kg/mm^2 compression stress. This two way memory effect is acheived through a training process (Guilemany et al. 1990).

An ideal solid state engine must be made with single crystals with total (Martensite---→ β) retransformation, since both polycrystal grain boundaries and stabilized martensite have an associated energy which diminishes the engine efficiency.

The thermal efficiency is given by the equation (Ahlers 1975) (Tong et al. 1974)(Wollats 1979)

$$\eta_t = \frac{\Delta H \, \Delta To}{To(C_p \Delta To + \Delta H(\sigma))} \qquad [1]$$

where:

C_p: specific heat of the alloy.

ΔH: transformation enthalpy.

$$\Delta To = To(\sigma) - To \qquad [2]$$

in which To, the equilibrium temperature, can be calculated by the expression (Salzbrenner 1980)

$$To = 1/2 \, (Ms + As) \qquad 3$$

in which Ms is the start (β ---→ Martensite) transformation temperature and As is the start (Martensite---→ β) retransformation temperature.

The temperature $To(\sigma)$ can be approximated as:

$$To(\sigma) = 1/2(Ms^{\sigma \to 0} + As^{\sigma \to 0}) \qquad [4]$$

containing $Ms^{\sigma \to 0}$ the start (β ---→ Stress Induced Martensite, S.I.M.) transformation temperature, and $As^{\sigma \to 0}$, the start (S.I.M.---→ β) retransformation temperature extrapoled to zero stress.

The stress induced transformation enthalpy can be expressed as (Wollats 1979):

$$\Delta H(\sigma) = \frac{(\Delta H \; To(\sigma))}{To} \qquad [5]$$

2. Experimental Procedure.-

The three single crystals were obtained by the Bridgman method (Guilemany et al.1988) and have a chemical composition in atomic percentage of 68.67% Cu, 16.22% Zn and 15.11% Al with an electron to atom ratio of 1.464.

The crystalline orientations of the planes perpendicular at the compression axes, determined by Laue method were (311), (321) and (322). The specific heat of these alloys is 0.595 J/gK (Hodgman 1970).

The calorimetric system used has already been described in previous papers (Muntasell et al. 1988)(Muntasell et al. 1989). The system allows the measurement of the characteristic temperatures Ms, Mf, As and Af, while the transformation enthalpy, ΔH, is calculated by integration of the calorimetric curve.

Cylindrical samples used (5 mm diameter, 6 mm high, 400 mg mass) underwent a heat treatment consisting of 10 minutes at 850°C and water quench to room temperature. This flow calorimeter measures differential signals (ΔT) by means of thermobatteries MELCOR. Temperature was measured by means of a

standard Pt-100 probe.

The compression tests were carried out on the same samples, after the calorimetric test, using a Houndsfield W machine at different temperatures (0, 10, 20, 30, 50 and 70°C). The rate at which stress was applied to the sample was 10 MN/m^2s (Gil 1989).

3. Results and Discussion.-

Table I gives the measured martensitic transformation temperatures, the equilibrium temperatures and enthalpies associated with the transformation. No considerable differences can be seen in these values with crystalline orientation. This is due to the fact that thermal origin transformation has 24 "Self Accommodation" martensite variants.

The measured transformation stress corrected by Schmid factor ($\beta \rightarrow$ S.I.M.) for each single crystal and test temperature, are shown in Table II. As the crystalline orientation are in the same stereographic triangle the single crystals will have identical Schmid factor, which in this case and in accordance with (Mellor 1989) (Lovey 1989) and (Gil 1989) is 0,4 in relation to slip plane.

As the temperature increases, an increase in stress can be observed. This increase can be explained by the fact that the stability of β-phase is greater as the temperature increases. The stress has to increase so that mechanical energy may overcome the thermodynamic stability.

From linear equations of the stress required to induce martensite (corrected by Schmid factor) versus test temperature (Table II) it was possible to obtain the Ms and As temperatures by extrapolation to zero stress. The equilibrium temperature under stress To(σ) is calculated by equation [4] . The above temperatures are shown in Table III as in enthalpy associated with stress induced martensitic transformation calculated by equation [5].

Thermal efficiency calculated from equation [1] shows that there is a strong influence single crystals orientation. Thermal efficiency was greater when the interplane distances in relation to compression axes were small. When the interplane distances are small, the martensitic plates have a greater amount of stored elastic energy, since in this case there is more internal stress and contact surfaces between martensite plates and β-martensite interphases. This brings about a great conversion to mechanical energy with the same calorific energy.

Acknowledgements.-

The present research was supported by CICYT project MAT 89-0407-C03-02.

References.-

Ahlers M. (1975): Scripta Met. 9, p.7174.
Gil F.J. (1989): Doctoral Thesis. University of Barcelona.
Guilemany J.M., Mellor B. and Fernández J. (1990): Scripta Met. To be submitted.
Guilemany J.M., Gil F.J.and Miguel J.R. (1988): Rev. Metall. 24 (3) p.175.
Hodgman C.D. (1970): Handbook of Chemistry and Physics 56 edition. Ed. CDH. Cleveland. U.S.A.
Lovey F.C. (1989): "Diffusionless and related phase transformations". Book of the course "The science and technology of shape memory alloys". COMETT 87/2/C-2/00863. Barcelona. p. 110.
Mellor B. (1989): "Martensitic transformation and the shape memory effect". Book of the course: "The science and technology of shape memory alloys", COMETT 87/2/C-2/00863. Barcelona. p.274.
Muntasell J., Tamarit J.L., Guilemany J.M., Gil F.J., Cesari E. (1988): Mat.Res.Bull.23 p.1585.
Muntasell J., Tamarit J.L., Guilemany J.M., Gil F.J., and Cesari E. (1989): Mat.Res. Bull. 24 p.450.
Salzbrenner R.J. and Cohen M. (1980): Acta Metall. 24, p.739.
Tong H.C. and Wayman C,M. (1974): Acta Metall 22, p.987.
Wolla ts P., Bonte M. and Roos J. (1979): Z.Metallkde 70, p.113.

TABLE I. Transformation and equilibrium temperatures. Martensitic thermal transformation enthalpy.

Crystalline Orientation	Ms (K)	Mf (K)	As (K)	Af (K)	To (K)	ΔH (J/g)
(311)	284	253	266	292	275	6.2
(321)	283	252	266	289	275	5.8
(322)	284	253	266	290	275	6.5

TABLE II. Transformation and retransformation stress corrected by Schmid factor for differents test temperatures.

Crystalline Orientation	T (°C)	$\sigma_{SCH}^{\beta\to M}$ (MN/m^2)	$\sigma_{SCH}^{M\to\beta}$ (MN/m^2)	Equation σ_{SCH}/T
(311)	0	17.6	4.8	
	10	33.2	17.6	
	20	45.8	22.8	$\sigma_{SCH}^{\beta\to M} = 23.20 + 1.15T$
	30	59.6	35.2	$\sigma_{SCH}^{M\to\beta} = 6.38 + 0.94T$
	50	87.1	59.6	
	70	98.0	68.8	
(321)	0	27.2	--	
	10	44.6	17.0	
	20	58.0	28.0	$\sigma_{SCH}^{\beta\to M} = 32.13 + 1.29T$
	30	77.6	40.0	$\sigma_{SCH}^{M\to\beta} = 7.26 + 1.03T$
	50	103.1	58.0	
	70	116.0	80.2	
(322)	0	24.5	6.8	
	10	48.8	14.6	
	20	66.0	26.0	$\sigma_{SCH}^{\beta\to M} = 34.97 + 1.21T$
	30	76.0	34.9	$\sigma_{SCH}^{M\to\beta} = 8.21 + 0.78T$
	50	102.2	45.6	
	70	111.8	63.0	

TABLE III. Temperatures and enthalpy values associated with stress martensitic transformation Thermal efficiency values.

Crystalline Orientation.	$Ms^{\sigma\to 0}$ (K)	$As^{\sigma\to 0}$ (K)	To (σ) (K)	$\Delta H^{\sigma\to 0}$ (J/g)	ΔTo (K)	η_t (%)
(311)	253	288	271	6.1	4	1.06
(321)	248	288	268	5.7	7	1.50
(322)	245	284	265	6.2	11	2.03

APPLICATION OF THE WAGNER-SCHOTTKY MODEL TO NONSTOICHIOMETRIC INTERMETALLIC PHASES

Regina KRACHLER and Herbert IPSER

Institut für Anorganische Chemie der Universität Wien
Währingerstr.42, A-1090 Wien, Austria

Abstract.-
The Wagner-Schottky model is a statistical thermodynamic model for crystalline ordered nonstoichiometric phases. From the intrinsic disorder at the stoichiometric composition it is possible to calculate the equilibrium point defect concentrations at any composition within the phase boundaries. Using the Wagner-Schottky approach the authors have treated the B2- and B8-structures in a more general way than previously. The model is applied to the B2-phases ß´-PdMn and ß´-NiAl as well as to the B8-phases in the Ni-Sb and the Ni-Te system.

1.- Introduction

If we keep a closed binary system at constant pressure and constant uniform temperature the following thermodynamic equilibrium condition is valid:

$$(dG)_{T,p,N_1,N_2} = 0 \qquad (1)$$

(N_1 and N_2 are the numbers of atoms of components 1 and 2.)

In their model Wagner and Schottky (1931) derived expressions relating the chemical activities of the components of a nonstoichiometric ordered binary compound to the deviation from stoichiometry. It is the existence of imperfections in the basically ordered crystal lattice that is responsible for the phenomenon of nonstoichiometry. Deviations from stoichiometry are caused by point defects.

Three types of point defects are important: vacancies, interstitial atoms and substitutional defects, and the thermodynamic properties of the crystal depend on the equilibrium concentrations of the different types of point defects.

Equation (1) enables us in principle to derive the equilibrium point defect concentrations as functions of the deviation from stoichiometry. Using the concentrations of the different defects at stoichiometry (which are entirely due to thermal excitation) as parameters, it is possible to calculate their concentrations as functions of the composition within the nonstoichiometric compound.

2.- Basic assumptions

The distribution of the point defects is assumed to be statistical. In the case of interactions between point defects additional energetic terms are used in the expression for the Gibbs free energy, as it has been done previously by other authors, for instance by Anderson (1946), by Lightstone and Libowitz (1969), and by Geffken et al. (1972). In cases where the distribution of the point defects is not statistical, the occurring superstructures in the crystal lattice can be treated in the model by further dividing the individual sublattices into "sub-sublattices".

We take into consideration only the interior of the crystal, not the surface or a gas phase in equilibrium with the crystal. All entropy contributions other than configurational entropy are taken to be independent of composition. With this last assumption we follow Chang (1974), Neumann et al. (1976) and other authors.

3.- The equilibrium condition

Assuming that the crystal has already reached equilibrium with respect to all lattice imperfections except point defects, the Gibbs free energy may be expressed as a function of the various point defect numbers v_i:

$$G = G(p,T,v_1,v_2,\ldots v_n) \qquad (2)$$

In complete thermodynamic equilibrium the point defect concentrations are no longer independent variables:

$$(G)_{N_1,N_2} = G(p,T) \qquad \text{equilibrium}$$

If we keep a certain amount of the crystal at constant temperature and constant pressure, the equilibrium condition (1) has the following general form ("equ" means equilibrium):

$$(\partial G/\partial v_1)_{equ} dv_1 + \ldots + (\partial G/\partial v_n)_{equ} dv_n = 0 \qquad (3)$$

Equation (3) is supplemented by a sufficient number of additional relations, containing the dv_i. The additional relations exist because of the conditions that N_1 and N_2 are constants and because of the special defect

mechanism under consideration, that makes some of the dv_i become zero and others become dependent of each other.

With the help of the additional relations it is possible to eliminate all the dv_i in equation (3). The explicit form of equation (2) (see Wagner and Schottky, 1931) enables us to derive the $(\partial G/\partial v_i)_{equ.}$. Together with some relations resulting from the conditions that the mole number and also the composition of the intermetallic phase are fixed quantities, the equilibrium condition (3) yields a system of x independent equations for x unknowns that can in principle be solved.

4 - B2-structure model (CsCl structure)

The CsCl-lattice can be seen as two interpenetrating primitive cubic sublattices. In the completely ordered crystal the positions of the α-sublattice are occupied by atoms of kind A and those of the ß-sublattice by atoms of kind B only. Traditionally the B2-phases are divided into two groups. The first group is characterized by anti-structure atoms on both sublattices. Interstitial atoms or vacancies are not allowed in this type of defect mechanism (anti-structure or substitutional type). In the other group the only allowed point defects are vacancies on α-sublattice sites and A-atoms on ß-sublattice sites. The last defect mechanism has been called triple-defect type by Wasilewski (1968). Based on the Wagner-Schottky model a number of authors have developed theoretical models for the B2-structure, among them Chang and Neumann (1982) and Libowitz (1971). They all developed different sets of equations to be applied separately to anti-structure and triple-defect B2-phases. However, diffusion measurements (Gupta and Liebermann 1971, Hilgedieck and Herzig 1983) as well as theoretical considerations (Neumann 1980) show that all B2-phases are members of the same family. Substitutional defects and vacancies should be allowed on both sublattices.

The existence of thermal anti-structure atoms in B2-phases is caused by interchange between atoms on their regular lattice sites and nearest-neighbor vacancies. It may be assumed now that (for not too large deviations from stoichiometry) the tendency for this interchange is for each sublattice independent of composition. With such an assumption we are able to consider both types of defects, i.e. substitutional defects and vacancies on both sublattices (Krachler et al. 1989).

The model contains the following parameters, which are the concentrations of the allowed point defects at stoichiometry (intrinsic disorder):

$$\underline{a} = (N_A^{\beta}/N^l)_{stoich};$$

$$\underline{b} = (N_B^{\alpha}/N^l)_{stoich};$$

$$\underline{c} = ((N_{\square}^{\alpha} + N_{\square}^{\beta})/N^l)_{stoich}$$

N^l: total number of lattice sites (both sublattices)

N_A^{β}, N_B^{α}: numbers of anti-structure atoms

$N_{\square}^{\alpha}$, $N_{\square}^{\beta}$: numbers of vacancies on the α- and ß-sublattices.

Figures 1 and 2 show applications, together with experimental data points.

5.- B8-structure model (NiAs structure)

The ideal NiAs-lattice can be visualized as a hexagonally close packed array of metalloid atoms (main group element) where the octahedral holes are filled with transition metal atoms. The allowed point defects are vacancies in the regular transition metal sites (octahedral holes) and interstitial transition metal atoms (in the trigonal-bipyramidal holes). There are two particular ways of arranging the vacancies in the transition metal sublattice: they may either be distributed over all sublattice sites or they may be restricted to alternate layers resulting in a partially filled up CdI_2-type structure. The intrinsic disorder is caused by transition metal atoms which leave the octahedral positions and enter the trigonal-bipyramidal holes (interstitial positions). It is assumed that the metalloid sublattice (ß-sublattice) remains un-disturbed. The transition metal sublattice (α-sublattice) is divided into two parts (α_1 and α_2) consisting of alternate layers. The interstitial sites form a third sublattice, the i-sublattice.

The model contains the following parameters:

$$\underline{\alpha} = (N_{\square}^{\alpha 1}/N^l)_{stoich};$$

$$\underline{\beta} = (N_{\square}^{\alpha 2}/N^l)_{stoich}$$

$N_{\square}^{\alpha 1}$, $N_{\square}^{\alpha 2}$: numbers of vacancies in the α_1 and α_2 sublattices

N^l: total number of lattice sites (α_1, α_2 and ß-sublattices)

$\underline{H_i}$ = interaction energy for one mole of pairs of nearest-neighbor interstitial atoms.

$\underline{H_V}$ = interaction energy for one mole of pairs of nearest-neighbor vacancies.

For $\underline{\alpha} = \underline{\beta}$ the vacancies in the α-sublattice are distributed over all sites whereas an increasing difference between $\underline{\alpha}$ and $\underline{\beta}$ means that the number of vacancies in alternate layers starts to differ, approaching a partially filled CdI_2-type lattice for which one of the disorder parameters becomes zero.

Figures 3 and 4 show applications, together with experimental data points.

Acknowledgement

We want to thank Prof. K.L. Komarek for his permanent interest in this work.

References

Anderson, J.S. (1946): Proc. Roy. Soc. 185 A, 69.
Chang, Y.A. (1974): Treatise on Materials Science, vol. 4, editor H. Herman (New York:Academic Press) p 173.
Chang, Y.A. and Neumann, J.P. (1982): Progress in Solid State Chemistry, vol. 14, eds. W.L. Worrell and G.R Rosenblatt (Oxford:Pergamon Press) p 221.
Ettenberg, M., Komarek, K.L. and Miller, E. (1970): J. Solid State Chem. 1, 583.
Geffken, R.M., Komarek, K.L. and Miller, E.M. (1972): J. Solid State Chem. 4, 153.
Gupta, D. and Liebermann, D.S. (1971): Phys. Rev. B4, 1070.
Hilgedieck, R. and Herzig, Ch. (1983): Z. Metallk. 74, 38.
Krachler, R., Ipser, H. and Komarek, K.L. (1984): Z. Metallk. 75, 724.
Krachler, R., Ipser, H. and Komarek, K.L. (1989): J. Phys. Chem. Solids 50, 1127.
Leubolt, R., Ipser, H. and Komarek, K.L. (1986): Z. Metallk. 77, 284.
Libowitz, G.G. (1971): Metall. Trans. 2, 85.
Lightstone, J.B. and Libowitz, G.G. (1969): J. Phys. Chem. Solids 30, 1025.
Neumann, J.P. (1980): Acta metall. 28, 1165.
Neumann, J.P., Chang, Y.A. and Lee, C.M. (1976): Acta metall. 24, 593.
Steiner, A. and Komarek, K.L. (1964): Trans. Met. Soc. A.I.M.E. 230, 786.
Wagner, C. and Schottky, W. (1931): Z. phys. Chem. B11, 163.
Wasilewski, R.J. (1968): J. Phys. Chem. Solids 29, 39.

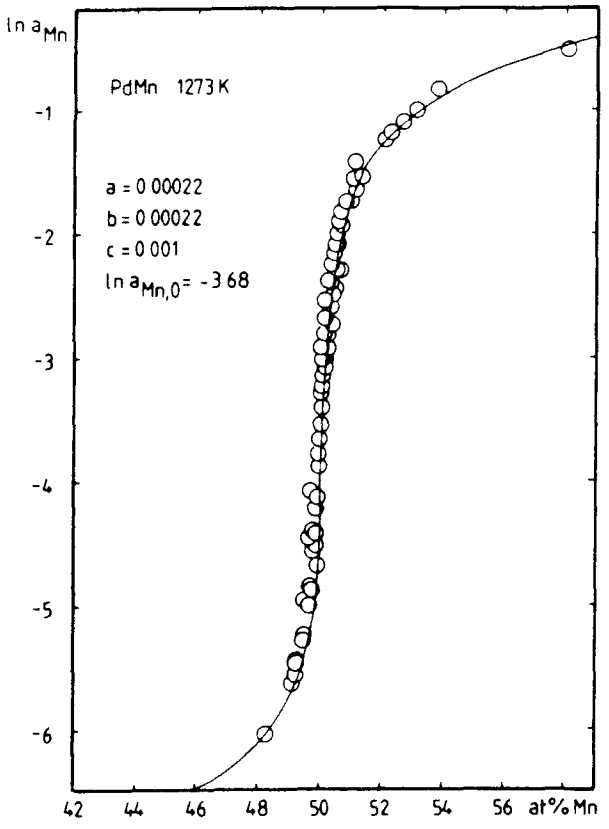

Fig.1. Activities of manganese in the ß´-PdMn phase at 1273 K. Standard state: ß-Mn(s). Experimental data points are from Krachler et al. (1984), the theoretical curve was calculated using the parameters given in the figure.

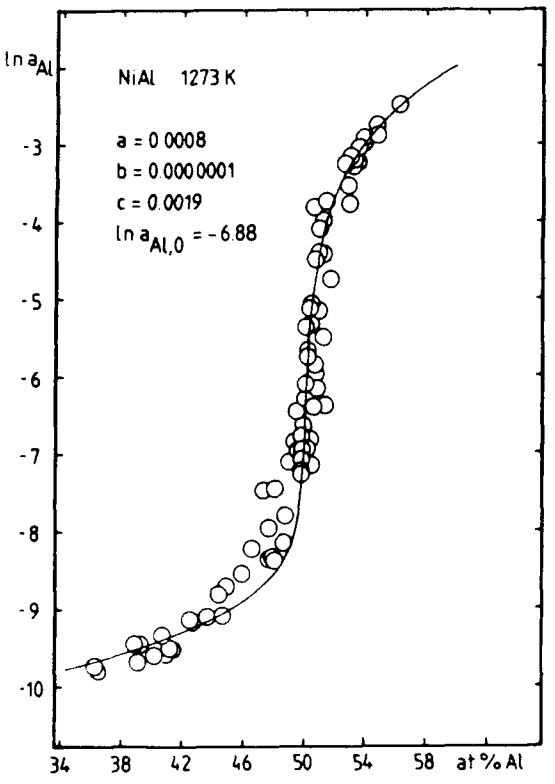

Fig.2. Activities of aluminum in the ß´-NiAl phase at 1273 K. Standard state: Al(l). Experimental data points are from Steiner and Komarek (1964). The theoretical curve was calculated using the parameters given in the figure.

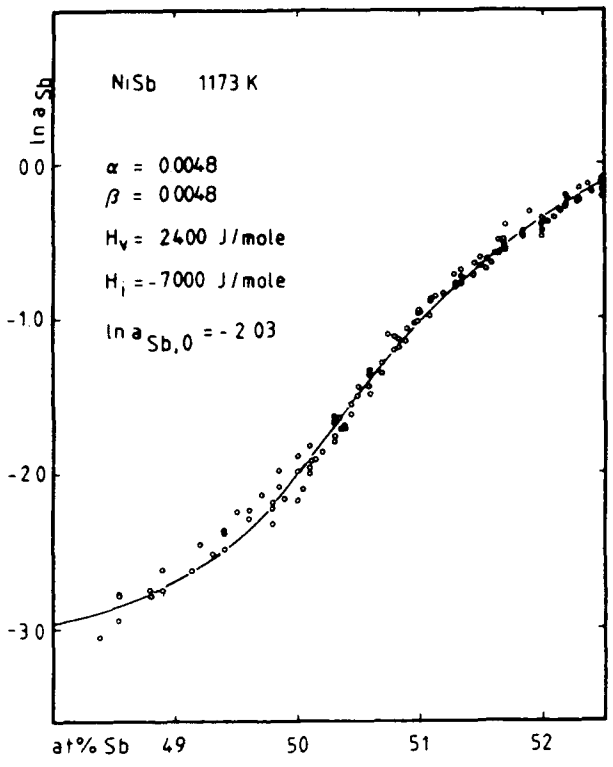

Fig.3. Activities of antimony in the γ-NiSb phase at 1173 K. Standard state: Sb(l). Experimental data points are from Leubolt et al. (19 . The theoretical curve was lated using the parameters given n the figure.

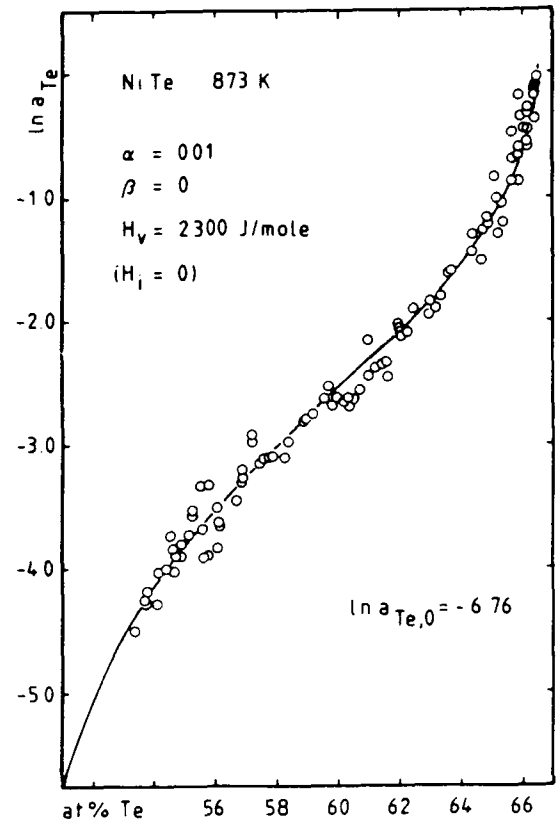

Fig.4. Activities of tellurium in the δ-NiTe phase at 873 K. Standard state: Te(l). Experimental data points are from Ettenberg et al. (1970). The theoretical curve was calculated using the parameters given in the figure.

Long Range Order Parameters for Multicomponent Compounds

Reinhard LÜCK, Norbert MÜNZER and Bruno PREDEL

Max-Planck-Institut für Metallforschung, Institut für Werkstoffwissenschaft and Institut für Metallkunde, Universität Stuttgart, Seestr. 75, D-7000 Stuttgart 1, F. R. Germany

Abstract

An ab initio description of the long range order of multicomponent alloys is carried out by a matrix, which is defined by the atomic fractions of each component for each sublattice. The large number of parameters can be reduced to some extend taking into account the boundary conditions. These parameters would be basic for a multicomponent Bragg-Williams theory. The processes of ordering and disordering are described by the loci of composition in geometrical representations for the different sublattices. Continous transitions as well as transformations in steps are possible.

1. INTRODUCTION

In the investigation of Heusler alloys (Heusler 1903) and related intermetallic compounds a change of the long range order (Webster 1969) may be observed during thermal treatment. Order-disorder transitions are possible in two steps (Wunsch 1981, Wachtel 1983). These transformations are of great interest, since the magnetic properties of these alloys are mainly influenced by lattice rearrangement on ordering and disordering. Since the ordering in multicomponent compounds cannot generally be described by one order parameter, an ab initio description for multicomponent compounds is developed in this paper.

2. BASIC IDEAS

Let ν_{IJ} be the fraction of I atoms ($I \in$ {A, B, C,..}) of the sites of the sublattice J ($J \in$ {X, Y, Z,..}). The following equation may be deduced accordingly to the definition:

$$\sum_{I}^{N} \nu_{IJ} = 1 \tag{1}$$

In the case of the stoichiometric composition the following equation also holds:

$$\sum_{J}^{N} \nu_{IJ} = 1 \tag{2}$$

Another possibility of defining is taking into account the fractions of the whole lattice:

$$\sum_{I}^{N}\sum_{J}^{N} \nu'_{IJ} = 1; \qquad \sum_{I}^{N} \nu'_{IJ} = \frac{1}{N}; \qquad \sum_{J}^{N} \nu'_{IJ} = \frac{1}{N} \tag{3}$$

with

$$\nu_{IJ} = N \cdot \nu'_{IJ} \tag{4}$$

A structure with N sublattices and N components needs N^2 quantities for the description. The $2N$ equations of Eqs. (1) and (2) result in $2N - 1$ conditions, since the last condition is obeyed automatically if the others are fulfilled. This procedure yields $(N - 1)^2$ free parameters.

A structure with two sublattices in a binary system can be described by one parameter. The long-range order parameter according to Bragg-Williams is well-known.

A structure with three equivalent sublattices in a ternary system (this is a fairly hypothetical case) could be described by the use of four long-range order parameters. Taking into account a condition of symmetry, which will be described later on, the number or free parameters will be reduced to three. Three parameters can be displayed in a three-dimensional diagram.

A structure with four equivalent sublattices, as in the Heusler alloys, in a quaternary system would need nine order parameters, the symmetry condition diminishes this number to six. Six parameters can only be displayed in a six-dimensional space.

A random distribution of atoms gives the relations

$$\nu'_{IJ} = \frac{1}{N^2} \quad \text{and} \quad \nu_{IJ} = \frac{1}{N} \tag{5}$$

Deviations from this values may be regarded as a measure of the order.

$$S_{IJ} = \nu_{IJ} - \frac{1}{N} \tag{6}$$

$$\sum_{I}^{N}(S_{IJ} + \frac{1}{N}) = 1 \quad \sum_{I}^{N} S_{IJ} = 0 \tag{7}$$

$$\sum_{J}^{N} S_{IJ} = 0 \tag{8}$$

A perfect order would result in the following equation

$$\nu_{IJ} = \delta_{IJ} \tag{9}$$

if the I and the J are defined accordingly, δ_{IJ} is the Kronecker symbol ($\delta_{IJ} = 1$ if $I = J$ and $\delta_{IJ} = 0$ else). Deviations from this may be considered as a measure of disorder:

$$\alpha_{IJ} = \delta_{IJ} - \nu_{IJ} \tag{10}$$

Eqs. (1) and (2) it follows

$$\sum_{I}^{N} \delta_{IJ} - \alpha_{IJ} = 1 \qquad \sum_{I}^{N} \alpha_{IJ} = 0 \tag{11}$$

$$\sum_{J}^{N} \delta_{IJ} - \alpha_{IJ} = 1 \qquad \sum_{J}^{N} \alpha_{IJ} = 0 \tag{12}$$

With Eqs. (10) and (11) a matrix of ν_{IJ} for $N = 4$ may be written as

$$\begin{pmatrix} \cdot & \cdot & \cdot \\ \cdot & \cdot & \cdot \\ \cdot & \cdot & \cdot \end{pmatrix}$$

Eq. (12) will yield other simplifications. In the following matrix Eq. (12) is taken into account for $N = 3$:

$$\begin{pmatrix} 1 - \alpha'_{12} - \alpha'_{13} & \alpha'_{12} + \Delta & \alpha'_{13} - \Delta \\ \alpha'_{12} - \Delta & 1 - \alpha'_{12} - \alpha'_{23} & \alpha'_{23} + \Delta \\ \alpha'_{13} + \Delta & \alpha'_{23} - \Delta & 1 - \alpha'_{13} - \alpha'_{23} \end{pmatrix}.$$

The expression Δ describes a circular exchange $x \rightarrow y \rightarrow z \rightarrow x$ which makes globally no sence, but locally, e. g. in the surroundings of antiphase boundaries, this may occur. In the following, this rotation can be neglected. The remaining three disorder parameters descibe the pairwise exchange for two of the sublattices.

In the case $N = 4$, the circular exchange is more complicated, three parameters Δ_i describe different circular four site exchanges. Four different circular three site exchanges can be composed by the circular four site exchanges. In binary systems with two sublattices no circular exchange exists.

$$\begin{pmatrix} \cdot & \cdot & \cdot & \cdot \\ \cdot & \cdot & \cdot & \cdot \\ \cdot & \cdot & \cdot & \cdot \\ \cdot & \cdot & \cdot & \cdot \end{pmatrix}$$

The remaining parameters are $\alpha_{12}, \alpha_{13}, \alpha_{14}, \alpha_{23}, \alpha_{24}, \alpha_{34}, \Delta_1, \Delta_2$ and Δ_3. If the circular exchange is neglected only six parameters are remaining. The rest matrices of the disorder parameters and of the occupation parameters are symmetric or can be transformed into the symmetric form by conventional methods.

The geometrical representation of the fractions of the different kinds of atoms in a sublattice will be carried out using a line for binaries, using a triangle for ternaries and for quaternaries a tetrahedron will be suitable. For the geometrical representations so many points are necessary as sublattices exist. In these geometrical representations Eq. (1) is regarded automatically. Eq. (2) may be transformed in geometrical rules, but the formulation is not simple in every case, especially if deviations from the stoichiometry occur.

Another possibility of geometrical representation is plotting fractions of each sublattice for all components, in this complementary representation Eq. (2) is regarded automatically. If the circular exchange is neglected the description will be slightly more clear (especially for $N = 3$ if for each sublattice a separate definition of the direction is chosen).

Limiting cases show an impressive clearness. Perfect long-range order requires that the loci of the sublattices are at the ends and in the corners, respectively (Fig. 1a). In the case of random solution the loci of all sublattices coincide and are situated at the points of the alloy composition (Fig. 1b). Partial orders may be described by the centers of edges or facets (Figs. 1c and 1d). The circular exchange is demonstrated together with partial order in Fig. 1c. The complementary representation giving the distribution of different sublattices for each component is demonstrated in Figs. 1e and 1f. Figs. 1e and 1f are in correspondence with Figs. 1b and 1c, respectively.

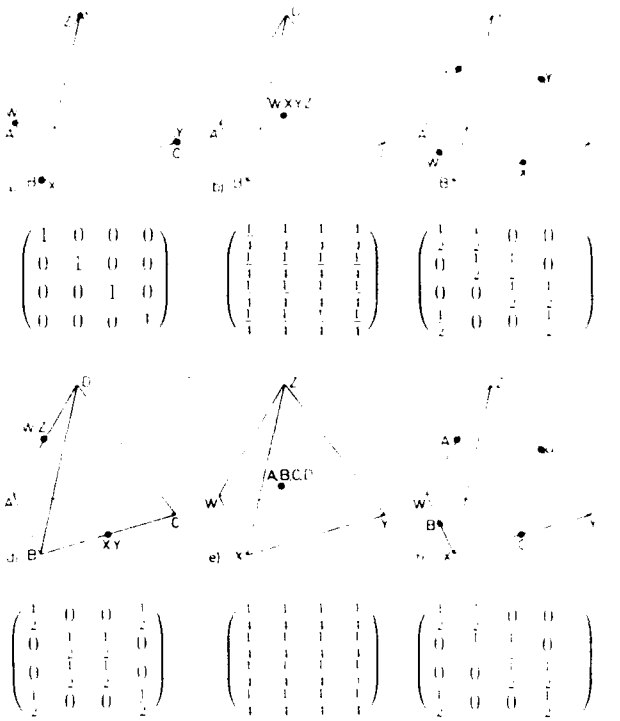

Fig. 1. Geometrical representations of matrices for quaternary systems. The matrices are shown for comparison. a.) Perfect order. b.) Random distribution. c.) Partial circular exchange in perfect order. d.) Partial order. e.) and f.) Complementary representation of the cases in b.) and c.)

3. ORDER-DISORDER PROCEDURES

Order-disorder procedures are described by curves connecting limiting cases. Figures 1 to 3 are constructed assuming a continous change of the degree of order, as it is known for higher order reactions. If the degree of order diminishes at a critical temperature discontinously to zero according to a first order reaction, a break of the curves through a 'two phase region' from the ordered state to the random solid solution must be imagined.

Figures 2 a to c represent the disordering in distinct steps. A different way of disordering is depicted in Figs. 2 d and e. A completely simultaneous disordering is given in Fig. 2 f.

If the process of disordering is partly simultaneous, curved loci as in Fig. 3 will arise.

In Heusler alloys the lattice sites A and C are occupied by the same species. Therefore the geometrical representation has to be modified (Fig. 4).

4. CONCLUSION

The representation used here may also be applied for deviations from stoichiometry and for vacancies. Equation (2) must be modified accordingly.

a)
$$\begin{pmatrix} 1 & 0 & 0 & 0 \\ 0 & 1-\frac{c}{2} & \frac{c}{2} & 0 \\ 0 & \frac{c}{2} & 1-\frac{c}{2} & 0 \\ 0 & 0 & 0 & 1 \end{pmatrix}$$

b)
$$\begin{pmatrix} 1 & \frac{c}{4} & 0 & 0 & \frac{c}{4} \\ 0 & \frac{1}{2} & \frac{1}{2} & 0 & 0 \\ 0 & \frac{1}{2} & \frac{1}{2} & 0 & 0 \\ \frac{c}{2} & 0 & 0 & 1-\frac{c}{2} & \end{pmatrix}$$

c)
$$\begin{pmatrix} \frac{1}{2}(1-\frac{c}{2}) & \frac{c}{4} & \frac{c}{4} & \frac{1}{2}(1-\frac{c}{2}) \\ \frac{c}{4} & \frac{1}{2}(1-\frac{c}{2}) & \frac{1}{2}(1-\frac{c}{2}) & \frac{c}{4} \\ \frac{c}{4} & \frac{1}{2}(1-\frac{c}{2}) & \frac{1}{2}(1-\frac{c}{2}) & \frac{c}{4} \\ \frac{1}{2}(1-\frac{c}{2}) & \frac{c}{4} & \frac{c}{4} & \frac{1}{2}(1-\frac{c}{2}) \end{pmatrix}$$

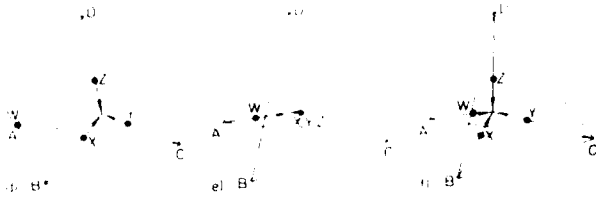

d)
$$\begin{pmatrix} 1 & 0 & 0 & 0 \\ 0 & 1-\frac{3}{4}\alpha & \frac{1}{4}\alpha & \frac{1}{4}\alpha \\ 0 & \frac{1}{4}\alpha & 1-\frac{3}{4}\alpha & \frac{1}{4}\alpha \\ 0 & \frac{1}{4}\alpha & \frac{1}{4}\alpha & 1-\frac{3}{4}\alpha \end{pmatrix}$$

e)
$$\begin{pmatrix} 1-\frac{3}{4}\alpha & \frac{1}{4}\alpha & \frac{1}{4}\alpha & \frac{1}{4}\alpha \\ \frac{1}{4}\alpha & \frac{1}{2}(1-\alpha) & \frac{1}{2}(1-\alpha) & \frac{1}{2}(1-\alpha) \\ \frac{1}{4}\alpha & \frac{1}{2}(1-\alpha) & \frac{1}{2}(1-\alpha) & \frac{1}{2}(1-\alpha) \\ \frac{1}{4}\alpha & \frac{1}{2}(1-\alpha) & \frac{1}{2}(1-\alpha) & \frac{1}{2}(1-\alpha) \end{pmatrix}$$

f)
$$\begin{pmatrix} 1-\frac{3}{4}\alpha & \frac{1}{4}\alpha & \frac{1}{4}\alpha & \frac{1}{4}\alpha \\ \frac{1}{4}\alpha & 1-\frac{3}{4}\alpha & \frac{1}{4}\alpha & \frac{1}{4}\alpha \\ \frac{1}{4}\alpha & \frac{1}{4}\alpha & 1-\frac{3}{4}\alpha & \frac{1}{4}\alpha \\ \frac{1}{4}\alpha & \frac{1}{4}\alpha & \frac{1}{4}\alpha & 1-\frac{3}{4}\alpha \end{pmatrix}$$

Fig. 2. Different procedures of disordering. a. to c.) Disordering in three distinct steps. d. and e.) Disordering in two distinct steps. f.) Disordering in one step.

Since the order of multicomponent compounds has to be described by a set of order parameters, it turns out that the energetic description will need a set of energy parameters.

a.)
$$\begin{pmatrix} 1-\frac{1}{2}\alpha_b & 0 & 0 & \frac{1}{2}\alpha_b \\ 0 & 1-\frac{1}{2}\alpha_a & \frac{1}{2}\alpha_a & 0 \\ 0 & \frac{1}{2}\alpha_a & 1-\frac{1}{2}\alpha_a & 0 \\ \frac{1}{2}\alpha_b & 0 & 0 & 1-\frac{1}{2}\alpha_b \end{pmatrix}$$

$$\begin{pmatrix} 1-\frac{1}{2}\alpha_c & \frac{1}{4}\alpha_c & \frac{1}{4}\alpha_c & \frac{1}{4}\alpha_c \\ \frac{1}{4}\alpha_c & (1-\frac{1}{2}\alpha_d)(1-\frac{1}{4}\alpha_c) & \frac{1}{2}\alpha_d(1-\frac{1}{4}\alpha_c) & \frac{1}{2}\alpha_d(1-\frac{1}{4}\alpha_c) \\ \frac{1}{4}\alpha_c & \frac{1}{2}\alpha_d(1-\frac{1}{4}\alpha_c) & (1-\frac{1}{2}\alpha_d)(1-\frac{1}{4}\alpha_c) & \frac{1}{2}\alpha_d(1-\frac{1}{4}\alpha_c) \\ \frac{1}{4}\alpha_c & \frac{1}{2}\alpha_d(1-\frac{1}{4}\alpha_c) & \frac{1}{2}\alpha_d(1-\frac{1}{4}\alpha_c) & (1-\frac{1}{2}\alpha_d)(1-\frac{1}{4}\alpha_c) \end{pmatrix}$$

c.)
$$\begin{pmatrix} (1-\frac{1}{2}\alpha_b)(1-\frac{1}{2}\alpha_c) & \frac{1}{4}\alpha_c & \frac{1}{4}\alpha_c & \frac{1}{2}\alpha_b(1-\frac{1}{2}\alpha_c) \\ \frac{1}{4}\alpha_c & (1-\frac{1}{2}\alpha_a)(1-\frac{1}{2}\alpha_c) & \frac{1}{2}\alpha_a(1-\frac{1}{2}\alpha_c) & \frac{1}{4}\alpha_c \\ \frac{1}{4}\alpha_c & \frac{1}{2}\alpha_a(1-\frac{1}{2}\alpha_c) & (1-\frac{1}{2}\alpha_a)(1-\frac{1}{2}\alpha_c) & \frac{1}{4}\alpha_c \\ \frac{1}{2}\alpha_b(1-\frac{1}{2}\alpha_c) & \frac{1}{4}\alpha_c & \frac{1}{4}\alpha_c & (1-\frac{1}{2}\alpha_b)(1-\frac{1}{2}\alpha_c) \end{pmatrix}$$

Fig. 3. Different procedures of partly simultaneous disordering. a.) According mainly to the procedures of Figs. 2a and 2b. b) According to Figs. 2d and 2e. c.) According to Figs. 2a, 2b and 2c.

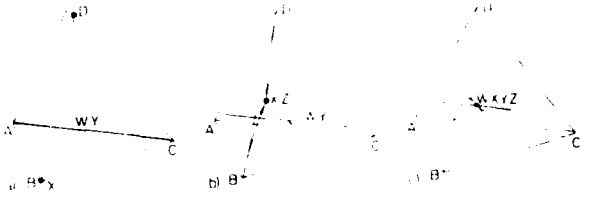

$$\begin{pmatrix} \frac{1}{4}\alpha_c & \frac{1}{2}(1-\frac{1}{2}\alpha_c) & \frac{1}{4}\alpha_c \\ (1-\frac{1}{2}\alpha_b)(1-\frac{1}{2}\alpha_c) & \frac{1}{4}\alpha_c & \frac{1}{2}\alpha_b(1-\frac{1}{2}\alpha_c) \\ \frac{1}{4}\alpha_c & \frac{1}{2}(1-\frac{1}{2}\alpha_c) & \frac{1}{4}\alpha_c \\ \frac{1}{2}\alpha_b(1-\frac{1}{2}\alpha_c) & \frac{1}{4}\alpha_c & (1-\frac{1}{2}\alpha_b)(1-\frac{1}{2}\alpha_c) \end{pmatrix}$$

If W ... aced by Y and A+C is replaced by A it follows

$$\begin{pmatrix} 1-\frac{1}{4}\alpha_c & \frac{1}{4}\alpha_c & \frac{1}{4}\alpha_c \\ \frac{1}{4}\alpha_c & (1-\frac{1}{2}\alpha_b)(1-\frac{1}{2}\alpha_c) & \frac{1}{2}\alpha_b(1-\frac{1}{2}\alpha_c) \\ \frac{1}{4}\alpha_c & \frac{1}{2}\alpha_b(1-\frac{1}{2}\alpha_c) & (1-\frac{1}{2}\alpha_b)(1-\frac{1}{2}\alpha_c) \end{pmatrix}.$$

Fig. 4. Geometric representation for a Heusler alloy. Component A and C may be identical. a.) Perfect order. b.) Disordering in two steps, partly simultaneous. c.) Random distribution.

REFERENCES

Heusler, F. (1903), Verh. Dtsch. Phys. Ges. **5**, 219.

Webster, P. J. (1969), Contemp. Phys. **10**, 559.

Wachtel, E., Henniger, F., and Predel, B. (1983), J. Magn. Magn. Mat. **38**, 305.

Wunsch, K. M., and Wachtel, E. (1981), J. Less-Common Met **80**, 23.

Enthalpy of formation and phase diagram of the Ga-Pb system

J.M. MIANE[+], P. REBOUILLON[+], R. BARET[+], M. GAMBINO[*] and J.P. BROS[*]

[+]Laboratoire de Chimie Générale, Faculté de Pharmacie
27, Bd J. Moulin 13385 Marseille CEDEX 5, FRANCE.

[*]Thermodynamique des Systèmes Métalliques, Université de Provence
3, Pl. V. Hugo 13331 Marseille CEDEX 3, FRANCE.

Abstract :

Using a high temperature Calvet calorimeter, the molar enthalpy of formation of liquid Ga-Pb alloys has been measured at 890 K on a large range of concentration.

D.T.A. experiments and heat capacities measurements in the solid and liquid states have been conducted using a D.S.C. calorimeter in order to confirm the limits of the miscibility gap.

1. Introduction :

As a part of our continuing thermodynamic study of binary or ternary alloys which presents a miscibility gap in the liquid state, we have investigated the Ga-Pb sytem.

This study deals with the enthalpies of formation of liquid Ga-Pb alloys at 890 K and the equilibrium phase diagram between 500 and 900 K.

2. Bibliographic survey :

2.1. Phase diagram equilibrium :

Due to Predel (1959) [PR1], by using D.T.A. measurements, this phase diagram equilibrium is resumed in the compilation of Elliott (1965) [ELL].

This system (fig. 1) presents a large miscibility gap between $0.024<x_{Pb}<0.954$ from 586 K to 880 K. Concentration ($x_{Pb}=0.954$) and temperature (T=586 K) correspond to monotectic reaction.

2.2. Thermodynamics properties :

In 1988, in their compilation Kawai and Shiraishi (1988) [KAW] have chosen the calorimetric measurements due to Predel and Stein (1971) [PR2]. These mixing enthalpies are in good agreement with the values obtained by Desideri and Piacente (1973) [DES] but they differ with Kwong and Munir (1973) [KWO] results, the both obtained from activities measurements (fig. 2).

3. Experiment :

3.1. Compound purity and measurements accuracy :

All measurements were performed under argon U atmosphere (cleaned by flow in titanium sponge at 1100 K) with high purity metals : gallium and lead with a purity of respectively, 99.995 % and 99.999 % from the Koch-Light Comp..

D.S.C. 111 apparatus allows us to reach the heat capacities values with a precision of 2 % and the values of the mixing enthalpy, which are measured with a Calvet calorimeter, are known with a precision of 3 %.

3.2. Heat capacities measurements :

By using a differential scanning calorimeter D.S.C 111 (SETARAM Soc.), with a linear programmation of the calorimeter temperature by steps [GA1], we have measured the heat capacities of nine Ga-Pb alloys ($0.1<x_{Pb}<0.9$ and $600<T/K<900$).

At the time of these experimentations, we have observed on the one hand, a large deviation from the Kopp-Neumann law in the miscibility gap region, and, on the other hand, a break in the curve of the heat capacities versus temperature when we reach the single liquid phase (fig. 3). This break allows us to determine the temperature limit between the miscibility gap and the monophase liquid region.

These results have been controlled by some D.T.A measurements and are gathered in figure 1 and table 1.

Table 1 :

Ga-Pb phase diagram: our results, literature data.

x_{Pb}	T/K		
	Cp	D.T.A.	Ref. Predel*
$0,02_4$			585
0,10	715	790	
0,15		801	
0,20	830		855
0,30	855		875
0,40	875		880
0,50	880	874	880
0,60	870		870
0,70	835		850
0,80	780		810
0,85		763	
0,90	680		710
$0,94_5$			585

*read on the Predel's graph [PR1]

These limit values determined both by heat capacities and thermal analysis are in good agreement. If all our results confirm the symmetry of the miscibility gap proposed by Predel (1959) [PR1], however, we have found some slight

differences from the coordinates of this limit.

Mixing enthalpies measurements:

In order to control the difference between the values proposed by Predel and Stein (1971) [PR2] determined by calorimetry) and Kwong and Munir (1973) [KWO] (derived from activities measurements), we have measured at 890 K the integral mixing enthalpy of eleven Ga-Pb liquid alloys by using a high temperature Calvet calorimeter (500K -1300 K). A detailed description of this apparatus has been already published by Gambino (1976) [GA2]. For our experimentations a complete automatisation has been carried out by Rebouillon (1989) [REB], (fig. 4).

Our experimental values presented in table 2 are described by the following equation:

$$\Delta_{mix}H_m = x_{Pb}(1 - x_{Pb})(21033,2 - 30261,4\ x_{Pb} + 27403,0\ x^2_{Pb} - 1,999\ 23x^3_{Pb})$$

Table 2

x_{Pb}	$\Delta_{mix}H_m$/J.mol^{-1} Experimental values
0.15	2186
0.29	3002
0.38	3065
0.40	3243
0.46	3201
0.51	3308
0.58	3092
0.62	3012
0.65	2752
0.71	2705
0.76	2588

These results have been compared with the literature (table 3) and are in good agreement with Kwong and Munir's (1973) determinations [KWO].

Table 3

$\Delta_{mix}H_m$/J.mol^{-1}

x_{Pb}	Predel 923 K	Kwong 1000 K	Desideri 1143 K	Kawai 1000 K	Exp.* 890 K
0.1	1172	1966	2100	1194	
0.2	3008	2343	3054	2990	2303
0.3	3519	3012	3556	3011	
0.4	3778	3347	3765	3800	3360
0.5	3853	3389	3840	3860	3394
0.6	3728	3096	3728	3700	3154
0.7	3227	2761	3284	2684	
0.8	2711	2008	2699	2770	2026
0.9	1629	1213	1611	1840	1222

* smoothed values.

4. Conclusion :

From these results we are able to specify the precedent determinations of the phase diagram in the liquid state and to confirm the mixing enthalpy of this system.

5. References :

[DES] Desideri A., Piacente V., (1973), J. Chem. Eng. Data,18,1,90-93.

[ELL] Elliott R.P., (1965), Constitution of Bynary Alloys, First supplement, Mc Graw-Hill Book Company.

[GA1] Gambino M., Rebouillon P., Bros J.P., (1989), J.Less-Common Metals ,154,195-205,

[GA2] Gambino M., (1976), Thèse Doct. es-Sc. Phys., Marseille.

[KAW] Kawai Y., Shiraishi Y., (1988), Handbook of Physico-Chemical Properties at Hight Temperature, The Iron and Steel Institute of Japan.

[KWO] Kwong A.F., Munir Z.A., (1973), J. Less-Common Metals,30,387-393.

[PR1] Predel B., (1959), Z. Metallkde,50,11,663-667.

[PR2] Predel B., Stein D.W., (1971) J. Less-Common Metals,24,159-171.

[REB] Rebouillon P., (1989), Thèse de l'Université de Provence-Sciences, France.

Fig. 1 Ga-Pb SYSTEM: PHASE DIAGRAM

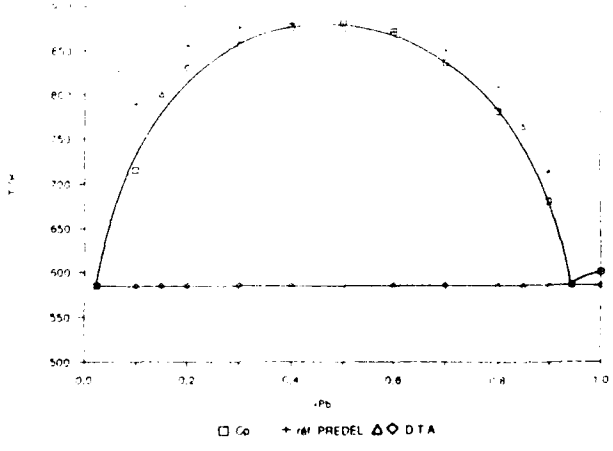

Fig. 2 Ga-Pb SYSTEM: MOLAR ENTHALPY

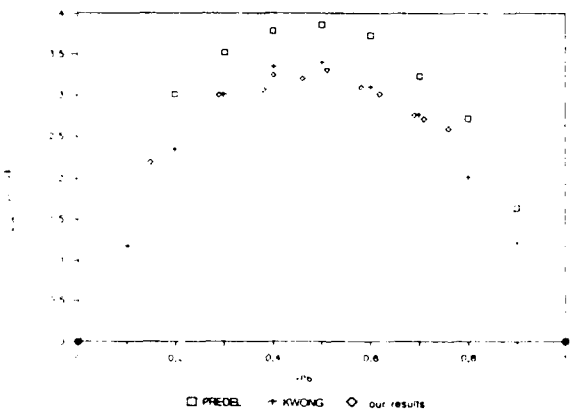

Fig. 3

Heat capacity measurements

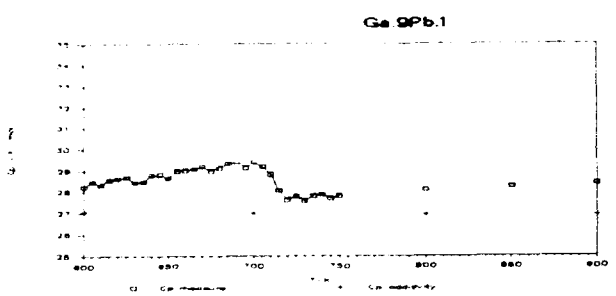

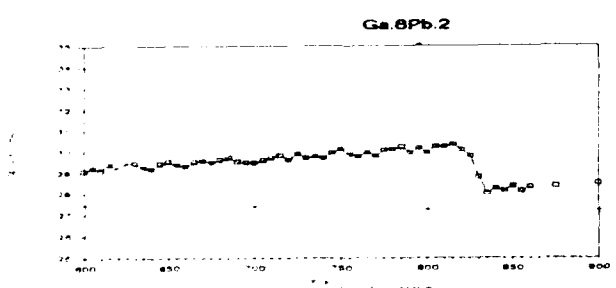

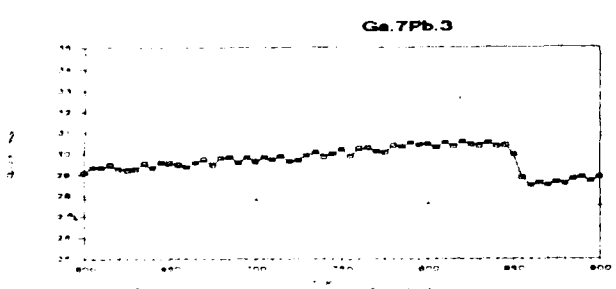

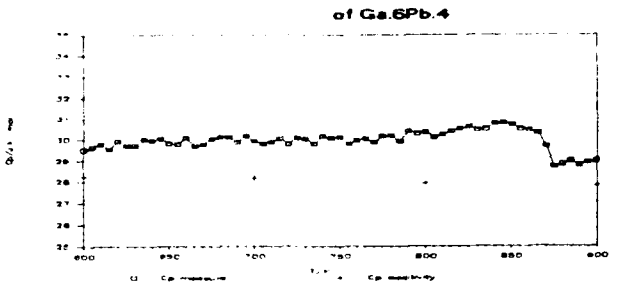

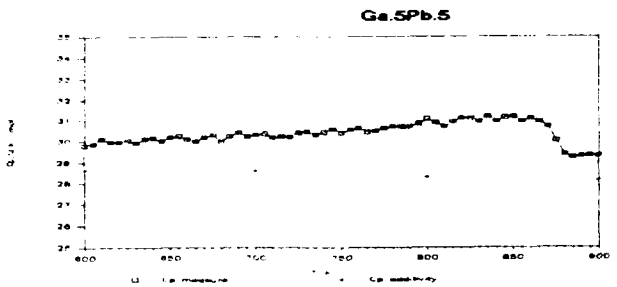

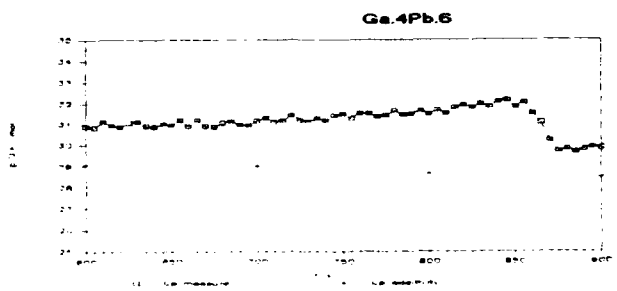

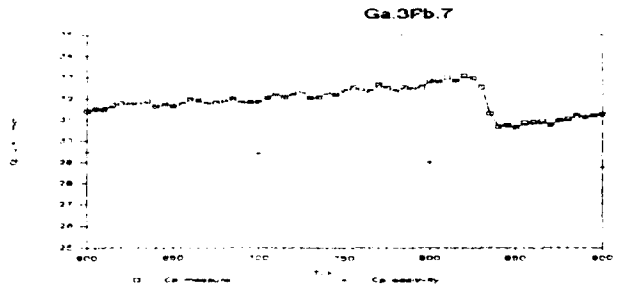

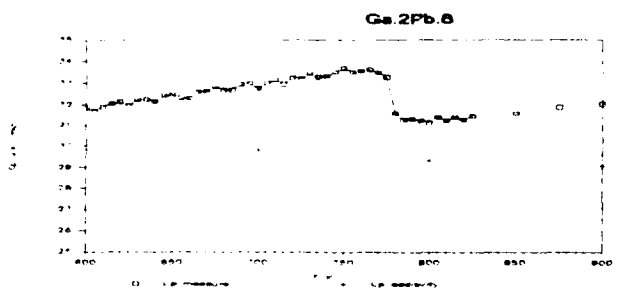

RARE EARTH-ALUMINIUM ALLOYS: OPTIMIZATION OF THERMODYNAMIC PROPERTIES AND PHASE DIAGRAM OF THE Ce-Al SYSTEM

Gabriele CACCIAMANI, Gabriella BORZONE and Riccardo FERRO
Istituto di Chimica Generale, Universita' di Genova, Viale Benedetto XV, 3,
I 16132 - Genova, Italia

Abstract.
Constitutional properties of the Ce-Al system are briefly summarized. The thermodynamic data concerning the formation of these alloys have been revised and compared with the experimental values recently obtained by our group in the measurements of the formation heats of the Ce-Al alloys. These data together with the already known phase diagram data, have been used to obtain an optimized description of the system.

1. - Introduction

The constitutional properties of the R-Al systems were recently assessed and presented by Gschneidner and Calderwood (1988 and 1989). In a recent paper Borzone et al. (1990) reported data concerning a thermodynamic investigation of the Ce-Al system.

2. - Ce-Al system

The phase diagram of the Ce-Al system was determined by Buschow and van Vucht (1966) and assessed by Gschneidner and Calderwood (1988). The following phases were reported:

α-Ce_3Al (low temperature phase), β-Ce_3Al (high temperature phase, congruent melting), CeAl (peritectic), $CeAl_2$ (congruent melting), $CeAl_3$ (peritectoidic), α-Ce_3Al_{11} (low temperature phase), β-Ce_3Al_{11} (high temperature phase, peritectic). No extended solid solubilities have been observed.

As for the thermodynamics of the R-Al alloys several investigations have been reported in literature (Gschneidner and Calderwood 1988 and 1989). In the specific case of the Ce-Al system the following thermodynamic properties have been described:

ΔH_f of solid alloys were investigated by acid solution calorimetry (Biltz and Pieper 1924), by liquid Al solution calorimetry (Colinet et al. 1985 and Sommer and Keita 1987), by direct calorimetry (Borzone et al. 1987). ΔH_{melt} of several compounds were measured by Sommer and Keita (1987); ΔG_{Ce} of solid alloys were studied by the e.m.f. method (Kober et al. 1982), ΔH_{mix} of liquid alloys were investigated by high temperature dissolution calorimetry (Esin et al. 1979, Zviadadze et al. 1976) and partial Gibbs free energy of mixing were measured by Knudsen effusion method (Shevchenko et al. 1979).

Several contradictions appear between the different measured values. A similar situation probably holds for several R-Al systems. This was noticed by Ran et al. (1989) while carrying out a thermodynamic optimization of the Al-Y system. Instead of using experimental values of ΔH_f they preferred to use a set of values estimated on the basis of the Miedema model. In the case of Ce-Al system we believe however that for the ΔH_f of the solid alloys the final values reported by Borzone et al. (1990) can be considered the most reliable. These values indeed were obtained from a new group of experimental data critically assessed taking into account the available information of other calorimetric investigations and the general alloying behaviour of cerium.

The assessed version of the phase diagram and the accepted trend of the ΔH_f are reported in figure 1.

3. - System optimization

The thermodynamic optimization of the system was carried out by using the Lukas program (Lukas et al. 1982).

The Gibbs free energy of the pure elements was expressed by the formula

$$G_{PE} = A - BT + CT(1 - \ln T) - DT^2/2 - E/(2T) - FT^3/6 \qquad (1)$$

and the coefficients A-F (reported in table 1) were interpolated from literature data (Chase et al. 1985).

The intermediate solid phases were described as stoichiometric and solid state transformations (when present) were ignored. Their Gibbs free energy is expressed by the formula

$$G_{SP} = G_{PE}(Ce) \cdot x_{Ce} + G_{PE}(Al) \cdot x_{Al} + \Delta H_f - T \cdot \Delta S_f \qquad (2)$$

The composition dependence of the excess functions of the liquid has been

TABLE 1 - Coefficients used in the analytical expression of the Gibbs free energy of the pure elements (see equation (1)).

Phase	A	B	C	D	E	F
γ-Ce	-6786.3	-125.24583	21.203316	.0163624	78324.	0.0
δ-Ce	-12102.9	-219.28903	37.614159	0.0	0.0	0.0
Ce(liq)	-7135.7	-217.40366	38.074402	0.0	0.0	0.0
Al(sol)	-10015.4	-148.49649	31.375809	-.0163929	-360661.	$2.0753\ 10^{-5}$
Al(liq)	-776.6	-145.62338	31.748199	0.0	0.0	0.0

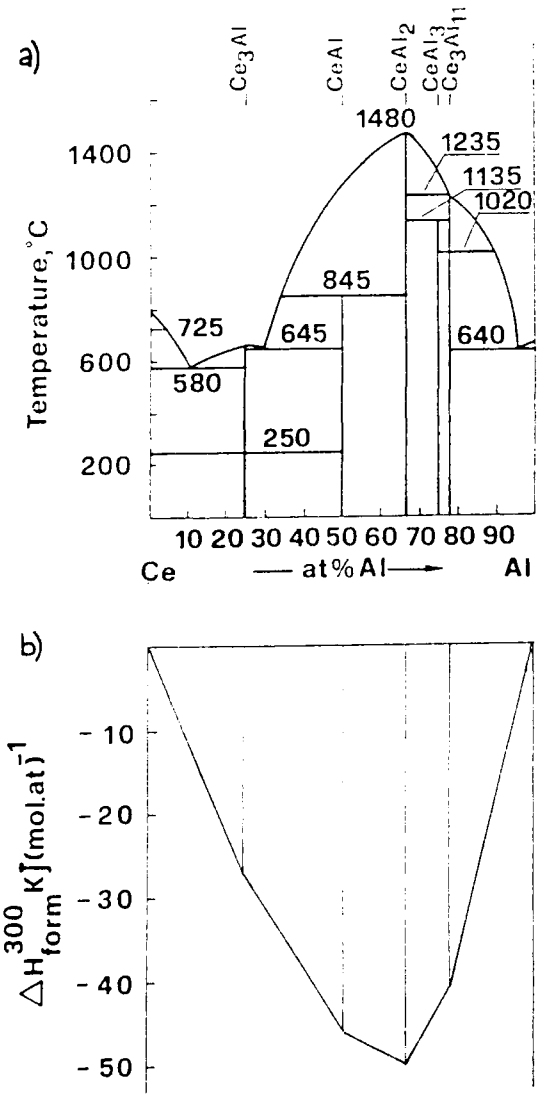

Fig.1 - Ce-Al system.
a) Phase diagram. The transformation temperatures of the different phases are indicated: 725°C γ-δ Ce; 250°C α-β Ce_3Al; 1020°C α-β Ce_3Al_{11}.
b) ΔH of formation of the solid Ce-Al alloys (Borzone et al. 1990).

TABLE 2 - Coefficients calculated (see equations (2) and (3)).

Phase	L_{0A}	L_{0B}	L_{1A}	L_{1B}
Liq.	-167593.1	-97.91327	36060	11.14867
Phase	**ΔH_f**		**ΔS_f**	
Ce_3Al	-27000*		-12.30281	
CeAl	-46000*		-20.39961	
$CeAl_2$	-50000*		-19.58768	
$CeAl_3$	-44000		-17.30780	
Ce_3Al_{11}	-41000*		-16.02630	

(*) These coefficients were not calculated but accepted from Borzone et al. (1990).

described by a series expansion of Legendre polynomials:

$$G^{ex} = x_{Ce} \cdot x_{Al} \cdot \Sigma(L_i \cdot P_i(x)) \qquad (i=0,1) \qquad (3)$$

where L_i are temperature dependent parameters of the form $L_{iA} - L_{iB} \cdot T$.

The thermodynamic descriptions of the Ce-Al phases were optimized by means of a least squares procedure described by Lukas et al. (1977).

Optimization was carried out using the following experimental data:

- Three phase equilibria and liquidus curves from the assessed phase diagram (Gschneidner and Calderwood 1988);

- ΔH_f of the solid phases (Borzone et al. 1990);

- ΔH_{dis} in liq. Al (Sommer and Keita 1987);

- ΔH_{melt} (Sommer and Keita 1987);

- ΔH_{mix} (Esin et al. 1979, Zviadadze et al. 1976).

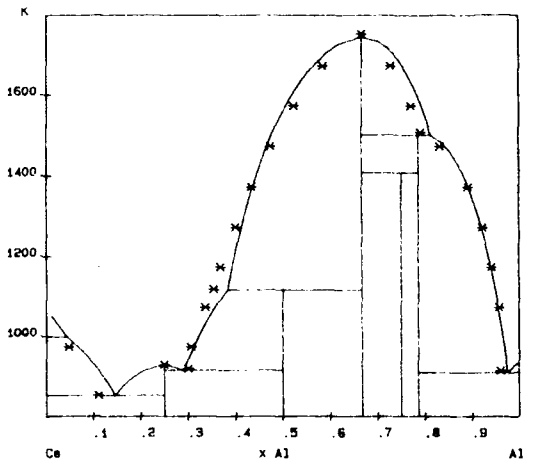

Fig.2 - Ce-Al system: computed phase diagram compared to the data points (*) belonging to the assessed liquidus curve (Gschneidner and Calderwood 1988).

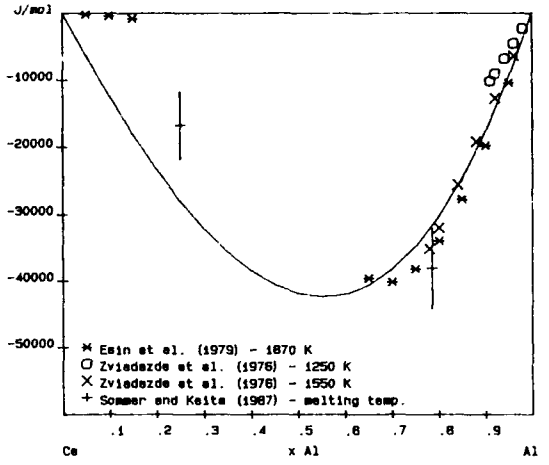

Fig.3 - Ce-Al system: computed and experimental ΔH_{mix}. The three Ce-richest experimental points after Esin et al. (1979) were not used in the calculation.

3.1 - Results and discussion

A preliminary calculation was carried out using all the experimental data cited above but the results were not completely satisfactory. A good agreement was obtained in a successive calculation after having rejected certain data reported in literature (Esin et al. 1979) for the ΔH_{mix} of the Ce-rich liquid alloys.

The parameters ΔH_f, ΔS_f and L_i occurring in the expressions (2) and (3) and now calculated are shown in table 2.

Figure 2 shows a comparison between the calculated and the experimental phase diagrams: the good agreement is apparent. Figure 3 summarises the trend of the calculated ΔH_{mix} in comparison to the experimental values (in a first approximation ΔH_{mix} was considered temperature independent because of the small differences reported for different temperatures and the low number of experimental points).

As a final consideration it should also be underlined that the overall consistence of the data seems to confirm the good reliability of the ΔH_f of the solid alloys recently determined and used in this optimization.

Acknowledgement

This research is part of the "Progetto finalizzato materiali" of the Italian "Consiglio Nazionale delle Ricerche" (CNR) which we thank for the financial support.

References

Biltz,W. and Pieper,H. (1924): Z. Anorg. Chem., 134, 13.
Borzone,G. Cacciamani,G. and Ferro,R. (1990): to be submitted.
Borzone,G. Cacciamani,G. Saccone,A. and Delfino,S. (1987): Proceeding XIII J.E.E.P., Lyon (France) 2-3/4/1987.
Buschow,K.H.J. and van Vucht,J.H.N. (1966): Z. Metallkd., 57, 162.
Chase,M.W.Jr. Davies,C.A. Downey,J.R.Jr. Frurip,D.J. McDonald,R.A. and Syverud,A.N. (1985): JANAF Thermochemical Tables, Third Edition, J. Phys. Chem. Ref. Data, 14, suppl.1.
Colinet,C. Pasturel,A. and Buschow,K.H.J. (1985): J. Chem. Thermodynamics, 17, 1133.
Esin,Yu.O. Ryss,G.M. Gel'd,P.V. (1979): Zh. Fiz. Khim., 53, 2380.
Gschneidner Jr.,K.A. and Calderwood,F.W. (1988): Bull. Alloy Phase Diagrams, 9, 658.
Gschneidner Jr.,K.A. and Calderwood,F.W. (1989): Bull. Alloy Phase Diagrams, 10, 28.
Kober,V.I. Nichkov,I.F. Raspopin,S.P. and Kondratov,A.S. (1982): Izv. Vyssh. Uchebn. Zaved., Tsvetn. Metall., 5, 101.
Lukas,H.L. Henig,E.Th. and Zimmermann,B. (1977): CALPHAD, 1, 225.
Lukas,H.L. Weiss,J. and Henig,E.Th. (1982): CALPHAD, 6, 229.
Ran,Q. Lukas,H.L. Effenberg,G. and Petzow,G. (1989): J. Less-Common Met., 146, 213.
Shevchenko,V.G. Kononenko,V.I. and Sukhman, A.L. (1979): Zh. Fiz. Khim., 53, 1351.
Sommer,F. and Keita,M. (1987): J. Less-Common Met., 136, 95.
Zviadadze,G.N. Chkhikvadze,L.A. and Kereselidze,M.V. (1976): Soobshch. Akad. Nauk Gruz. SSR, 81, 149.

THE METASTABLE PHASE IN Fe-C ALLOYS

Anatoly LJAKUTKIN
Institute of Nuclear Physics AS Kazakh SSR,Alma-Ata,480082

Abstract.-

The metastable bcc phase is crystallized from melts in Fe-C Alloys with contents of carbon up to 1.5 wt pct where the fcc phase is stable at high temperature. The measurements was conducted by the magnetic susceptibility method.

In the course of investigations of the phase transformations in Fe-C alloys by the Thermal Magnetic Analysis Method (in which the magnetic susceptibility of a dia - or paramagnetic substance is measured as a function of temperature) it was established that the melts of Fe-C alloys with contents of C up to 1.5 wt pct is crystallized into metastable bcc δ -phase , in spite of stability of fcc γ -phase at high temperature at alloys with contents of C more than 0.51 wt pct (Ljakutkin et al. 1984). This metastable δ -phase is transformated into stable γ -phase after certain supercooling the value of what was up to 100 C.

It was established also that melt of pure Fe is crystallised in any event into bcc δ -phase even then the supercooling of melt was bellow than 1400 C i.e. in the region of existence of fcc γ -phase . This is the evidence of preference bcc structure at high temperature and that a pattern of metallic melts is in more accordance with bcc than fcc structure. The solidification into a intermediate phases was discovered in some fcc metals (Ni,Co,Cu,Pt) (Ljakutkin 1982; Ljakutkin 1988).

The obtained results can be explained by the assumption that solidification occur in accordance with the diagram of metastable equilibrium (if the lines of solidus and liquidus of δ -phase is continued in the region of carbon contents more than 0.51 wt pct) (Ljakutkin et al. 1984).

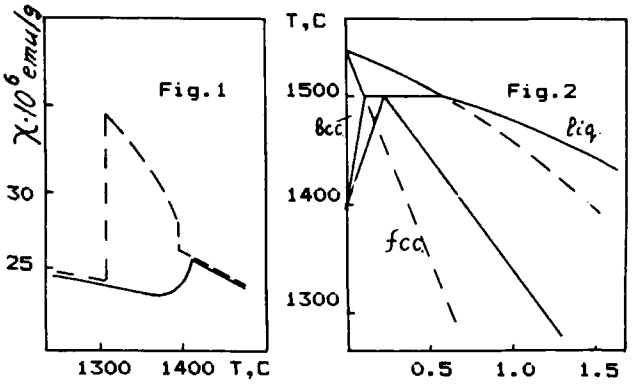

Fig.1. The temperature dependence of MS for alloy Fe-1.5C wt pct. —— heat. ;- - - cool.
Fig.2. Diagram Fe-C. The metastable equilibbrium is shown by the dotted lines.

References

Ljakutkin A. V. , Grigorovith V. K. and Ivakhnenko I. S. (1984) : Docl. Acad. Nauk SSSR , vol. 275, p 1449 (in Russian).

Ljakutkin A.V. (1982) : Phys . Metall. Metalloved. , vol. 54, p.129 (in Russian).

Ljakutkin A.V. (1988): Journ. Therm. Anal.: vol. 33, p. 865.

AUTHORS

REAL SOCIEDAD ESPAÑOLA DE FISICA

GRUPOS ESPECIALIZADOS

ADSORCION

PRESIDENTE

Juan de Dios López González
Departamento de Química Inorgánica UNED
Senda del Rey, s/n 28040 - MADRID
Telef. 4.49.03.06 Ext. 1094

CALORIMETRIA Y ANALISIS TERMICO

PRESIDENTE

Fernando Fernández Martín
Instituto del Frío C.S.I.C.
Ciudad Universitaria 28040 MADRID
Telf. 2.44.56.00 Ext. 31

CRISTALOGRAFIA

PRESIDENTE

Jose María Amigó Descarrega
Depto Cristalografía. Facultad de Ciencias
Dr. Moliner, 50, 46100 - Burjassot (VALENCIA)
Teléf. (96) 3.86.43.00

DIDACTICA DE LA FISICA Y QUIMICA

PRESIDENTE

Salvador Senent Pérez
P. de las Perdices, 23
Ciudalcampo, 28700. S.S. Reyes (MADRID)
Teléf. 6.57.01.19

ELECTRICIDAD Y MAGNETISMO

PRESIDENTE

Pedro Cartujo Estébanez
Depto. de Electrónica
Facultad de Ciencias. Universidad de Granada.
18071 - GRANADA
Teléf. (958) 20.22.12

ESPECTROQUIMICO

PRESIDENTE

Alfredo Sanz Medel
Depto. de Química Analítica. Facultad de Ciencias
Universidad de Oviedo. 33007 - OVIEDO
Teléf. (985) 27.12.44

FISICA DE LA ATMOSFERA Y DEL OCEANO

PRESIDENTE

Sergio Alonso Oroza
Depto. de Física. Facultad de Ciencias
Universidad de Baleares. 07071-PALMA DE MALLORCA
Teléf. (971) 20.71.11

FISICA ATOMICA MOLECULAR

PRESIDENTE

Gerardo Delgado Barrio

Insto. de Estructura de la Materia. C.S.I.C.
Serrano, 119. 28006 - MADRID
Teléf. 2.61.94.00

FISICA DEL ESTADO SOLIDO

PRESIDENTE

Francisco Baltá Calleja

Insto. Estructura de la Materia. C.S.I.C.
Serrano, 119. 29006 - MADRID
Teléf. 2.61.84.00 - Ext. 223

FISICA NUCLEAR

PRESIDENTE

Elvira Valgañon Moya

Insto. Estructura de la Materia. C.S.I.C.
Serrano, 199 - 29006 - madrid
Teléf. 2.61.94.00

FISICA TEORICA

PRESIDENTE

J. Luis Sánchez Gómez

Depto. de Física Teórica. Facultad de Ciencias
Universidad Autonoma. 28049-Cantoblanco (MADRID)
Teléf. 7.34.01.00 - Ext. 1881

POLIMEROS

PRESIDENTE

Arturo Horta Zubiaga

Depto. de Química Física UNED
Senda del Rey, s/n - 28040 - MADRID
Teléf. 2.43.71.69 - Ext. 1316

REOLOGIA

PRESIDENTE

José Alemán Vega

Insto. de Ciencia y Tecnología de Polímeros C.S.I.C.
28006 - MADRID
Teléf. 2.62.29.00

TERMODINAMICA

PRESIDENTE

Juan de la Rubia Pacheco

Depto. de Termología. Facultad de Ciencias
Universidad de Valencia. 46100 - Buejassot (VALENCIA)
Teléf. (96) 3.86.43.00. 3.86.32.81
Fax. 36.42.35

TRIBOLOGIA

PRESIDENTE

Pedro Andrés Sanz

CENIM, Gregorio del Amo, s/n
28040 - MADRID
Teléf. 2.53.89.00